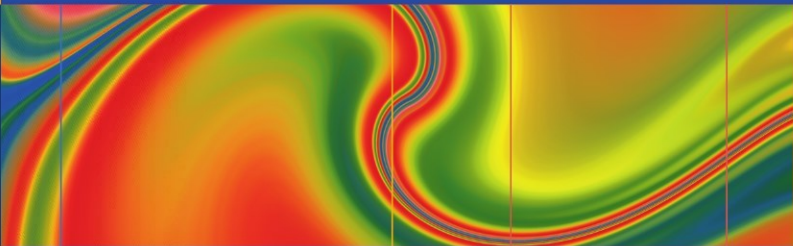


Sven Plein
John Greenwood
John Ridgway



Cardiovascular MR Manual

 Springer

Cardiovascular MR Manual

Sven Plein • John P. Greenwood
John P. Ridgway

Cardiovascular MR Manual



Springer

Authors

Sven Plein

Multidisciplinary Cardiovascular Research Centre (MCRC), University of Leeds, Department of Cardiology, G-Floor, Jubilee Wing, Leeds General Infirmary, Great George Street, Leeds, LS1 3EX United Kingdom

John P. Ridgway

Multidisciplinary Cardiovascular Research Centre (MCRC), University of Leeds, Department of Cardiology, G-Floor, Jubilee Wing, Leeds General Infirmary, Great George Street, Leeds, LS1 3EX United Kingdom

ISBN 978-1-84996-361-9

John P. Ridgway

DOI 10.1007/978-1-84996-362-6

Department of Medical Physics and Engineering
Leeds Teaching Hospitals NHS Trust
Leeds General Infirmary
Leeds LS1 3EX
UK

Springer London Dordrecht Heidelberg New York

e-ISBN 978-1-84996-362-6

British Library Cataloguing in Publication Data

A catalogue record for this book is available from the British Library

Library of Congress Control Number: 2010933605

© Springer-Verlag London Limited 2011

Apart from any fair dealing for the purposes of research or private study, or criticism or review, as permitted under the Copyright, Designs and Patents Act 1988, this publication may only be reproduced, stored or transmitted, in any form or by any means, with the prior permission in writing of the publishers, or in the case of reprographic reproduction in accordance with the terms of licenses issued by the Copyright Licensing Agency. Enquiries concerning reproduction outside those terms should be sent to the publishers.

The use of registered names, trademarks, etc., in this publication does not imply, even in the absence of a specific statement, that such names are exempt from the relevant laws and regulations and therefore free for general use.

Product liability: The publisher can give no guarantee for information about drug dosage and application thereof contained in this book. In every individual case the respective user must check its accuracy by consulting other pharmaceutical literature.

Cover design: eStudioCalamar, Figueres/Berlin

Printed on acid-free paper

Springer is part of Springer Science+Business Media (www.springer.com)

Foreword

Cardiovascular magnetic resonance (CMR) has become an established imaging modality with an expanding range of clinical indications. While in the past the CMR imaging was available in only a few specialist centres, the use of CMR is now becoming much more widespread. All clinicians working in Cardiology or Imaging should therefore have a general understanding of the diagnostic information that can be obtained from CMR, the indications for referral as well as contraindications and limitations of the technique. For cardiologists and radiologists in particular, CMR will become a routine diagnostic tool and training curricula in Cardiology or Radiology will require a compulsory period of training in CMR.

This book is conceived as a compact introductory text to CMR and as a practical guide for daily use. The book begins with a detailed didactic overview of the physics of magnetic resonance imaging – a subject that many clinicians find difficult to understand, but one that is essential for the appropriate use of this technology, as it determines image quality and most appropriate use. We have taken a very practical approach to explaining MRI physics, cross-referencing consistently to the subsequent clinical chapters and showing how an understanding of basic MRI physics translates into generating better images.

The second part of the book explains the practicalities of CMR from the referral to screening, set-up of the study and reporting. It then outlines the most commonly acquired

image components used in CMR and explains with tips and tricks how the user can generate good quality images.

The third part of the book gives details of how CMR is used in clinical practice. It covers the most common referrals for CMR imaging in a structured way with imaging protocols and case examples for each indication.

Throughout the book, we have used graphs and tables as well as boxes that highlight important aspects. The emphasis of each chapter is on providing practical, hands-on information.

We hope that this compendium will be a useful resource for clinicians wishing to learn the basics of CMR and a handy guide for everyday use in clinical practice.

Sven Plein
John P. Greenwood
John P. Ridgway

Contents

Part I How Does CMR Work?

1 What's Inside the Magnet and Why?	3
1.1 The Main Magnet.	4
1.2 The Gradient Coil Assembly	6
1.3 Integral Radiofrequency (RF) Body Transmitter Coil	8
1.4 Receiver Coil	9
2 The MRI Environment	11
2.1 The Examination Room and RF Shielding	11
2.2 The Magnetic Fringe Field Hazard and the Controlled Area	11
2.3 Active and Passive Magnetic Shielding	14
3 Protons and Spins: The Origin of the MRI Signal	17
3.1 MRI Images: What Are We Looking At?	17
3.2 Proton Spin and Net Magnetization	17
3.3 What Determines the Size of the Net Magnetization?	18
4 Generating a Signal: RF Pulses and Echoes	21
4.1 How Do We Generate a Signal?	21
4.2 What Does the RF Pulse Do to the Magnetization?	22
4.3 Longitudinal and Transverse Components of Magnetization	24

4.4	Flip Angle and Common RF pulses.....	24
4.4.1	Variable-Flip Angle RF Excitation Pulse	24
4.4.2	90° RF Excitation Pulse	25
4.4.3	180° RF Pulse (Refocusing Pulse)	27
4.4.4	180° RF Pulse (Inversion Pulse).....	27
4.5	What Does the MRI Signal Look Like?.....	28
5	Relaxation Times, Gradient Echoes, and Spin Echoes .	31
5.1	Relaxation: What Happens After the RF Excitation Pulse?	31
5.1.1	What is T1 Relaxation?.....	31
5.1.2	Transverse Relaxation and MRI Signal Decay	33
5.1.3	What is T2 Relaxation?.....	34
5.1.4	What is T2* Relaxation?.....	35
5.2	MR Echoes.....	37
5.2.1	Gradient Echoes	37
5.2.2	Spin Echoes.....	39
6	Making an Image: Locating and Encoding Signals in Space.....	45
6.1	Selecting an Image Slice	45
6.2	Encoding the MR Signal Within the Slice.....	47
6.3	Phase Encoding	47
6.4	Frequency Encoding.....	49
6.5	How is the Frequency-Encoded Signal Decoded?.....	51
6.6	How do we make sure that the Gradients we apply for Imaging don't Destroy the signal?	54
6.7	Why isn't a Single Phase and Frequency Encoded Signal enough to Reconstruct an Image?.....	55
6.8	Field of View in the Phase Encoding Direction.	56
6.9	Phase Encoding, Image Matrix, and Acquisition Time.....	57

7 Image Space and k-Space	61
8 Imaging Parameters and Image Attributes	69
8.1 Spatial Resolution and Image Acquisition Time ..	69
8.2 Noise and Signal-to-Noise Ratio	70
8.3 Factors That Determine Image Quality	71
8.3.1 Intrinsic Signal Amplitude	71
8.3.2 Signal Averaging.	72
8.3.3 SNR and Receiver Bandwidth	73
8.4 Imaging Parameters: Practical Examples.	74
8.5 2D and 3D Imaging	79
9 Improving SNR with Surface Coils and Array Coils	83
10 Pulse Sequences and Image Contrast	87
10.1 Dependence of the MR Signal on TR and TE ..	87
10.2 Image Contrast and Weighting.	90
10.3 Long TR and Short TE.	92
10.4 Short TR, Short TE	93
10.5 Long TR, Long TE.	94
10.6 Short TR, Long TE.	95
11 Gradient Echo Versus Spin Echo	97
12 Black Blood Versus Bright Blood Imaging.	103
12.1 Black Blood (Spin Echo Pulse Sequence)	103
12.2 Black Blood – Double Inversion Preparation Pulses	105
12.3 Bright Blood (Gradient Echo Pulse Sequence) .	107
13 Dealing with Cardiac Motion: How Do We Image the Beating Heart?	111
13.1 Still Imaging.	112
13.2 Cine Imaging	114
13.3 Triggering Versus Gating for Cine Imaging. . . .	115

13.4	Prospective Versus Retrospective ECG Gating	117
13.5	Spoiled Gradient Echo versus bSSFP	118
14	Dealing with Respiratory Motion	123
14.1	Respiratory Compensation (Respiratory Gating) .	123
14.2	Respiratory Gating using Navigator Echoes ...	125
15	Fast Imaging: How Do We Speed Up the Image Acquisition?.....	127
15.1	Turbo (or Fast) Spin Echo	127
15.2	Turbo (or Fast) Gradient Echo	129
15.3	Echo Planar-Imaging (EPI)	131
15.4	Reducing the Total Number of Phase Encoding Steps Acquired for Each Image	133
15.5	Parallel Imaging.....	135
16	Special Pulse Sequences for Cardiac Imaging	139
16.1	Selective Tissue Saturation	139
16.2	Frequency Selective Fat Suppression.....	141
	16.2.1 Pros and Cons of Frequency Selective Fat Suppression (cf. STIR) ..	143
16.3	STIR and Turbo STIR	143
	16.3.1 Pros and Cons of STIR (cf. Frequency Selective Fat Suppression)	145
16.4	Black Blood FSE/TSE (Double Inversion)	145
16.5	Black Blood turboSTIR (Triple Inversion Recovery).....	147
16.6	Inversion Recovery Fast/Turbo Gradient Echo ..	149
16.7	Navigator-Gated 3D Fast/Turbo Gradient Echo (Coronary Artery Imaging).....	151
	16.7.1 Key Features of a Navigator-Gated 3D Coronary Artery Imaging Sequence ...	153
16.8	Cine Gradient Echo	153
16.9	Velocity Encoded Cine Gradient Echo (Velocity Mapping)	155
16.10	Myocardial Tagging (Binomial Pulses)	159
16.11	Saturation Recovery, Single-Shot Fast Gradient Echo for Dynamic, Contrast-Enhanced Myocardial Perfusion Imaging.....	162

17 Common Artifacts	167
17.1 Image Aliasing	167
17.2 Aliasing Artifacts with Parallel Imaging	169
17.3 Ghosting Artifacts from Motion (Respiratory)	171
17.4 Ghosting Artifacts from Motion (Pulsatile Flow)	172
17.5 Flow-Related Signal Loss and Flow Jets	174
17.6 Chemical Shift Artifact	175
17.7 Magnetic Susceptibility Artifacts.	178
17.8 Metallic Artifact.	180
17.9 Radiofrequency Interference Artifacts.	182

Part II How CMR is Performed

18 The Basics of a CMR Study	187
18.1 The Referral	187
18.2 Indications for CMR	189
18.3 Contraindications/Safety	190
18.3.1 Screening.	191
18.3.2 Contraindications to CMR Scanning	192
18.4 Setting Up a CMR Study	199
18.4.1 Equipment.	199
18.4.2 ECG Signals	200
18.4.3 Patient Preparation	201
18.4.4 Commencing the Scan	202
References.	203
19 Components of CMR Protocols	205
19.1 Introduction	205
19.2 Localizing Images and Simple Planning	206
19.2.1 Interactive Planning	211
19.3 Anatomical and Morphological Imaging.	211
19.3.1 T1-Weighted (Black Blood) Imaging	212
19.3.2 T2-Weighted (Black Blood) Imaging	214
19.3.3 T2* Relaxometry	216
19.4 Cine Imaging (Including Real-Time Cine Imaging).	218
19.4.1 Real-Time Cine Imaging.	219
19.4.2 Quantitation.	220

19.5	Myocardial Tagging	223
19.6	Phase Contrast Velocity Encoding	225
19.7	Contrast-Enhanced MR Angiography (Excluding Coronary Arteries)	228
19.8	Myocardial Perfusion CMR	231
19.8.1	Reproducible Planning of Three Short Axis Slices	233
19.8.2	Dark Rim Artifact	235
19.8.3	Interpretation of CMR Myocardial Perfusion Images	236
19.9	Early and Late Gadolinium Enhancement	239
19.9.1	Protocol for Early and Late Gadolinium Enhancement Imaging	241
19.10	Coronary Artery Imaging	244
19.10.1	Whole Heart Technique	245
19.10.2	Targeted Technique	248
20	Anatomy by CMR	251
20.1	Cross-sectional Anatomy	251
20.2	Customized Views	259
20.3	Comparison with Other Imaging Modalities	259
21	The CMR Report	261
21.1	A Structured Approach to Reporting a CMR Study	261
21.2	The Report	263
	Reference	264
Part III Clinical Indications for CMR Imaging		
22	Diseases of the aorta	267
22.1	Introduction	268
22.2	CMR versus Other Imaging Modalities	268
22.3	CMR in the Assessment of Aortic Atherosclerosis and Dissection	269
22.3.1	Acute Intramural Hematoma	269
22.3.2	Penetrating Atherosclerotic Ulcer	270
22.3.3	Aortic Dissection	271
22.4	Aortic Aneurysm	272

23 Cardiomyopathies	279
23.1 General Overview	279
23.2 Dilated Cardiomyopathy (DCM)	280
23.2.1 Introduction	280
23.2.2 CMR versus Other Imaging Modalities in DCM	281
23.2.3 Findings on CMR	282
23.2.4 Differential Diagnosis	282
23.2.5 Case Example	283
23.3 Hypertrophic Cardiomyopathy (HCM)	284
23.3.1 Introduction	284
23.3.2 CMR versus Other Imaging Modalities	285
23.3.3 Findings on CMR	285
23.3.4 Differential Diagnosis	286
23.3.5 Case Example	287
23.4 Arrhythmogenic Right Ventricular Cardiomyopathy (ARVC)	290
23.4.1 Introduction	290
23.4.2 CMR versus Other Imaging Modalities	292
23.4.3 Findings on CMR	293
23.4.4 Differential Diagnosis	293
23.4.5 Case Example	294
23.5 Left Ventricular Non-Compaction Cardiomyopathy (LVNC)	298
23.5.1 Introduction	298
23.5.2 CMR versus Other Imaging Modalities	298
23.5.3 Role of CMR in LVNC	298
23.5.4 Findings on CMR	299
23.5.5 Differential Diagnosis	299
23.5.6 Case Example	300
23.6 Inflammatory Diseases: Myocarditis	302
23.6.1 Introduction	302
23.6.2 CMR versus Other Imaging Modalities	303
23.6.3 Findings on CMR	304
23.6.4 Differential Diagnosis	304
23.6.5 Case Example	304
23.7 Inflammatory Diseases: Sarcoidosis	309
23.7.1 Introduction	309
23.7.2 Findings on CMR	309

23.7.3	Differential Diagnosis	310
23.7.4	Case Example	310
23.8	Inflammatory Diseases: Vasculitis (Churg–Strauss Syndrome)	314
23.8.1	Introduction	314
23.8.2	Findings on CMR	314
23.8.3	Differential Diagnosis	315
23.8.4	Case Example	315
23.9	Infiltrative/Storage Diseases: Amyloidosis	317
23.9.1	Introduction	317
23.9.2	Findings on CMR	317
23.9.3	Differential Diagnosis	318
23.9.4	Case Example	319
23.10	Infiltrative/Storage Diseases: Siderotic Cardiomyopathy	322
23.10.1	Introduction	322
23.10.2	CMR versus Other Imaging Modalities	322
23.10.3	Findings on CMR	323
23.10.4	Differential Diagnosis	323
23.10.5	Case Example	324
23.11	Tako-Tsubo Cardiomyopathy	327
23.11.1	Introduction	327
23.11.2	CMR versus Other Imaging Modalities	327
23.11.3	Findings on CMR	328
23.11.4	Differential Diagnosis	328
23.11.5	Case Example	329
	References	331
24	Pericardial Disease	333
24.1	Pericardial Effusion	333
24.1.1	Introduction	333
24.1.2	CMR versus Other Imaging Modalities	334
24.1.3	Findings on CMR	334
24.1.4	Case Example	336
24.2	Constrictive Pericarditis	340
24.2.1	Introduction	340
24.2.2	CMR versus Other Imaging Modalities	341
24.2.3	Findings on CMR	341
24.2.4	Case Example	343

24.3	Pericardial Tumors	347
24.3.1	Introduction	347
24.3.2	CMR versus Other Imaging Modalities	347
24.3.3	Findings on CMR	348
24.4	Congenital Abnormalities of the Pericardium	355
24.4.1	Introduction	355
24.4.2	CMR versus Other Imaging Modalities	356
24.4.3	Findings on CMR	356
24.4.4	Case Example	357
25	Cardiac Masses	361
25.1	Introduction	362
25.2	Benign Cardiac Tumors	364
25.2.1	Myxoma	364
25.2.2	Lipoma	364
25.2.3	Papillary Fibroelastoma	366
25.2.4	Fibroma	366
25.2.5	Rhabdomyoma	368
25.2.6	Hemangioma	368
25.3	Malignant Cardiac Tumors	368
25.3.1	Sarcoma	368
25.3.2	Lymphoma	369
25.3.3	Metastatic Tumors	370
25.4	Other Masses and Tumors	370
25.4.1	Thrombus	370
25.4.2	Cysts	372
25.4.3	Pseudotumors	373
	Further Readings	374
26	Valvular Heart Disease	375
26.1	Introduction	376
26.2	CMR Versus Other Imaging Modalities	376
26.3	Congenital	378
26.4	Regurgitation	379
26.5	Stenosis	380
26.6	Prosthetic Valves	382
26.7	Vegetations	382
26.8	Paravalvular Abscesses	382

27 Ischemic Heart Disease	387
27.1 Introduction	387
27.2 Stress Myocardial Perfusion Imaging for the Detection of Myocardial Ischemia	388
27.2.1 Introduction.	389
27.2.2 Myocardial Perfusion CMR Versus Other Imaging Modalities	389
27.2.3 Diagnostic Performance	391
27.2.4 Prognostic Performance	393
27.2.5 How to Perform a Myocardial Perfusion CMR Study	394
27.2.6 Safety Considerations	397
27.2.7 Analysis of CMR Perfusion Images . . .	398
27.2.8 Case Examples	400
27.3 CMR Stress Wall Motion Imaging for the Detection of IHD	405
27.3.1 Introduction.	405
27.3.2 CMR Versus Other Imaging Modalities .	405
27.3.3 Diagnostic Performance	406
27.3.4 Prognostic Performance	406
27.3.5 Method	408
27.3.6 Safety Considerations	408
27.3.7 Analysis.	410
27.3.8 Case Example	412
27.3.9 Which Stress Modality Should I Choose?	413
27.4 CMR for Assessment of Viability	414
27.4.1 Introduction.	414
27.4.2 CMR Versus Other Imaging Modalities	414
27.4.3 CMR Methods for Viability Assessment	415
27.4.4 Case Examples	418
27.5 CMR in Acute Coronary Syndromes	422
27.5.1 Introduction.	422
27.5.2 CMR Versus Other Imaging Modalities	422
27.5.3 Methods.	423
27.5.4 Case Examples	426

27.6	Positive Cardiac Enzymes and Normal Coronary Arteries.....	431
27.6.1	Example Case	433
27.7	Potential Future Developments	434
27.7.1	Hardware Development	434
27.7.2	Software Development	434
27.7.3	New Methods	435
	References.....	436
28	Basic Adult Congenital Heart Disease (ACHD).....	439
28.1	Introduction	440
28.2	CMR Versus Other Imaging Modalities.....	440
28.3	Coarctation of the Aorta.....	441
28.4	Tetralogy of Fallot	444
28.5	Transposition of the Great Arteries	448
28.6	Coronary Anomalies	451
28.7	Partial Anomalous Pulmonary Venous Return (PAPVR).	452
28.8	Summary	454
29	Pulmonary Vein Assessment	457
29.1	Introduction	457
29.2	CMR Versus Other Imaging Modalities.....	458
29.3	CMR Protocol and Findings.....	459
29.4	CMR Analysis	459
30	Interventional Cardiovascular Magnetic Resonance Imaging.....	463
30.1	Introduction	463
30.2	Interventional MRI Systems	463
30.2.1	XMR Facility Design	463
30.3	MR Visualization Strategies.....	465
30.3.1	Performing XMR Procedures	466
30.3.2	Physiological Information.....	467
30.3.3	Early Experiences	469
30.4	Future Perspectives	471
	References.....	474
Index.....		475

Contributors

Dr. Sven Plein, MD, PhD

Senior Lecturer & Consultant Cardiologist
University of Leeds, Leeds, UK

Dr. John P. Greenwood, MBChB, PhD, MRCP(UK)

Senior Lecturer & Consultant Cardiologist
University of Leeds, Leeds, UK

Dr. John P. Ridgway, PhD

Department of Medical Physics & Engineering, Leeds
Teaching Hospitals NHS Trust Leeds General Infirmary,
Leeds, UK

Dr. Adam Mather

Research Fellow, University of Leeds, Leeds, UK

Dr. Neil Maredia

Research Fellow, University of Leeds, Leeds, UK

Dr. Charles Peebles, MBBS, MRCP, FRCR

Consultant Cardiothoracic Radiologist, Cardiothoracic
Radiology Department, Southampton General Hospital,
Southampton, UK

Dr. Daniel Messroghli, MD

Research fellow, Congenital Heart Defects and Pediatric
Cardiology, German Heart Institute, Berlin, Germany

Dr. Andrew M. Crean

Associate Professor

Peter Munk Cardiac Center (Cardiac Imaging),
Toronto General Hospital, Toronto ON, Canada

Dr. Amedeo Chiribiri

Clinical Research Fellow Division of Imaging Sciences,
King's College London, St Thomas' Hospital London,
London, UK

Dr. Gerald F. Greil

Consultant Paediatric Cardiologist/Senior Clinical Lecturer,
Division of Imaging Sciences, King's College London,
St. Thomas' Hospital, London, UK

Dr. Tarique M. Hussain

Research Fellow, Division of Imaging Sciences,
King's College London,
St. Thomas' Hospital, London, UK

Dr. Kawal Rhode

Lecturer, Division of Imaging Sciences,
King's College London,
St. Thomas' Hospital, London, UK

Part I

How Does CMR Work?

Chapter 1

What's Inside the Magnet and Why?

The use of Magnetic Resonance (MR) in medicine involves the interaction of magnetic fields with biological tissue. For magnetic resonance imaging, (MRI), three types of magnetic field are used to generate images.

- *A strong, constant magnetic field.* This has the symbol \mathbf{B}_0 and defines the nominal operating field strength of a particular MRI system. This is measured in units of Tesla, (T) with 1 T equal to approximately 20,000 times the earth's magnetic field.
- *A gradient magnetic field* that can be rapidly switched on and off. This magnetic field has a strength that increases with position along a chosen direction and is measured in units of milliTesla per meter (mT/m).
- *A radiofrequency (RF) magnetic field* that oscillates at a characteristic frequency in the MegaHertz range, the exact value of which is determined by the nominal field strength of the main magnet. This is given the symbol \mathbf{B}_1 .

A typical MRI system therefore consists of three main components that generate these three fields, the main magnet, the gradient coil assembly, and the integral radiofrequency body transmitter coil. These are described in the sections that follow which will use the convention of Cartesian axes (x , y , z) in the directions as shown in Fig. 1.1.

1.1 The Main Magnet

The most common main magnet configurations are *superconducting*, with a *horizontal patient bore* with field strengths of 1.0 T, 1.5 T, and 3.0 T.

Superconducting magnets consist of several circular magnet coils each consisting of many turns of wire (windings) carrying a high electrical current. This generates a *strong, constant magnetic field*, \mathbf{B}_o , in a horizontal direction through the center of the coils (parallel to the z axis as shown in Fig. 1.1a).

The windings are made of a material that becomes superconducting when cooled to liquid helium temperatures (approx. 4 K or -269°C). They are immersed in liquid helium contained within a vessel (the “*cryostat*”) surrounded by two vacuum layers to reduce the boil-off rate of the liquid Helium

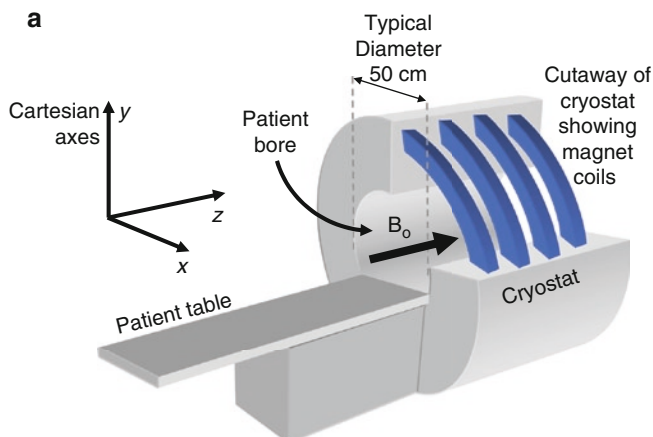


FIGURE 1.1. (a) The Key features of superconducting magnet design showing the cartesian axes with the horizontal z axis, the static \mathbf{B}_o field direction, the patient bore, and magnet coils. (b) Internal construction of magnet cryostat. The spherical homogenous volume is indicated by the dotted line. (c) A vertical field, open magnet configuration. The z axis is vertical for this configuration.

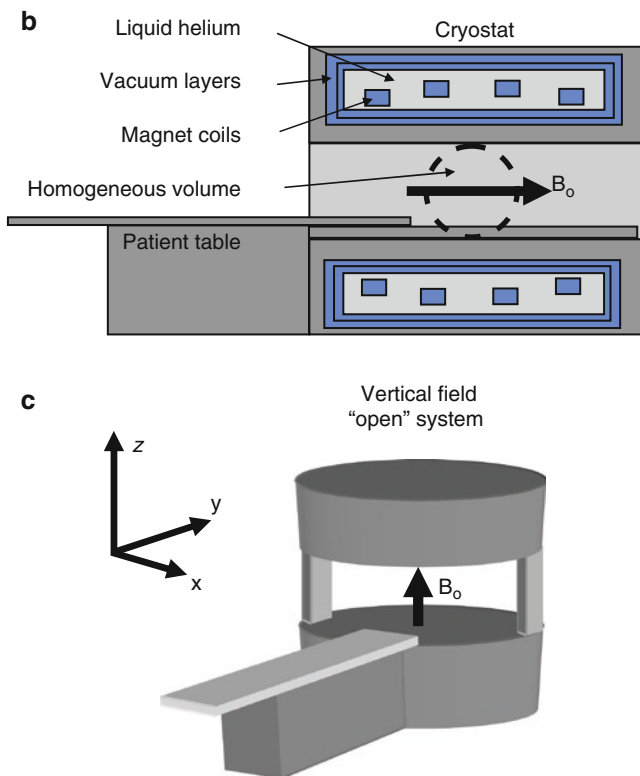


FIGURE 1.1. (continued).

(Fig. 1.1b). The Cryostat has a central bore open at both ends of the magnet (the *patient bore*).

The magnet coils are positioned to generate a highly uniform magnetic field at the center of the patient bore typically over a spherical region between 45–50 cm in diameter, known as the *homogeneous volume*. The extent of this region determines the *maximum field of view* that can be imaged at one time.

The magnetic field is brought within a specified limit of homogeneity by a process known as shimming. At the time of installation, small pieces of steel are placed around the inside of the magnet bore to modify the magnetic field so that it has the best uniformity within the homogenous volume. This process is known as *passive shimming* and it takes into account

the effect that any steel within the building structure might have. It is also possible to perform *active shimming* of the magnetic field by using small magnetic fields generated by additional electromagnetic coils to correct any remaining variations in the magnetic field. This may be done by using either the *gradient coils* (see Sect. 1.2) or dedicated *shim coils*. A standard shim is determined at installation to provide the best uniformity over the whole imaging volume. *Dynamic shimming* may also be performed on a scan by scan basis in order to provide the best magnetic field homogeneity over a particular region for specific applications.

Once the magnet has been energized after installation, it *remains on at all times*. Superconductivity is maintained by minimizing the boil-off rate of liquid helium using a cooling system and periodically topping it up. Current systems can maintain sufficient levels of helium for several years before topping up.

As the magnet remains on all the time, (even outside normal working hours), the strong magnetic field presents a constant hazard and safety measures must therefore be applied at all times (See Chap. 2).

Vertical field “open” MR systems are also commercially available, currently having field strengths of up to 1.0 T (Fig. 1.1c). Open MR systems often use magnet designs that are based on permanent magnets or iron cored resistive magnets, but these have lower field strengths than superconducting systems.

1.2 The Gradient Coil Assembly

This consists of a set of three cylindrical copper windings (*gradient coils*) positioned inside the inner bore of the cryostat (Fig. 1.2). Each gradient coil generates a *magnetic field gradient* This is a field applied in the same direction as the main magnetic field that either adds or subtracts in such a way as to create a net total field that varies in strength with

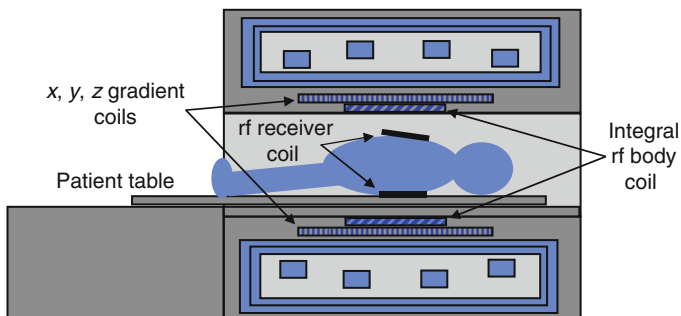


FIGURE 1.2. The relative locations of the gradient coils, integral rf body coil, and rf receiver coils.

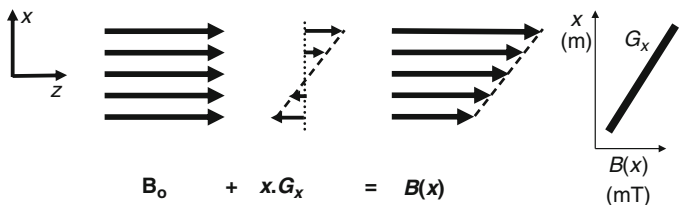


FIGURE 1.3. This diagram shows how a gradient field of slope G_x is superimposed onto the main magnetic field, \mathbf{B}_0 to produce a total field that varies in the x direction, $B(x)$. The strength of the magnetic field is represented by the length of the arrows in each case. The direction of each magnetic field is along the z axis, but the direction of the gradient (change in strength) is along the x axis.

position along each of the x , y , and z directions (Fig. 1.3). This also varies the resonant frequency and enables the MRI signals subsequently emitted to be related to particular locations (see Chap. 6). The use of the three gradients enables the signal to be encoded in three dimensions and provides the unique ability to directly acquire cross sectional images in any orthogonal or oblique plane. The gradient magnetic fields can be independently switched on or off rapidly in less than a millisecond and may be kept on for a few milliseconds at

a time. As the fields are switched rapidly within the main magnetic field they cause the gradient coils to vibrate creating the familiar loud banging noise that is associated with MRI systems.

The rapidly switched gradient magnetic fields are active only during image acquisition; however, they present two additional hazards:

- The rapidly changing electromagnetic field (often denoted dB/dt) can cause peripheral nerve stimulation of patients.
- The banging noise is sufficiently loud to warrant the use of hearing protection by patients and caregivers who remain in the examination room.

1.3 Integral Radiofrequency (RF) Body Transmitter Coil

This consists of a cylindrical copper antenna mounted inside the gradient coil assembly (Fig. 1.2). It generates a much smaller magnetic field, \mathbf{B}_1 that oscillates in a direction at right angles to the main magnetic field along the x or y axes. The frequency of oscillation (known as the *resonant frequency* or *Larmor frequency*) corresponds to the nominal operating frequency of the MRI system which in turn is determined by the nominal field strength of the main magnetic field. The operating frequency is typically in the Megahertz range (as used by short wave radios) and hence \mathbf{B}_1 is known as the *radiofrequency* (rf) magnetic field. The resonant frequencies for the most common nominal field strengths are given below:

Field strength (T)	Resonant frequency (MHz)
1.0	42.6
1.5	63.9
3.0	127.8

The rf magnetic field produced by the integral body coil is used to transmit energy into the patient. It is normally delivered in the form of a short pulse, known as a *rf pulse* (see Chap. 4). When applied at the resonant frequency, this causes the hydrogen nuclei in the patient's tissue to absorb the energy, to resonate, and then to re-emit the energy, also in the form of an oscillating RF magnetic field.

The radiofrequency field creates a further hazard as it has the potential to cause heating of body tissue. The rate of energy deposition is characterized by the *Specific Absorption Rate* (SAR) with units Watts per Kilogram of tissue (W/kg) and is carefully monitored and controlled.

1.4 Receiver Coil

The oscillating magnetic field (MRI Signal) emitted is detected by a rf receiver coil. For Cardiac MRI, this is usually a dedicated *receiver coil* or *coil array*, whose design is tailored to maximize signal detection around the heart and to minimize the detection of “noise” from elsewhere in the body and surrounding environment (see Fig. 1.2). The MRI signal is small; the voltage induced in the receiver coil is typically measured in microVolts and so it is very sensitive to interference from external sources of electrical noise. The integral body transmitter can also be used as a receiver coil. Although it is less sensitive than a dedicated receiver coil, it can provide a more uniform detection field which is sometimes advantageous.

For more on currently available MR system configurations visit the
MR Manufacturer links:

GE

www.ge.com/medical

Philips

www.medical.philips.com

Siemens

www.med.siemens.com

Toshiba

www.toshiba.com

Summary

- Cardiac Magnetic Resonance Imaging uses three types of magnetic field to generate images:
 - A strong constant magnetic field is generated by the main magnet
 - A rapidly switched gradient magnetic field is generated by an assembly of three gradient coils (one for each direction, x , y , and z) mounted inside the main magnet
 - A radiofrequency (rf) magnetic field is generated by the integral rf body transmitter coil mounted inside the gradient coil
- A separate rf receiver coil that is tailored to maximize signal from the heart is normally used to detect the emitted MR signal

Chapter 2

The MRI Environment

2.1 The Examination Room and RF Shielding

The examination room contains the magnet assembly and patient table (Fig. 2.1). To prevent environmental electrical noise from interfering with the MRI signal, this room is enclosed within a *rf shield* (or *Faraday cage*) made of copper or aluminum sheet. The door into the examination room forms part of this shield and must always be closed during the MR examination. The observation window also forms part of this shield.

2.2 The Magnetic Fringe Field Hazard and the Controlled Area

The main magnet generates the strongest magnetic field at its center and also has a *fringe field* that is always present and extends well beyond outside the magnet, decreasing with distance from the magnet. This can create an extremely hazardous environment unless control measures are put in place. For this reason, the general public must be excluded from entering the fringe field above a certain threshold. Currently, this threshold is set at 0.5 mT, as magnetic fields above this value have been shown to adversely affect the operation of *cardiac pacemakers*. A *controlled area* is therefore defined to include the examination room and any adjacent rooms necessary to fully enclose the *0.5 mT fringe field contour* (Fig. 2.1). Access to this area is restricted to authorized staff with

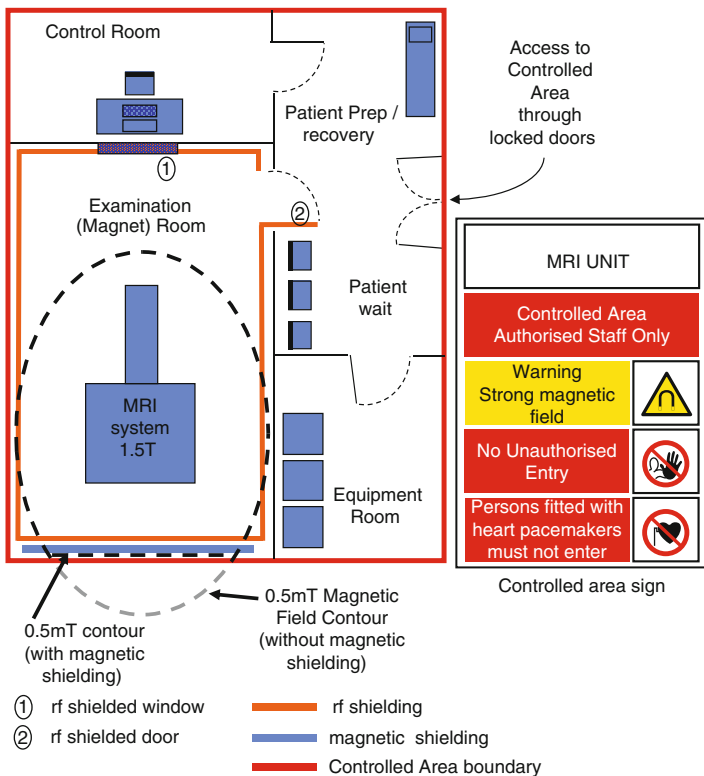


FIGURE 2.1. Typical layout of an MRI unit showing the examination (magnet) room, control room, equipment room, and ancillary rooms. The boundary of the controlled area is shown in red. Steel sheet shielding has been used to prevent the 0.5 mT fringe field from extending outside the controlled area. The examination room is completely enclosed by a copper RF shield (RF cabin). An example sign for the controlled area access doors is shown.

appropriate training. Patients and visitors should not enter unless they have first been screened for the presence of pacemakers and other contraindicated implants (see [Section 18.3](#) for a list of other MR contraindications).

A second very important reason to restrict access to the controlled area is to prevent accidents caused by ferromagnetic objects being attracted by the magnet and becoming

projectiles. All equipment or other items that are taken into the examination room must first be carefully checked to ensure that they are not ferromagnetic.

Specific items should be identified as being safe, unsafe, or conditional (Fig. 2.2) using the labeling system introduced by the ASTM. (ASTM International, Standard practice for marking medical devices and other items for safety in magnetic resonance environments, F2503-05).

Items such as watches, credit cards, and mobile phones may also be damaged by the magnetic field and should not be taken into the magnet room.

Though the above hazards have the potential to cause serious harm, there are relatively few deaths recorded due to MR equipment. Most recorded fatalities have been caused by pacemaker malfunction with one fatality caused by a gas cylinder becoming a projectile. If the above control measures are strictly adhered to, the MR environment can be managed relatively safely.



FIGURE 2.2. Labeling system developed by the ASTM to identify ancillary equipment as MR safe, Conditional, or Unsafe.

2.3 Active and Passive Magnetic Shielding

Most commercially available magnets have *active shielding* (additional windings within the cryostat located just outside the main magnet coils) that produces a counteracting field that in turn reduces the extent of the fringe field. This reduces the requirement for the controlled area and enables magnet systems to be installed in relatively small departments. Magnetic shielding using steel plate is often additionally used (known as *passive shielding*) to further reduce the extent of the fringe field to prevent it from extending outside the controlled area (Fig. 2.1). For example, magnetic shielding is commonly used in multistorey buildings to prevent the fringe field from extending into areas in the floors above and below the magnetic location.

National and international guidance is published for the safe installation and operation of magnetic resonance imaging systems. Useful information and links can be found in the following:

- MHRA Device Bulletin DB2007(03) Safety Guidelines for Magnetic Resonance Imaging Equipment in Clinical Use. <http://www.mhra.gov.uk/Publications/Safetyguidance/DeviceBulletins>
- American College of Radiology (ACR) Guidance Document for Safe MR Practices: 2007, AJR 2007; 188:1–27.

Summary

- The examination room is enclosed within a rf shield (Faraday cage) made of copper or aluminum to prevent external rf “noise” from interfering with the MR signal.
- The main magnet generates a fringe field that can both adversely affect the operation of pacemakers and other implants *and* cause ferromagnetic items to accelerate toward the magnet causing a projectile hazard.
- A controlled area must be defined that encloses the 0.5 mT fringe field contour (pacemaker line).
- Access to the controlled area is restricted to authorized staff and patients who have been screened for pacemakers and other contraindicated implants.
- Items of equipment must not be taken into the MR examination room unless they are clearly identified to be safe in the MR environment.
- Magnetic shielding can be used to restrict the extent of the fringe field.

Chapter 3

Protons and Spins: The Origin of the MRI Signal

3.1 MRI Images: What Are We Looking At?

The primary origin of the MR signal is from water and fat within the patient's tissue; specifically, it is from the *hydrogen nuclei* (consisting of a single proton) contained within *free water* and *lipid molecules* (Fig. 3.1). Hydrogen is one of a number of elements whose nuclei exhibit magnetic resonance properties, but the high intrinsic sensitivity and natural abundance in the form of water and lipid molecules makes it particularly favorable for imaging. Other nuclei of potential interest for cardiac applications in the future may include ^{31}P , ^{23}Na , and ^{13}C , but their sensitivity for imaging is low as they are normally present in the body only in trace amounts.

3.2 Proton Spin and Net Magnetization

Hydrogen nuclei (protons) possess an intrinsic property known as *Nuclear Spin*. This, combined with their positive charge gives rise to a small magnetic field for each proton known as a *magnetic moment*. Normally, the magnetic moments (spins) are randomly oriented, but in the presence of the externally applied B_0 field, they tend to align either with or against the externally applied magnetic field. An *equilibrium* state is quickly attained where there is a small excess

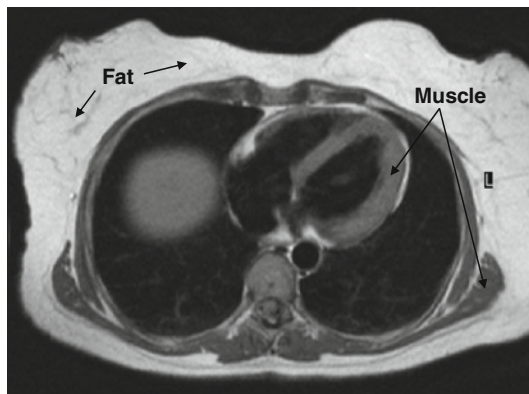


FIGURE 3.1. Transverse section through the thorax. Visible signal originates from either water-based tissue such as muscle or from lipid molecules within fat.

alignment with the field (typically just a few spins per million) as this is the more favorable direction of alignment. A more accurate description of this process relies on statistical quantum mechanics. It becomes easier, however, to develop a simpler picture by considering a population of billions of protons. In this model (known as the classical model), the excess of proton magnetic moments combines to form a net magnetic field or *net magnetization* (Fig. 3.2). This is often given the symbol \mathbf{M} and at equilibrium, it is aligned along the +ve z axis (along B_0) and has its maximum value, \mathbf{M}_0 . It is often shown as an arrow or vector.

3.3 What Determines the Size of the Net Magnetization?

The size of this net magnetization is one of the key determinants of the maximum signal intensity that can be generated and used to form images. The exact proportion of excess spins that gives rise to the net magnetization at equilibrium is

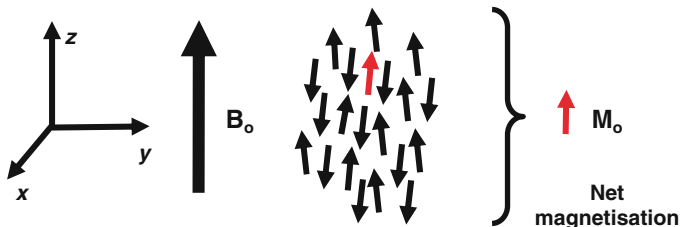


FIGURE 3.2. Proton magnetic moments, represented by arrows align either with or against the direction of the magnetic field, B_o (that is, along the z -axis). In this example, there is an excess of just one proton (shown in red) aligned with the field out of a population of 21, giving rise to the Net Magnetization M_o .

described by the *Boltzmann Equation* which shows that it depends on both the temperature (37°C for in vivo imaging) and the applied magnetic field strength, B_o as determined by the main magnet (see box). The greater the field strength, the greater is the size of the Net Magnetization (that is, the greater the excess of protons aligned with the magnetic field).

The Boltzmann Equation tells us that the excess of protons aligned with the field at equilibrium is determined by the temperature and the applied magnetic field strength

At 1.5 T, the excess is about *4 protons per million*

At 3.0 T, the excess is *7 protons per million* (assuming body temperature)

Therefore, the *higher* the field strength, the *greater* the available signal

The presence of the Net Magnetization aligned with the magnetic field at equilibrium is not measurable as an MR signal. The next section shows that in order to produce a signal, energy must first be delivered to the system of protons in a very specific form.

Summary

- The origin of the MR signal is from hydrogen nuclei (single protons) contained within free water and lipid molecules.
- Hydrogen nuclei (protons) possess a property known as nuclear spin that gives rise to a small magnetic field known as a magnetic moment.
- When a large magnetic field is applied, a small proportion of the magnetic moments of a large population of hydrogen nuclei combine to form a Net Magnetization aligned in the same direction as the applied magnetic field.
- The greater the strength of the applied magnetic field, the greater the value of the Net Magnetization.
- The value of the Net Magnetization determines the maximum available MR signal.

Chapter 4

Generating a Signal: RF Pulses and Echoes

4.1 How Do We Generate a Signal?

In order to generate a signal from the net magnetization that is detectable, the radiofrequency (rf) magnetic field described in Chap. 1 is generated by the rf transmitter coil (the integral body coil) and used to deliver energy into the population of protons. This field must be applied at a particular frequency, known as the *Larmor frequency*, that is determined by the strength of the magnetic field (see table in Sect. 1.3) such that:

$$\text{Larmor frequency} = \text{constant} \times B_0$$

This equation is known as the *Larmor equation*. The Larmor frequency is proportional to the strength of the magnetic field and is typically in the Megahertz range, for example, for 1.5 T, the Larmor frequency is 63 MHz. This is also known as the *resonant frequency*, as the protons absorb energy (or resonate) only at this characteristic frequency. The constant in the Larmor equation is known as the *gyromagnetic ratio* and has a value that is characteristic for a particular nucleus (42.6 MHz/T for the proton). The rf field is normally applied as a short pulse, known as an *rf pulse*.

Is the Larmor Frequency the Same for Other Nuclei?

As we saw in Chap. 3, magnetic resonance imaging is normally performed using hydrogen nuclei; however, there are other MR-active nuclei such as the most common isotopes of phosphorus (^{31}P) and Sodium (^{23}Na), as well as a much less common one of carbon (^{13}C). In each case, the constant in the Larmor equation is different, leading to different resonant frequencies for each nucleus for a particular magnetic field strength. MR systems that have *multi-nuclear capability* can perform imaging and spectroscopy of these and other nuclei.

4.2 What Does the RF Pulse Do to the Magnetization?

Before the rf pulse is switched on, the proton population, and therefore the Net Magnetization, M_o , is at *equilibrium*, aligned along the z -axis. (Fig. 4.1a). When the rf pulse is switched on, the proton magnetic moments start to rotate together about the main magnetic field. This causes the *net magnetization* to move away from its alignment with the z -axis and to rotate around it (Fig. 4.1b). Remember that the Net Magnetization is the result of the sum of the individual magnetic moments. So long as they rotate together (a condition known as *coherence*) they will produce a Net Magnetization that is rotating. The speed of this rotational motion, known as *precession*, is also at the Larmor frequency. (The Larmor frequency is therefore also sometimes referred to as the as the frequency of precession). The greater the amount of energy applied by the rf pulse, the greater the angle that the net magnetization makes with the B_o field (or the z axis). If the rf pulse were to remain on (that is, a continuous rf field, constantly delivering energy), the net magnetization will continue to move away from the z axis, pass

through the plane of the x and y axes (Fig. 4.1d) and eventually become aligned along the -ve z axis (Fig. 4.1g), and then continue to rotate back up towards the +ve z axis and so on. In practice, the rf field is delivered as a short pulse that is switched off once the angle of precession has reached a prescribed value, usually somewhere between 0° and 180° (Figs. 4.1b–g). This angle that the net magnetization is rotated through by the rf pulse is known as *the flip angle*.

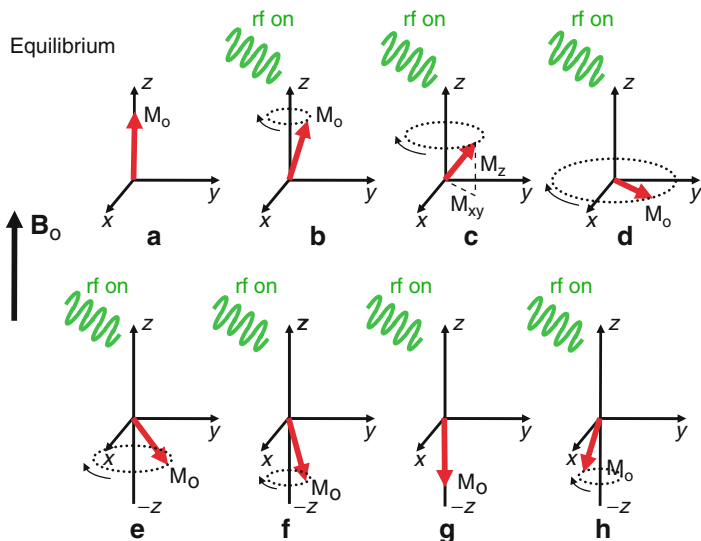


FIGURE 4.1. Initially, M_o is at equilibrium (a). As the rf field is applied, M_o makes an increasing angle with the z -axis (b) and rotates in the direction of the curved arrow. For as long as the rf field is applied, the angle with the z axis continues to increase (b–f) until M_o lies along the -ve z -axis (g). If the rf field continues to be applied, the angle will increase beyond 180° , driving the magnetization back toward the +ve z axis once more (h). At any instant, the magnetization can be split into two components, M_z and M_{xy} , (c). The rotating M_{xy} component generates the detectable MR signal once the applied rf field is switched off. The maximum detectable signal amplitude occurs when M_o lies entirely in the plane of the x and y axes (d) as this gives the largest M_{xy} component.

4.3 Longitudinal and Transverse Components of Magnetization

Once the rf pulse has caused the net magnetization to make an angle with the z -axis, it can be split into two components (Fig. 4.1c). One component is parallel to the z -axis. This is known as the z -component of the magnetization, M_z , also known as the *longitudinal component*. The other component lies at right angles to the z axis within the plane of the x and y axes and is known as the x - y component of the magnetization, M_{xy} , or the *transverse component*. This rotates at the Larmor frequency within the xy plane and it is this transverse component of the net magnetization that produces the detectable signal as it rotates by generating its own small, oscillating magnetic field which can be detected by an rf receiver coil once the transmitted rf pulse is switched off.

4.4 Flip Angle and Common RF Pulses

The flip angle of an rf pulse is determined by the energy delivered by the pulse which in turn depends upon both its amplitude and its duration. The greater the energy delivered, the greater the flip angle. RF pulses that generate an MR signal by delivering energy to the spin system, causing the magnetization to move away from its equilibrium position are known as *excitation pulses*. Commonly used rf excitation pulses are identified by their flip angle as follows:

4.4.1 Variable-Flip Angle RF Excitation Pulse

In this case, the net magnetization is rotated through a pre-defined angle of less than 90° (often referred to as a *low flip angle*, often represented by the symbol α or assigned a specific value, for example, 30°). Only a proportion of the net magnetization is transferred from the z axis into the xy plane, with

some remaining along the z axis. While a *variable or low flip angle* rf pulse produces an intrinsically lower signal than the 90° excitation pulse described next, it can be repeated more rapidly as it always leave some of the magnetization along the z -axis. This excitation pulse is used to generate the signal in gradient echo pulse sequences (see Chap. 11) to control the amount of magnetization that is transferred between the z -axis and the xy plane for *fast imaging* applications (Fig. 4.2).

4.4.2 90° RF Excitation Pulse

The 90° rf excitation pulse delivers just enough energy to rotate the net magnetization through 90° . When the Net magnetization is at equilibrium, aligned along the z -axis, this

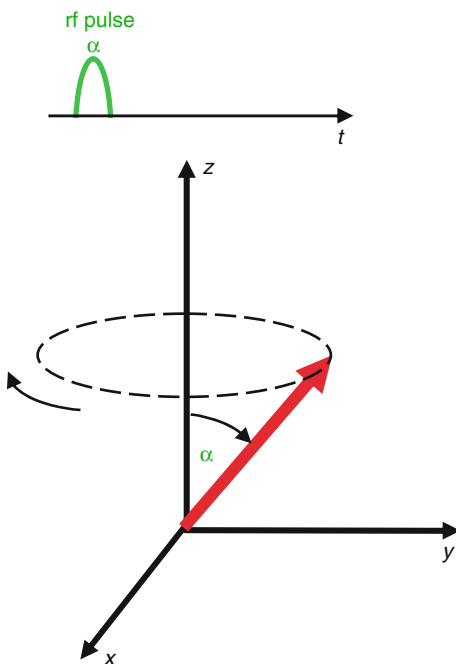


FIGURE 4.2. Variable flip angle (α) rf pulse.

transfers all of the net magnetization from the z -axis into the xy (transverse) plane. This leaves no magnetization along the z -axis immediately after the pulse and the system of protons is said to be *saturated*. The 90° rf pulse is sometimes referred to as a *saturation pulse*. When applied once, a 90° rf pulse produces the largest possible transverse magnetization and MR signal and therefore provides better image quality than an rf pulse with a lower flip angle. It cannot be repeated as rapidly, however, as the z -component of the magnetization needs time to recover. The 90° excitation pulse is used to initially generate the signal for spin echo-based pulse sequences (see Chap. 11) (Fig. 4.3).

The next most common rf pulse delivers enough energy to rotate the net magnetization through 180° . This is used in one of two ways:

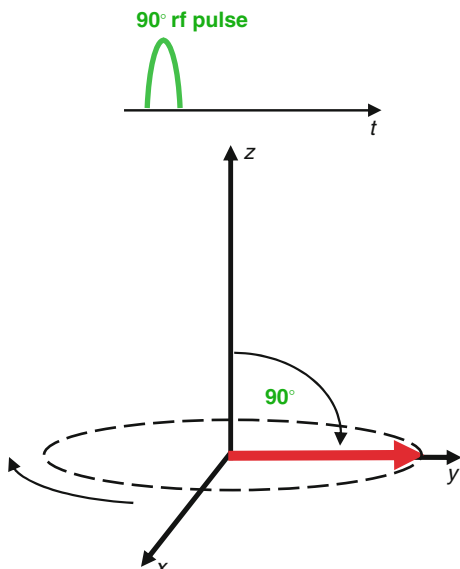


FIGURE 4.3. 90° rf pulse.

4.4.3 180° RF Pulse (Refocusing Pulse)

The 180° refocusing pulse is used in spin echo pulse sequences after the 90° excitation pulse, where the net magnetization has already been transferred into the x - y plane. It instantaneously swaps the direction of the magnetization in the x - y plane through 180° . This is used to reverse the loss of coherence caused by magnetic field inhomogeneities (see Sect. 5.2.2) (Fig. 4.4).

4.4.4 180° RF Pulse (Inversion Pulse)

The 180° inversion pulse is normally used when the net magnetization is at or close to equilibrium and will therefore rotate it from the positive to the negative z axis. It is known as an inversion pulse as it inverts the excess population of proton magnetic moments from being aligned to antialigned

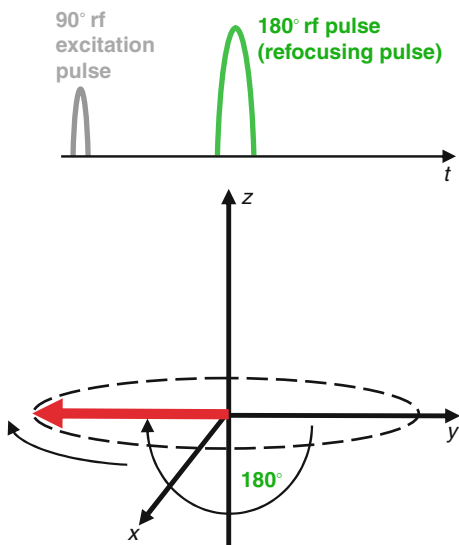


FIGURE 4.4. 180° rf refocusing pulse.

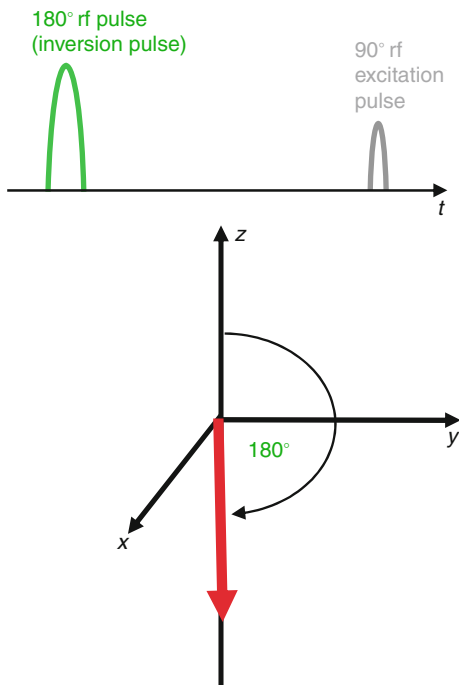


FIGURE 4.5. 180° rf inversion pulse.

with the magnetic field. Because the resultant magnetization lies only along the z axis, this pulse does not result in a detectable signal. It is used to prepare the z -magnetization in *inversion recovery* pulse sequences and in Black Blood preparation schemes (see Sects. 12.2 and 16.3). This type of pulse is therefore also often referred to as a magnetization preparation pulse (Fig. 4.5).

4.5 What Does the MRI Signal Look Like?

The simplest way of generating an MRI signal is to apply a 90° RF excitation pulse to a spin system at equilibrium. This rotates all of the net magnetization that is aligned long the

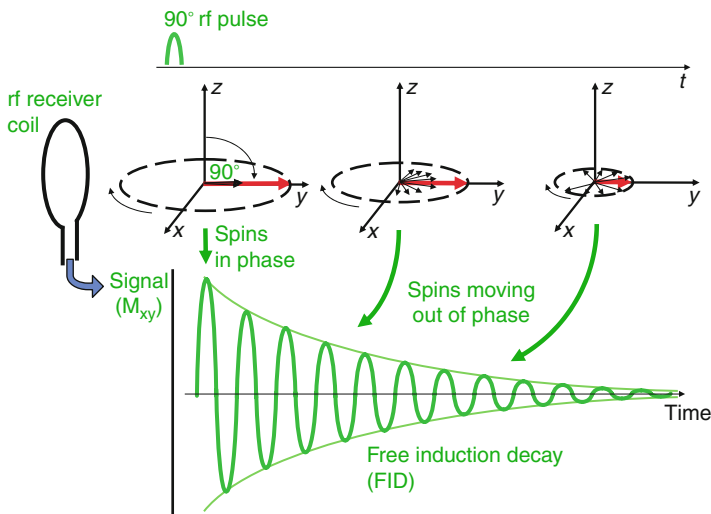


FIGURE 4.6. The net transverse magnetization (red arrow) generated by a 90° rf pulse generates an oscillating magnetic field as it rotates in the xy plane that can be detected by a rf receiver coil. Initially, the signal has a maximum amplitude as the population of proton magnetic moments (spins) is in phase. The amplitude of the signal detected decays as the proton magnetic moments move out of phase with one another (shown by the small *black arrows*). The resultant decaying signal is known as the free induction decay (FID).

z -axis into the x - y plane. The resulting rotating transverse component of magnetization produces an oscillating magnetic field that can be detected with a receiver coil (Fig. 4.6).

The signal that the receiver coil detects is seen as an oscillating magnetic field that gradually decays (known as a *Free Induction Decay or FID*). The reason for the decay can be understood by remembering that the net magnetization is the result of the sum of the magnetic moments (spins) of a whole population of protons. Immediately after the rf pulse, they rotate together in a coherent fashion, that is, as they rotate they point in the same direction within the xy plane. This angle of the direction they point at any instant is known as the phase angle and the spins are said at this initial stage to

be “in phase.” Over time, this coherence is gradually lost and the magnetic moments no longer rotate together. They are thus said to move “out of phase.” The net sum of the magnetic moments is thus reduced, resulting in a reduction in the measured net (transverse) magnetization which is observed as a decay of the signal strength.

Summary

- RF excitation pulses are used to generate an MR signal by flipping the net magnetization away from its equilibrium position along the z -axis.
- The flip angle of the RF pulse determines the angle that the net magnetization makes with the z -axis after the RF pulse.
- After excitation by the RF pulse, the net magnetization can be split into two components: One that remains along the z axis (longitudinal component) and one that rotates at the Larmor frequency around the z -axis in the xy plane (transverse component).
- The rotating transverse component generates an oscillating magnetic field that can be detected by a RF receiver coil as an MR signal.
- The freely decaying MR signal is known as a free induction decay (FID).

Chapter 5

Relaxation Times, Gradient Echoes, and Spin Echoes

5.1 Relaxation: What Happens After the RF Excitation Pulse?

Immediately after the rf pulse, the spin system starts to return back to its original state, that is, equilibrium. This process is known as *relaxation*. In fact, there are two distinct relaxation processes that relate to the two components of the net magnetization, the longitudinal (z) and transverse (xy) components. The first *longitudinal relaxation* process, commonly referred to as *T1 relaxation*, is responsible for the regrowth of the z component along the longitudinal (z) axis to its original value at equilibrium. This is explained in Sect. 5.1.1. The second *transverse relaxation* process is responsible for the decay of the xy component as it rotates about the z axis and hence the observed decay of the MR signal. There are two types of transverse relaxation, known as *T2 relaxation* and *T2* relaxation* and these are explained in Sects. 5.1.2–5.1.4. Longitudinal and transverse relaxation both occur at the same time; however, transverse relaxation is typically a much faster process in human tissue, that is, the signal decays away long before the spin system returns to equilibrium.

5.1.1 What is T1 Relaxation?

T1 relaxation describes the recovery of the z -component (M_z) of the magnetization following an rf pulse as the

population of protons returns to its equilibrium state. In the previous example of a 90° pulse (*saturation pulse*), the z -magnetization is *saturated* (reduced to zero) immediately after the pulse, but then returns along the z -axis toward its equilibrium value initially rapidly, slowing down as it approaches its equilibrium value. The return of the M_z component along the z axis is an exponential process with a time constant $T1$ (Fig. 5.1). The shorter the $T1$ time constant, the faster the relaxation process and the return to equilibrium.

Recovery of the z -magnetization after a 90° rf pulse is sometimes referred to as *saturation recovery*.

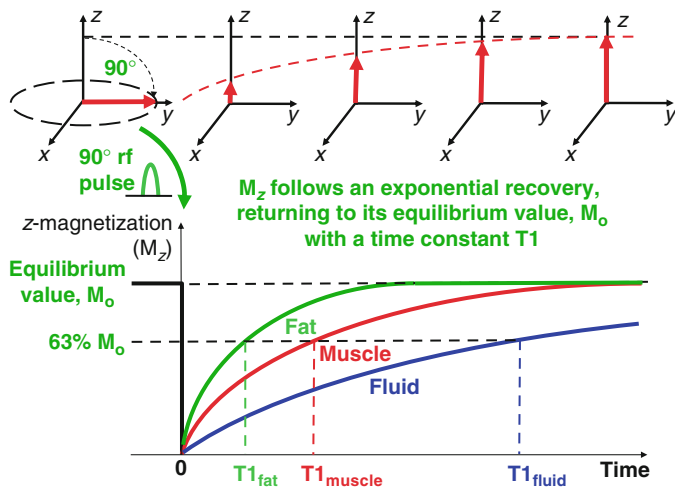


FIGURE 5.1. Following a 90° rf pulse, the z component of the net magnetization, M_z , is reduced to zero, but then recovers gradually back to its equilibrium value if no further pulses are applied. The recovery of M_z is an exponential process with a time constant $T1$. This is the time at which the magnetization has recovered to 63% of its original value. Different tissues have different $T1$ values. Fat has the shortest $T1$ value of all tissues (fat recovers the fastest), while fluid has the longest $T1$ value (fluid recovers the slowest).

What's the Significance of the T1 Value?

T1 relaxation involves the release of energy from the proton spin population as it returns to its equilibrium state. The rate of relaxation is related to rate at which energy is released to the surrounding molecular structure. This in turn is related to the size of the molecule that contains the hydrogen nuclei, and in particular, the rate of molecular motion, known as the tumbling rate of the particular molecule. As molecules tumble or rotate they give rise to a fluctuating magnetic field which is experienced by protons in adjacent molecules. When this fluctuating magnetic field is close to the Larmor frequency, energy exchange is encouraged. For example, lipid molecules are of a size that gives rise to a tumbling rate which is close to the Larmor frequency, and therefore, extremely favorable for energy exchange. Fat therefore has one of the fastest relaxation rates of all body tissues and therefore the shortest T1 relaxation time. Larger molecules have much slower tumbling rates that are unfavorable for energy exchange, giving rise to long relaxation times. For free water, its small molecules have much faster molecular tumbling rates which are also unfavorable for energy exchange and therefore it has a long T1 relaxation time. The tumbling rates of water molecules that are adjacent to large macromolecules can however be slowed down toward the Larmor frequency shortening the T1 value. Water-based tissues with a high macromolecular content (for example, muscle) tend to have shorter T1 values. Conversely, when the water content is increased, for example, by an inflammatory process, the T1 value also increases.

5.1.2 Transverse Relaxation and MRI Signal Decay

In Sect. 4.5 we saw that the decay of the MR signal (or Free Induction Decay) is due to a loss of coherence as the magnetic moments (spins) of proton population move out of phase. The causes of this loss of coherence are twofold:

1. The presence of interactions between neighboring protons.
2. Local variations (inhomogeneities) in the applied magnetic field.

The transverse relaxation caused by (1) alone is known as T_2 relaxation. The transverse relaxation actually observed in an FID is the combination of (1) and (2) and is known as T_2^* relaxation.

5.1.3 What is T_2 Relaxation?

The rate of precession for an individual proton depends on the applied magnetic field. It is however possible for the magnetic moment of one proton to slightly modify the magnetic field of a neighboring proton (Fig. 5.2). As the protons are

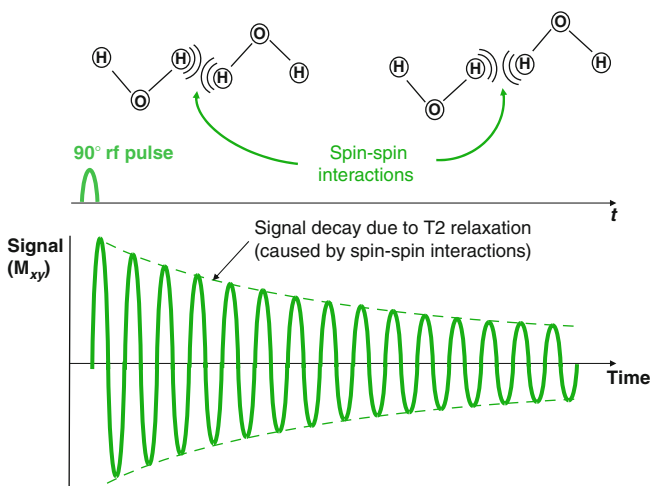


FIGURE 5.2. The FID signal decays due to spin-spin interactions. This is where the magnetic moment of one proton moves transiently adjacent to another proton, slightly modifying the local magnetic field of its neighbor and therefore causing the Larmor frequency to briefly alter. This in turn leads to a loss of phase coherence (dephasing). Due to the random nature of molecular motion, this process is irreversible.

constituents of atoms within molecules, they are moving rapidly and randomly, and so, such effects are transient and random. The net effect is for the Larmor frequency of the individual protons to fluctuate in a random fashion, leading to a loss of coherence across the population of protons. That is, the spins gradually acquire different phase angles, pointing in different directions to one another and are said to move out of phase with one another (this is often referred to as *dephasing*).

The resultant decay of the transverse component of the magnetization (M_{xy}) has an exponential form with a time constant, T_2 , hence this contribution to transverse relaxation is known as *T₂ relaxation*. As it is caused by interactions between neighboring proton spins, it is also known as *spin-spin relaxation*. Due to the random nature of the spin-spin interactions, T_2 relaxation is irreversible.

What's the Significance of T₂ Value?

T_2 relaxation is related to the amount of spin-spin interaction that takes place. Free water are small molecules that are relatively far apart and moving rapidly, and therefore, spin-spin interactions are less frequent and T_2 relaxation is slow (leading to long T_2 relaxation times). Water molecules bound to large molecules are slowed down and more likely interact, leading to faster T_2 relaxation and shorter T_2 relaxation times. Water-based tissues with a high macromolecular content (for example, muscle) tend to have shorter T_2 values. Conversely, when the water content is increased, for example, by an inflammatory process, the T_2 value also increases.

5.1.4 What is T_{2^*} Relaxation?

The second cause for the loss of coherence (dephasing) relates to nonuniformities in the applied magnetic field, B_o . If this field varies with position, then, so does the Larmor

frequency (Fig. 5.3). Protons at different spatial locations will therefore rotate at different rates, causing further dephasing and the signal to decay more rapidly. In this case, as the cause of the variation in Larmor frequency is fixed, the resultant dephasing is potentially reversible.

The combined effect of T_2 relaxation and the effect of magnetic field nonuniformities is referred to as T_{2^*} relaxation and this determines the actual rate of decay observed when measuring an FID signal.

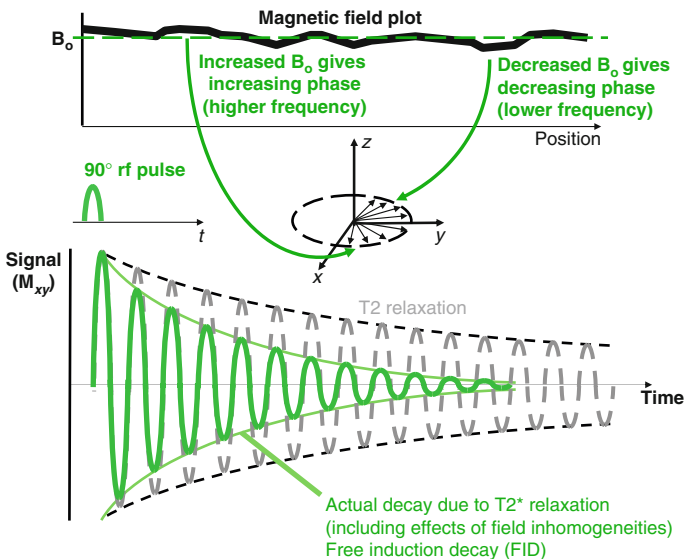


FIGURE 5.3. A further cause of loss of phase coherence is that the applied magnetic field, B_0 is not uniform. While the nominal magnetic field value is assumed to be uniform (shown by the dotted green line) the actual field value is variable. Where the magnetic field is decreased, the Larmor frequency is decreased and the relative phase of the proton magnetic moments decreases over time relative to the proton magnetic moments at the nominal Larmor frequency. Where the field is increased in value, this results in an increasing phase. This causes additional dephasing and accounts for the more rapid decay of the FID signal, known as T_{2^*} decay.

5.2 MR Echoes

While the FID can be detected as a MR signal, for MR imaging, it is more common to generate and measure the MR signal in the form of an echo. This is because the magnetic field gradients that are used to localize and encode the MR signals in space (as we shall see in Chap. 6) cause additional dephasing which disrupts the FID. The two most common types of echo used for MR imaging are *gradient echoes* and *spin echoes*. The following sections describe how these echoes are generated.

5.2.1 Gradient Echoes

Magnetic field gradients are used to produce a change in field strength and hence a corresponding change in Larmor frequency along a particular direction. When a magnetic field gradient is switched on, it causes proton spins to lose coherence or dephase rapidly along the direction of the gradient as they precess at different frequencies (Fig. 5.4). This dephasing causes the amplitude of the FID signal to rapidly drop to zero.

The amount of dephasing caused by one magnetic field gradient can however be reversed by applying a second magnetic field gradient along the same direction with equal amplitude but with the opposite slope (Fig. 5.5). If the second gradient is applied for the same amount of time as the first gradient, the dephasing caused by the first gradient is cancelled and the FID reappears. It reaches a maximum amplitude at the point at which the spins dephased by the first gradient have moved back into phase or “rephased” (ignoring any effects of T2* relaxation).

If the second gradient then continues to be applied, the FID signal dephases and disappears once more (Fig. 5.6). The signal that reappears (rephases) through the switching of the gradient direction is known as a *gradient echo*.

The time from the point at which the transverse magnetization (the FID) is generated by the RF pulse, to the point at

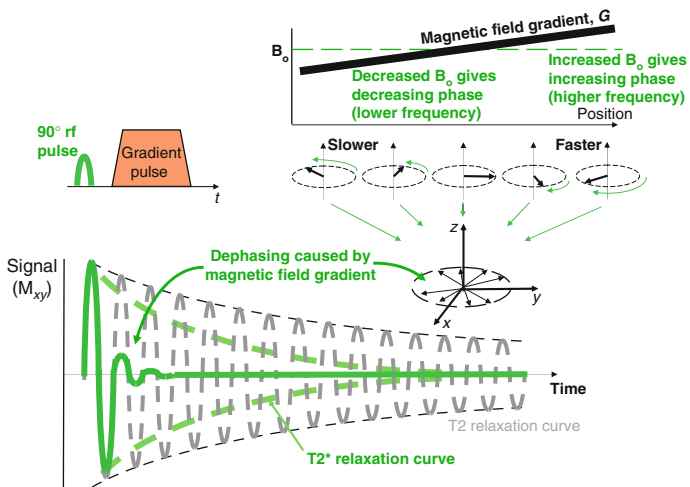


FIGURE 5.4. This shows how the application of a magnetic field gradient causes loss of detectable MRI signal. The range of frequencies along the direction of the gradient causes the spins to rapidly dephase, resulting in a rapid reduction of the transverse magnetization.

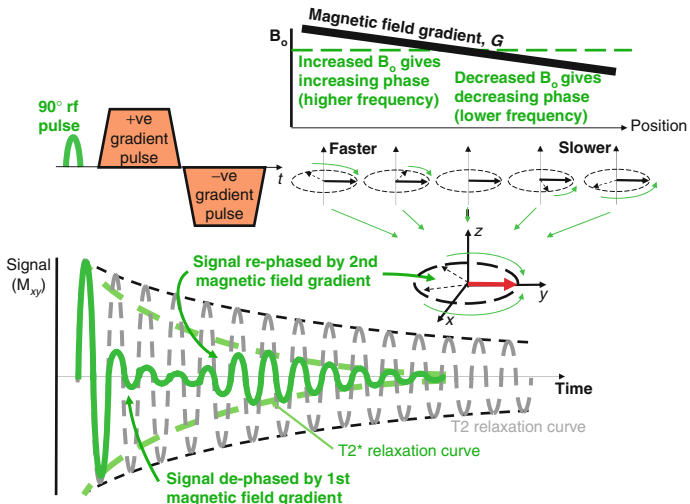


FIGURE 5.5. This shows how the application of a second magnetic field gradient reverses the dephasing caused by the first gradient pulse, resulting in recovery of the FID signal.

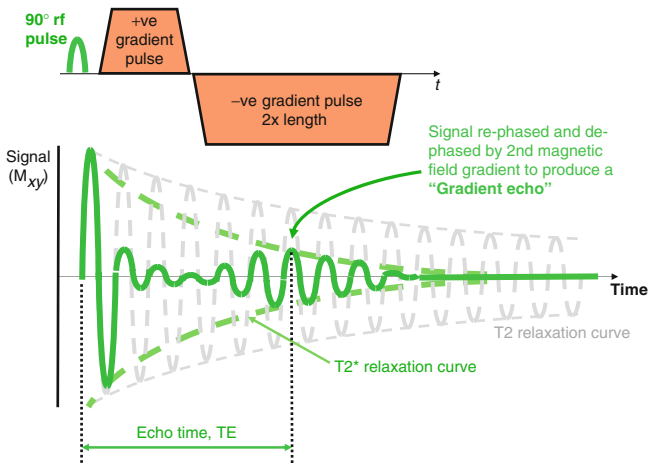


FIGURE 5.6. Extension of the time duration of the second gradient to twice that of the first gradient causes the FID to first rephase and then dephase. The resultant transient signal is known as a gradient echo. The maximum amplitude of the echo depends on the $T2^*$ relaxation rate and the echo time TE.

which the gradient echo reaches its maximum amplitude is known as the *Echo Time* (abbreviated as *TE*). If the echo time is chosen to be longer, more natural $T2^*$ dephasing occurs and the maximum echo amplitude becomes smaller. In practice, the *TE* is set by the MR system operator (in milliseconds) as it determines, amongst other things, the influence of $T2^*$ on the image contrast.

5.2.2 Spin Echoes

In Sect. 5.1 we learned that while the dephasing caused by $T2$ relaxation was a random, irreversible process, the additional dephasing caused by the presence of magnetic field nonuniformities was potentially reversible. At a certain time after the initial generation of the FID signal, a proportion of the relative phase change for each proton spin will be related to the local value of the applied magnetic field. The application of a 180° refocusing pulse rotates the spins

through 180° , effectively changing the sign of the relative phase change within the xy plane (Fig. 5.7). Where the previous relative phase change was positive due to a locally increased field, the 180° pulse causes it to become negative and vice versa. As the local field variations remain fixed, the spins still continue to have the same Larmor frequency, and so a spin in an increased field continues to gain in phase, while a spin in a decrease field continues to lose phase. Because the sign of their phase shifts has been swapped halfway through by the 180° refocusing pulse, the spins all come back into phase causing the FID to increase in amplitude, reaching a maximum at the echo time, TE. For the spin dephasing caused by the field nonuniformities to be completely reversed at time TE, the 180° pulse must be applied at time $TE/2$. The signal that appears (rephases) through the

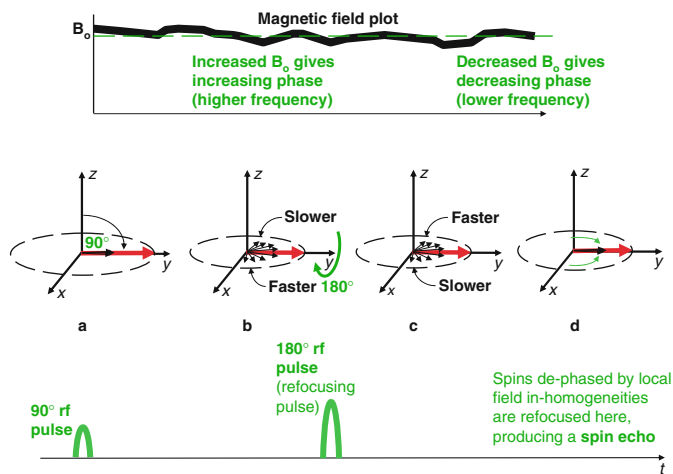


FIGURE 5.7. The presence of magnetic field inhomogeneities causes the proton magnetic moments to dephase (a–b). The application of a 180° rf pulse causes an instantaneous change in sign of the phase shifts by rotating the spins about the y axis (b–c). The proton magnetic moments then move back into phase, reversing the dephasing effect of the magnetic field inhomogeneities (c–d).

application of the 180° rf refocusing pulse is known as a *spin echo* (Fig. 5.8). After reaching a maximum amplitude at time TE, the signal again dephases due to the $T2^*$ relaxation process.

For the purposes of imaging, a magnetic field gradient is also applied during both the dephasing period and during the measurement of the spin echo (Fig. 5.9). In general, because of the 180° refocusing pulse, the amplitude of the spin echo signal is greater than the gradient echo signal. Spin echo images are therefore generally of higher image quality. Imaging based on spin echo is also less affected by the presence of field inhomogeneities caused by metallic artifacts (for example, sternal wires or metallic heart valves – see also Sect. 17.8). Gradient echo imaging is however more affected by the presence of magnetic field inhomogeneities caused by iron and so can be useful, for example, in the assessment of patients with increased iron deposition within the heart and liver.

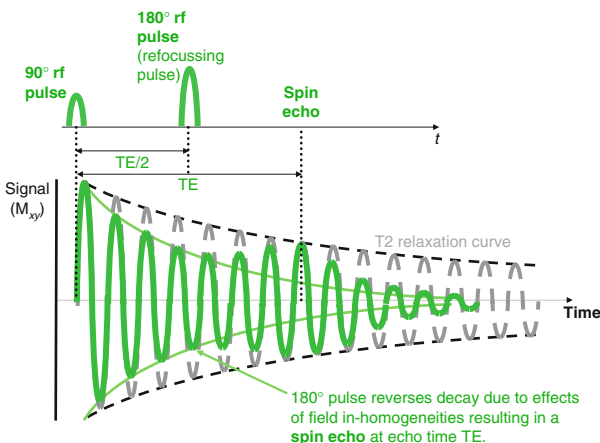


FIGURE 5.8. The MRI signal that is refocused by the 180° pulse is known as a spin echo. To produce an echo at time TE, the 180° pulse is applied at time $TE/2$.

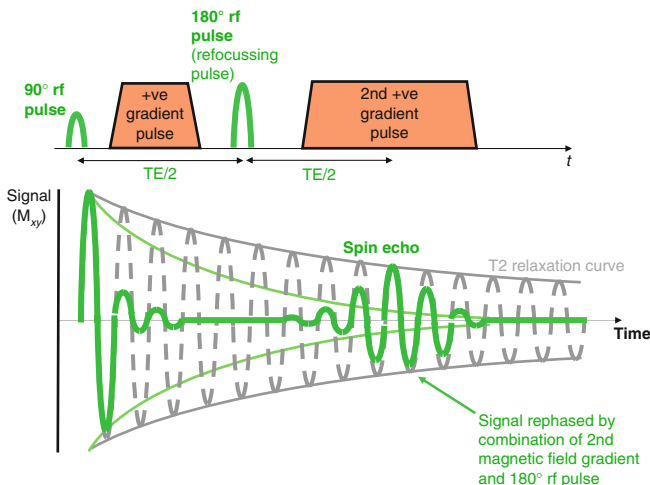


FIGURE 5.9. In addition to the effect of the 180° refocusing pulse, gradients are applied to dephase and rephase the signal for imaging purposes (see Chap. 6). Note that the second gradient has the same sign as the first as the 180° pulse also changes the sign of the phase shifts caused by the first gradient.

Summary

- Following rf excitation, two relaxation processes occur as the spin system gradually returns back to its equilibrium state.
- As the spin system releases its energy, the longitudinal component returns to its equilibrium value through longitudinal relaxation. This is an exponential process with time constant, T1 (also known as T1 relaxation).
- The rotating transverse component decays more rapidly than that due to transverse relaxation. This is also an exponential process and has two causes:
 - Loss of coherence of the rotating proton spins due to the interaction of neighboring magnetic moments (spin-spin interactions). This has a time constant, T2 and is known as T2 relaxation.
 - Loss of coherence between rotating spins due to magnetic field inhomogeneity. This together with T2 relaxation leads to a more rapid decay with a combined time constant, T2*.
- In practice, the FID signal is disrupted by the presence of the magnetic field gradients used to generate images.
- Instead, signal echoes are generated and used for the formation of images.
- Gradient echoes are generated by switching the direction of a gradient to first dephase, then rephase the MR signal.
- Spin echoes are generated by applying a 180° rf refocusing pulse to reverse the decay caused by magnetic field inhomogeneities.
- The time from the rf pulse to the maximum amplitude of the echo is known as the echo time, TE.

Chapter 6

Making an Image: Locating and Encoding Signals in Space

Single MR echoes produced by rf pulses alone cannot be used to produce an image as they do not contain any information about position. This information is introduced by using the gradient coils described in Sect. 1.2 to generate magnetic field gradients. When a gradient is applied in a particular direction, this causes the strength of the magnetic field and hence, the Larmor frequency to depend on position along that direction. MR echoes that are generated and measured in the presence of magnetic field gradients therefore contain spatial information that can be used to build up an image. The sections that follow describe the most commonly used method to build up a cross-sectional image (or image slice) using rf pulses and gradient magnetic fields.

6.1 Selecting an Image Slice

First, the resonance of protons is confined to a slice of tissue. This is done by applying a gradient magnetic field at the same time as the rf excitation pulse (Fig. 6.1). The frequency of the rf pulse corresponds to the Larmor frequency at a chosen point along the direction of the applied gradient. The result is for resonance only to occur for protons in a plane that cuts through that point at right angles to the gradient direction, effectively defining a slice of tissue. This process is known as *slice selection* and the gradient is known as the

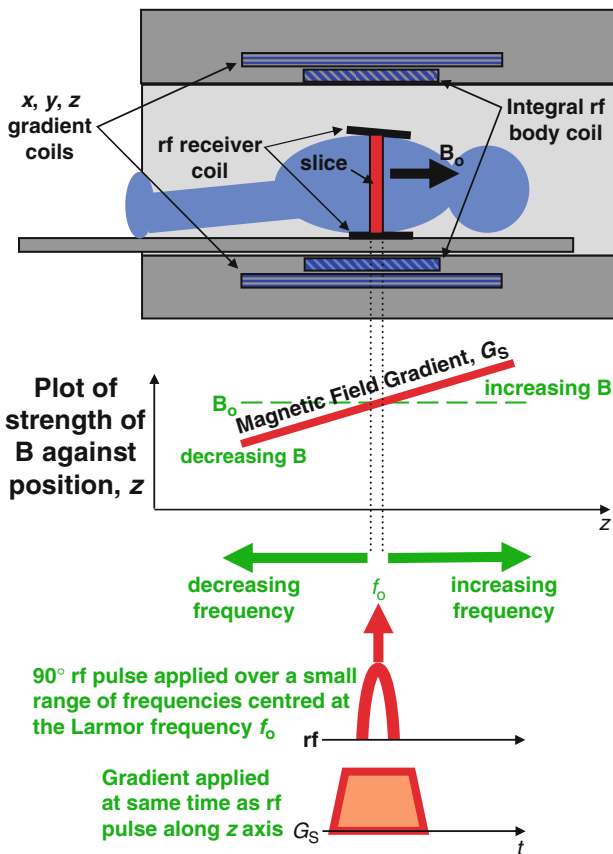


FIGURE 6.1. Slice selection is achieved by applying a magnetic field gradient for the duration of the rf excitation pulse. The gradient causes the Larmor frequency to be dependent on location along the gradient (in this example in the z direction). Resonance only occurs where the Larmor frequency matches the frequency of the RF pulse, defining a plane (slice) of tissue perpendicular to the z axis. The RF pulse has a small range of frequencies, thus causing resonance over a small range of locations, defining the thickness of the slice.

slice selection gradient, G_s . The orientation of the slice is determined by the direction of the applied gradient known as the *slice selection direction* (in the example of Fig. 6.1 this is the z -direction).

Rather than just a single frequency, the rf pulse is comprised of a small range of frequencies, known as the *bandwidth* of the rf pulse. This gives the slice a thickness. The thickness of the slice is determined by the combination of the rf pulse bandwidth and the steepness (or strength) of the gradient.

6.2 Encoding the MR Signal Within the Slice

Once the slice selection process has created resonance within the slice of tissue, two further gradients are applied in sequence, this time within the plane of the image slice but at right angles to each other. The first of these two gradients is known as the *phase encoding gradient, G_p* , while the second is known as the *frequency encoding gradient, G_F* . Each of these gradients causes the protons to rotate at different frequencies according to their relative position along each gradient. Where the gradient increases the magnetic field, the protons acquire a higher frequency of precession, while where the gradient decreases the magnetic field, the protons acquire a lower frequency of precession. The protons are therefore also constantly changing their relative phase according to their position along the gradient. One consequence of this is that the magnetic field gradients cause de-phasing in the direction along which the gradient is applied.

6.3 Phase Encoding

The *phase encoding gradient, G_p* , is applied only for a specified time, such that when it is switched off, the protons will have changed their relative phase by a prescribed amount depending on their position along the gradient (Fig. 6.2). This

process is known as *phase encoding* and the direction of the applied gradient is known as the *phase encoding direction*. In the example in Fig. 6.2, the phase encoding direction is along the y axis. This example also shows the effect of a phase encoding gradient with a particular amplitude and duration, such that the protons at the edges of a predefined field of

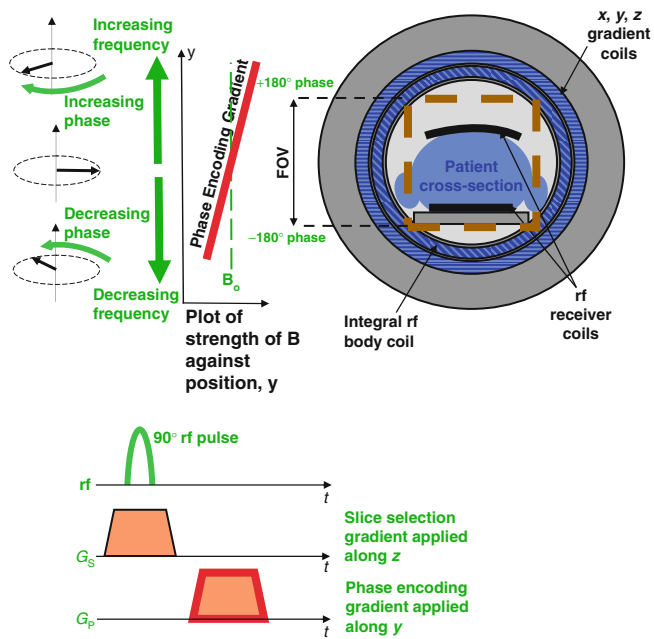


FIGURE 6.2. Phase encoding is achieved by applying a gradient magnetic field (known as the phase encoding gradient, G_p), in a direction along the selected image plane (in this case the phase encoding direction is along the y direction). The amplitude (steepness) and duration of the gradient are chosen to cause a range of phase shifts of the proton magnetic moments dependent on their position along the gradient. In this example the edges of a predefined field of view have acquired phase shifts of $+180^\circ$ and -180° relative to the center of the field of view.

view have acquired a phase change of $+180^\circ$ and -180° relative to the center of the field of view.

6.4 Frequency Encoding

The *frequency encoding gradient*, G_F , is applied for longer, and at the same time the signal is measured or digitally sampled (Fig. 6.3). The signal is comprised of a range of frequencies (or bandwidth), corresponding to the Larmor frequencies of the proton magnetic moments at their different locations along the gradient (Fig. 6.4). This process is known as *frequency encoding*, the direction of the frequency encoding gradient defines the *frequency encoding direction*.

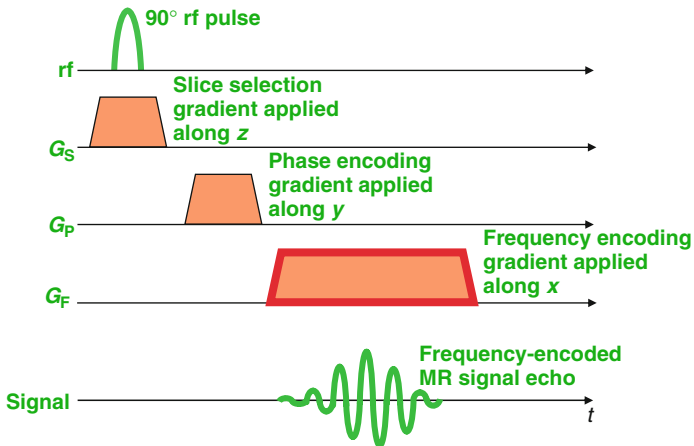


FIGURE 6.3. Following the phase encoding gradient, the frequency encoding gradient, G_F , is also applied in the plane of the selected slice but perpendicular to the phase encoding direction. The MR signal echo is measured during this period.

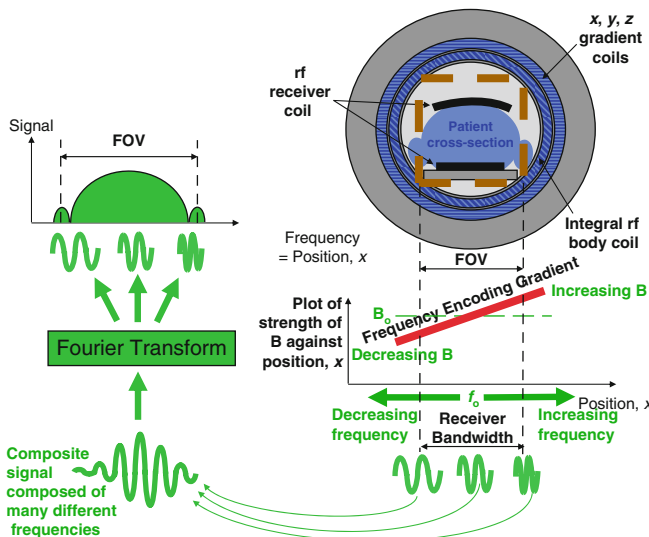


FIGURE 6.4. The frequency encoding gradient changes the Larmor frequency according to position along its direction. The detected MR signal from a subject that extends in that direction is therefore comprised of many different frequencies. This signal is analyzed by a Fourier transform to determine the contribution of each of the frequency components, each corresponding to a unique location along the frequency encoding gradient. The field of view is predefined and matched to a specific range of frequencies (the receiver bandwidth).

In summary, to localize the MR signal in three dimensions, three separate magnetic field gradients are applied.

The example in Figs. 6.1–6.4 these gradients are applied in sequence as follows:

Slice-section gradient, G_s applied along the z -axis

Phase-encoding gradient, G_p applied along the y -axis

Frequency-encoding Gradient, G_f applied along the x -axis

This defines a slice perpendicular to the z axis, that is, a slice oriented in the transaxial plane. Other slice orientations can easily be obtained by re-assigning each of the gradients to a different axis as shown in Table 6.1. Note that for each orientation there are two possible combinations for the phase and frequency encoding directions with the second combination shown in parentheses. The choice of phase encoding direction is important as it influences the direction in which motion artifacts appear across the image.

It is also possible to obtain an angled slice by simply combining gradients along two or more axes to perform each of the localization tasks. *The ability to define an arbitrary slice orientation is a key strength of magnetic resonance imaging.*

TABLE 6.1. Assignment of the slice selection, phase encoding, and frequency encoding functions to the appropriate magnetic field gradient axes allows the arbitrary definition of the image slice orientation.

	Slice selection, G_s	Phase encoding, G_p	Frequency encoding, G_f
Transaxial	z	y (or x)	x (or y)
Coronal	y	x (or z)	z (or x)
Sagittal	x	y (or z)	z (or y)

6.5 How is the Frequency-Encoded Signal Decoded?

The frequency encoded signal is analyzed using a *Fourier transform*. This is a mathematical tool that transforms the time-dependent MR signal into its different frequency

components. The amplitude of each frequency component can be mapped onto a location along the *frequency encoding gradient* to determine the relative signal at each location. A *field of view* is also predefined in this direction, and the range of frequencies across this field of view is directly related to the frequency at which the signal is digitally sampled, known as the *receiver bandwidth*.

The field of view in the frequency encoding direction is defined by the operator in millimeters or centimeters. This, in combination with the choice of receiver bandwidth, determines the amplitude (or slope) required for the frequency encoding gradient (Fig. 6.4).

Before the signal is digitally sampled it commonly undergoes a process known as *demodulation* (Fig. 6.5). This process removes the high frequency content but preserves the range of frequencies, so that they are centered around zero Hertz, rather than the Larmor frequency. This makes the sampling process simpler. (It is easier to digitally sample a signal in the kHz range than a signal in the MHz range although some MR systems now directly sample the high frequency signal).

The choice of receiver bandwidth also determines the rate (or frequency) at which the MR signal is digitally sampled as it is measured. A rule, known as Nyquist's theorem states that in order to faithfully detect a signal, it must be sampled at a frequency that is twice the maximum frequency contained within the signal. So if the signal contains the frequency range $\pm\Delta f$, then it must be sampled at a frequency $2\Delta f$.

If the sampling frequency is set at this value, signals with frequencies outside the range $\pm\Delta f$, (from outside the defined field of view) are not properly detected. In fact they appear to have the same frequency as a signal from a point within the defined field of view. If it is not dealt with, this would cause an artifact known as image aliasing, seen as “wrap around” or “folding-in” of features from outside the field of view into the image. In practice this is easily removed in the frequency encoding direction (see Sect. 17.1).

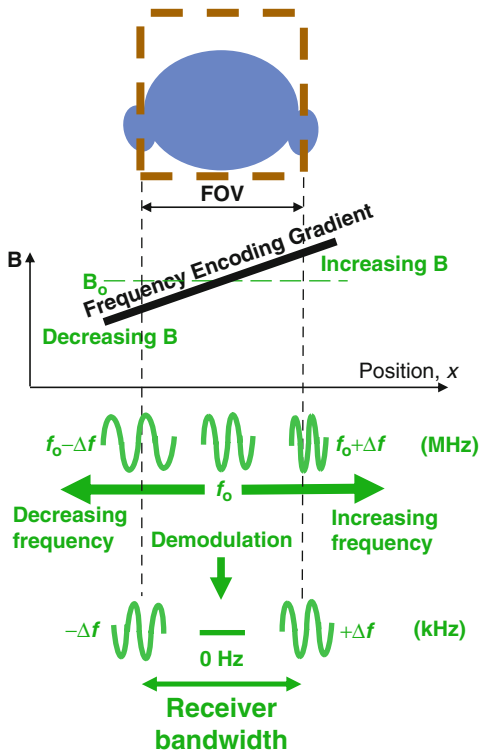


FIGURE 6.5. The field of view (fov) in the frequency encoding direction is determined by the slope of the frequency encoding gradient and the selected receiver bandwidth. The MR signal originating from within this fov contains frequencies in the range $\pm\Delta f$ (the receiver bandwidth) centered on the Larmor frequency, f_o . Before the signal is digitally sampled, it is demodulated, removing the high frequency content. The result is a signal with the same range of frequencies (same bandwidth) but centered around zero Hertz.

6.6 How do we make sure that the Gradients we apply for Imaging don't Destroy the signal?

Pulse sequences must be designed to provide the maximum possible signal at the center of the MR signal echo. This requires that any de-phasing caused by one of the imaging gradients must be reversed by another gradient along the same direction, but with opposite slope, so that the proton magnetic moments are brought back into phase. This is particularly important in the slice selection and frequency encoding gradient directions. The frequency encoding gradient is normally preceded by a de-phasing gradient (Fig. 6.6)

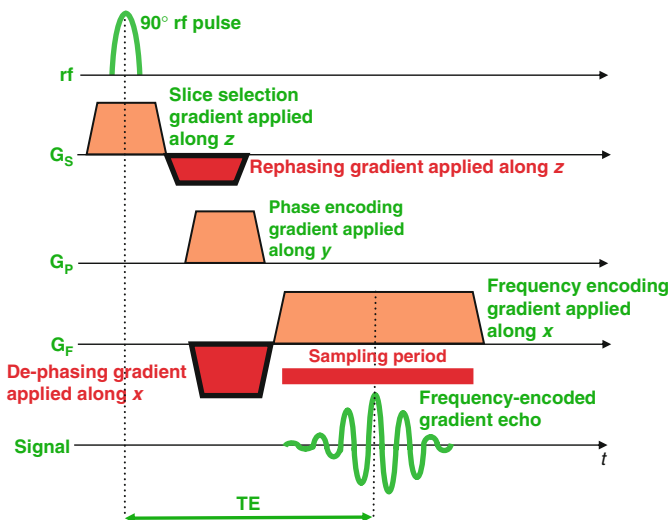


FIGURE 6.6. Additional gradient pulses are required both immediately after the slice selection gradient and immediately before the frequency encoding gradient (shown in red). These additional pulses ensure that any de-phasing of the transverse magnetization caused by the imaging gradients is cancelled once the echo time, TE, is reached. This results in the echo having its maximum possible signal at this point.

so that when the frequency encoding gradient is applied, the de-phasing is reversed by the first half of the frequency encoding gradient and the signal echo reaches its maximum amplitude at the center of the sampling period, (see Sect. 5.2.1 on “Gradient Echo”). For the same reason, the slice selection gradient is followed by a re-phasing gradient. This ensures that de-phasing that occurs along the slice selection gradient is reversed. The re-phasing gradient is only half the length of the slice selection gradient since the transverse magnetization is only generated halfway through the applied rf pulse. De-phasing therefore only occurs during the second half of the slice selection gradient.

6.7 Why isn't a Single Phase and Frequency Encoded Signal enough to Reconstruct an Image?

While analysis of this signal by the Fourier Transform provides the frequency content of the signal, the phase changes imparted by the phase encoding gradient cannot be decoded by a similar process. The Fourier Transform can only analyze a signal that changes over time. To enable this, a number of signal echoes must be generated and measured by repeating the above process (slice selection, phase encoding, and frequency encoding), each time applying the same slice selection and frequency encoding gradient, but a different amount of phase encoding so that the resulting changes in phase over time can be analyzed in a similar way (Fig. 6.7). In practice, the strength (or slope) of the phase encoding gradient is increased for each repetition in equal increments. The time interval between each repetition is known as the *Repetition Time, TR*. TR is another important parameter that can be set by the operator in milliseconds. As we will see in later sections it not only determines how fast MR images can be acquired (see Chap. 8), but also affects the image contrast (see Chap. 10).

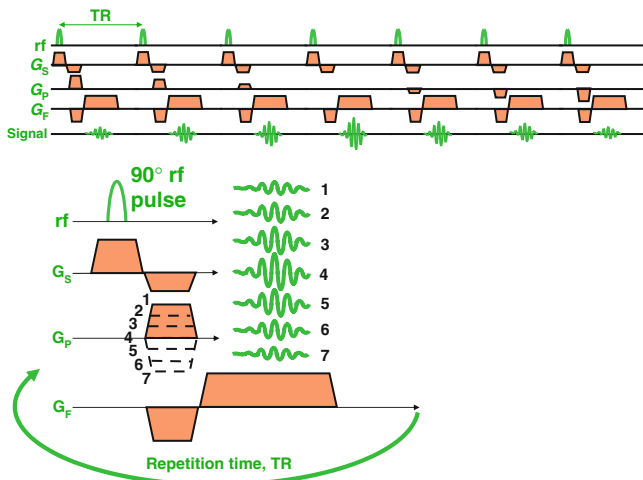


FIGURE 6.7. To fulfill the phase encoding process, the pulse sequence must be repeated a number of times, with a different amplitude (slope) of phase encoding gradient being applied each time. In this example, seven values of phase encoding gradient slope are used (shown by the dotted lines), causing different amounts of change in phase according to position along the direction of the gradient. Note that as the strength of the phase encoding gradient increases, this increases the amount of de-phasing along the gradient. When the strength (or slope) of the phase encoding gradient is zero (step 4), there is no de-phasing and the signal has its maximum possible amplitude.

6.8 Field of View in the Phase Encoding Direction

The amount that signal phase changes with each phase encoding step, increases with distance from the center of the phase encoding gradient (Fig. 6.8). The edge of the field of view in the phase encoding direction is defined to be where the phase changes by 180° with each phase encoding step. Thus the phase of protons located at one extreme edge of the field of view will change in steps of $+180^\circ$ relative to those at the center, while the phase of those protons located at the

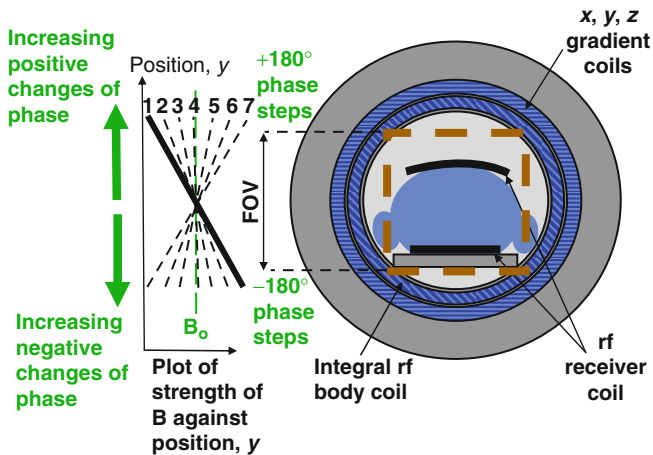


FIGURE 6.8. The phase of the proton magnetic moments at a given location changes with each phase encoding step according to their position along the phase encoding gradient. The field of view in this direction is defined such that the signal generated by proton magnetic moments at its edges have phase changes of $\pm 180^\circ$ relative to that generated at the center of the field of view.

opposite edge of the field of view will change in steps of -180° relative to those at the center. Protons located outside this field of view in the phase encoding direction appear to have the same behavior as a point located within the field of view. This causes image aliasing (see Sect. 17.1).

6.9 Phase Encoding, Image Matrix, and Acquisition Time

For each repetition, and therefore, phase encoding step, the signal echo is measured and stored as an array of numbers or matrix (Fig. 6.9). Once all the signals for a prescribed number of phase encoding steps have been acquired, they are analyzed together as a group by a two-dimensional (2D) Fourier Transform in order to decode both the frequency and the phase information. The number of pixels calculated by this process in the phase encoding direction is determined by the

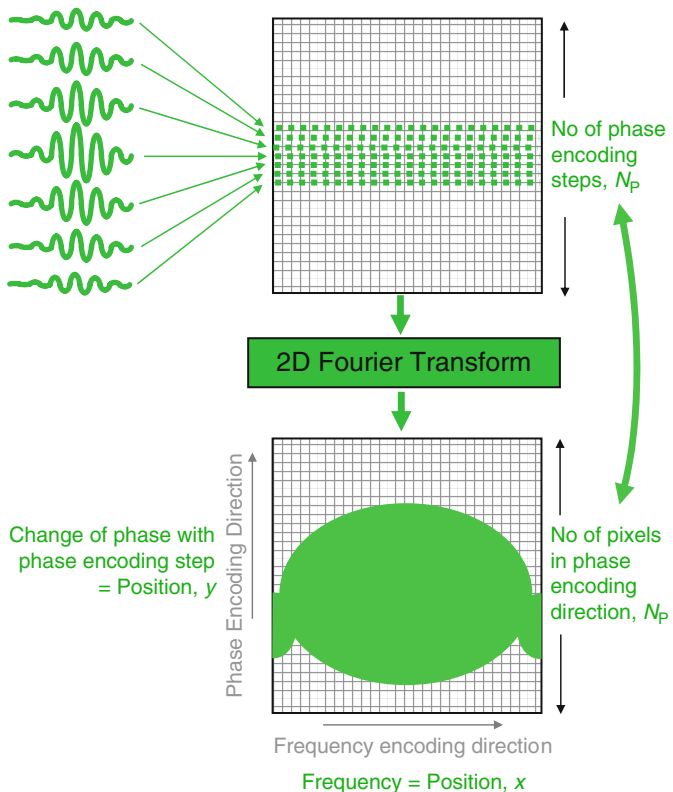


FIGURE 6.9. The MR signals derived from each phase encoding step are stored in a matrix. Two dimensional Fourier transformation of this matrix results in the reconstruction of the image. The number of phase encoding steps determines the number of pixels in the image along the phase encoding direction. The location of MR signal contributions along the frequency encoding direction (x) is related to their frequency, while their location along the phase encoding direction (y) is related to their change in phase with each phase encoding step.

number of phase encoding steps used. The spatial resolution of the reconstructed image, therefore, depends on the number of phase encoding steps, and is hence often limited by the image acquisition time (see box).

Number of pixels in phase = Number of phase encoding steps
encoding direction, N_p

Image acquisition time = $TR \times N_p$

If a greater spatial resolution is required in the phase encoding direction (for a fixed field of view), the number of acquired pixels N_p (acquired image matrix size) must be increased and so must the number of phase encoding steps. This requires a greater number of repetitions, and therefore a longer image acquisition time.

Summary

- The MR signal is localized in three dimensions by using the three magnetic field gradient coils to superimpose three magnetic field gradients in sequence onto the static magnetic field in three different directions.
- Each gradient field varies the magnetic field, and therefore the Larmor frequency, along the direction in which it is applied.
- The slice selection gradient is applied at the same time as the rf pulse, causing resonance in a slice of tissue at right angles to the gradient direction.
- The phase encoding gradient encodes the phase of the signal according to position along its direction.
- The frequency encoding gradient encodes the frequency of the signal according to position along its direction.
- The sequence of slice selection, phase encoding, and frequency encoding is repeated many times, with a repetition interval, TR, each time with a different amount of phase encoding (known as a phase encoding step).
- The MR image is reconstructed using an algorithm, known as a two-dimensional (2D) Fourier transform.
- This is applied to the resultant signals to decode the contributions from different locations based on their frequency and the change in phase with each phase encoding step.

Chapter 7

Image Space and k-Space

The way that the MR signals are generated and encoded by the use of magnetic field gradients gives rise to a particular relationship between the data points in the signal and those in the image. A single data point in an MR signal contributes a particular attribute to the whole image. Conversely, a single pixel in the image may have contributions from all of the MR signals collected. Just as each pixel occupies a unique location in image space, each point of an MR signal echo belongs to a particular location in a related space known as *k*-space (Fig. 7.1).

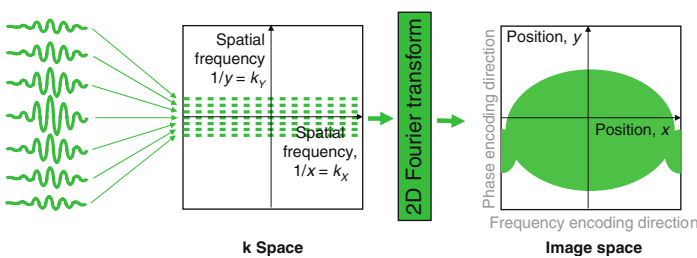


FIGURE 7.1. k-space is related to the image space by the Fourier transform. The coordinates of image space are the spatial coordinates x and y . The Coordinates of k-space are the spatial frequencies $k_x = 1/x$ and $k_y = 1/y$. The sampled data points from the MR signals therefore contribute different spatial frequencies to the image.

There is an inverse relationship between the image space and k-space. Whereas the coordinates of the image are spatial position (x, y), the coordinates of k-space are $1/x$ and $1/y$, sometimes referred to as *spatial frequencies*. The value of each point in k-space therefore relates to how much of a particular spatial frequency is contained within the image.

A spatial frequency is difficult to picture. An image consisting of a single spatial frequency looks like a wave propagating across the image with bright and dark peaks and troughs (Fig. 7.2). A *low spatial frequency* (arising from a point near the center of k space) has peaks and troughs far apart and thus contributes mostly the signal content and contrast of the image. A *high spatial frequency* (arising from a point near the edge of k-space) has peaks and troughs close

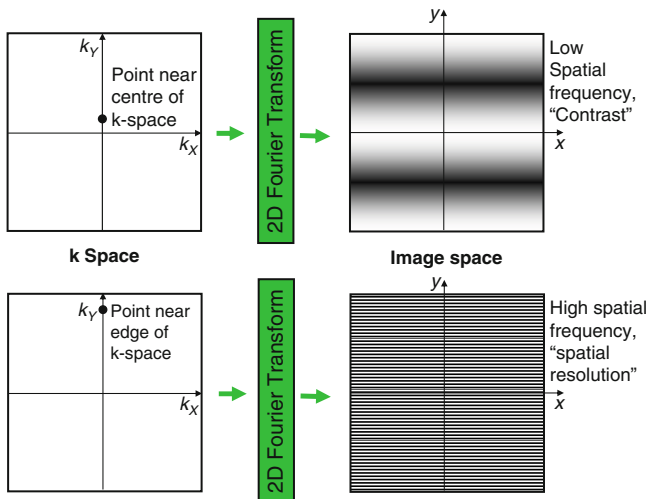


FIGURE 7.2. A single spatial frequency (single point in k-space) can be represented as a wave in image space. A point close to the center of k-space contributes a low spatial frequency, represented by a wave with broad peaks and troughs. This provides the signal content for large regions of uniform signal in the image. A point at the edge of k-space contributes a high spatial frequency and is represented by a fine “toothcomb” wave. The highest spatial frequency content defines the spatial resolution of the image.

together and thus contributes fine detail or edges, effectively defining the *spatial resolution* of the image.

The location of a particular signal data point in k-space depends on the strength and duration of each gradient that has been applied from the time when the transverse magnetization was first generated by the rf excitation pulse to when that particular point was measured. If no gradients are applied (or if the sum of the areas of the positive and negative gradients applied up to that point, when added together, completely cancel out) then the point collected is at the center of k-space. As no gradients are applied, there is no de-phasing and the signal therefore has a high amplitude and contributes mainly signal content to the image.

As gradients are applied, they move the signal data point away from the center of k-space. The stronger the gradients are and the longer they are applied for, the further from the center of k space they move the data point. The phase encoding gradient moves the data points along k_y , the frequency encoding gradient along k_x . At the same time, the gradient de-phases the signal and so the amplitude of the signal decreases away from the center of k-space.

To make an image that is a totally faithful representation of the imaged subject, it is important that the whole range of spatial frequencies is acquired (up to a maximum that defines the spatial resolution of the image), that is, that the whole of k-space is covered. For standard imaging this is done by filling k-space with equally spaced parallel lines of signal data, line by line, along the k_x direction. This is known as a *Cartesian acquisition* (Fig. 7.3).

As the data points from each signal echo are sampled, with the frequency encoding gradient applied, a line of k-space is filled from left to right of k-space (The de-phasing gradient moves the acquisition from the center of k-space to the left of k-space ready for the signal to be sampled). The phase encoding gradient moves the acquisition either up or down in the k_y direction by a prescribed distance. Usually the amplitude of the phase encoding gradient is incremented in steps such that the next adjacent line in k-space is filled with each successive repetition, starting at one edge of k-space and finishing at the

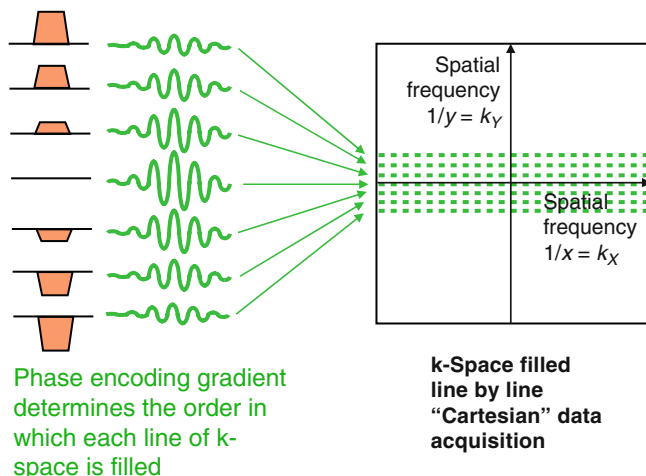


FIGURE 7.3. In a Cartesian data acquisition, the MR signals are sampled and the data points stored line by line along the k_x direction. The position along k_x depends on the time point during the application of the frequency encoding gradient. The location of each line of data points in the k_y direction is determined by the amplitude and duration of the phase encoding direction at each phase encoding step.

opposite edge (Fig. 7.4). This is known as a *linear phase encoding* order.

Choosing a different phase encoding step order is particularly important in some dynamic applications such as angiography. Here, it is important to acquire the contrast information immediately once the contrast agent reaches a particular vessel segment. In this case, the phase encoding gradient is incremented from zero, but with alternating sign, starting at the center of k space and working outward to the edges of k-space. This is known as *centric* or *low-high k-space order*.

Although the majority of cardiac applications use a Cartesian k-space acquisition scheme, it is possible to cover k-space using different schemes such as *radial* or *spiral k-space trajectories*. These have particular advantages as well as some potential technical drawbacks.

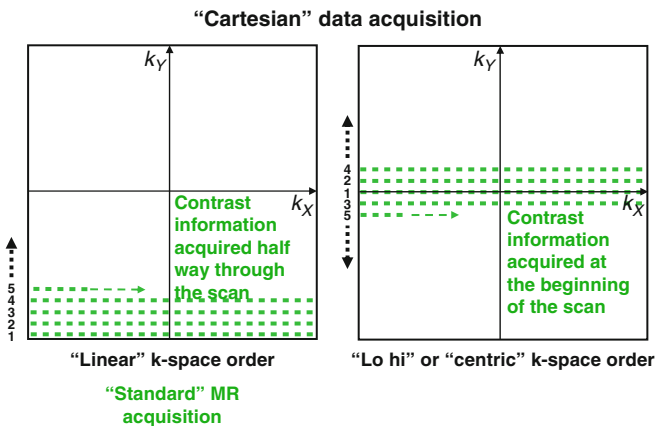


FIGURE 7.4. For a standard Cartesian MR data acquisition, lines of k-space are filled starting at one edge of k-space, incrementing line by line until the opposite edge of k-space is reached. This is known as linear k-space order. For some fast imaging applications where it is important to acquire the contrast information first, lines of k-space are filled from the center outward to both edges in an alternating fashion. This is known as “centric” or “lo-hi” k-space order.

Once the data acquisition is complete and k-space is filled to a sufficient extent to obtain the desired image resolution, the two-dimensional Fourier transform is applied to all the data points in k-space, transforming the data from k-space into the image space.

The number of acquired pixels in image space (the *acquired image matrix*) is equal to the number of data points acquired in k-space (Fig. 7.5). The number of lines of data points acquired in the k_y direction is equal to the number of phase encoding steps (i.e., repetitions with different phase encoding gradient amplitudes). The number of data points along each line in the k_x direction is equal to the number of samples taken of the MR signal echo as it is measured (see box). The number of sampled data points from each echo therefore determines the acquired image matrix size in the frequency encoding direction.

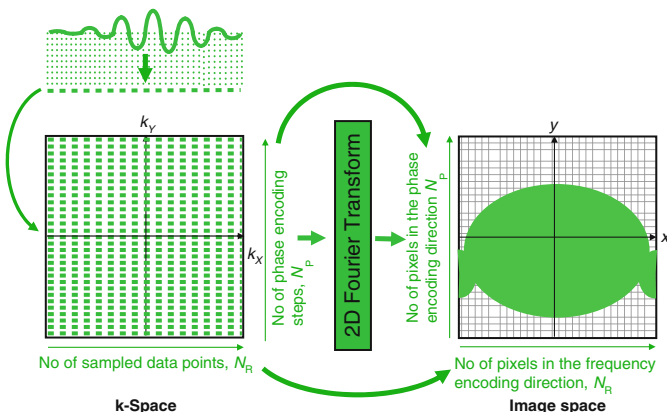


FIGURE 7.5. The number of data points in k-space determines the number of pixels in the image following the two-dimensional Fourier transform. The number of points along k_x is determined by the number of samples taken from the MR signal. The number of points along k_y is determined by the number of phase encoding steps.

How is a Data Point in k-Space Related to the MR Signal?

The MR signal is an oscillating magnetic field produced by the transverse component of the net magnetization as it rotates. The RF receiver coil converts the signal into an electrical signal, which is then digitally sampled to generate a series of numbers, which are then stored as rows of data points in k-space

Summary

- The MR signals are digitally sampled and stored as data points in a domain known as k-space.
- The information stored in k-space is related to the image via the Fourier transform, which forms the basis of the image reconstruction process.
- A single data point in k-space contributes to the whole image. The number of data points acquired in each direction k-space is the same as the number of data points in each direction of the image (the acquired image matrix).
- Data points near the center of k-space provide most of the signal content and therefore the image contrast (low spatial frequency content).
- Data points near the edge of k-space provide fine detail, defining the spatial resolution of the image (high spatial frequency content).
- Cartesian data acquisition fills k-space with data points line by line. The order in which lines of k-space are filled can determine contrast properties for some fast imaging applications such as angiography.

Chapter 8

Imaging Parameters and Image Attributes

8.1 Spatial Resolution and Image Acquisition Time

The *acquired matrix size*, together with the *field of view* in each direction determines the *pixel dimension* in each direction and therefore the *nominal spatial resolution* of the image. These parameters, together with the thickness of the selected 2D image slice, also determine the voxel dimensions and hence the *voxel volume* (Fig. 8.1). The voxel volume determines the number of protons that contribute to each pixel location. This strongly influences the size of the signal and is consequently a major determinant of *image quality*.

The acquired image matrix size also determines the image acquisition time. In the *phase encoding direction*, increasing the number of samples requires additional phase encoding steps, thus requiring additional repetitions of the MR signal acquisition. Thus the image acquisition time is very sensitive to the chosen spatial resolution in the phase encoding direction. In the simplest case, as we saw in Chap. 6,

$$\text{Image acquisition time} = \text{TR} \times N_p.$$

In the *frequency encoding direction*, however, increasing the number of samples, and hence the spatial resolution can be achieved without affecting the overall acquisition time. Although this increases overall sampling time of each echo, it

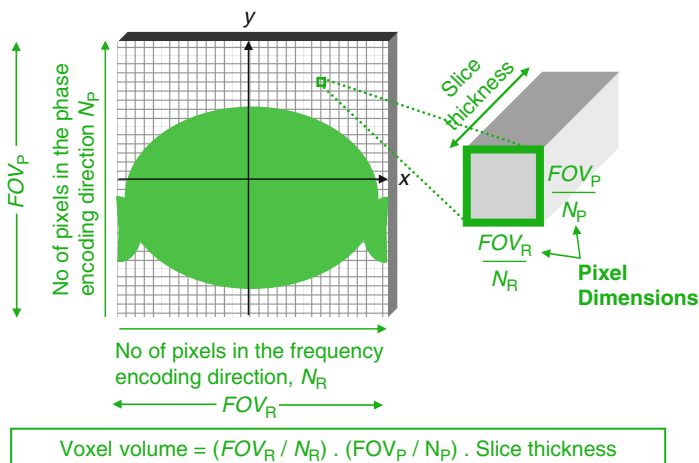


FIGURE 8.1. The image matrix size and field of view in each direction determine the acquired pixel dimensions. These dimensions, together with the slice thickness determine the voxel volume.

only lengthens the TR if the shortest possible TR and TE are already selected.

If time were no object (unfortunately not the case for cardiac imaging!), then one could increase the number of digital samples and phase encoding steps so that the spatial resolution could be increased without limit. There is, however, a second major limiting factor. As the spatial resolution increases, the pixel dimensions become smaller, the voxel volume becomes smaller and the number of protons contributing to the signal in a voxel reduces and so the signal within the corresponding image pixel (the pixel intensity) diminishes proportionately. As the signal becomes smaller, the pixel intensity approaches the noise level and the image quality is severely degraded. It is this that ultimately limits the spatial resolution of the MR technique.

8.2 Noise and Signal-to-Noise Ratio

The “noise” in MRI is electrical noise that is evenly spread across all frequencies. At higher field strengths (0.5 T and

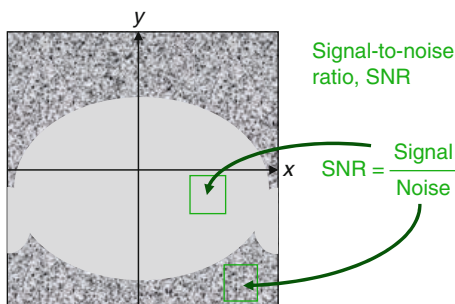


FIGURE 8.2. Background noise is visible in areas of low signal, such as outside the body and in the lung fields. The signal-to-noise ratio for a particular tissue area can be calculated from the mean pixel value within a region of interest placed over that area, divided by the mean pixel value from a region of interest placed in the background noise.

above) the main source of this noise is from the patient. The primary measure of image quality in MRI is the *signal-to-noise ratio or SNR*. It is measured as the ratio of the signal amplitude to the amplitude of the noise. In a typical image, noise can be seen as a salt-and-pepper pattern in background areas where there is little or no MR signal, for example, outside the body or in the lung fields (Fig. 8.2).

8.3 Factors That Determine Image Quality

8.3.1 Intrinsic Signal Amplitude

Image quality depends on *signal-to-noise ratio*. In addition to the noise level, SNR depends on the *pixel intensity*, which is determined by the *amplitude* of the MR signal. This, in turn, depends on a multitude of factors as follows:

- The number of protons within a voxel, which depends on the *proton density* and the *voxel volume* (Sect. 8.1).
- The *net magnetization*, which is in turn dependent on the *field strength* (Sect. 3.3). A higher static magnetic field strength (e.g., moving from 1.5–3.0 T), increases the available signal.

- The *tissue relaxation properties* of the particular tissue, T1 and T2, in combination with the selected *pulse sequence* and *timing parameters*, such as *TR* and *TE* (Chaps. 5 and 10).
- *Dephasing* of the net magnetization due to the presence of magnetic field gradients, for example, caused by *tissue susceptibility (T2*)*, or due to fluid motion or water diffusion along the imaging gradients.

8.3.2 Signal Averaging

As noise is random, averaging two or more signals together can have a beneficial effect upon the SNR. For example, if two signals are averaged, the relative noise component is reduced by a factor $1/\sqrt{2}$ and so the SNR increases by a factor of about 41%. This effect is manifested in a number of ways. First, as the signal is sampled many times, either through digital sampling of each signal echo, or by repeated sampling of the signal echo for different phase encoding steps, the SNR increases according to the square root of the total number of samples. Additionally, it is possible to repeat each phase encoding step a number of times in order to improve the SNR, a process known as signal averaging (Fig. 8.3).

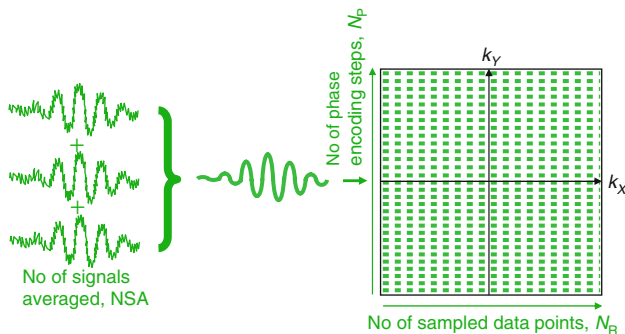
The drawback of the signal averaging approach is that the imaging time increases in proportion to the number of averages, whilst only gaining by the square root of the same factor in SNR. For techniques where speed is not of primary importance signal averaging is often used to improve image quality, whereas for cardiac imaging, the requirement for fast acquisition times limits its use.

The Nomenclature of Signal Averaging

Philips: Number of Signals Averaged, (NSA)

Siemens: Number of Acquisitions (ACQ)

GE: Number of Excitations, (NEX)



$$\text{Total no of signal samples} = \frac{\text{No of sampled data points, } N_R}{\text{No of phase encoding steps, } N_P} \times \text{No of signals averaged, } NSA$$

FIGURE 8.3. Image SNR ratio is related to the total number of times the MR signal is sampled. This is related to the number of times each signal is digitally sampled and the number of phase encoding steps. The MR signal acquisition at each phase encoding step is also sometimes repeated and averaged to increase the SNR. In this example, the number of signals averaged, NSA = 3.

8.3.3 SNR and Receiver Bandwidth

As noise is spread evenly across all frequencies, the level of noise in the image is extremely sensitive to the *receiver bandwidth* of the image acquisition (Fig. 8.4). A high (or wide) bandwidth includes more of the noise spectrum, reducing the SNR. A low (or narrow) bandwidth only accepts noise from a narrow range of frequencies and therefore increases the SNR.

One might expect, therefore, to always use a narrow bandwidth to maximize the SNR. There are a number of reasons why not. First, chemical shift artifact in the frequency encoding direction (see Sect. 17.6) becomes more pronounced at narrow bandwidths. The low bandwidth usually also means that the frequency encoding gradient is not particularly steep, so that any intrinsic magnetic field distortion becomes more apparent, leading to geometric image distortion. Second, a narrow bandwidth necessitates slower digital sampling rates of the signal, resulting in an increased signal sampling time.

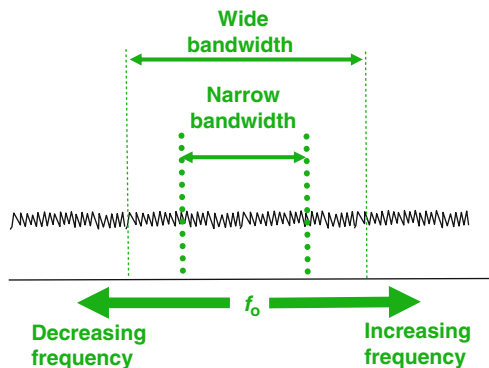


FIGURE 8.4. Noise in MRI is spread evenly across all frequencies. A wide receiver bandwidth includes more noise, leading to a poorer SNR. A narrow receiver bandwidth reduces the amount of noise and therefore increases the image SNR.

This limits the minimum possible TE and TR and therefore the minimum image acquisition time. In practice there is usually a compromise, dependent upon the requirements of the particular pulse sequence and application, balancing the image quality (SNR) against the acquisition speed and artifact level. In some instances, artifacts are tolerated in order to reduce noise in the image. In other instances one is prepared to accept a noisy image in the exchange for imaging speed. In practice, altering the bandwidth of a given pulse sequence should be left to expert users as it can have a substantial, detrimental effect on image quality.

8.4 Imaging Parameters: Practical Examples

In summary, imaging parameters affect the three aspects of an MR acquisition, *image acquisition time*, *spatial resolution*, and *image quality (or SNR)*. An improvement in one of these

aspects necessitates a reduction in at least one of the other two aspects. This is illustrated in the following two examples:

Example 8.1

Twofold increase in the in-plane spatial resolution (Fig. 8.5) (i.e., a decrease in the in-plane voxel dimensions by twofold in each direction).

There are at least two distinct ways of doing this:

- a. Keep the matrix size the same and reduce the field of view by half in both directions.
 - The image acquisition time stays the same (same number of phase encoding steps).
 - The voxel volume decreases fourfold
 - The SNR decreases fourfold.
 - There is an increased possibility of image aliasing as the subject may now be larger than the field of view (see Sect. 17.1).
- b. Keep the field of view the same and increase the image matrix size by twofold in each direction.
 - The number of phase encoding steps is increased twofold. The total image acquisition time is doubled.
 - The number of digital samples for each signal is increased twofold. If the bandwidth stays the same (signal sampling rate) the signal echo takes twice the time to sample. (for all but the fastest techniques, this is probably not important).
 - The fourfold decrease in SNR due to the fourfold reduction in voxel volume is countered by the fourfold increase in the total number of signal samples, giving a twofold ($\sqrt{4}$) increase in SNR. This leads overall to a net twofold decrease in SNR.
 - In (a) the imaging time stays the same, but the image quality (SNR) is drastically reduced. In (b), the reduction in image quality (SNR) is less, but the image acquisition time is increased.

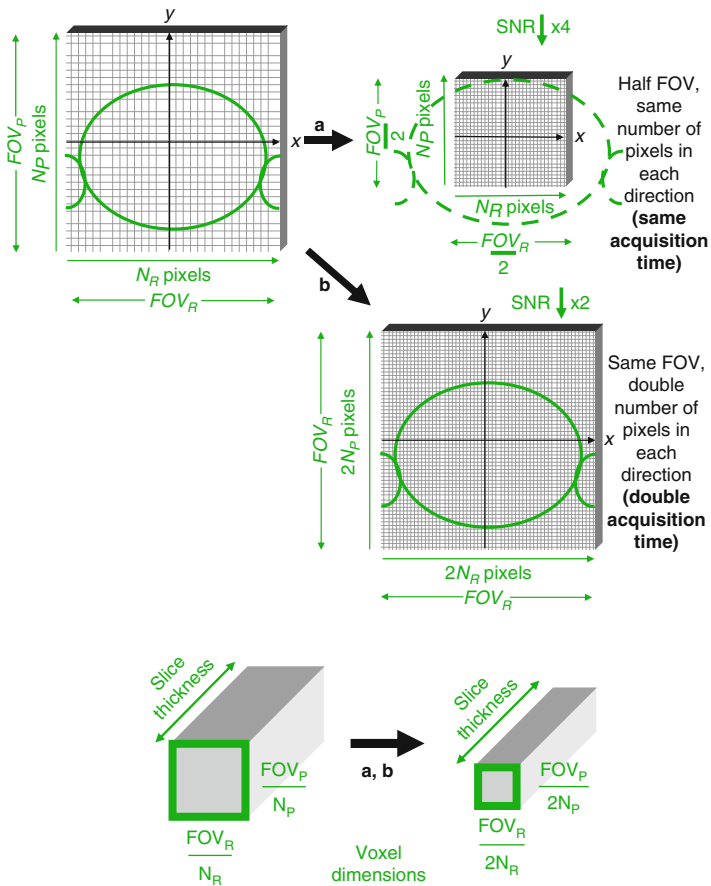


FIGURE 8.5. Two alternatives to double in-plane spatial resolution. **(a)** Halving the field of view in both directions leads to a fourfold reduction in SNR with no change in imaging time. **(b)** Doubling the image matrix in both directions keeps the field of view the same but doubles the image acquisition time.

Example 8.2

Decreased image acquisition time by half (Fig. 8.6).

There are again at least two distinct approaches:

- Half the image matrix dimension in the phase encoding direction, keeping the field of view constant in both directions.
 - The number of phase encoding steps is decreased by twofold leading to a twofold reduction in image acquisition time.
 - The spatial resolution is reduced in the phase encoding direction by twofold.
 - The total number of signal samples is halved leading to a $\sqrt{2}$ -fold reduction in SNR.
 - This is countered by a twofold increase in the pixel dimension in the phase encoding direction, leading in turn to a twofold increase in voxel volume and therefore a net increase in SNR by a factor of $\sqrt{2}$.
 - The field of view is preserved.
- Halve both the image matrix dimension and the field of view in the phase encoding direction, keeping the pixel dimensions constant.
 - The number of phase encoding steps is decreased twofold leading to a twofold reduction in image acquisition time.
 - The spatial resolution is preserved.
 - The total number of signal samples is halved leading to a $\sqrt{2}$ -fold reduction in SNR.
 - As the voxel volume is unchanged, this leads to a net $\sqrt{2}$ -fold reduction in SNR.
 - As the field of view is reduced, there is a possibility of image aliasing as the subject may now be larger than the field of view (see Sect. 17.1).

Summary of Factors Affecting Image Quality (SNR)

$$\text{SNR is proportional to } \frac{(\text{Voxel Volume}) \times \sqrt{(\text{No of signal samples})}}{\sqrt{\text{Bandwidth}}}$$

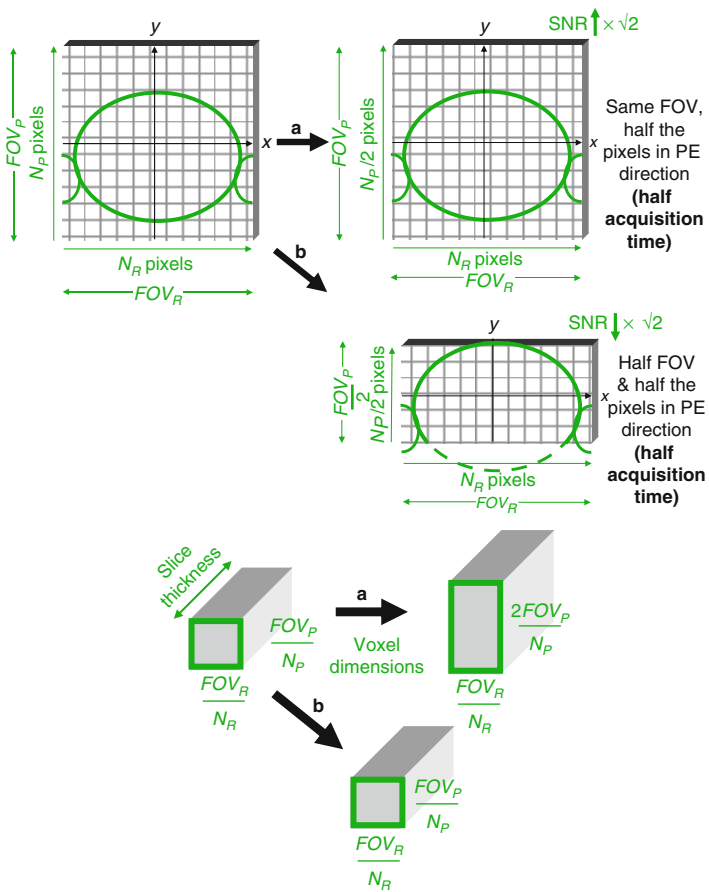
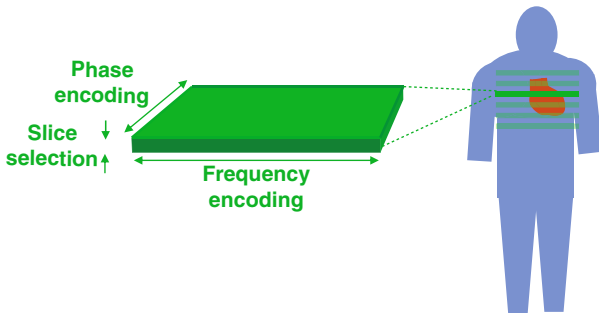


FIGURE 8.6. Two alternatives to halve image acquisition time: **(a)** Halving the image matrix in the phase encoding steps leads to a two-fold reduction in spatial resolution in that direction, but a net increase in image quality (SNR). **(b)** Halving both the image matrix and the field of view in the phase encoding direction maintains the same spatial resolution but leads to a net ($\sqrt{2}$) decrease in image quality (SNR).

8.5 2D and 3D Imaging

For the major part of anatomical and functional Cardiac MR imaging, *two-dimensional (2D) image acquisition* techniques are used to acquire 2D slices through the heart (Fig. 8.7). Complete anatomical coverage is then achieved either by repeating the acquisition to acquire multiple parallel 2D slices, or by acquiring images in different image planes. For 2D imaging, the thickness of the slice is limited by the need to maintain adequate image quality (SNR). The acquisition time is related to the number of phase encoding steps (determined by the resolution in the phase encoding direction).

For selected techniques a *three-dimensional (3D) image acquisition* is more appropriate. In this case, a volume, rather than a slice of tissue is selected by the excitation pulse and subsequently encoded in three directions by applying frequency encoding in one direction, and phase encoding in the remaining two directions (Fig. 8.8). The phase encoding applied in the “slice” direction effectively partitions in the



$$\text{Total acquisition time} = \text{TR} \times \text{No of phase encoding steps, } N_P \times \text{No of signals averaged, } \text{NSA}$$

FIGURE 8.7. Two-dimensional imaging is performed by slice selection and then using the MR signal frequency and phase to spatially encode the signal according to position within image plane in the two remaining directions. Volume coverage is achieved by repeating the acquisition at different slice locations.

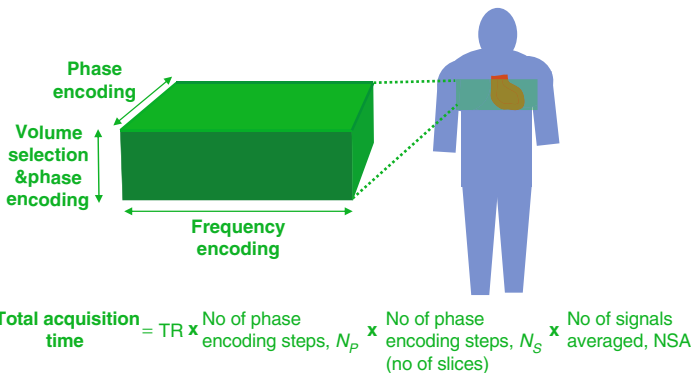


FIGURE 8.8. 3D imaging is performed by selecting a volume, and then spatially encoding the signal in all three directions. The signal frequency is used to encode one direction and the signal phase is used for the other two directions. The image acquisition time is increased, relative to the 2D acquisition, by the number of phase encoding steps used to spatially encode the slice locations in the volume-selection direction.

volume into slices with the number of encoding steps being determined by the number of reconstructed slices required. For every phase encoding step in the “slice” direction, the sequence must step through all the phase encoding steps in the “in-plane” phase encoding direction. The imaging time is therefore related to the number of phase encode steps (in-plane encoding) multiplied by the number of phase encode steps (slice encoding).

3D imaging has the following advantages:

- Thinner slices can be achieved (resolution is closer to “isotropic”)
- Slices are contiguous (no gap)
- SNR is greater compared to the equivalent 2D technique by a factor equal to the square root of the number of encoded slices

Summary

- Signal to noise ratio (SNR) is a major determinant of image quality in MRI.
- There is an interdependence between SNR, spatial resolution (voxel volume), receiver bandwidth, and image acquisition time.
- Increasing spatial resolution (same field of view) reduces SNR and increases image acquisition time.
- Increasing spatial resolution by decreasing field of view reduces SNR for same imaging time
- Reducing image acquisition time reduces spatial resolution or SNR or both.
- Signal averaging increases SNR but also increases image acquisition time.
- Increasing receiver bandwidth leads to faster echo sampling, shorter TE and TR hence shorter image acquisition time, but reduces SNR.
- In comparison to 2D imaging, 3D imaging allows thinner, contiguous slices to be acquired with improved SNR but with a longer acquisition time.

Chapter 9

Improving SNR with Surface Coils and Array Coils

Perhaps the most important aspect of MR in optimizing *SNR* is the choice of receiver coil. The *integral body coil* has a large field of view (Fig. 9.1a), but for imaging a smaller region of interest, it is much more appropriate to use a smaller, more tailored, *surface coil* (Fig. 9.1b). This has two advantages:

1. It is closer to the origin of the signal from the region of interest.
2. It detects less of the noise originating from outside of the region of interest.

These are the key principles of surface coil imaging. In general, the smaller the coil the better, although it is important that the coil is not too small that it cannot detect signal at depth.

Coil arrays are now in common use (Fig. 9.2). They combine the advantages of a small coil, maximizing SNR, while allowing imaging of a larger field of view. As the noise detected by each coil array element arises from a different region, the sum of the noise detected combines differently compared to a single large coil, giving an advantage of increased SNR. Coil arrays with elements distributed around the subject can also be used to provide information about the spatial distribution of the signal, allowing a reduced amount of phase encoding to be performed, and therefore, reducing the imaging time. This technique is known as *parallel imaging* (see Sect. 15.5). Most rf receiver coils used for adult imaging are *multielement coil arrays*, both providing good SNR over the entire thorax and enabling parallel imaging to be employed.

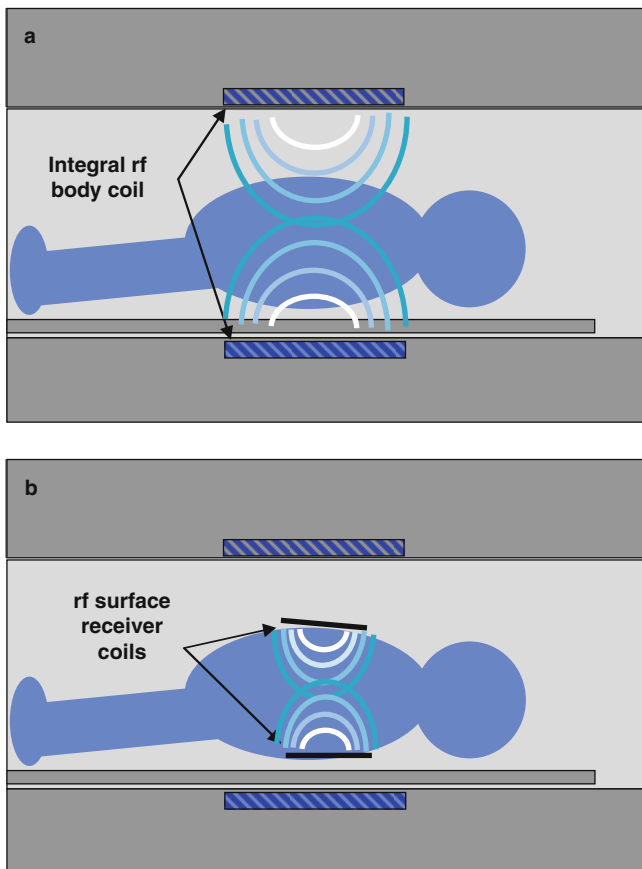


FIGURE 9.1. The integral body coil (**a**) has a large, uniform field of view coverage but receives more noise from a larger part of the body, resulting in a reduced SNR. Surface coils (**b**) have a smaller field of view but receive noise from a smaller part of the body, resulting in a higher SNR. As the sensitivity of the coil falls rapidly with distance from the coil, the image uniformity of the surface coil is poorer. This can partially be compensated by using two surface coils on either side of the body as shown.

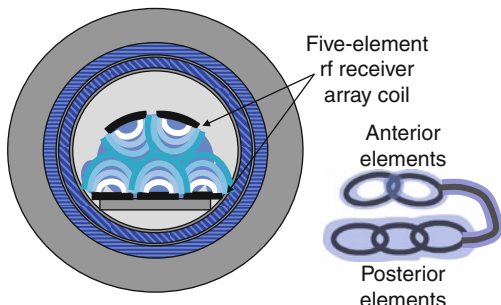


FIGURE. 9.2. Coil arrays consist of multiple receiver coil elements arranged in an array. Dedicated cardiac coils typically consist of four to six elements arranged as shown. The MR signal detected by each coil element can be directed through a separate receiver channel, providing high SNR imaging over a large field of view and enabling parallel imaging techniques to be employed.

RF Coils for Pediatric CMR

A good example of the use of surface coils is in pediatric cardiac MR. Whereas for adult imaging, the field of view used for most imaging protocols will not vary considerably, for pediatric subjects, the field of view will vary widely from teenagers with almost the same field of view as adults, to neonates with a very small field of view. Not only does the field of view change but so does the demand for spatial resolution. The smaller structures within a neonatal heart will require significantly higher spatial resolution. As we saw from Example 8.1 in Sect. 8.4, the need to increase spatial resolution over a small field of view drastically reduces the SNR. The appropriate choice of surface coil is therefore an essential step in designing pediatric imaging protocols in order to recover the SNR and to provide adequate image quality.

Summary

- The choice of appropriate receiver coil is one of the most important factors in maximizing image quality.
- Dedicated receiver coils improve SNR by being closer to the region of interest while receiving less noise from outside the region of interest.
- Appropriate coil selection is particularly important for pediatric applications.
- Coil arrays with multiple receiver elements provide improved SNR over a large field of view.
- Multielement coils can also be used to provide information about the spatial distribution of the signal, reducing the number of phase encoding steps needed, and therefore, the image acquisition time (known as Parallel Imaging).

Chapter 10

Pulse Sequences and Image Contrast

10.1 Dependence of the MR Signal on TR and TE

The MR signal intensity at a particular location is represented by the image *pixel intensity*. In Chaps. 8 and 9 it was shown that the strength of the MR signal relative to the background noise (SNR) depends on a number of *instrumental factors* including the magnetic field strength, the choice of receiver coil and system electronics, as well as *image acquisition parameters* including the field of view, image acquisition matrix size and slice thickness (defining the voxel volume), the number of signal samples, and the receiver bandwidth. It also depends on the sequence of rf and gradient pulses used to generate the MR signal echo, commonly referred to as the *pulse sequence*. The two main types of pulse sequences are *gradient echo* and *spin echo* pulse sequences. The choice of pulse sequence and its imaging parameters, including the timing parameters, *repetition time, TR* and *echo time, TE*, determine the intrinsic strength of the MR signal from a particular tissue according to its proton density value and relaxation properties.

For a simple pulse sequence that uses a single rf excitation pulse (Fig. 10.1), the transverse magnetization at the time of measurement depends on the following:

- The net longitudinal magnetization at *equilibrium*, M_o . This is determined by the proton density of the tissue and the applied magnetic field strength.
- The value of the longitudinal (z) magnetization, M_z , immediately before each rf excitation pulse is applied. This depends on the time allowed for recovery of the z -magnetization between pulses (usually the *repetition time*, TR), and the rate of recovery, determined by the *T1 relaxation time* of the particular tissue.
- The *flip angle* of the rf excitation pulse. This determines the proportion of that magnetization that is transferred into the transverse (xy) plane by the rf pulse and, therefore, the initial value of the transverse magnetization before it decays. In Fig. 10.1, the flip angle is 90° and all of the z -magnetization is transferred into the xy -plane.
- The rate of decay of the amplitude of the transverse magnetization, determined by the *T2 relaxation time* of the particular tissue, together with the effect of magnetic field inhomogeneities (combined as the *T2* relaxation time*).
- The time after the excitation pulse at which the center of the signal echo is generated and sampled (the *echo time*, TE).

All of the above factors combine to determine the amplitude of the transverse magnetization at the echo time for a particular tissue. This is translated into image pixel intensity according to the aforementioned instrumental factors (specific to each patient/receiver coil setup) and image acquisition parameters.

The above sequence describes a single repetition period, TR . After the excitation pulse, the longitudinal (z) component of magnetization recovers back toward its equilibrium value at a rate determined by its longitudinal (*T1 relaxation time*) (Fig. 10.1). The time at which the next excitation pulse is applied after the previous excitation pulse (the *repetition time*, TR) will determine the amount of recovery and

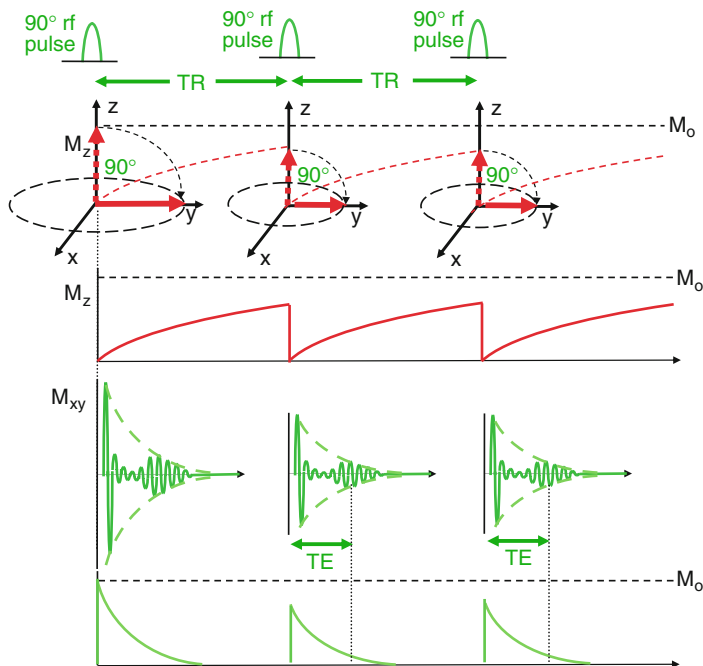


FIGURE 10.1. Simple pulse sequence using a 90° rf pulse. The initial z -magnetization is M_0 . Each rf pulse fully transfers the z -magnetization, M_z , into the xy -plane. Recovery of the z -magnetization with a time constant $T1$ during the repetition time, TR , determines its value prior to the next rf pulse. This in turn determines the magnetization transferred into the xy -plane after each rf pulse. The transverse magnetization, M_{xy} , then decays with a time constant $T2^*$. This and the choice of echo time, TE , at which the gradient echo is formed determine the MR signal echo amplitude.

therefore the value of the z -magnetization before the next rf excitation pulse is applied. This then influences the signal amplitude in the following repetition period.

In summary, the amplitude of the MR signal echo depends on the following:

- Decay of the transverse component of magnetization (T_2 and T_{2^*} relaxation), and the chosen echo time, TE
- Recovery of the z -component of magnetization (T_1 relaxation), the chosen repetition time, TR, and the flip angle.
- Different tissues have different characteristic relaxation times. This gives rise to different signal amplitudes depending on the choice of the pulse sequence timing parameters TR and TE and the flip angle.

TR and flip angle control the differences due to T_1 relaxation.

TE controls the differences due to T_2 and T_{2^} relaxation.*

10.2 Image Contrast and Weighting

One of the most important advantages of MR imaging over other imaging modalities is the ability to generate contrast between different soft tissue types. This is because different types of soft tissues have different characteristic T_1 and T_2 relaxation times. Sect. 10.1 showed that the dependence of the signal from a particular tissue on its T_1 and T_2 (or T_{2^*}) relaxation properties is controlled by the choice of the pulse sequence parameters, TR, TE, and flip angle.

For *spin echo* pulse sequences the addition of a 180° *refocusing pulse* determines that the amplitude of the spin echo at the TE is influenced by T_2 relaxation. As the excitation flip angle is fixed at 90° , the TR and TE are the only parameters used to control the image contrast. Typically, they are chosen to weight the image contrast so that it is primarily dependent upon either the differences in T_1 relaxation times (*T_1 weighted*), or the differences in T_2 relaxation times (*T_2 weighted*).

For *gradient echo* pulse sequences the absence of a 180° refocusing pulse determines that the amplitude of the gradient echo at the TE is influenced by T_{2^*} relaxation. A *variable flip angle* for the excitation pulse, as well as the TR and TE, is used to control image contrast. Typically, these three

parameters are chosen to weight the image contrast so that it is primarily dependent upon either the differences in T1 relaxation times (*T1 weighted*), or the differences in T2* relaxation times (*T2* weighted*).

For both spin echo and gradient echo pulse sequences, if the parameters are chosen so that the image contrast is neither dependent on the differences in T1 nor T2 (or T2*), the tissue signal is said to be primarily dependent on the proton density of the tissue and the image contrast is “*proton density*” weighted.

Sequence type	Parameters	Contrast weighting
Spin echo	TR, TE	T1, T2, or proton density
Gradient echo	TR, TE, flip angle	T1, T2*, or proton density

In the following examples, a simple pulse sequence with a fixed, 90° excitation pulse is used to demonstrate how the two parameters, TR and TE, can be chosen to produce different contrast weightings. While the pulse sequence shown is a gradient echo sequence without a 180° refocusing pulse, the trends for TR and TE are the same for spin echo sequences, except that for the spin echo sequence, the amplitude of the signal echo at the TE is governed by the T2 relaxation time rather than the T2* relaxation time. In these examples the terms “long” and “short” are used to describe the TR and TE as follows:

- *Long TR* means much longer than the T1 relaxation times of most of the tissues.
- *Short TR* means comparable to or shorter than the T1 relaxation times of most of the tissues.
- *Short TE* means much shorter than the T2* (or T2 for spin echo) values of all the tissues.
- *Long TE* means comparable to or longer than the T2* relaxation times of most of the tissues.

The possible combinations of TR and TE are as follows:

10.3 Long TR and Short TE

The choice of a long TR allows the z -magnetization to recover close to the equilibrium values for most of the tissues (Fig. 10.2). The 90° excitation pulse therefore transfers a similar amount of signal into the xy -plane for all tissues. The choice of a short TE limits the amount of $T2^*$ decay for any tissue at the time of measurement. This results in a high signal from all tissues, with little difference between them. So the signal amplitude is not particularly affected by the $T1$ relaxation properties, or by the $T2^*$ relaxation properties. The primary determinant of the signal amplitude is therefore the equilibrium magnetization of the tissue and the image contrast is said to be “*Proton density*” weighted. This type of weighting is useful where the depiction of anatomical structure is required, without the need to introduce soft tissue contrast.

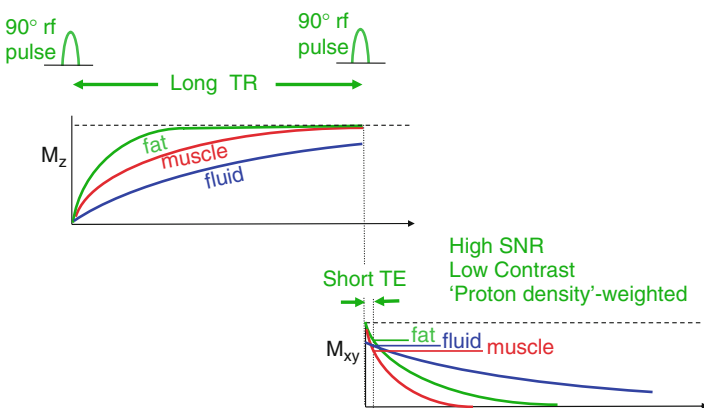


FIGURE 10.2. Pulse sequence with a “long TR” and “short TE” produces “Proton Density”-weighted contrast.

10.4 Short TR, Short TE

The choice of a short TR determines that tissues with a short T1 (e.g., fat) will recover more than those with a long T1 (e.g., fluid) (Fig. 10.3). This determines the initial value of the transverse magnetization, M_{xy} , when the next rf pulse is applied. Tissues that have recovered more quickly will have a greater longitudinal magnetization before the next rf pulse, resulting in a greater transverse magnetization after the rf pulse. The short TE limits the influence of the different T2* decay rates. The resultant contrast is therefore said to be *T1 weighted*. These images are typically characterized by bright fat signal and a low signal from fluid and are useful for anatomical imaging where high contrast is required between, fat, muscle, and fluid.

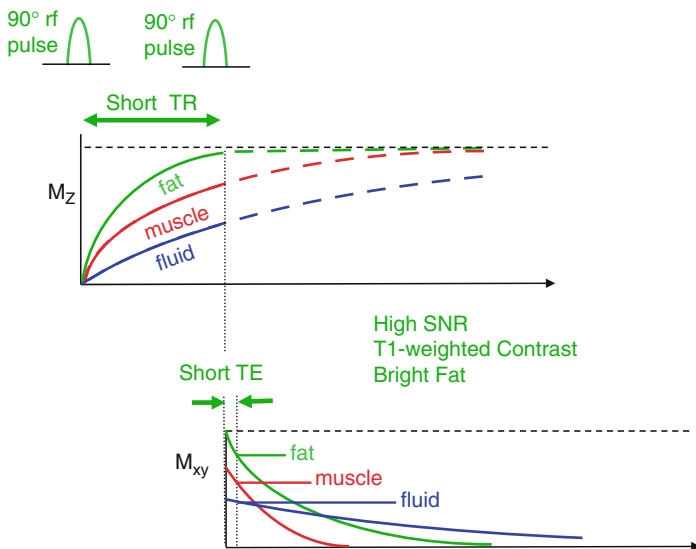


FIGURE 10.3. Pulse sequence with a “short TR” and “short TE” produces T1-weighted contrast.

10.5 Long TR, Long TE

As with Fig. 10.2, the long TR allows recovery of the z -magnetization for most tissues, therefore, reducing the influence of differences in T1 relaxation time (Fig. 10.4). The longer echo time, however, allows more decay of the xy component of the magnetization. The differential rate of decay between a tissue with a short T2* (muscle) and a tissue with a long T2* (e.g., fluid) leads to a difference in signal that is said to be *T2* weighted*. (For spin echo sequences this combination of TR and TE provides images that are T2 weighted.) The short T2* leads to a reduced signal, while the long T2* leads to a high signal intensity. These images are characterized by bright fluid and are useful for the depiction of fluid collections and the characterization of cardiac masses and edema. For T2* weighted gradient echo, the image contrast is also strongly influenced by the presence of magnetic susceptibility effects and can be used to detect the presence of iron, for example, where there is hemorrhage or iron loading of tissue.

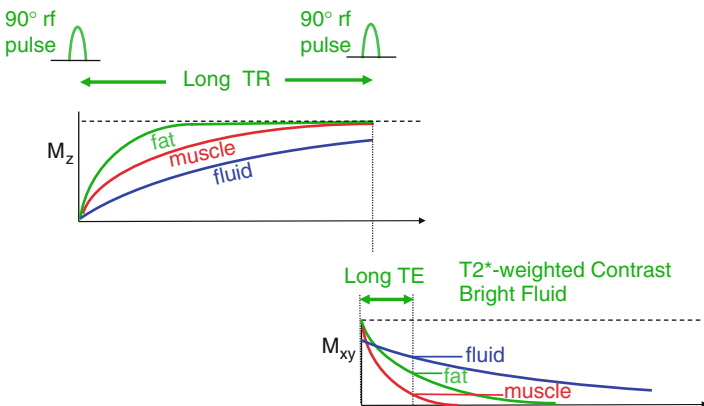


FIGURE 10.4. Pulse sequence with a “long TR” and “long TE” produces T2*-weighted contrast.

10.6 Short TR, Long TE

This combination of timing parameter choices is generally not a good idea (Fig. 10.5). The short TR reduces signal from tissue with long T₁ relaxation times. The long TE reduces signal from tissues with short T_{2*} values. Since the T₁ and T₂ (and T_{2*}) relaxation times for most tissues follow similar trends, the result is a reduced signal from everything as well as poor contrast, that is, a poor image.

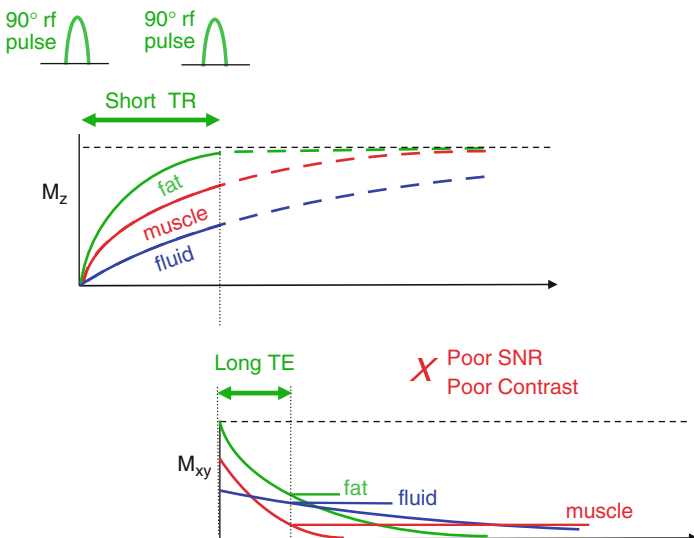


FIGURE 10.5. Pulse sequence with a “long TR” and “long TE” produces a poor contrast, low SNR image.

Summary

- Soft tissue contrast in MRI arises due to the differences between the tissues characteristic relaxation times.
- The type of pulse sequence and its parameters determines whether the image contrast is weighted by the T1, T2, or T2* relaxation processes.
- For spin echo (SE) pulse sequences, the TR controls the T1 weighting while the TE controls the T2* weighting.
- For gradient echo (GE) pulse sequences, the TR and the flip angle control the T1 weighting, while the TE controls the T2* weighting.
- Contrast weightings for TR and TE parameter choices with fixed flip angle:

	Short TE	Long TE
Long TR	<p>“Proton density” weighted</p> <p>Good SNR</p> <p>No contrast</p>	<p><i>T2* weighted</i></p> <p><i>(T2 weighted for SE)</i></p> <p>Bright fluid</p>
Short TR	<p><i>T1 weighted</i></p> <p>Bright fat</p> <p>Low fluid signal</p>	<p>Poor SNR, poor contrast image</p>

Chapter 11

Gradient Echo Versus Spin Echo

Spin Echo pulse sequences follow similar contrast behavior to that described in the previous section; however, there are some key differences between Gradient Echo and Spin Echo pulse sequences (Fig. 11.1).

In the case of spin echo, a 180° refocusing pulse is applied at a time equal to half the echo time. This reverses the effect of the field inhomogeneities and the amplitude of the transverse magnetization at the echo times dependent on the pure T2 relaxation time of the tissue. As the T2 values for tissues are longer than the T2* values, the echo times chosen to achieve T2 weighting with Spin Echo are also longer than the echo times required to achieve T2* weighting with gradient echo sequences.

The spin echo pulse sequence uses an excitation pulse that is normally 90° , so at each excitation pulse all of the z magnetization is transferred into the transverse plane. This combined with the refocusing pulse gives the largest possible signal provided the magnetization is allowed to recover sufficiently between repetitions.

These two attributes make the spin echo technique ideally suited when the primary goal is to achieve good image quality, with a reduced sensitivity to artifacts caused by magnetic field inhomogeneities.

The gradient echo pulse sequence uses an excitation pulse with a variable flip angle, α , that is normally less than 90° (typically 30° or less). While this initially results in a smaller

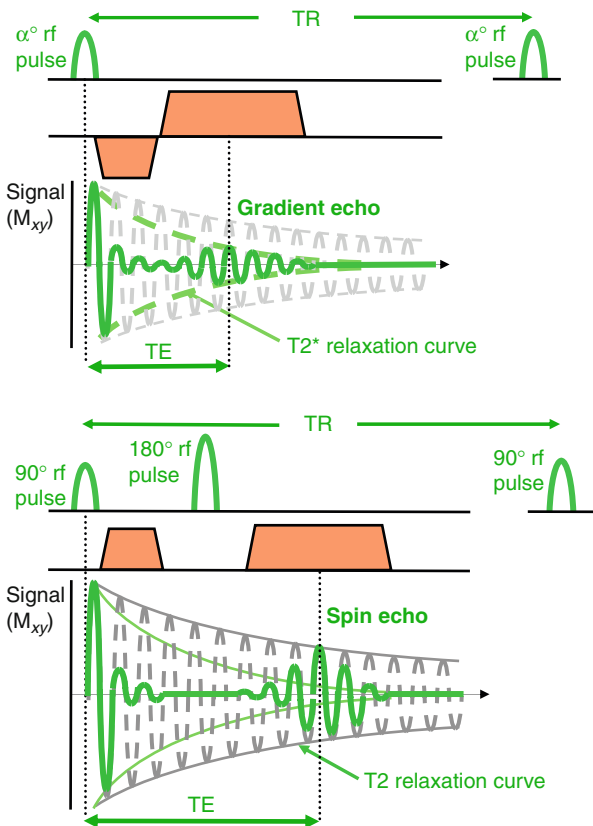


FIGURE 11.1. Comparison between a gradient echo pulse sequence (top) and a spin echo sequence (bottom). The gradient echo sequence uses variable rf excitation pulses with flip angles, α , that are typically much less than 90° . The Gradient echo signal amplitude is determined by T_2^* decay and is therefore smaller. Echo times also tend to be shorter. The spin echo pulse sequence uses a 90° excitation pulse and a 180° rf pulse to reverse the effects of field inhomogeneities. The spin echo signal amplitude is determined primarily by T_2 decay and is therefore larger.

transverse magnetization, as only a proportion of the z -magnetization is transferred into the xy plane, the recovery of the z magnetization toward the equilibrium value is faster, allowing the repetition time to be reduced. In this case a much larger transverse magnetization is achieved compared to that generated by a 90° pulse in combination with a very short TR. This is known as *low flip angle* imaging and is the basis for fast imaging with gradient echo pulse sequences. Much shorter repetition times can be used for gradient echo than for spin echo pulse sequences. *Fast gradient echo* pulse sequences are used where imaging speed is more important than SNR.

The contrast behavior described in this section is only true for a gradient echo pulse sequence provided the TR is not too short (>100 ms). For fast imaging, very short TR values (<10 ms) are used and the contrast behavior of the gradient echo sequence can change. The contrast behavior described here is only applicable at very short TR values if particular type of gradient echo pulse sequence, *Spoiled gradient echo* is used (See Sect. 13.5) (Fig. 11.2).

Further differences between spin echo and gradient echo pulse sequences arise due to the absence of the 180° refocusing pulse in the gradient echo sequence. This leads to signal loss in the presence of magnetic susceptibility effects (see Sect. 17.7), and at the boundaries between water and fat-based tissues (See Sect. 17.6). Flowing blood also appears differently between the two sequences. All of the above key differences are summarized in Table 11.1. Note that the description of TR as long or short is dependent on the choice of flip angle. A TR that may be described as short when a high flip angle is selected (e.g., TR = 200 ms, flip angle 70°), becomes a long TR when a low flip angle is selected (e.g., TR = 200 ms, flip angle 30°).

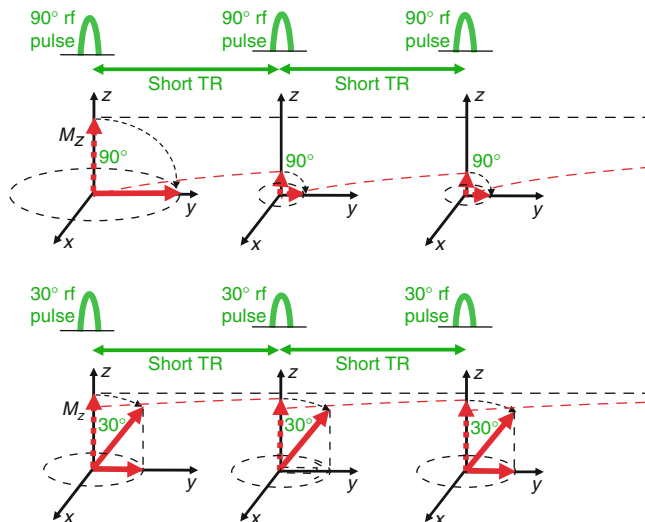


FIGURE 11.2. Gradient echo sequences can use a variable (*low*) flip angle for the excitation pulse, which allows much shorter TR values to be used without losing too much signal. When a 90° rf pulse is used (*top row*), the short TR allows very little recovery between rf pulses. The z -magnetization quickly reduces, resulting in a low signal amplitude when it is transferred into the xy plane. The use of a low flip angle (in this case, 30°, *bottom row*), allows the z -magnetization to remain much closer to its equilibrium value. This, when transferred into the xy plane, results in a much larger signal in comparison.

TABLE 11.1. Summary of differences between conventional gradient echo and spin echo sequences.

	Gradient echo (spoiled)	Spin echo
RF pulses	Variable excitation pulse	Excitation pulse and 180° refocusing pulse
Signal amplitude depends on decay of transverse magnetization according to	T2*	T2
Flip angle (excitation pulse)	5°–70°	90°
Short echo time (minimize T2 or T2* weighting)	1–3 ms	6–25 ms
Long echo time (for T2 or T2* weighting)	7–15 ms	60–100 ms
Short repetition time (T1 weighting)	3–400 ms (depends on flip angle)	400–800 ms
Long repetition time (minimizes T1 weighting)	400 ms – (depends on flip angle)	1,500–2,500 ms
Shortest practical TR	2–5 ms	200 ms
Intravoxel signal loss (susceptibility, iron)	Yes	No
Intravoxel signal loss (fat/water boundaries)	At out-of phase echo times	No
Signal from blood flowing through the slice	Bright (inflow enhancement)	Dark (spin washout)

Summary

- The Contrast behavior of Conventional Spin Echo and Gradient Echo follow similar trends, but there are also key differences:
- Spin Echo (SE)
 - High Quality T1- and T2-weighted imaging
 - Insensitive to magnetic susceptibility ($T2^*$) effects including iron
 - Dark Blood appearance (flowing blood)
 - Relatively long TR required – cannot be used for fast imaging applications
- Gradient Echo (GE)
 - Relatively reduced signal
 - Short TR possible with variable low flip angle – suited to fast imaging applications
 - Bright blood appearance
 - Increasing sensitivity to magnetic susceptibility ($T2^*$) effects including iron as TE is increased.

Chapter 12

Black Blood Versus Bright Blood Imaging

12.1 Black Blood (Spin Echo Pulse Sequence)

The spin echo pulse sequence generates images that have intrinsic black blood contrast. This is because it uses two pulses, the 90° and 180° pulses, to produce the spin echo signal (Fig. 12.1). Both of these pulses are slice-selective but are separated by a time equal to half the echo time. The transverse magnetization of blood flowing through the slice that moves out of the slice between the two pulses is not refocused by the 180° pulse and does not contribute to the generation of a spin echo. If the flow is sufficiently rapid for all the blood receiving the 90° pulse to move out of the slice, this results in a signal void, also known as a “*Black Blood*” or “*Dark Blood*” appearance. This effect is also known as the *spin washout effect*, referring to the “washout” of proton spins from the image slice that would otherwise be refocused and contribute to the spin echo signal.

When there is significant blood flow *through* the slice, the black blood appearance provides high intrinsic contrast between the blood pool and the heart and blood vessel walls, which is ideal for anatomical imaging (Fig. 12.2a).

Where blood is moving *slowly*, however, or moves within the plane of the image slice, this effect is reduced and the dark blood contrast is lost (Fig. 12.2b).

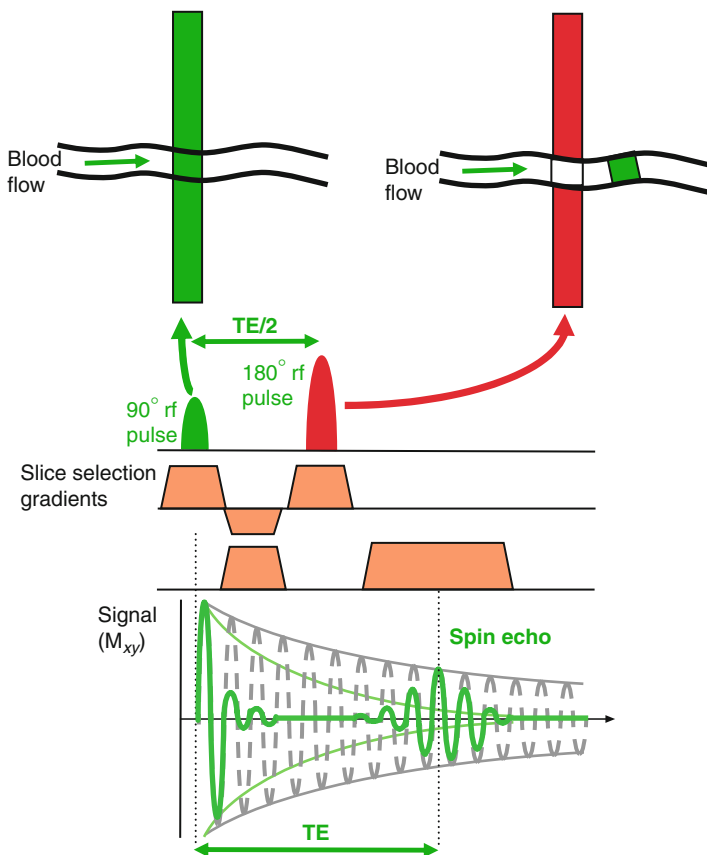


FIGURE 12.1. Black blood appearance using spin echo pulse sequences is caused by the motion of blood through the image slice between the 90° and 180° pulses. The 90° pulse (green) causes resonance in all the tissue within the slice; however, a spin echo signal is only produced when the same tissue and blood also receive the 180° refocusing pulse (red). Blood that moves out of the slice during the time between the 90° and 180° pulses does not produce a spin echo, resulting in a signal void.

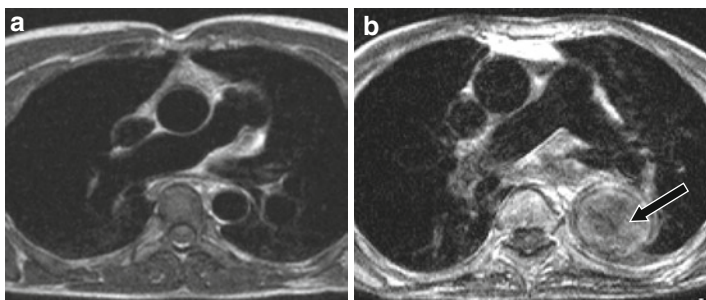


FIGURE 12.2. The image in (a) is acquired using a spin echo pulse sequence. High blood flow velocities through the major vessels generate good contrast between the blood vessel walls and the blood due to the spin washout effect. Image (b) shows an image acquired in a patient with a dilated descending aorta. The slow blood flow reduces the spin washout effect and signal is seen from the blood within the descending aorta (arrow).

12.2 Black Blood – Double Inversion Preparation Pulses

Reliance on the spin washout effect to produce dark blood contrast often leads to inconsistent results due to insufficient blood flow. In order to improve the effectiveness of black blood imaging it is common to use a *black blood preparation scheme* in combination with the spin echo pulse sequence. The preparation scheme consists of the addition of two 180° rf pulses followed by a delay, prior to the spin echo pulse sequence (Fig. 12.3). The effect of this preparation scheme is described as follows:

- The first 180° pulse inverts the magnetization of all blood and tissues within range of the rf body transmitter coil.
- The second 180° pulse re-inverts the magnetization only within a slice that encompasses the slice to be imaged.
- The net effect of these two pulses is to invert the magnetization of blood and tissue outside the slice, while the magnetization within the slice remains close to its equilibrium value.

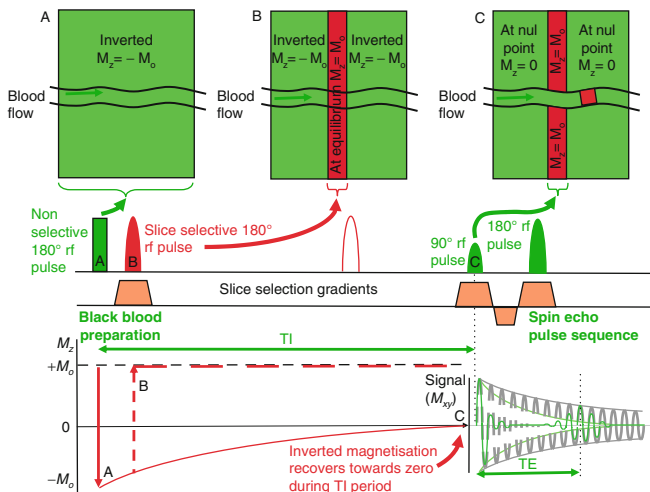


FIGURE 12.3. Black blood imaging commonly uses a double inversion preparation pulse scheme to make the suppression of the blood signal more effective. The first inversion pulse, A, inverts the magnetization of all the tissue within range of the rf transmitter coil. The second inversion pulse, B, restores the magnetization of the tissue within the intended image slice. The net effect of pulses A and B is to invert the magnetization of all the tissue outside the intended image slice (shown in green). After a prescribed recovery period, chosen as the time taken for the blood magnetization to reach zero (solid red line), an excitation pulse, C, is applied to generate a signal dependent on the current value the z-magnetization of tissue and blood within the slice. During that same period, blood from outside the slice that has been inverted (green) is likely to have replaced the non-inverted blood within the slice (red), resulting in a signal void within the vessel.

- There is then a time delay before the excitation pulse (*Time from Inversion, TI*). During this time, the inverted blood magnetization recovers due to T1 relaxation from its initial negative value, toward its positive equilibrium value.
- The *TI* is calculated to be equal to the time it takes the inverted magnetization of blood to pass through zero. At that time, the 90° excitation pulse of the spin echo pulse sequence is applied.

- At the same time, blood flow causes the blood with inverted magnetization to move into the image slice, replacing the blood that has remained at equilibrium. As the spin echo pulse sequence is applied at the same time as the inverted blood magnetization reaches zero, no signal is produced from the blood.

The double inversion pulse black blood preparation scheme provides much better signal suppression as the time delay used here is much greater than the half echo time period that gives rise to the intrinsic black blood contrast of the conventional spin echo pulse sequence (Fig. 12.4).

Signal Voids and Vessel Patency

When a signal void is seen within the vessel lumen on spin echo images, it usually suggests that there is significant blood flow, confirming vessel patency. Conversely, if signal is seen within a vessel, this does not necessarily mean that it is occluded. It could either mean that there is thrombus or that the blood is moving slowly through, or remaining within in the image slice. This requires further imaging, such as velocity mapping, for confirmation.

12.3 Bright Blood (Gradient Echo Pulse Sequence)

In contrast to the spin echo sequence, the gradient echo sequence only uses one rf pulse to generate the signal and so the spin washout effect does not apply and the signal from flowing blood is usually visible. Indeed, rather than suffering from a reduction in signal, flowing blood often appears with an apparently increased signal, compared to the surrounding tissues. The gradient echo pulse sequence is therefore commonly referred to as a *bright blood* imaging technique.

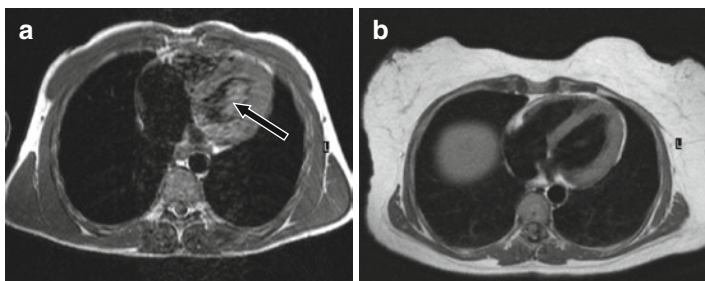


FIGURE 12.4. Image (a) is acquired using a conventional spin echo pulse sequence. Note the imperfect suppression of the blood pool signal (arrow). This is because the spin washout effect is not always effective, either due to slower flow in diastole, or due to blood flowing more within the plane of the image slice. The image in (b) is acquired in diastole using a black blood preparation pulse. Suppression of the blood pool signal is more consistent using this method.

Gradient echo sequences are often used with a very short repetition time, (TR), for the purpose of fast imaging (e.g., TR < 10 ms). This means that the magnetization of tissue that remains in the image slice becomes saturated as rf pulses are rapidly applied to the same tissue, as there is little time for recovery of the z -magnetization between pulses. This has the effect of reducing the signal from stationary tissue or blood that remains within the slice (Fig. 12.5). Blood moving into the slice, however, has not received any previous pulses and the spin population is therefore fully magnetized. The moving blood is therefore able to generate a much higher signal than the surrounding tissue, thus the blood signal appears enhanced or bright. This effect is known as *inflow enhancement*.

When there is significant blood flow through the slice, the bright blood signal provides good intrinsic contrast between the blood pool and the heart and blood vessel walls (Fig. 12.6). The use of a much shorter repetition time compared to spin echo, for example, makes this technique useful for functional

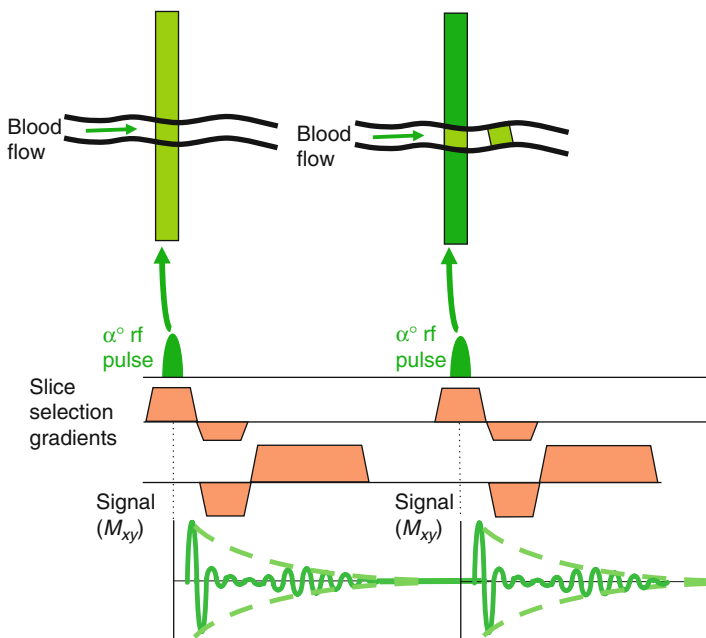


FIGURE 12.5. Gradient echo pulse sequences are often characterized by bright appearance of flowing blood. This is because they often use very short repetition times. This results in limited recovery of the tissue magnetization between pulses. Tissue that remains within the slice therefore has a reduced signal. Blood that flows through the image slice is constantly being replaced by fully magnetized blood which is able to generate a much higher signal when the excitation pulse is applied.

imaging of the heart and great vessels. The flow enhancement effect is also used as the basis for time-of-flight MR angiography (TOF MRA). Where the blood flow is moving slowly through the slice or in a direction within the plane of the image slice, this effect is reduced and the bright blood contrast is reduced.

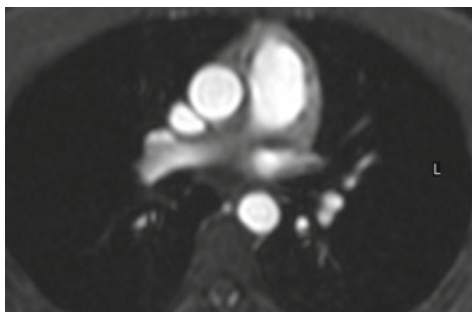


FIGURE 12.6. A Gradient echo pulse sequence showing “bright blood” appearance within the major blood vessels, due to the inflow enhancement effect.

Summary

- Spin echo pulse sequences exhibit intrinsic black blood contrast, caused by the movement of blood out of the image slice between the 90° and 180° pulses.
- In the presence of slow blood flow, the intrinsic black blood contrast of spin echo pulse sequences becomes inconsistent.
- Black blood contrast can be improved by using a black blood preparation scheme, in combination with a spin echo pulse sequence.
- The black blood preparation scheme consists of two 180° inversion pulses, one nonselective and one slice selective, to invert the blood magnetization outside the image slice.
- As the magnetization recovers toward zero, the inverted blood moves into the slice. The spin echo pulse sequence is applied as the inverted blood magnetization reaches zero leading to no signal from blood.
- Gradient echo pulse sequences commonly exhibit an intrinsic “bright blood” appearance from flowing blood.
- Gradient echo sequences use a short TR, which causes saturation of the magnetization and a reduction in signal of stationary tissue within the slice.
- Flowing blood entering the slice is fully magnetized and is able to yield a higher signal than the surrounding tissue, resulting in a bright blood appearance.

Chapter 13

Dealing with Cardiac Motion: How Do We Image the Beating Heart?

Imaging the beating heart is a challenge for MR imaging. To capture an image of the heart that is unaffected by motion would require an image to be acquired in just a few tens of milliseconds. In Chap. 8 it was shown that the minimum possible image acquisition time is limited by the repetition time and the need to acquire a sufficient number of phase encoding steps to achieve a particular image matrix size and therefore spatial resolution. To achieve an image acquisition in a few tens of milliseconds means both limiting the number of phase encoding steps (and thus the spatial resolution and SNR), and making the TR as short as possible. As Chap. 15 on Fast Imaging will show, this can be done but is often at the cost of accepting a significant reduction in image quality. One of the current main focuses of the development of MR technology is to devise imaging schemes that allow the fastest possible imaging whilst maintaining acceptable image quality.

For standard MR imaging, in order to achieve acceptable image quality, the image acquisition time is too long to “freeze” heart motion. MR signals are therefore acquired over several heart beats, synchronizing the pulse sequence and therefore the signal acquisition to a particular time point in the cardiac cycle. Cardiac synchronization is achieved by using the patient’s ECG signal, obtained by applying ECG pads and leads onto the patient’s chest (Fig. 13.1)

Software is used to detect the “R” wave of the ECG and to generate a synchronization pulse, which is then used to

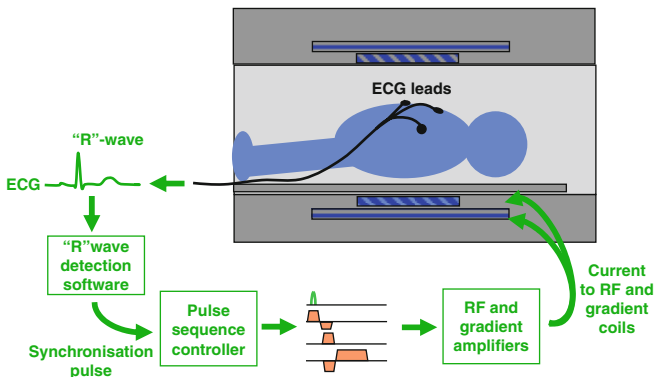


FIGURE 13.1. Cardiac synchronization is achieved by obtaining an ECG signal from the patient. A software algorithm is then used to detect the QRS complex and generate a synchronization pulse. This can then be used as a trigger pulse to initiate the pulse sequence controller. This produces rf and gradient pulse waveforms that are amplified to drive the rf transmitter and gradient coils. This is then repeated, with each cardiac cycle triggering a new repetition of the pulse sequence.

synchronize the MR data acquisition. This enables images of the beating heart to be obtained either at a single time point (Still imaging) or at multiple time points through the cardiac cycle (Cine imaging).

13.1 Still Imaging

For still imaging, the ECG synchronization is known as triggering. The synchronization pulse is used as a trigger to initiate the pulse sequence at a particular time point after the R-wave in each cardiac cycle. This time point is known as the trigger delay and is selectable by the system operator to determine the point in the cardiac cycle at which the heart is to be imaged (Fig. 13.2).

Examples of still imaging are given in Table 13.1. This type of imaging can be used for anatomical imaging, tissue characterization, myocardial viability assessment or coronary angiography.

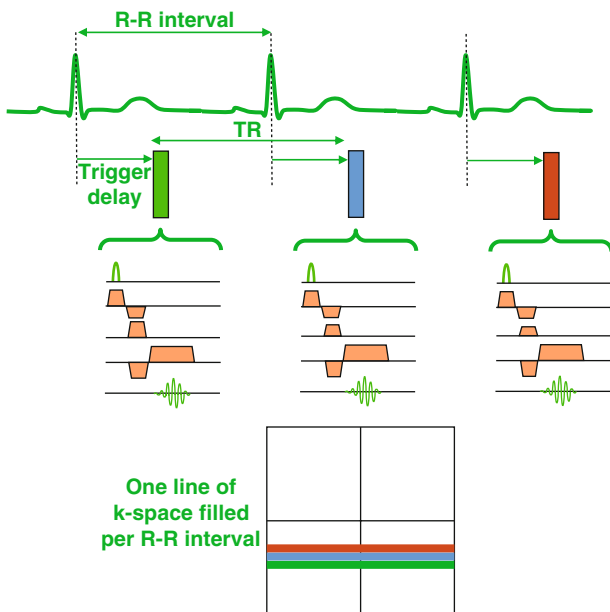


FIGURE 13.2. Still imaging is achieved by acquiring data at a single time point in the cardiac cycle after the cardiac synchronization pulse, determined by an operator-selected trigger delay. One line of k-space is filled with each heart beat. Once k-space has been filled, a single image is reconstructed, corresponding to that time point.

TABLE 13.1. Common applications for ‘still’ imaging techniques.

“Still” imaging technique	Pulse sequence	Information
T1w or T2w black blood SE (Sect. 16.4 and Sect. 19.3)	Double inversion 2D T1w SE	Anatomy and tissue characterization
Black blood STIR (Sect. 16.5 and Sect. 19.3)	Triple inversion 2D T2w SE	Tissue characterization/edema
Late enhancement (Sect. 16.6 and Sect. 19.9)	Inversion recovery 2D gradient echo	Tissue characterization/myocardial scar
Coronary MRA (Sect. 16.7 and Sect. 19.10)	3D gradient echo	Coronary vessel lumen

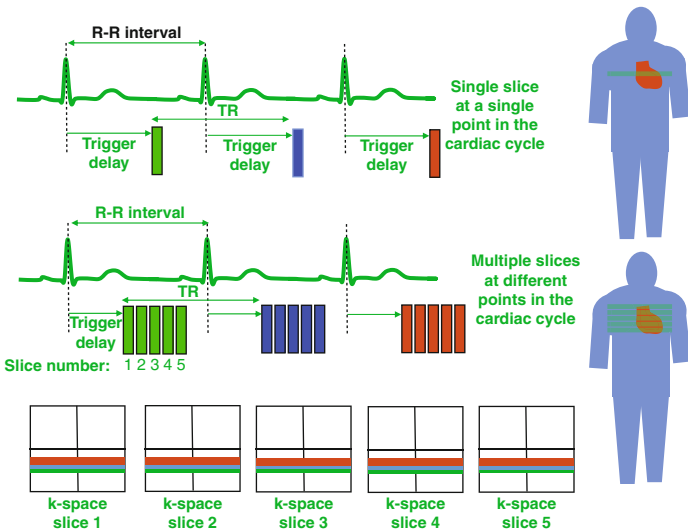


FIGURE 13.3. Multiple slice acquisitions can be achieved by acquiring data from multiple slice locations at different time points within the cardiac cycle. The total imaging time is the same as for a single slice acquisition.

In order to improve the efficiency of still imaging, MR signal data can be acquired from multiple slice locations within each cardiac cycle (Fig. 13.3). At the end of the acquisition, the multiple slices are reconstructed with each slice acquired at a different time point in the cardiac cycle.

13.2 Cine Imaging

Cine imaging involves the acquisition of data at multiple time points, known as cardiac phases, throughout the cardiac cycle (Fig. 13.4). The trigger delay for the first time point is set to the shortest possible time after the R wave to enable images to be acquired from the beginning of the cardiac cycle. Data acquired within each cardiac phase fills a separate k-space, resulting in the reconstruction of a separate image corresponding to each

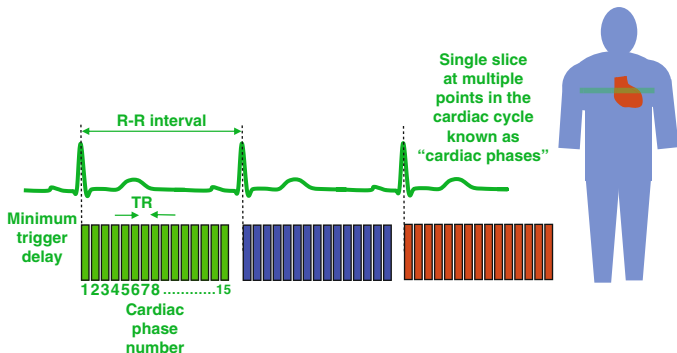


FIGURE 13.4. Cine imaging is achieved by acquiring data for a single slice location at multiple time points throughout the cardiac cycle. Multiple images are then reconstructed at the corresponding time points, known as cardiac phases. These images may then be viewed as a movie to allow the visualization of cardiac motion and blood flow patterns.

cardiac phase. The images for all the cardiac phases are then viewed as a movie sequence or cine, allowing functional assessment of the heart, its wall motion, and a visual, qualitative assessment of blood flow.

13.3 Triggering Versus Gating for Cine Imaging

For cine imaging, cardiac synchronization can be performed in either of two ways: ECG triggering or ECG Gating.

ECG triggering can be used to commence data acquisition immediately after the QRS complex (Fig. 13.5a). Data is then acquired for multiple consecutive cardiac phases until nearly at the end of the cardiac cycle. Data acquisition is then stopped until the synchronization pulse from the next “R”-wave is received. This method requires the system to estimate an average R-R interval for the patient being imaged (This can be either entered by the operator or captured from the ECG trace

by the MR system). This is then used to determine the average length of the cardiac cycle over which data can be acquired and therefore how many cardiac phases can be acquired. A consequence of this approach is that there is a “blind spot” where no data is acquired at the end of the cardiac cycle while the system waits for the next trigger pulse. This is a disadvantage if imaging of diastolic function or mitral and tricuspid valve function is important.

An alternative is to use ECG gating. (Fig. 13.5b). Here the pulse sequence runs continuously with a short TR. The

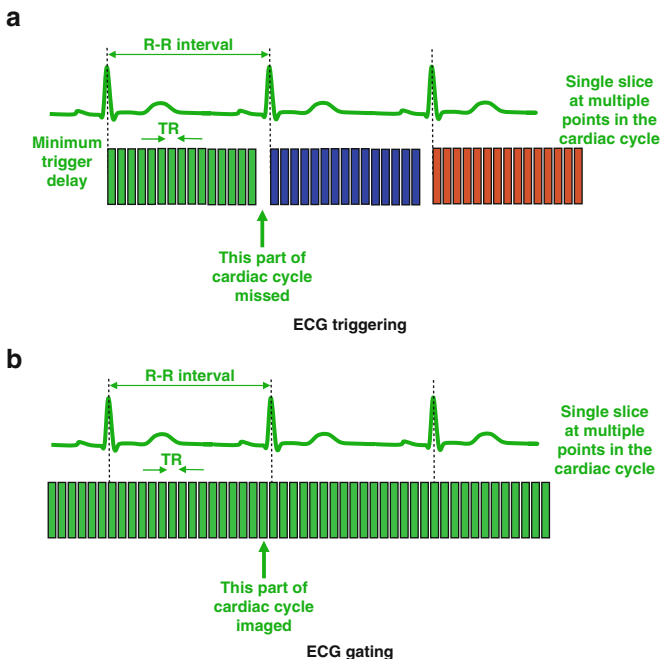


FIGURE 13.5. (a) ECG triggering initiates the data acquisition immediately after the QRS complex and must stop before the next QRS complex. This results in the last part of the cardiac cycle not being imaged. (b) For ECG gating data acquisition is continuous. If the data is sorted retrospectively, data can be assigned accurately to the end of the cardiac cycle, ensuring the whole of the cardiac cycle is imaged.

synchronization pulse is used to mark when a repetition of the pulse sequence is coincident with the “R”-wave. The signals from this and subsequent repetitions are then related to the corresponding time points in the cardiac cycle. This can be done either prospectively or retrospectively.

13.4 Prospective Versus Retrospective ECG Gating

Prospective gating allocates the MR signal data to points in the cardiac cycle as it is acquired. As with triggering, the number of imaged time points is preselected. This selection allows for an estimate of the shortest heart beat that is likely to occur during the acquisition. This will always lead to the last few time points in most heart beats being excluded, resulting in a “blind spot” at the end of the cardiac cycle.

Retrospective gating allocates the MR signal data at the end of the entire k-space acquisition. This approach provides more flexibility when imaging patients with beat-to-beat variations in heart rates (most patients!) The method acquires data from the whole of each heart beat, so that heart beats of different lengths will have different numbers of data points recorded. At the end of the data acquisition, an average heart beat interval is calculated from the whole acquisition. Data points acquired from short heart beats are stretched and data from long heart beats are compressed to fit the average heart beat interval, ensuring that all points in the cardiac cycle are imaged. This is particularly important for functional imaging where diastolic ventricular function, mitral or tricuspid valve function, diastolic flow measurement or atrial contraction are of interest.

Retrospective gating works well for normal beat-to-beat variations in the R-R interval. There is also usually an option for data points acquired from excessively long or short heart beats to be rejected and reacquired. This is known as arrhythmia rejection. In cases where there are many arrhythmias, however, rejection of data is not practical and the only option

is to use a “real-time” image data acquisition for which ECG synchronization is not required (see Sect. 16.8).

13.5 Spoiled Gradient Echo versus bSSFP

In general, cine imaging requires very short repetition times to be used, and therefore, can only be achieved using gradient echo-based pulse sequences.

There are two main types of gradient echo pulse sequence used for cine imaging. These have the generic names, spoiled gradient echo and balanced steady state free precession (bSSFP). MR manufacturers also have their own names for these pulse sequences and these are also given in the following sections.

Spoiled Gradient Echo

Siemens:	FLASH	Fast Low Angle Shot
Philips:	T1 FFE	T1-weighted Fast Field Echo
GE:	SPGR	Spoiled GRASS (Gradient Recalled Acquisition in the Steady State)

The need for very short TR values means that the transverse magnetization generated by one rf excitation pulse still exists when the next rf pulse is applied. This can potentially contribute to, or interfere with, the signal during the following TR. In spoiled gradient echo, this signal is de-phased (or spoiled) using a spoiler gradient at the end of each TR period, so that its contribution to subsequent TR periods is removed (Fig. 13.6a). The resultant sequence, with a short TR and TE, essentially behaves as a T1-weighted pulse sequence. As a very short TR is used, tissue or blood that remains in the slice becomes saturated (Fig. 13.7). This sequence thus relies on the flow of blood to generate contrast as described in Sect. 12.3.

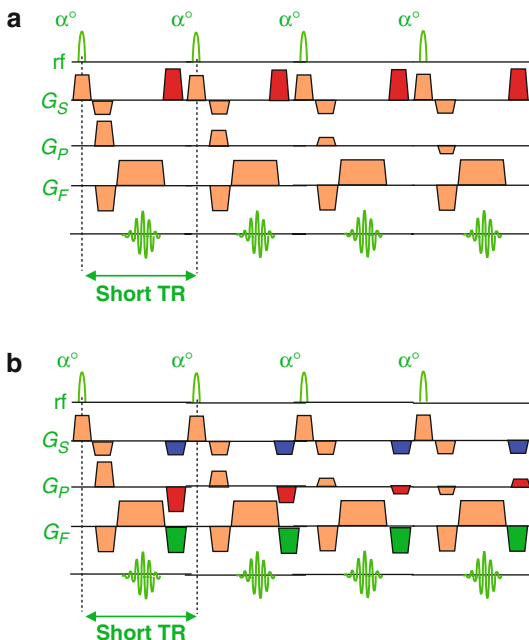


FIGURE 13.6. (a) Spoiled gradient echo pulse sequence. The spoiler gradients (shown in red) destroy any residual transverse magnetization prior to the next Rf pulse. The contrast is therefore essentially T1 weighted. (b) bSSFP pulse sequence. Additional gradient pulses (shown in blue, red and green) are added to ensure that the all transverse magnetization is in phase when the next rf pulse is applied. This modifies the contrast behavior so that it is related to the T2/T1 ratio.

Balanced Steady State Free Precession (bSSFP)

Siemens:	True FISP	True Fast Imaging with Steady Precession
Philips:	bFFE	Balanced Fast Field Echo
GE:	FIESTA	Fast Imaging Employing Steady State Acquisition

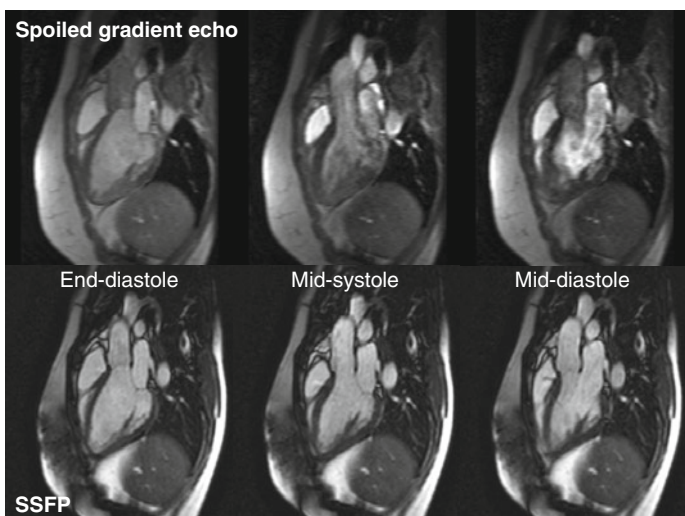


FIGURE 13.7. Images taken from a cine gradient echo series using (*top row*) spoiled gradient echo pulse sequence and (*bottom row*) a balanced SSFP pulse sequence. The images shown correspond to the end diastolic, mid-systolic, and mid-diastolic time points within the cardiac cycle. Note how the blood signal intensity varies through the cardiac cycle when using the spoiled gradient echo pulse sequence due to the speed and direction of flow, enabling the qualitative assessment of blood flow patterns. The blood signal intensity is more consistent through the cardiac cycle bSSFP, providing better definition of the endo-cardial boundary and the valve leaflets.

Balanced SSFP gradient echo sequences are designed to ensure that the transverse magnetization is not spoiled but fully re-phased at the end of each TR period (Fig. 13.6b) when the next rf pulse is applied. This then carries over into the next repetition and is superimposed onto the transverse magnetization generated by that rf pulse. After a number of repetitions this gives rise to a steady state condition where the transverse magnetization from two or three successive repetition periods combine to give a much greater signal.

The contrast behavior of bSSFP sequences is very different to the spoiled gradient echo sequences (Fig. 13.7). bSSFP

contrast is related to the T2/T1 ratio, with fluid and fat in particular appearing as brighter than other tissues. Because the transverse magnetization originating from several TR's are combined, the SNR for bSSFP is much greater compared to spoiled gradient echo. The increased SNR allows a higher bandwidth to be used, resulting in a shorter TE, TR, and therefore, improved imaging efficiency. However, if the magnetic field is not uniform, the transverse magnetization from different TRs can destructively cancel rather than add together in areas of magnetic field inhomogeneity, making the bSSFP technique prone to dark banding artifacts across the image. Patient-specific dynamic shimming (see Sect. 1.1) is therefore very important to achieve images that are free of banding artifacts over the region of interest. Keeping the TR as short as possible also helps to minimize the banding artifacts observed in bSSFP imaging.

Cine imaging is generally used to image cardiac function and blood flow patterns. The choice of whether to use a spoiled gradient echo or bSSFP pulse sequence depends on the information required. Table 13.2 describes the most common applications of cine imaging techniques and choice of pulse sequence in each case.

TABLE 13.2. Common applications for cine gradient echo techniques.

Cine imaging technique	Pulse sequence	Information
Cine gradient echo (Sect. 16.8 and Sect. 19.4)	Spoiled gradient echo	Function, qualitative flow assessment, flow jets, regurgitation
Cine SSFP imaging (Sect. 16.8 and Sect. 19.4)	Balanced SSFP	Function, volumetric measurements
Velocity mapping (Sect. 16.9 and Sect. 19.6)	Spoiled gradient echo	Flow velocity, flow rate
Myocardial tagging (Sect. 16.10 and Sect. 19.5)	Gradient echo or bSSFP	Intramyocardial motion/contraction

Summary

- In order to acquire images of the beating heart, the MR pulse sequence and data acquisition must be synchronized with the patient's ECG signal.
- Still imaging uses the ECG signal to "trigger" the image data acquisition at a single chosen time point (trigger delay) after the R-wave.
- Still imaging is used to image cardiac anatomy, for tissue characterization or to image the coronary arteries.
- Cine imaging acquires image data at multiple time points (cardiac phases) throughout the cardiac cycle to produce a sequence of images that can be viewed as a movie.
- Cine imaging that uses ECG triggering does not image the last part of the cardiac cycle.
- Retrospective gating allows the pulse sequence to run continuously and the acquired data is assigned retrospectively to the cardiac phases. This ensures that the whole cardiac cycle is imaged.
- Cine gradient echo imaging is used to image cardiac function, ventricular wall motion and to qualitatively assess blood flow patterns.
- Two main types of gradient echo sequence are used for cine imaging, Spoiled gradient echo and balanced steady state free precession (bSSFP).
- For the spoiled gradient echo technique, the bright blood contrast is highly dependent on speed and direction of flow, and flow jets are highly visible.
- For the bSSFP technique, the Bright Blood contrast depends more on the relaxation properties of blood and is more consistent, but flow jet are less visible.

Chapter 14

Dealing with Respiratory Motion

For conventional imaging methods, the phase encoding gradient is incremented with each successive heart beat, acquiring a single line of k-space each heart beat and resulting in imaging times of several minutes. This means that images using these techniques are degraded by *respiratory motion* (see Sect. 17.3).

Image degradation caused by respiratory motion can be reduced by using one of three possible approaches:

- Respiratory Compensation methods (*Respiratory Gating*)
- *Fast imaging* techniques with patient *breath holding*
- *Ultra-fast (single-shot)* imaging techniques (*real-time imaging*)

In practice, most cardiac imaging is performed with patient breath holding combined with fast imaging techniques and these are described in Chap. 15. Respiratory compensation methods are described in this section.

14.1 Respiratory Compensation (Respiratory Gating)

These require the patient's respiratory cycle to be monitored. The simplest way to do this is to use a pneumatic bellows system attached to the abdomen by a Velcro band (Fig. 14.1). The data acquisition is then controlled or gated (Fig. 14.2),

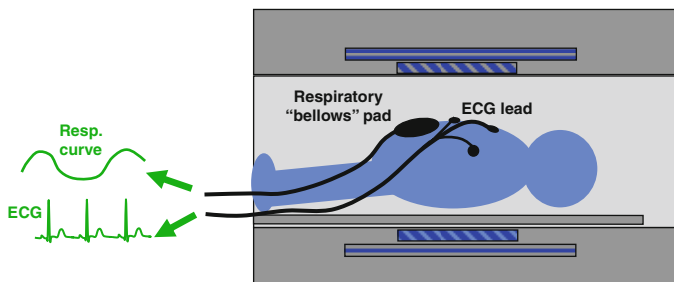


FIGURE 14.1. The patient respiratory cycle is monitored by placing a pneumatic bellows device on the patient's abdomen held in place using a Velcro band. The change in pressure caused by movement of the abdomen generates a waveform that is related to the respiratory cycle.

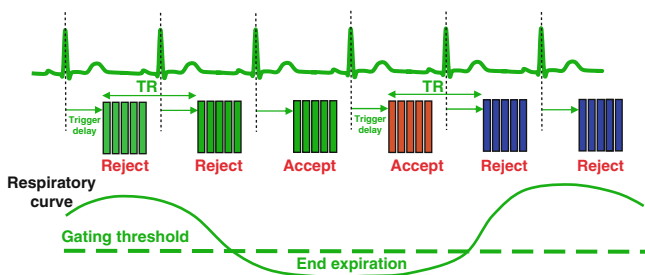


FIGURE 14.2. A respiratory gating threshold is set automatically such that data is accepted and stored in k-space if the data acquisition occurs when the respiratory curve is below the threshold (assumed to correspond to end-expiration). When the respiratory curve lies above the threshold the acquired data is rejected and the same line of k-space is reacquired until data acquisition again falls within the end-expiratory period.

such that data is acquired predominantly from one part of the respiratory cycle (usually end expiration, as it is assumed that most patients spend longer periods there). Typically a gating threshold is set automatically and data from each cardiac cycle is either accepted or rejected depending on whether it

is acquired either above or below the respiratory gating threshold. More sophisticated methods acquired data throughout a greater part or the whole of the respiratory cycle, but restrict the acquisition of the central lines of k-space to within the gating threshold. In this case, the phase encoding steps can be reordered on the fly, according to the respiratory cycle.

14.2 Respiratory Gating using Navigator Echoes

A more accurate method is to use real-time monitoring of the diaphragm position by the use of *navigator echoes* (Fig. 14.3).

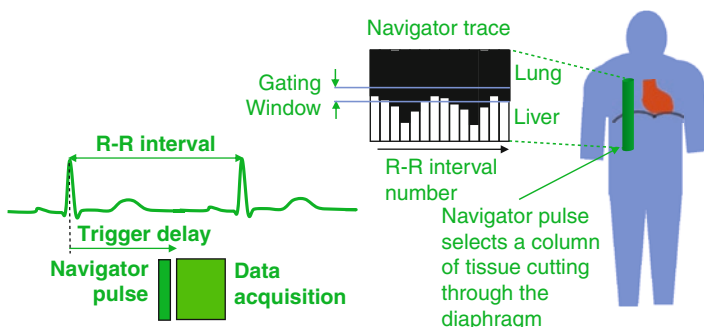


FIGURE 14.3. Respiratory gating using navigator echoes use a specially designed rf pulse (or pulses) to excite a column of tissue through the diaphragm immediately before each image data acquisition. A line of signal is reconstructed from each navigator echo and displayed as a trace. The boundary between the low signal intensity in the lung and the relatively high signal intensity in the liver creates an edge that can easily be detected and used as a gating signal, which accurately reflects the diaphragm position and is used to determine whether the data is accepted or rejected. The accuracy of this method allows narrow gating windows to be set (typically 5 mm) for high resolution applications such as coronary artery imaging.

Summary

- MR images acquired using conventional spin echo or gradient echo methods over several minutes are degraded by respiratory motion artifacts.
- The effects of respiratory motion can be limited by:
 - Respiratory compensation or gating
 - Patient breath holding combined with fast image acquisition
 - Ultra-fast (real-time) image acquisition.
- Respiratory gating only accepts image data that is acquired at one phase of the respiratory cycle (usually end expiration).
- The respiratory position is monitored either by a pneumatic bellows device, or by the acquisition of navigator echoes.
- The navigator echo is produced immediately prior to data acquisition by an rf pulse scheme that excites a column of tissue that cuts through the patient's diaphragm.
- This allows more accurate monitoring of the diaphragm, position for high resolution applications such as coronary artery imaging.

Chapter 15

Fast Imaging: How Do We Speed Up the Image Acquisition?

Conventional imaging techniques acquire only one phase encoding step (one line of k-space) per heart beat. It therefore invariably takes several minutes to acquire an anatomical image dataset with conventional spin echo (SE) or a cine image dataset with conventional gradient echo sequences (FLASH, SPGR, FFE).

In order to overcome this limitation to achieve shorter image acquisition times, *fast imaging* techniques acquire more than one line of k-space in each heart beat. This fills up k-space more rapidly, leading to shorter image acquisition times. Pulse sequences that use this principle are known as *fast* or *turbo* pulse sequences. It can be applied to both spin echo and gradient echo pulse sequences.

15.1 Turbo (or Fast) Spin Echo

Philips, Siemens	TSE	Turbo Spin Echo
GE	FSE	Fast Spin Echo

The spin echo (SE) pulse sequence generates a spin echo signal by the use of an excitation pulse followed by a 180° refocusing pulse. Further echoes can be generated from the same transverse magnetization by applying additional 180° refocusing pulses. Each time the echo is de-phased due to the presence of magnetic field inhomogeneities, the de-phasing can be

reversed by the application of a further 180° pulse. The turbo/fast spin echo pulse sequence generates multiple echoes by applying multiple 180° pulses after the initial 90° pulse (Fig. 15.1). After each 180° pulse there is a corresponding spin echo. Each echo is used to fill a new line of k-space by applying a different amount of phase encoding to each one, prior to data sampling.

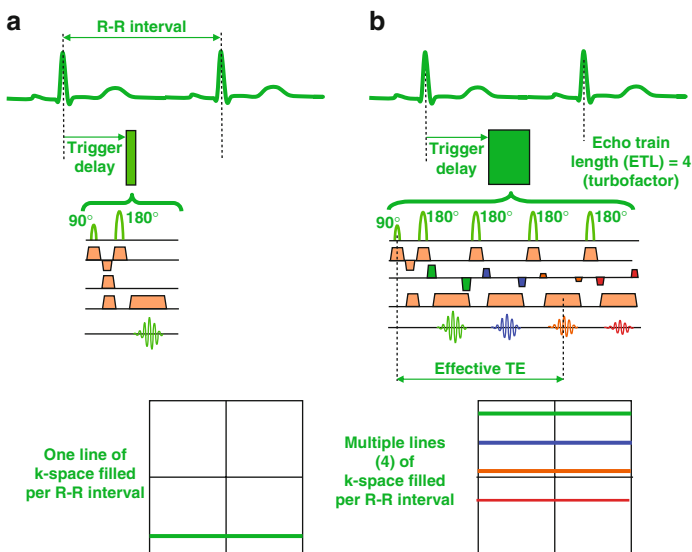


FIGURE 15.1. The conventional spin echo pulse sequence (a) applies a single 180° pulse following the 90° pulse to generate a single spin echo. One line of k-space is filled each R-R interval. The fast/turbo spin echo pulse sequence (b) applies multiple 180° pulses following the 90° pulse to generate multiple spin echoes. Multiple lines of k-space are filled within each R-R interval by applying a different amplitude of the phase encoding gradient to each echo. In this diagram each phase encoding gradient is color coded corresponding to the line of k-space filled. The phase encoding applied to each echo is removed by applying an equal and opposite phase encoding gradient after each echo is sampled. In this example, four 180° pulses are applied to generate four spin echoes (known as turbofactor= 4). This provides a fourfold reduction in scan time.

The number of echoes acquired for each excitation pulse is known as the *echo train length (ETL)* or “*turbofactor*” and this defines the acceleration factor for the pulse sequence. Typically, echo train lengths of 15 or 16 are used in order to reduce the imaging time to within a breath hold period. Each successive echo in the echo train has a different echo time. The amplitude of each echo diminishes as its echo time increases according to T2 decay. The echo which is acquired closest to the center of k-space (with the smallest phase encoding gradient) defines the *effective echo time* for the sequence, as this is the echo time that has the greatest influence on the image contrast.

For cardiac imaging, fast (or turbo) spin echo pulse sequences are commonly used in combination with a double inversion “black-blood” magnetization preparation scheme (Sect. 12.2) to acquire anatomical images of the heart and major vessels. One or two slices are typically acquired within each breath hold period.

15.2 Turbo (or Fast) Gradient Echo

Acceleration of cine gradient echo imaging is achieved by simply repeating the gradient echo pulse sequence a number of times rapidly acquiring a number of lines of k-space within each cardiac phase (Fig. 15.2). Each group of k-space lines acquired is known as a *shot*. This is repeated for each cardiac phase and then for each heart beat, each time acquiring a different group of lines in each successive heart beat until the whole of k-space is filled. This is known as *multiple shot imaging*, and is also known as *segmented k-space* gradient echo imaging, as k-space is segmented into a series of groups of lines.

The parameter that defines the *number of lines of k-space* acquired in each shot is dependent upon the manufacturer as follows:

Philips	Turbofactor
Siemens	No of segments
GE	Views per segment

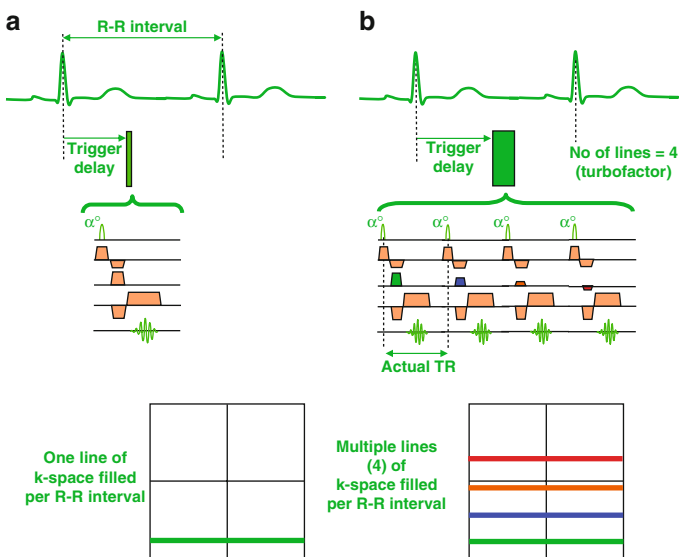


FIGURE 15.2. The conventional gradient echo pulse sequence (a) applies a single low flip angle rf pulse to generate a single gradient echo. One line of k-space is filled each R-R interval for each cardiac phase. The fast/turbo gradient echo pulse sequence (b) rapidly repeats the low flip angle rf pulse to generate multiple gradient echoes. Multiple lines of k-space are filled within each R-R interval by applying a different amplitude of phase encoding gradient to each echo. In this diagram each phase encoding gradient is color coded corresponding to the line of k-space filled. In this example, four rf pulses are applied to generate four gradient echoes, known as turbofactor= 4 (Philips), no of segments = 4 (Siemens), no of views per segment = 4 (GE). This provides a fourfold reduction in scan time.

This determines the acceleration factor for a particular pulse sequence. For functional imaging it also determines the length of the acquisition window corresponding to each phase of the cardiac cycle. Increasing the “turbofactor” decreases the scan time (shortens the length of breath hold) but increases the acquisition window for each cardiac phase, thus limiting the number of cardiac phases that can be imaged (the cine frame rate or temporal resolution). In order to

maximize the number of cardiac phases and minimize the breath hold period, a very short TR must be used.

For breath hold cine gradient echo imaging, this method of accelerated image acquisition can be applied to both the commonly used types of gradient echo pulse sequence described in Sect. 13.4. The vendor-specific names for the “turbo” or “fast” versions of these sequences are given below:

Fast Spoiled Gradient Echo

Siemens	TFL	TurboFLASH
Philips	T1-TFE	T1-weighted Turbo Field Echo
GE	FSPGR	Fast Spoiled GRASS

Steady State Free Precession (SSFP)

Siemens	Segmented True FISP	
Philips	BTFE	Balanced Turbo Field Echo
GE	FIESTA	Fast Imaging Employing Steady State Acquisition

When the whole of k-space is filled in a *single shot*, the cine sequence can be acquired within a single heart beat and cardiac synchronization is no longer necessary. This is known as “*real-time*” imaging.

15.3 Echo Planar-Imaging (EPI)

One of the fastest techniques available is known as echo-planar imaging (EPI). This is a gradient echo technique that generates multiple gradient echoes following a single RF pulse (Fig. 15.3). The first echo is generated as usual by applying a de-phasing gradient followed by a frequency encoding gradient applied in the opposite direction. Once the first echo has been sampled and de-phased, the frequency encoding gradient is then successively reapplied with alternating sign, each time re-phasing and de-phasing the transverse

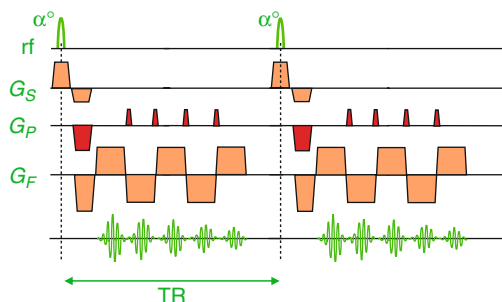


FIGURE 15.3. The Echo-Planar Imaging (EPI) pulse sequence is a gradient echo pulse sequence that rapidly alternates the direction of the frequency encoding gradient. Each time the gradient is switched a gradient echo is formed. Multiple lines of k-space are filled within each R-R interval by applying a small phase encoding gradient (shown in red) prior to sampling each echo. In this example, the frequency encoding gradient is switched five times after the initial de-phasing gradient to generate five gradient echoes. This provides a fivefold reduction in scan time.

magnetization to form a new gradient echo. The amplitude of each successive echo rapidly diminishes according to $T2^*$ decay so it is necessary to switch the gradient rapidly and acquire the echoes before the signal decays into the background noise level. To ensure that each echo fills a different line in k-space, a small phase encoding gradient is applied as the frequency encoding gradient is switched in order to increment the amount of phase encoding applied to each echo. In order to sample each echo as quickly as possible, a high bandwidth is used. The use of a high bandwidth, together with the low signal level caused by $T2^*$ decay, results in a low SNR for this technique. EPI is therefore only used for applications where reduced image quality is acceptable in return for greater imaging speed. For cardiac imaging, a hybrid approach is often employed that combines the segmented gradient echo approach and an EPI readout with a short echo train length (known as segmented EPI). Such an approach has been used for perfusion imaging.

15.4 Reducing the Total Number of Phase Encoding Steps Acquired for Each Image

Another common approach to achieve faster imaging is to reduce the number of phase encoding steps required to complete the data acquisition. This can be done by reducing the image acquisition matrix (scan percentage, phase percentage) or by reducing the field of view in the phase encoding direction (*Rectangular Field of View*). Both these approaches have drawbacks as illustrated by the examples in Sect. 8.4.

The number of phase encoding steps can also be reduced by exploiting the symmetry properties of k-space by using *Half Fourier Imaging* (also known as *Half Nex*, *0.5 Nex*, or *Half Scan*). In this case the acquisition is completed when just over half the lines of k-space are acquired (Fig. 15.4). The missing information from the lines not acquired can be predicted by using the symmetry properties of k-space. Typically 65% of the lines are acquired, giving a corresponding

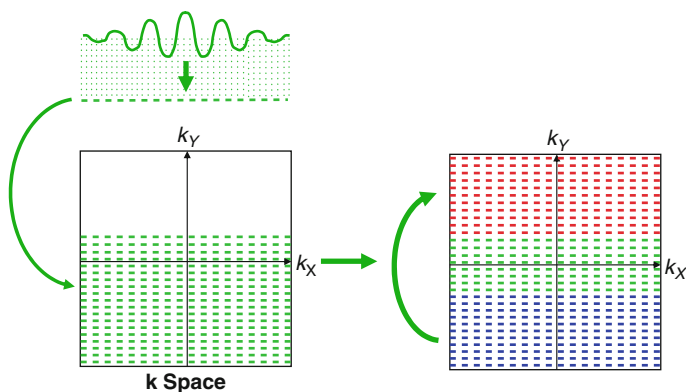


FIGURE 15.4. Half Fourier image acquisition fills only about 65% of the lines of k-space. The symmetry of k-space allows the missing information to be synthesized. The acquired lines of k-space shown in blue are used to synthesize the missing lines in red.

reduction in scan time. As fewer lines are acquired, the SNR is reduced due to the reduction in the number of signal samples (see Chap. 8).

An alternative approach is sometimes used in gradient echo imaging where less de-phasing is applied prior to echo sampling and the echo is re-phased early by the readout gradient. Because the center of the echo occurs earlier than with full echo sampling, this results in a shorter minimum TE and shorter minimum TR, allowing faster imaging. This is known as *partial echo or asymmetric echo* imaging. As with Half Fourier imaging, a reduced number of points in k-space is sampled, resulting in a reduced image SNR (Fig. 15.5).

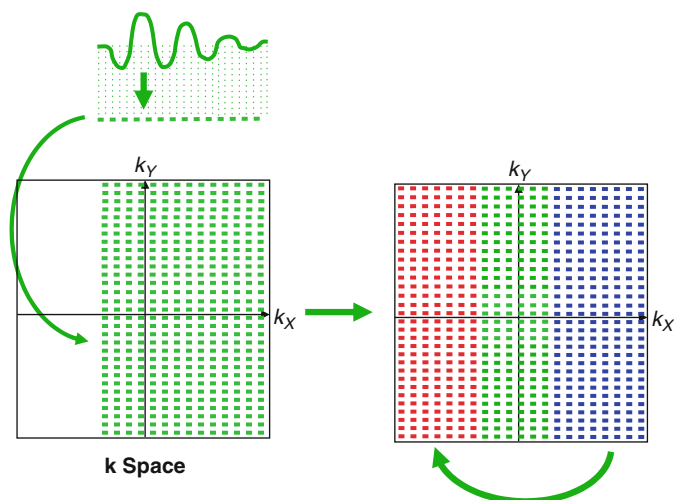


FIGURE 15.5. Partial echo or asymmetric echo is achieved by applying less de-phasing to the FID so that when the readout gradient is applied the center of the echo is attained earlier. This essentially truncates the front of the signal echo, resulting in a shorter TE, and therefore, a shorter minimum TR and a faster imaging acquisition. As with Half Fourier imaging, the symmetry of k-space is exploited with the acquired lines in blue used to synthesize the information for the missing lines in red.

15.5 Parallel Imaging

Parallel imaging is an additional method that can be used to achieve shorter imaging acquisition times by exploiting the spatial distribution of coil elements in an array coil. Here, the number of phase encoding steps required to reconstruct the image is reduced by a certain factor, known as the *Reduction factor*. MR signal data covering the full extent of k-space is acquired, but lines of k-space spaced further apart (k-space is under-sampled). This would normally result in aliasing of information in the image. For example, for a reduction factor of 2, alternate lines of k-space are skipped. This is equivalent to acquiring a rectangular field of view of 50%. In order to reconstruct a full field of view and avoid image aliasing, parallel imaging relies on the distribution of at least two elements of an rf coil array, along the phase encoding direction, to provide the information missed by under-sampling k-space. The reconstruction process requires knowledge of the coil sensitivity profile (a 3D plot of how the detected signal varies with distance from each coil element). Comparing the signal from each coil element, together with the coil sensitivity profile, allows reconstruction of an image without aliasing. This reconstruction step can either be performed in the image space (SENSE) or in k-space (SMASH). A knowledge of the coil sensitivity map or signal intensity distribution for each patient, coil array element, and image slice geometry is essential for this technique to work. Sensitivity maps are formed from the central lines of k-space and can either be acquired as a separate *Reference scan* with SENSE, or concurrently as part of the acquisition (mSENSE, GRAPPA) (Fig. 15.6 and Table 15.1).

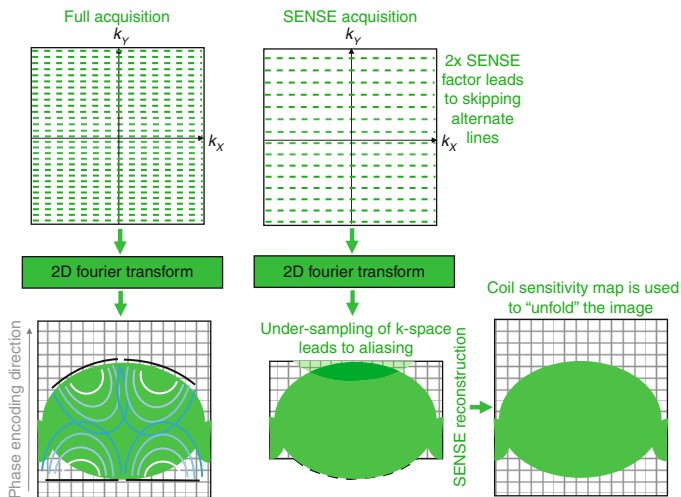


FIGURE 15.6. Parallel imaging uses the spatial distribution of coil array elements and their characteristic sensitivity maps to provide spatial information. This allows under-sampling of k-space (skipping of phase encoding steps) during the acquisition, shortening the image acquisition time. In this example, a SENSE factor of two leads to skipping of alternate lines of k-space. Without the SENSE reconstruction this would lead to an effective reduction of the field of view and image aliasing or “foldover.” The coil element sensitivity maps acquired from the reference data are used during the image reconstruction to “unfold” the image to a full field of view.

TABLE 15.1. Parallel imaging techniques offered by the different vendors.

	Image-based reconstruction (SENSE)	k-space-based reconstruction
Sensitivity map (reference scan)	Separate acquisition	Concurrent
Philips	SENSE	
Siemens		mSENSE GRAPPA
GE	ASSET	ARC

SENSE: SENsitivity Encoding

mSENSE: Modified SENSE

GRAPPA: GeneRalized, Autocalibrating Partially Parallel Acquisition

ASSET: Array Spatial Sensitivity Encoding Technique

ARC: Auto-calibrating Reconstruction for Cartesian Sampling

Summary

- The key principle of fast imaging techniques is to acquire more than one line of k-space within each heart beat.
- This fills up k-space more rapidly, leading to shorter image acquisition times.
- Fast (or turbo) spin echo fills multiple lines of k-space by generating multiple spin echoes with multiple 180° refocusing pulses.
- Fast (or turbo) Gradient echo fills multiple lines of k-space within the same heart beat by rapid repetition of several TR periods (a shot).
- The number of lines of k-space acquired in each determines the acceleration factor:
 - Turbofactor (Philips)
 - No of segments (Siemens)
 - No of views per segment (GE)
- The symmetry property of k-space also allows image acquisition time to be reduced by sampling only just over one half of k-space, either by omitting phase encoding steps (Half Fourier, Half Scan, Half NEX) or by not sampling first part of the echo (Partial Echo, asymmetric echo).
- Parallel imaging exploits the spatial distribution of elements of array coils to reduce the amount of phase encoding required, resulting in faster image acquisition times.

Chapter 16

Special Pulse Sequences for Cardiac Imaging

Spin echo and Gradient echo pulse sequences form the basis for all the advanced pulse sequences that are used in cardiac applications. For most cardiac synchronized applications, the “fast” or “turbo” variant of the pulse sequence is used, that is, *fast or turbo spin echo* and *fast or turbo gradient echo* (see Chap. 15). Depending on the application, further pulses may be added as *preparation pulses* in order to modify the contrast or to suppress the signal from particular tissue types or regions. The addition of preparation pulses is known as *magnetization preparation*. The following sections describe the most common preparation scheme and pulse sequence combinations that are in use for cardiac imaging. Where possible, the common generic and vendor-specific names are given for each technique.

16.1 Selective Tissue Saturation

Common names:	Sat Bands
	REST Slabs
	Presat (Presaturation band)

Spatially selective tissue saturation is a magnetization preparation scheme that is used to suppress the signal from a prescribed region of tissue. It may be a region that is outside the field of view in the phase encoding direction, where the signal is suppressed in order to prevent aliasing (Sect. 17.1), or a region that is subject to physiological motion (respiratory,

peristaltic, or swallowing) in order to prevent motion artifacts (Sect. 17.3). Saturation regions may also be used to suppress the signal from blood flowing into the image slice to remove artifacts caused by pulsatile blood flow (Sect. 17.4). In this case they are positioned at an upstream location parallel to the image slice. The saturation region is selected as a slab (thick slice) of tissue, by using a selective 90° rf pulse in combination with one or more selection gradients (Fig. 16.1). The combination of gradients determines the orientation of the slab. The rf pulse saturates the magnetization within the slab and the transverse magnetization is de-phased using a spoiler gradient. The pulse sequence used for image data acquisition is then applied immediately afterward. As the magnetization of the tissue within the slab is saturated, it does not contribute any signal, and the region appears on the image as a

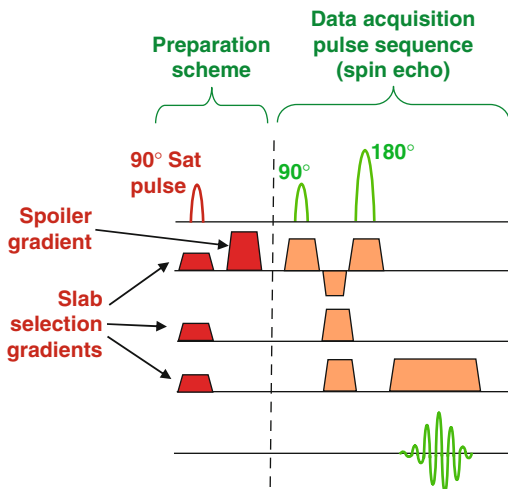


FIGURE 16.1. Selective tissue saturation is achieved by applying a 90° saturation pulse in combination with selection gradients immediately prior to the imaging pulse sequence (in this case, spin echo). This causes saturation of the magnetization within a slab of tissue. The spoiler gradient de-phases any signal contribution from the saturation region.

signal void. Saturation Regions can be placed by the operator manually using the graphical user interface and for some applications they may be placed automatically.

Application	Placement of saturation region
To prevent aliasing	Slab at right angles to image slice, over the tissue outside the field of view in the phase encoding direction
To prevent motion artifact (respiratory, peristaltic, swallowing)	Slab at right angles to image slice, over the tissue that is moving and in line with the region of interest in the phase encoding direction
To prevent suppress signal from flowing blood	Slab parallel and adjacent to the image slice, upstream relative to the direction of flow

16.2 Frequency Selective Fat Suppression

Common names:

(GE, Siemens)	CHESS (CHEmical Shift Selective) pulse
	Fat Sat
(Philips)	SPIR (Spectral Inversion Recovery) (<i>SPIR is not really inversion recovery; it uses a 120° rf pulse, producing a partial inversion</i>)

The suppression of signal from fat is often desirable as the high intensity fat signal can mask other lower intensity features. One method of achieving this is to exploit the difference in Larmor frequency between the hydrogen nuclei in lipid molecules and water molecules (see also Sect. 17.6). There is a difference of 3.5 parts per million in the frequency between them (Fig. 16.2a). At 1.5 T this is a difference of approximately 220 Hz. The signal from the lipid molecules is suppressed by applying a 90° rf pulse at the Larmor frequency of fat (Fig. 16.2b). As no magnetic field gradient is applied, this pulse will saturate (reduce to zero) the z -magnetization of fat within the entire imaging volume, provided that the

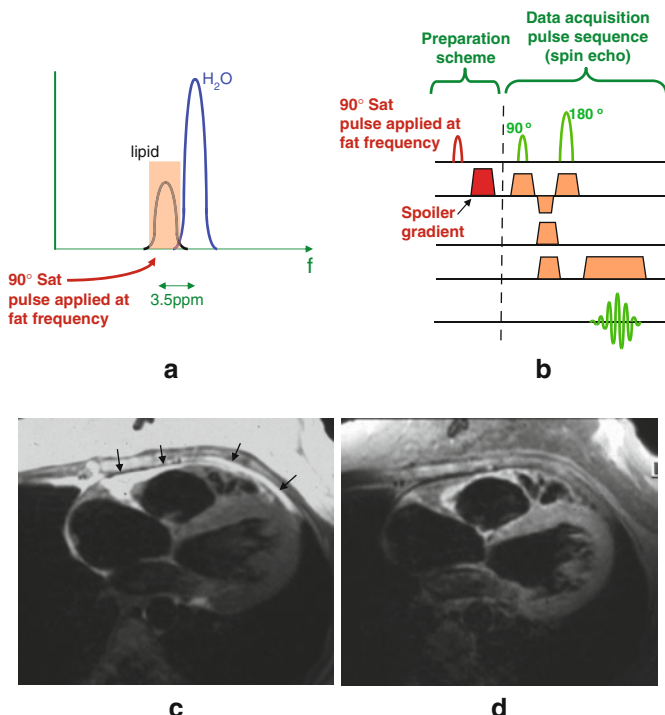


FIGURE 16.2. Frequency selective fat suppression is achieved by exploiting the difference in the Larmor frequency between lipid and water (**a**). The fat suppression preparation scheme applies a 90° saturation pulse at the Larmor frequency of fat immediately prior to the imaging pulse sequence (**b**). The transverse magnetization produced by this pulse is suppressed by a spoiler gradient. As the magnetization of fat is saturated (reduced to zero), it does not contribute to the signal generated by the spin echo pulse sequence. The image in (**c**) is acquired using a T1-weighted spin echo pulse sequence and an anterior surface receiver coil. Bright signal from pericardial fat is seen anterior to the heart. The image in (**d**) is acquired using the same pulse sequence, but with a frequency selective fat suppression pulse. Note that the signal from fat is now suppressed, providing better assessment of the myocardial thickness around the right ventricular outflow tract.

Larmor frequency is constant (i.e., the magnetic field is uniform throughout the volume). The transverse magnetization produced by the rf pulse is de-phased using a *spoiler gradient* and the pulse sequence used for image data acquisition is then applied immediately afterward. As the fat magnetization is already saturated, it does not contribute any signal and appears on the image as a signal void. For fat suppression to be effective using this method, the magnetic field must be particularly uniform and *dynamic shimming* over the field of view is mandatory.

16.2.1 Pros and Cons of Frequency Selective Fat Suppression (cf. STIR)

Pros	Cons
Can be applied to any pulse sequence (gradient echo, spin echo)	Requires <i>dynamic shimming</i> to ensure a highly uniform magnetic field across the region of interest
Can be applied to T1- or T2-weighted pulse sequences without altering the intrinsic contrast	Does not work well in the presence of metal due to local magnetic field inhomogeneities
Does not significantly increase the time duration of the pulse sequence	Does not work well at low field strengths <1.0 T, where the Larmor frequency difference becomes too small

16.3 STIR and Turbo STIR

Another method of suppressing the signal from fat exploits the differences in T1 relaxation time between fat and other tissues. It uses a preparation scheme with a 180° inversion rf pulse, followed by a delay prior to the imaging pulse sequence (Fig. 16.3). This is known as an *Inversion Recovery (IR)* pulse sequence and the delay is known as the *Time from Inversion, TI*. The inversion pulse is usually slice selective and

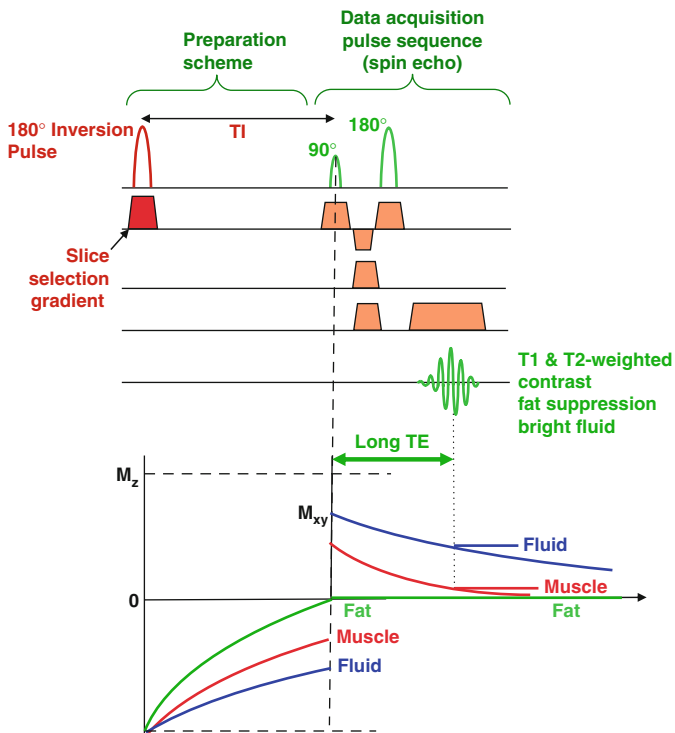


FIGURE 16.3. The STIR pulse sequence consists of a slice-selective 180° inversion pulse followed by a time delay, TI, prior to the imaging pulse sequence (in this case spin echo). The inversion pulse inverts the magnetization of all tissues. The magnetization recovers according to the T1 relaxation time of each tissue. The TI is chosen so that the imaging pulse sequence is applied when the fat magnetization is zero. In the resultant image, the fat signal is suppressed while fluid signal is bright.

inverts the magnetization of all the tissue within the image slice. During the subsequent TI period, the magnetization of each tissue recovers according to its characteristic T1 relaxation time. As fat has the shortest T1 of all the tissues, its magnetization is the fastest to recover back toward its equilibrium value. The TI is chosen so that the imaging pulse sequence is applied at the time when the magnetization value

of fat is zero (typically 160 ms at 1.5 T). It therefore contributes no signal to the acquired image. This particular instance of inversion recovery sequence with a short TI value is known as a *Short TI Inversion Recovery* or *STIR* pulse sequence. It is normally combined with spin echo pulse sequences. When combined with fast or turbo spin echo it may be referred to as *TurboSTIR*. In addition to the suppressed fat signal, a useful characteristic of this pulse sequence is the high signal from fluid. The high fluid signal weighting can be further increased by increasing the TE to introduce T2 weighting in addition to the intrinsic T1 weighting. This pulse sequence is therefore particularly suited for the detection of inflammatory processes and edema. For CMR applications, it is usually combined with a black blood preparation scheme ([Sect. 16.5](#)).

16.3.1 Pros and Cons of STIR (cf. Frequency Selective Fat Suppression)

Pros	Cons
Does not require a highly uniform magnetic field and fat suppression works well in the presence of distortion of the magnetic field by metallic implants	Single type of pulse sequence and a limited range of contrast weighting
Combined T1 and T2 weighting gives High fluid signal, useful for edema, inflammation	IR pulse and TI delay significantly increases the time duration of the pulse sequence
Works well at low field strengths <1.0 T	Cannot be used with contrast agent as this reduces the T1 of the other tissues

16.4 Black Blood FSE/TSE (Double Inversion)

The most commonly-used advanced pulse sequence for anatomical imaging combines the *black blood preparation* scheme described in [Sect. 12.2](#) with the *fast (or turbo) spin echo* pulse sequence described in [Sect. 15.1](#). The black blood preparation

scheme provides consistently high contrast between the heart and vessel walls and the blood pool. The use of the fast (or turbo) spin echo pulse sequence with an echo train length (turbofactor) of between 15 and 20 shortens the image acquisition time so that it falls within a typical breath hold period. One or two slices are typically acquired within each breath hold period. Adjustment of the k-space order within the echo train controls the effective echo time and therefore the T2-weighting of the contrast. For T1 weighting, a short effective echo time is chosen and the pulse sequence is triggered every heart beat to keep the repetition time short (Sect. 19.3.1). For T2 weighting, a long effective echo time is used and the pulse sequence is triggered only every two or three heart beats to make a long repetition time (Sect. 19.3.2). Frequency selective fat suppression may also be applied to suppress the signal from fat if required (Sect. 16.2).

The time delay after the black blood preparation scheme is automatically calculated by the MR system software to provide the best suppression of signal from blood. This depends on the TR of the pulse sequence, which is determined by the patient's heart rate and the number of heart beats between each trigger pulse.

A common problem with this pulse sequence is loss of signal from the myocardium due motion of the re-inverted myocardial tissue out of the image slice between the time of the black blood preparation scheme and the time of the fast (turbo) spin echo data acquisition. This effect can be reduced by increasing the thickness of the slice of tissue that is re-inverted by the second 180° pulse of the black blood preparation scheme. While the image slice thickness may be typically 6–8 mm, a typical value for the black blood inversion preparation pulse is 20 mm. The exact choice depends on how much displacement of the myocardium there is through the slice and requires some adjustment depending on the trigger delay, slice orientation, and location within the heart (Fig. 16.4).

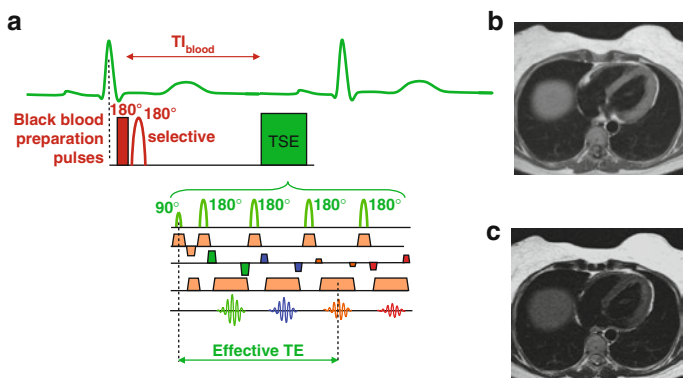


FIGURE 16.4. The black blood fast (turbo) spin eco pulse sequence used for anatomical imaging (a). The black blood preparation scheme is applied at the beginning of the cardiac cycle with the image acquisition in diastole. The exact duration of the black blood inversion, TI_{Blood} , is calculated to provide the best blood suppression and depends on the heart rate and the number of heart beats between each trigger pulse (typically $TI_{Blood} = 400\text{--}600\text{ ms}$). The image in (b) is acquired with short effective echo time every heart beat to generate $T1$ -weighted contrast. The image in (c) is acquired with a long effective echo time every two heart beats to generate $T2$ -weighted contrast. Note the lower signal from the myocardium compared to that in image (b), due to the short $T2$ relaxation time of myocardial muscle.

16.5 Black Blood turboSTIR (Triple Inversion Recovery)

The black blood preparation scheme can also be combined with the turboSTIR pulse sequence described in Sect. 16.3. This provides a pulse sequence that has strong fluid weighting but with no signal from blood within the cardiac chambers and it is particularly useful for the assessment of myocardial edema (Sect. 19.3.2). This pulse sequence consists of the two 180° pulses for the black blood preparation,

followed by a third 180° pulse to provide the STIR contrast. It is therefore sometimes known as a triple inversion recovery pulse sequence. The sequence has two inversion times, TI_{Blood} and TI_{fat} . TI_{fat} has the same value for fat suppression as in the STIR sequence (approx. 160 ms). Calculation of the value for TI_{Blood} is more complicated and depends on the heart rate, the number of heart beats between trigger pulses, and whether the third inversion pulse is slice selective or not. The setting of other imaging parameter values is similar to the black blood FSE/TSE pulse sequence in Sect. 16.4 (Fig. 16.5).

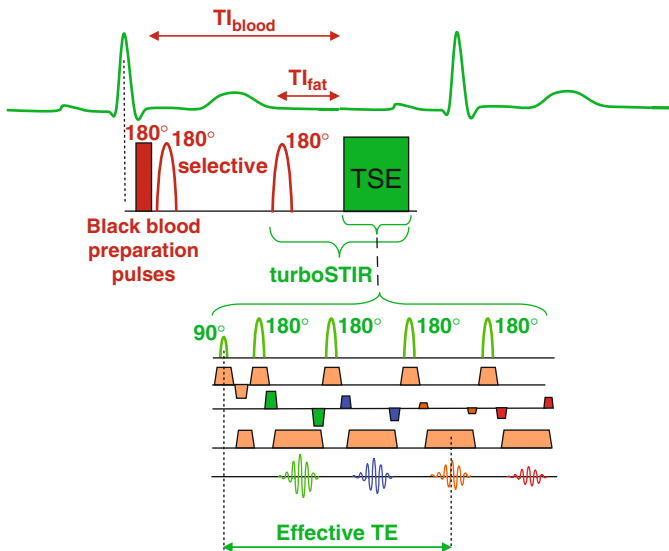


FIGURE 16.5. The black blood turboSTIR (Triple Inversion) pulse sequence used to achieve image contrast with a high signal from fluid. The black blood preparation scheme is applied at the beginning of the cardiac cycle with a further 180° inversion pulse approx. 150 ms prior to image acquisition in diastole. The exact duration of the black blood inversion, TI_{Blood} is calculated to provide the best blood suppression.

16.6 Inversion Recovery Fast/Turbo Gradient Echo

Common names:	Late enhancement
	Delayed enhancement
	Viability Imaging

Inversion recovery preparation schemes can also be combined with fast (or turbo) gradient echo pulse sequences. The most common application for this combination is for the imaging of the myocardium after intravenous administration of an MR contrast medium to differentiate viable myocardial tissue from nonviable, infarcted myocardial tissue (see Sect. 19.9). The *contrast agent* is based on the element *Gadolinium*. Gadolinium is a highly *paramagnetic* substance that mediates the T1 relaxation time of water molecules when it is in close proximity to them. The T1 relaxation time is therefore reduced, demonstrated by an increase in signal intensity when using T1-weighted imaging methods. The contrast agent is carried within the blood pool into the myocardial muscle where it enters extracellular space. Wash-in and wash-out of the contrast is relatively fast for normal myocardium, whereas wash-in and wash-out is delayed for infarcted muscle. Delayed imaging after contrast agent injection using a T1-weighted pulse sequence is therefore able to demonstrate areas of infarction as areas with increased signal where there is a greater concentration of contrast agent. The inversion recovery technique provides T1-weighting and enhances the signal difference between normal and infarcted myocardium by suppressing the signal from normal myocardium (Fig. 16.6). The use of the fast or turbo gradient echo pulse sequence allows image acquisition to be kept within a breath hold period. The delay required following administration of the contrast agent and the enhanced signal from infarcted tissue gives this technique the name *late enhancement* (previously *delayed enhancement*). As this technique is able to differentiate normal (viable) myocardial tissue from infarcted

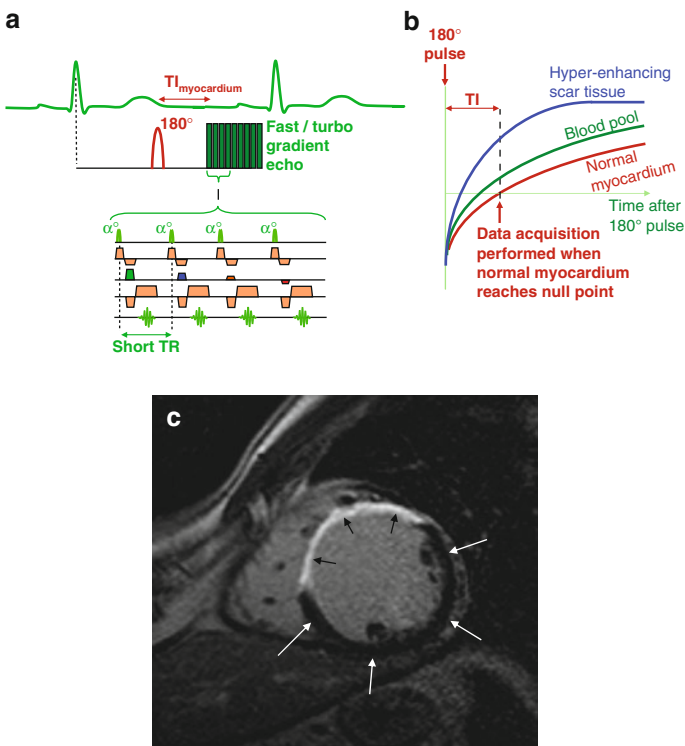


FIGURE 16.6. Late enhancement imaging is performed using an inversion recovery fast (or turbo) gradient echo pulse sequence (**a**). The fast (or turbo) gradient echo pulse sequence allows the image acquisition to be completed within a few heart beats. Image acquisition is normally performed in diastole to minimize the effects of heart motion. The 180° inversion pulse is followed by a delay, $TI_{\text{myocardium}}$, selected to suppress the signal from normal myocardium. The graph in (**b**) shows the relaxation curves for normal myocardium, the blood pool, and scar tissue. The higher concentration of contrast agent within scar tissue results in a faster T1 relaxation rate and therefore an increased signal compared to the blood pool and normal myocardium. Nulling the signal from normal myocardium maximizes the scar tissue contrast. The image in (**c**) shows the enhanced signal from scar tissue (*small black arrows*), and the nulled signal within the normal, viable myocardium (*white arrows*).

(nonviable) myocardial tissue, it is also sometimes referred to as *viability imaging*.

The quality of late enhancement imaging depends on the effective suppression of the signal from normal myocardium. This requires very precise selection of the appropriate inversion time, $TI_{\text{myocardium}}$, which depends on many factors, including the dose of contrast, the delay after administration, and the rate of renal excretion. The TI is therefore chosen by performing a number of fast, low-resolution test image acquisitions at different TIs, typically within the range from 200–250 ms in steps of 25–50 ms. The TI from the test image that demonstrates the best suppression of normal myocardium is then used to perform imaging at full resolution. This can also be achieved by performing a so-called *TI-scout*, which acquires images at multiple time delays after a single inversion pulse within the same acquisition.

16.7 Navigator-Gated 3D Fast/Turbo Gradient Echo (Coronary Artery Imaging)

Imaging of the coronary arteries is one of the most challenging applications of cardiac MR imaging due to their small size and their motion with the cardiac and respiratory cycles. The most common pulse sequence used to image the coronary vessel lumen is a *three-dimensional (3D) gradient echo* pulse sequence, combined with a series of preparation pulses to optimize the vessel contrast (Sect. 19.10). The use of a gradient echo pulse sequence for data acquisition provides a relatively enhanced signal from flowing blood. The 3D data acquisition allows thin slices to be acquired to achieve a high resolution data set (Sect. 8.5). The acquisition of a high resolution 3D data set requires a long acquisition time, even when using a fast/turbo sequence. This acquisition method cannot therefore be combined with breath holding and the acquisition must therefore be both cardiac triggered and respiratory gated.

The preparation scheme includes a rf pulse that is used to produce a *navigator echo* that is used to gate the MR acquisition with respect to the respiratory cycle (see Sect. 14.2). *Frequency selective fat suppression* (Sect. 16.2) is used to suppress the fat signal surrounding the coronary arteries. The image data acquisition is also preceded by a *T2-preparation* scheme. This scheme uses the same series of pulses as a fast spin echo train (90° – 180° – 180° – 180° – 180°) which produces a transverse magnetization that is T2 weighted. The final pulse in this scheme is a 90° that restores this magnetization along the *z*-axis. This pulse scheme helps to suppress the signal from the myocardium (short T2) relative to the blood signal (long T2) (Fig. 16.7).

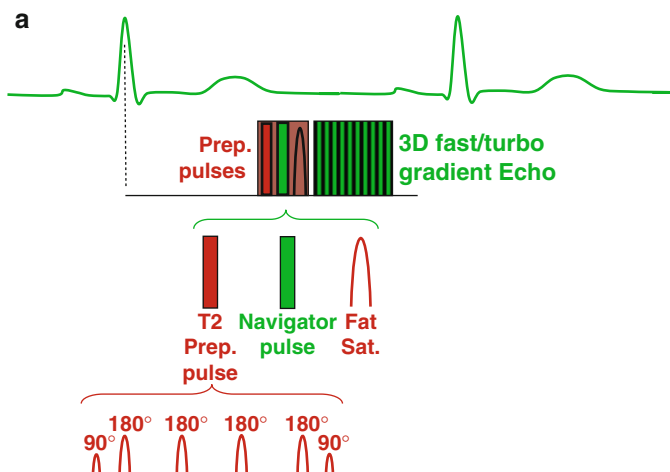


FIGURE 16.7. Navigator-gated three-dimensional (3D) fast gradient echo pulse sequence for coronary artery imaging (a). The preparation scheme consists of a T2-preparation pulse, a navigator rf pulse and a frequency selective fat suppression pulse. The data acquisition window is positioned in mid-diastole to minimize the effect of cardiac motion. The coronary artery image in (b) is generated from a 3D data set acquired using the pulse sequence in (a). This produced by post-processing the 3D data set on a workstation to produce a curved reformat that follows the course of the left anterior descending artery (arrows).

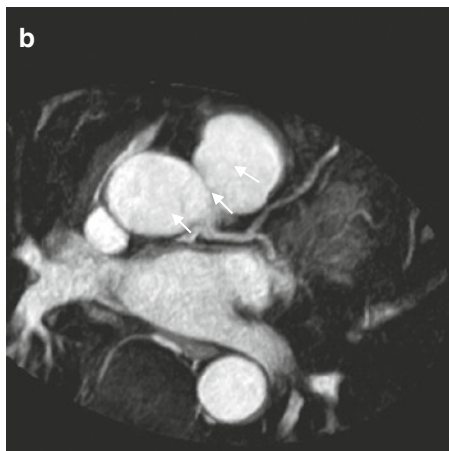


FIGURE 16.7. (continued).

16.7.1 Key Features of a Navigator-Gated 3D Coronary Artery Imaging Sequence

Fast/turbo gradient echo pulse sequence	Enhanced signal from flowing blood and fast image data acquisition window (short TR)
3D data acquisition	Thin slices, high isotropic resolution
Cardiac triggered with data acquisition window in mid diastole	Minimize cardiac motion
Respiratory navigator	Minimize effects of cardiac motion
T2 preparation pulse scheme	Enhance contrast between coronary artery and muscle
Frequency selective fat suppression	Suppress fat bright signal surrounding arteries

16.8 Cine Gradient Echo

Imaging of *cardiac function*, including the assessment of wall motion and volumetric assessment is done using a “*bright-blood* cine gradient echo” technique that acquires images at

multiple heart phases which are displayed as a movie (Sect. 13.2). The most common approach to cine imaging is to combine *retrospective gating* (Sect. 13.4) with a fast or turbo gradient echo method (Sect. 15.2). This allows imaging of the entire cardiac cycle within a single breath hold period (Fig. 16.8). The choice of gradient echo pulse sequence depends on the field strength and the specific application (Sect. 13.5). At 1.5 T the *balanced SSFP* gradient echo sequence is used for most functional imaging applications volumetric assessments due to its high contrast between blood and myocardium throughout the cardiac cycle (Sect. 19.4). The *spoiled gradient echo* pulse sequence is often used for assessment of valvular disease and flow jets, due to its greater flow sensitivity (Chap. 26).

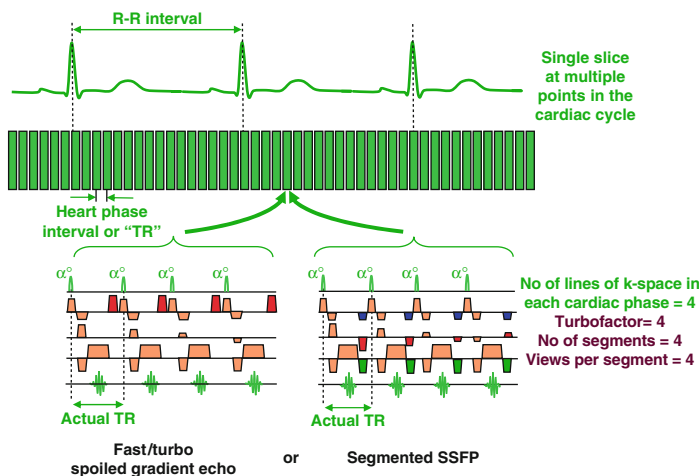


FIGURE 16.8. A retrospectively gated cine gradient echo pulse sequence used for “bright blood” functional imaging. Either spoiled gradient echo or balanced SSFP Pulse sequences may be used for this application. The number of lines of k-space acquired in each cardiac phase (in this example = 4) determines the acquisition time for this sequence (typically within a single breath hold period). Increasing the number of lines (the turbofactor, number of segments or number of views per segment) shortens the acquisition time but increases the time between heart phases (the heart phase interval or “TR”), resulting in poorer temporal resolution.

A key parameter for this pulse sequence is the number of lines of k-space acquired within each heart phase (*turbofactor, no of segments* or *number of views per segment*). Increasing the value of this parameter shortens the acquisition time (Sect. 15.2), but also increases the time between cardiac phases. This reduces the number of *cardiac phases* within the cardiac cycle and therefore the cine frame rate or “temporal resolution” of the image acquisition (the ability to resolve faster motion). “*Real-time*” imaging is achieved by selecting a very high turbofactor, such that the whole image acquisition is completed in a single cardiac phase in a single heart beat (a *single-shot* acquisition). (see also Section 19.4.1) Since all the phase encoding steps are acquired in a single heart beat, cardiac synchronization is not required for real time imaging.

16.9 Velocity Encoded Cine Gradient Echo (Velocity Mapping)

Qualitative assessment of *blood flow* patterns can be performed using cine gradient echo pulse sequences. Spoiled gradient echo (non-SSPF) pulse sequences are particularly useful for the visualization of flow jets associated with regurgitant and stenotic valves, stenotic vessels and septal defects, due to their inherent sensitivity to the presence of these flow jets (See Sect. 17.5). This sensitivity arises due to the motion of spins within the flowing blood along the magnetic field gradients that are applied as part of the gradient echo pulse sequence. The formation of the gradient echo requires that any de-phasing of the magnetization caused by either the slice selection or frequency encoding gradients to be reversed at the echo time (TE). This is achieved by applying two gradients along the same direction but with opposite signs. This combination is known as a *bipolar gradient* pulse pair. The second gradient reverses (re-phases) the de-phasing caused by the first gradient. For stationary tissue this is generally true, but for spins within flowing blood that change their position along the gradient during the interval between the de-phasing and re-phasing

gradients, the complete reversal of the phase changes that cause de-phasing is not achieved (Fig. 16.9). As a result, the phase of the transverse magnetization within flowing blood is different from the phase of transverse magnetization within stationary tissue and the difference is proportional to the velocity of the blood in the direction of the applied gradient. For a certain velocity, the size of this phase difference depends on the flow sensitivity of the pulse sequence. This depends on the amplitude (or slope) of the bipolar gradients, their duration and the time interval between the two gradient pulses.

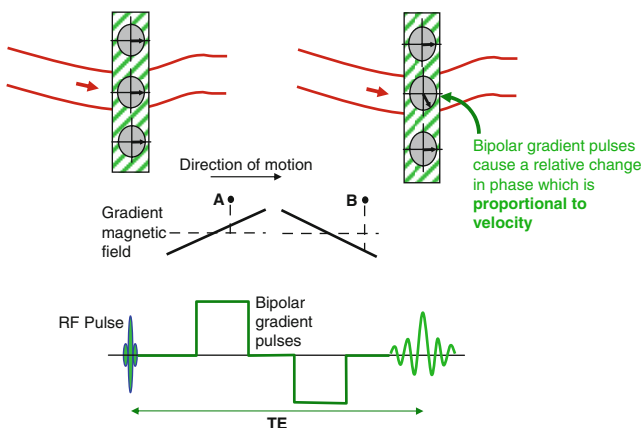


FIGURE 16.9. All imaging pulse sequences use magnetic gradients for purposes such as slice selection and frequency encoding. These usually consist of two gradients applied in the same direction but with opposite sign (known as a bipolar gradient pulse pair). The second “re-phasing” gradient pulse reverses the de-phasing caused by the first gradient to ensure the transverse magnetization is fully re-phased at the echo time, TE. Whilst this is achievable for stationary tissue, proton magnetic moments (spins) within flowing blood that move along the gradient during the time interval between the two gradient pulses do not experience the same change in magnetic field when the second gradient magnetic field is applied. The transverse magnetization within the flowing blood therefore acquires a different phase relative to the transverse magnetization within the stationary tissue. This difference in phase is proportional to the blood flow velocity along the direction of the gradient.

This inherent flow sensitivity is exploited to enable the quantification of *blood flow velocity* by generating images, known as *Phase Maps* that depend upon the phase of the transverse magnetization, rather than its magnitude (see Sect. 16.9). There are, however, a number potential of causes of relative change in phase of the transverse magnetization. These include:

- Phase changes due to motion along more than one gradient direction (multiple velocity components)
- Phase changes due to magnetic field inhomogeneities

The phase changes due to the above causes must be accounted for in order to isolate the change that is due to motion along the desired gradient direction. This is achieved by performing two consecutive acquisitions for each phase encoding step (Fig. 16.10). The two acquisitions are identical other than that

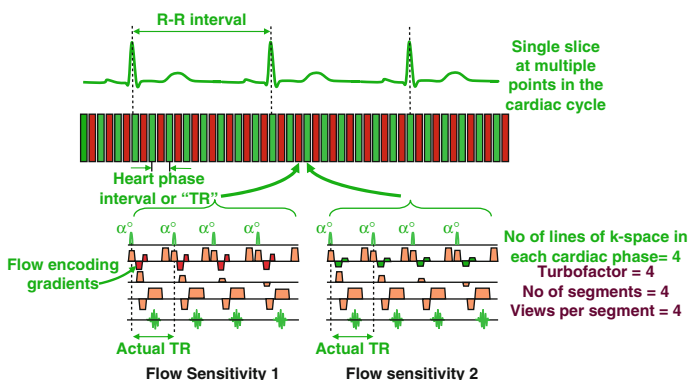


FIGURE 16.10. Velocity mapping uses a fast or turbo cine gradient echo pulse sequence combined with retrospective gating. Two acquisitions are performed for each encoding step with different flow sensitivities. This is achieved by changing the amplitude of the bipolar flow encoding gradients between the two acquisitions. In this example, the 4 k-space lines for each cardiac phase are played out twice; once for each flow sensitivity. Alternatively, the change in flow sensitivity may be interleaved with the change in phase encoding step. In either case the use of two acquisitions for velocity encoding doubles the time between the cardiac phases (heart phase interval or “TR”), leading to poorer temporal resolution compared with an equivalent cine gradient echo pulse sequence without velocity encoding.

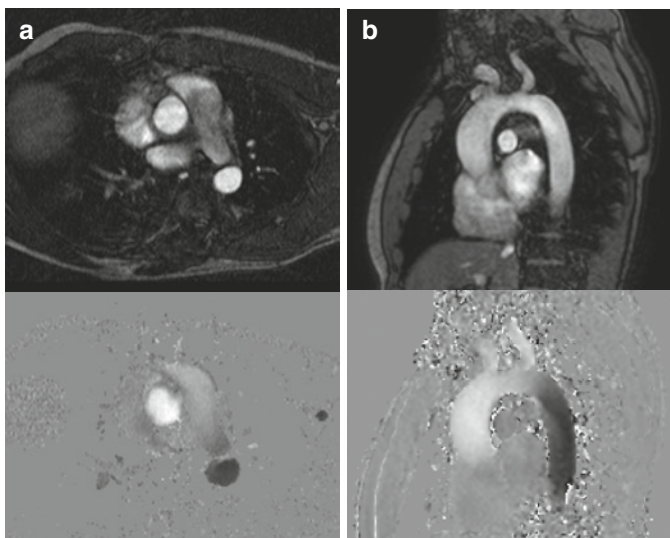


FIGURE 16.11. Examples of velocity-encoded cine gradient echo imaging. The images in (a) show the signal “magnitude” (top) and velocity map (bottom) of an axial slice acquired through the level of the great arteries. Velocity encoding is for through-plane flow (inferior-superior direction) with flow toward the head displayed as higher intensity gray levels (toward white) while flow towardsthe feet is displayed as lower gray levels. Stationary tissue (zero velocity) is displayed as mid-gray. The images in (b) show an oblique sagittal image slice through the aortic arch. In this case the velocity encoding direction is selected to be along the image plane in the superior-inferior direction. In both examples, the images shown correspond to mid-systole, and therefore show significant forward blood flow through the aorta.

they have different flow sensitivities in the chosen direction of flow measurement. This is known as the *velocity encoding direction* and is determined by the amplitude, duration, and time separation of the bipolar flow-encoding gradients in that direction. Once the image data acquisition is complete, phase maps from the two acquisitions are calculated and subtracted

to produce a *velocity map*. The subtracted velocity map contains only phase shifts that are related to velocity components in the flow-encoding direction. Phase changes due to other causes, including velocity components in other directions and magnetic field inhomogeneities are removed by the subtraction.

Velocity maps are generally displayed using a grey scale with stationary tissue being displayed as mid-grey, with velocities in forward (positive) and reverse (negative) directions being represented as higher (toward white) and lower (toward black) intensities (Fig. 16.11).

The maximum measurable *velocity range*, sometimes known as the *VENC*, is defined by the MR operator. It is determined by the difference in the flow sensitivities of the two acquisitions. The imaging of blood flow with velocities that are higher than the chosen VENC results in aliasing of the velocity value, with positive velocities being displayed as negative velocities and vice versa (Fig. 16.12). Selecting a VENC that is too low is a common pitfall of velocity-encoded cine MR imaging. The presence of flow jets or turbulence presents a further pitfall when attempting to quantify blood flow velocities as they can cause signal loss (see Sect. 17.5). At low signal magnitudes, calculation of the signal phase becomes unreliable, resulting in spurious velocity measurements. This pitfall can be avoided by selecting a short echo time for the cine velocity mapping gradient echo pulse sequence (Fig. 16.13).

16.10 Myocardial Tagging (Binomial Pulses)

Imaging of heart wall motion is routinely performed using cine gradient echo pulse sequences. In addition, it is possible to assess intramyocardial motion by “tagging” the myocardium at end diastole with a line or grid pattern, which then deforms as the heart wall contracts (Sect. 19.5). Myocardial tagging is done using a specialized preparation scheme consisting of series of nonselective rf pulses, (together known as a composite or binomial rf pulse) combined with a series of gradient pulses, known as modulating gradients (Fig. 16.14). The

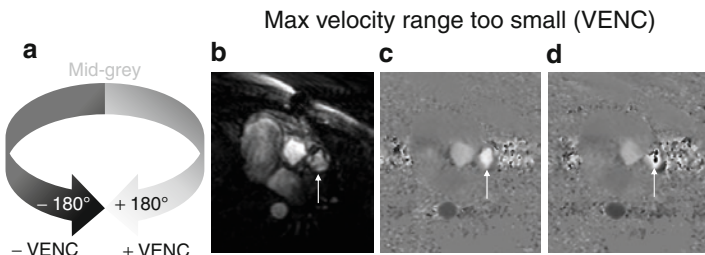


FIGURE 16.12. The selection of the velocity encoding sensitivity (VENC) determines the maximum velocity that can be measured with a velocity-encoded cine pulse sequence, corresponding to a velocity-related phase shift of $\pm 180^\circ$ in the flow encoding direction (a). Blood flow velocities above that selected range are aliased, appearing as velocities in the opposite direction. The image in (b) shows a magnitude image taken from a cine series at the level of the pulmonary valve (arrow). (c) shows the corresponding velocity map during early systole, showing high forward blood flow velocity through the pulmonary valve (arrow). The image in (d) shows a velocity map further into systole, where the velocity at the center of the pulmonary outflow tract has increased to a value greater than the VENC. Velocity aliasing is seen as a few black pixels at the center of the vessel. This acquisition would normally be repeated with a higher VENC in order to remove the aliasing.

effective flip angle of the composite rf pulse is around 90° . The modulating gradients are applied in between the rf pulses and along a direction that is parallel to the image slice. The tagging preparation scheme is applied immediately after the R-wave (at end diastole) and superimposes a “magnetization” pattern across the image slice consisting of lines of tissue that are alternately saturated or at equilibrium. A cine image data acquisition is then performed using a gradient echo pulse sequence.

On the first image of the cine series (immediately after the tagging pulse), the magnetization pattern appears as a series of low-signal-intensity parallel lines across the image. As the heart contracts through systole, the magnetization pattern deforms as it follows the contraction of the myocardial muscle

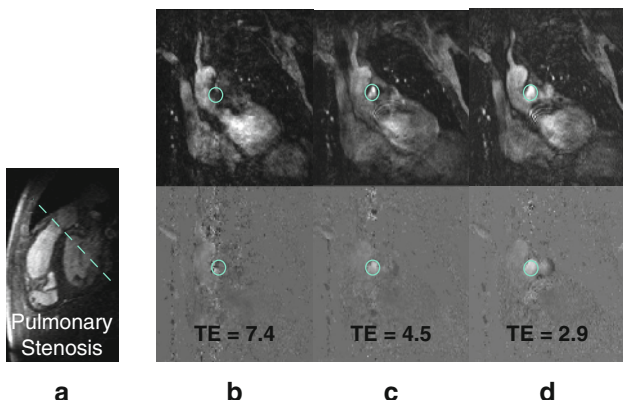


FIGURE 16.13. The *dotted line* in (a) shows the image orientation used to acquire velocity encoded measurements at the level of the pulmonary valve in a patient with pulmonary valve stenosis. The subsequent images show the magnitude image (*top*) and corresponding velocity map acquired through the valve during mid-systole. A circle indicates the location of the pulmonary artery cross section. In (b) an echo time of 7.4 ms is used, resulting in complete loss of signal in the magnitude image and an unreliable velocity calculation. In (c) a shorter echo time of 4.5 ms is used, resulting in reduced signal loss, although the velocity map is still unreliable and underestimates the velocity within the pulmonary artery. In (d) an echo time of 2.9 ms is used, minimizing the signal loss and providing a more reliable estimate of velocity.

(Fig. 16.15). As the pattern is generated through saturation of the tissue magnetization, the pattern fades during the cardiac cycle as T1-relaxation causes the magnetization to return toward its equilibrium value. Typically, two line patterns are generated at right angles to form a grid pattern. This can be done by using two tagging preparation pulses within the same acquisition (known as grid tagging), or by performing two separate acquisitions with line tagging at right angles, and subsequently combining the two data sets as a post-processing step.

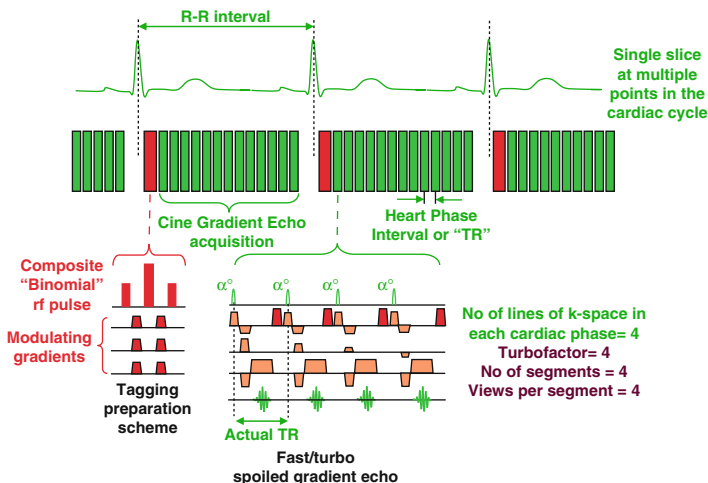


FIGURE 16.14. Myocardial tagging pulse sequence with a tagging preparation scheme applied immediately after the R-wave followed by a fast cine gradient echo acquisition. The tagging preparation scheme consists of a composite “binomial” rf pulse (in this example consisting of three nonselective rf pulses) combined with modulating gradient pulses. The modulating gradients (two pulses in this example) are applied in between the rf pulses along a direction parallel to the image slice. This generates a magnetization pattern across the image consisting of parallel lines of saturated tissue.

16.11 Saturation Recovery, Single-Shot Fast Gradient Echo for Dynamic, Contrast-Enhanced Myocardial Perfusion Imaging

Assessment of myocardial perfusion is achieved by imaging the heart during the first pass of an MR contrast agent through the coronary circulation and the myocardial

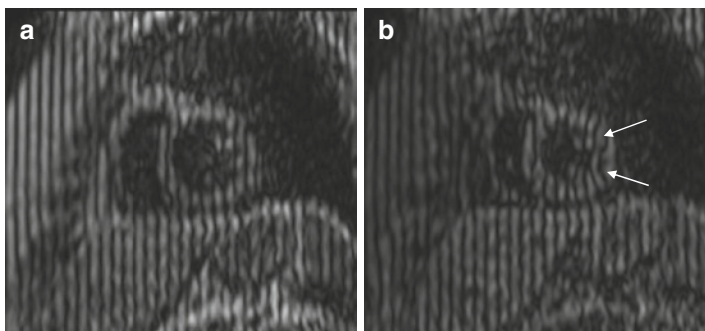


FIGURE 16.15. Example images from a myocardial tagging cine pulse sequence. Image (a) is taken from the cine series immediately after the tagging preparation scheme has superimposed a magnetization pattern of vertical lines across the image slice. Image (b) is taken from the same cine series at end-systole when the left ventricle has fully contracted. Note the deformation of the line pattern due to contraction of the myocardial muscle, especially in the left ventricular free wall (arrows). Analysis of the tagged line displacement can provide a quantitative assessment of myocardial strain.

tissue. This requires a technique that is rapid enough to acquire an entire image at several slice locations within a single heart beat. A single-shot gradient echo-based technique is used for data acquisition (Fig. 16.16). Fast gradient echo, balanced SSFP, and segmented EPI pulse sequences have all been used and each has advantages and disadvantages (see Sect. 19.8). T1 contrast is generated by using a saturation recovery (90°) preparation pulse as the effect of this pulse is independent of heart rate variations. Methods to further accelerate the data acquisition such as *half Fourier* imaging and *parallel imaging* are also commonly used in order to improve the spatial resolution of the technique.

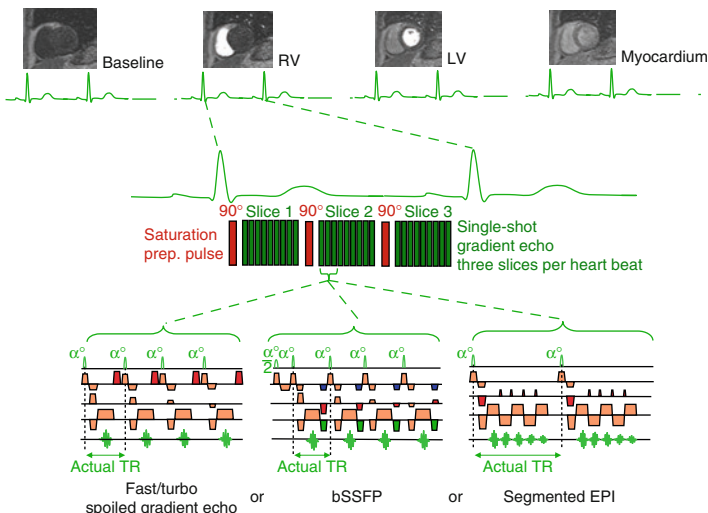


FIGURE 16.16. A schematic diagram showing the key features of a myocardial perfusion imaging sequence. Imaging is performed as a dynamic series, during which a short bolus of MR contrast agent is injected intravenously. The image acquisition is performed using single-shot gradient echo-based acquisition with a 90° saturation-recovery preparation pulse. The single shot acquisition must be sufficiently rapid to enable the acquisition of a complete image at several slice locations (in this example, 3 slices) within a single heart beat. The pulse sequence may be a fast (or turbo) gradient echo, balanced SSFP, or segmented EPI pulse sequence. The saturation recovery preparation generates T1-weighted contrast so that contrast agent appears bright in areas of high concentration. Typical appearances of the images during the first pass of contrast agent through the heart are shown including a baseline image (before contrast medium arrives in the heart), as the contrast arrives in the right ventricle, the left ventricle, and then, as it perfuses, the myocardium.

Summary

- Fast (or turbo) spin echo pulse sequences and fast (or turbo) gradient echo pulse sequences form the basis for all advanced cardiac MR imaging techniques.
- Magnetization preparation schemes are used to modify contrast or suppress signal from specific tissues or regions.
- Different combinations of the above provide the following special pulse sequences for cardiac imaging:
 - Selective (regional) tissue saturation
 - Frequency selective fat suppression
 - Use of short TI inversion recovery for fat suppression and high fluid signal weighting (STIR, turboSTIR)
 - Use of black blood preparation for T1- and T2-weighted fast(turbo) spin echo for anatomical imaging
 - Combination of black blood preparation with turboSTIR technique for imaging of myocardial edema.
 - Inversion recovery fast(turbo) gradient echo in combination with contrast medium for imaging of myocardial infarction (late enhancement imaging).
 - Combination of 3D fast(turbo) gradient echo with respiratory navigator gating for coronary artery imaging
 - Retrospectively-gated cine gradient echo imaging for imaging cardiac function
 - Velocity-encoded cine gradient echo imaging for flow quantification
 - Myocardial tagging pulse combined with cine gradient echo imaging for the assessment of intramyocardial contraction
 - Use of a saturation recovery preparation combined with single-shot, fast gradient echo for dynamic, contrast enhanced myocardial perfusion imaging.

Chapter 17

Common Artifacts

17.1 Image Aliasing

Common names:	Aliasing
	Fold-over
	Back-folding
	Wrap-around

Image aliasing occurs when the imaged subject is larger than the field of view in the phase encoding direction. Aliasing is a consequence of the phase encoding process: While the number of phase encoding steps used to complete the image acquisition is sufficient to uniquely encode all the locations within the field of view, locations outside the field of view are not uniquely encoded (Fig. 17.1). At the edge of the field of view, the phase increments in steps of 180° with each phase encoding step (see Sect. 6.8). A little further beyond the edge of the field of view (point A), phase changes in steps of 185° are indistinguishable from phase changes in steps of -175° corresponding to locations just inside the opposite edge of the field of view. Signal originating at point A is therefore reconstructed to appear at point B and aliasing occurs (Fig. 17.2a).

A number of common solutions that can be used to reduce or remove image aliasing are listed in Table 17.1.

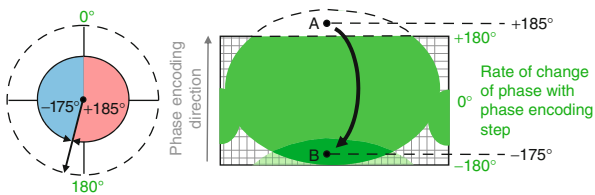


FIGURE 17.1. Diagram demonstrating the cause of image aliasing or foldover. The phase encoding process is designed to encode locations in the phase-encoding direction only within the predefined field of view. As the phase encoding gradient is incremented, the phase of the transverse magnetization at locations within the field view changes with steps in the range of $+180^\circ$ to -180° , enabling reconstruction at the correct location. The location at A, outside the field of view, has a phase that changes in steps of $+185^\circ$. This is indistinguishable from the phase change of -175° at point B, inside the field of view. Signal from point A therefore appears at point B.

Why Doesn't Aliasing Occur in the Frequency Encoding Direction?

In theory, aliasing could also occur in the frequency encoding direction but this is easily avoided by data *over-sampling*. Over-sampling doubles the rate at which the MR signal echo is digitally sampled to acquire double the number of data samples. This doubles the frequency range (bandwidth) that can be accurately detected, effectively doubling the field of view in the frequency encoding direction. Once the image has been reconstructed, image data outside the prescribed field of view are discarded. As over-sampling when frequency encoding is achieved by doubling the sampling rate, the sampling time of the MR signal echo is unchanged and there is no penalty of increased imaging time (unlike phase-oversampling). Frequencies originating from outside the prescribed field of view can also be easily removed prior to image reconstruction by analogue or digital filtering with high-pass filters when the signal is digitally sampled and stored. Both of these methods are commonly used together in practice.

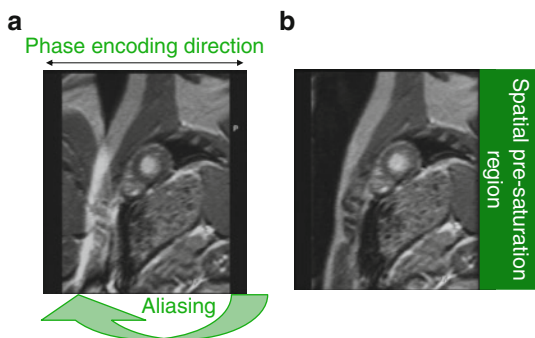


FIGURE 17.2. Short-axis image of the heart (a) showing aliasing of signal from the posterior chest wall from outside the field of view onto the anterior chest wall. The use of a selective tissue saturation region placed outside the field of view posteriorly (b) suppresses the signal from the posterior chest wall and removes the aliased signal.

TABLE 17.1. Common solutions to remove/reduce image aliasing.

Solution	Disadvantage/comment
Increase field of view	Reduced spatial resolution
Acquire additional phase encoding steps (phase-oversampling, foldover suppression, no phase wrap)	Increases image acquisition time
Swap phase and frequency direction	May introduce aliasing in the other direction
Use selective tissue saturation (sat bands) See Fig. 17.2b	Slight increase in image acquisition time
Use a surface coil or switch off unwanted elements of array coil	May reduce SNR over part of region of interest

17.2 Aliasing Artifacts with Parallel Imaging

Common name:	Residual foldover
--------------	-------------------

Image aliasing can be a particular problem when using Parallel Imaging techniques such as SENSE. These techniques achieve a reduction in image acquisition time by

reducing the number of acquired phase encoding steps, and under-sampling k-space. This has the same effect as reducing the field of view in the phase encoding direction, which causes image aliasing. The subsequent SENSE reconstruction, making use of coil sensitivity information, removes any aliasing due to this under-sampling process and reconstructs a full field of view image. If the field of view in the phase encoding direction after SENSE reconstruction is still too small to encompass the subject, this will cause aliasing that cannot be removed by the SENSE reconstruction. Furthermore, it appears at the center of the image rather than the edge (Fig. 17.3).

The approaches to remove SENSE aliasing artifacts are the same as the approaches listed in Table 17.1 for standard aliasing. An additional option here is to fractionally reduce the SENSE factor at the expense of a slightly longer acquisition time.

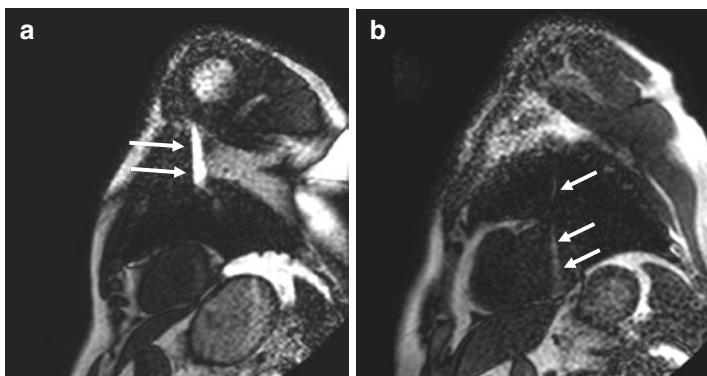


FIGURE 17.3. (a, b) Short axis images taken from a dynamic series of saturation recovery-prepared gradient echo perfusion imaging sequence acquired with parallel imaging (SENSE factor 2). Note the SENSE aliasing artifact at the center of the field of view (straight arrows). In these examples the artifact could be removed by repeating the acquisition after re-centering the field of view to the right, ensuring that the posterior chest wall is included in the field of view.

17.3 Ghosting Artifacts from Motion (Respiratory)

Patient motion during the image acquisition typically results in smearing or ghosting of signal across the image in the phase encoding direction. This is because the phase encoding process is the method by which signal is correctly assigned to a location in the phase encoding direction. If tissue is changing position between each TR (or phase encoding step) this leads to misplacement of the signal in the image. Motion that is random or asynchronous with the TR typically results in smearing of signal in the phase encoding direction. A typical example of such an artifact is that caused by *respiratory motion* (Fig. 17.4).

Motion artifacts are more prominent if the motion occurs when the data acquisition is close to the center of k-space (usually the middle of the image acquisition). Motion that is more periodic (cardiac or respiratory) will result in discrete, repeated ghosts in the phase encoding direction. Motion that has a periodicity that is close to a multiple of the pulse sequence TR results in particularly strong ghosting. Common solutions to remove or reduce respiratory ghosting are given in Table 17.2.

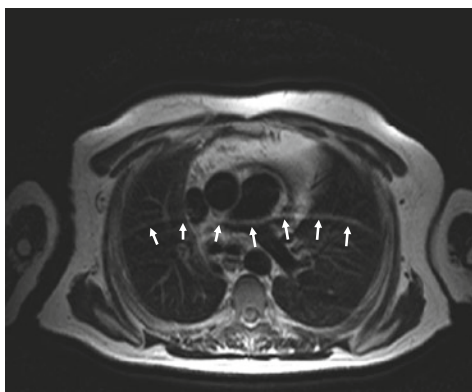


FIGURE 17.4. An axial black-blood turbo spin echo image through the great vessels where the patient has been unable to completely suspend respiration. A respiratory ghost artifact is clearly seen (arrows). Note that the shape of the artifact is the same as the anterior chest wall, suggesting that this is the main source of the artifact.

TABLE 17.2. Common solutions to remove/reduce respiratory ghosting.

Solution	Comment
Patient breath-holding combined with fast imaging techniques	Limits acquisition time and therefore spatial resolution)
Respiratory gating using bellows or navigator echoes	Increases image acquisition time (due to rejection of data)
Swap phase and frequency direction	May introduce ghosting in the other direction
Use selective tissue saturation (sat bands) to suppress the signal from anterior abdominal wall	Slight increase in image acquisition time

17.4 Ghosting Artifacts from Motion (Pulsatile Flow)

Another type of *ghosting* caused by motion is that seen from blood vessels carrying *pulsatile blood flow*. Even if the vessel itself is not moving during the cardiac cycle, ghosts are often still visible. This is particularly common with arterial vessels that carry highly pulsatile blood flow, or with pulsatile cerebro-spinal fluid (CSF) motion in the spinal column. The ghosting in this case is due to motion of proton magnetic moments (spins) in the blood (or CSF) along the gradient magnetic fields used for imaging. Motion along magnetic field gradients results in the transverse magnetization of flowing blood having a different phase relative to that of stationary tissue (see Sect. 16.9 and Fig. 16.9). This relative phase difference is proportional to the velocity of motion. If the blood flow velocity is constant, the relative phase difference is always the same and is ignored by the image reconstruction process. For pulsatile flow, unless the pulse sequence is synchronized with the cardiac cycle, the velocity and, therefore, the relative phase difference will be different for each repetition of the pulse sequence. The varying phase change with each repetition is misinterpreted by the image reconstruction process as being a result of the phase encoding process. This results in a series of ghost images of the

vessel appearing in line with the true vessel in the phase encoding direction (Fig. 17.5). Common solutions for removal of ghosting related to pulsatile flow are given in table 17.3.

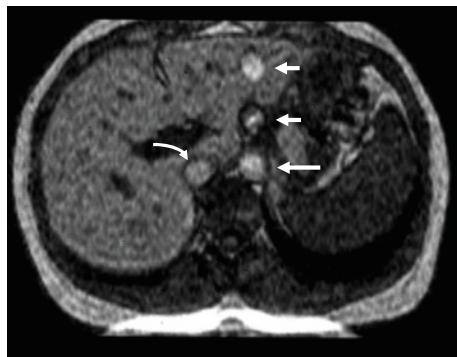


FIGURE 17.5. An axial Spoiled Gradient Echo image through the abdomen showing the abdominal aorta (*large arrow*) and ghosting due to pulsatile blood flow (*small arrows*). Note the absence of ghosting from the much less pulsatile inferior vena cava (*curved arrow*). The phase encoding direction is anterior-posterior. Note also aliasing from the anterior abdominal wall onto the posterior abdominal wall.

TABLE 17.3. Common solutions to remove/reduce ghosting from pulsatile flow.

Solution	Comment
Use cardiac synchronization (ECG triggering or gating) (Chap. 13)	Limits acquisition time and therefore spatial resolution
Use flow compensation (see Box)	Increases image acquisition time (increases minimum TE)
Use selective tissue saturation parallel to the image slice positioned “upstream” (parallel sat bands) to suppress the blood signal flowing into the slice (Sect. 16.1)	Slight increase in image acquisition time
Swap phase and frequency direction	May introduce ghosting in the other direction

What is Flow Compensation?

Flow compensation applies a modification to the gradient pulses to reduce the flow sensitivity of a pulse sequence. It is normally achieved by adding one or more gradient pulses to the pulse sequence where there is already a bipolar gradient pulse. The purpose of the additional gradient pulse(s) is to reduce or nullify the velocity-dependent phase shift caused by motion along the gradient. This reduces flow de-phasing and ghosting artifacts from pulsatile flow.

Common names:	Flow Compensation
	Gradient Moment Nulling
	Gradient Motion Rephasing

17.5 Flow-Related Signal Loss and Flow Jets

Gradient echo-based pulse sequences normally produce images with a “bright-blood” appearance. In the presence of flow jets, however, a signal void is often seen at the location of the jet (Fig. 17.6). This effect is commonly observed while imaging regurgitant valves, stenotic vessels, or the flow through septal defects. The signal void is caused by a de-phasing of the magnetization in the presence of the jet. This is another consequence of the velocity-related phase shift caused by motion along the magnetic field gradients (Sect. 16.9 and Fig. 16.9). The flow jet contains a large range of velocities (sometimes referred to as a *velocity gradient*). This causes a large range of phase shifts, causing de-phasing of the transverse magnetization and therefore resulting in signal loss. The *flow-related signal void* is often qualitatively related to the size and severity of the flow jet and is sometimes used to grade regurgitation, for example. Qualitative assessment of this kind must be done with caution, as the size of the signal void also depends on the pulse sequence type,

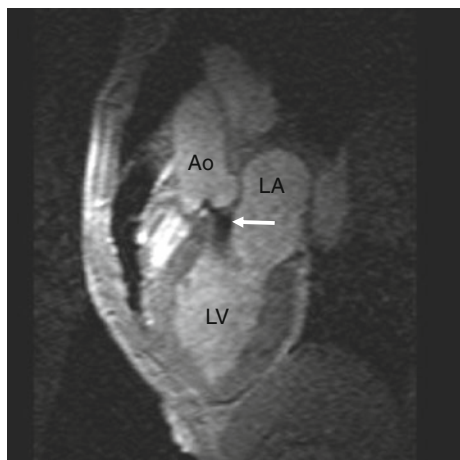


FIGURE 17.6. An image taken from a cine Gradient Echo series, corresponding to diastole. The image is a left ventricular outflow tract (LVOT) view, showing the Aorta (Ao), Left Ventricle (LV) and Left Atrium (LA). The aortic valve is closed while the mitral valve is open. Note the signal void due to the regurgitant flow jet through the aortic valve (*arrow*).

the echo time, and a number of other parameters that affect the imaging gradients strength and duration. For example, increasing the echo time increases the apparent size of the flow jet. Additionally, the same flow jet visualized using a balanced SSFP pulse sequence is smaller than when visualized using a spoiled gradient echo pulse sequence with equivalent imaging parameters. Common solutions to minimise flow-related signal loss are given in table 17.4.

17.6 Chemical Shift Artifact

Chemical shift artifact occurs due to the difference in resonant frequency between fat and water-based tissue. The Larmor frequency for hydrogen nuclei within lipid molecules is lower than that within water molecules by approximately

TABLE 17.4. Common solutions to remove/reduce flow-related signal loss.

Solution	Comment
Reduce echo time	A TE of less than 3.5 ms significantly reduces signal loss but may require use of a high receiver bandwidth, and or partial (asymmetric) echo sampling, reducing SNR
Use flow compensation (see Box)	Increases image acquisition time (increases minimum TE)
Use a balanced SSFP pulse sequence	Balanced SSFP pulse sequences are less flow sensitive than spoiled gradient echo pulse sequences

3.5 parts per million (Fig. 17.7a). This shift in frequency due to the difference in the molecular structure of these two molecules is known as the *chemical shift*. The way in which chemical shift artifacts appear depends on the pulse sequence and its imaging parameters.

When using Spin Echo-based pulse sequences, the chemical shift artifact is most commonly seen when a low imaging bandwidth is selected (e.g., on T2-weighted imaging). As frequency is used to encode position (in the frequency encoding direction), the signals from fat- and water-based tissues become mis-registered relative to one another in the frequency encoding direction (Fig. 17.7). This effect is particularly marked when using a low imaging bandwidth as the bandwidth corresponding to each pixel becomes comparable to, or smaller than the chemical shift between fat and water. The amount of mis-registration may be several pixels, resulting in overlapping of signal at some interfaces and a gap in signal at others.

When using Gradient echo pulse sequences, a second chemical shift artifact effect is seen as a signal void in pixels that contain both fat- and water-based tissue. This is again the result of the signals from the lipid and water at the same location having different frequencies. Immediately after the

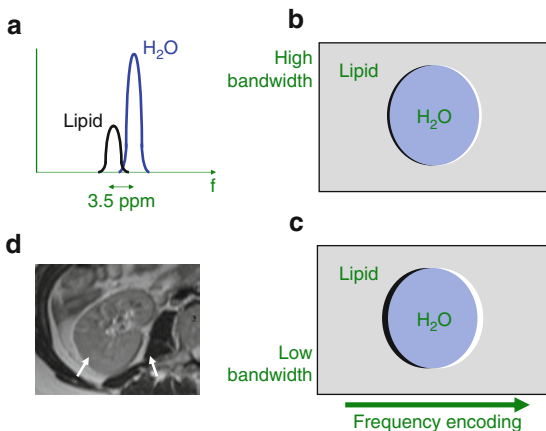


FIGURE 17.7. The Larmor frequency for hydrogen nuclei within lipid molecules is lower than the Larmor frequency for those within water molecules (a). This results in a relative shift in the true position of lipid-based tissue and water-based tissue in the frequency encoding direction (b). This shift is increased when selecting a lower bandwidth (c). This results in bright (signal overlap) or dark (signal gap) artifacts at the interfaces between water and lipid-based tissues, such as the kidneys surrounded by fat (arrows in d).

rf excitation pulse the two signals are in phase but gradually move out of phase as the signals evolve until they cancel (Fig. 17.8). At a later time, they move back into phase, their signals combining. As the two signals continue to evolve, they alternately move out of phase and back into phase. The time at which the gradient echo is sampled (the TE) will determine whether the signals cancel or combine. As this effect depends on the difference in Larmor frequency between fat and water, the chosen echo times will depend on field strength (see Table 17.5). If the TE for the pulse sequence is chosen to coincide with the point when the signals cancel, all pixels containing fat and water appear as a signal void (out-of-phase image, Fig. 17.9a). If the echo time is chosen at the point where the signals are in phase and combine then the same pixels will have a high signal (In-phase image, Fig. 17.9b).

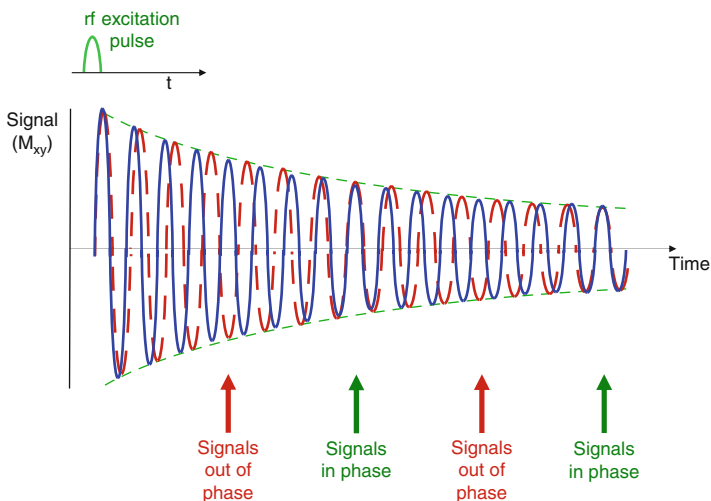


FIGURE 17.8. Diagram showing FID signals from water- (blue) and lipid- (red) based tissue. Immediately after the rf excitation pulse, the two signals are in phase. As the FID signals evolve they alternately move out-of-phase (peaks and troughs oppose each other) and back into phase (peaks and troughs coincide).

TABLE 17.5. Echo times for in-phase and out-of-phase gradient imaging.

Field strength (T)	Out of phase (ms)	In phase (ms)	Out of phase (ms)	In phase (ms)
1.0	3.4	6.8	10.2	13.6
1.5	2.3	4.6	6.9	9.2
3.0	1.2	2.3	3.4	4.6

17.7 Magnetic Susceptibility Artifacts

Magnetic susceptibility artifact arises from variations in the local magnetic field caused by the presence of materials with differing magnetic susceptibility. This is a property of any material that, when placed in a magnetic field, causes the

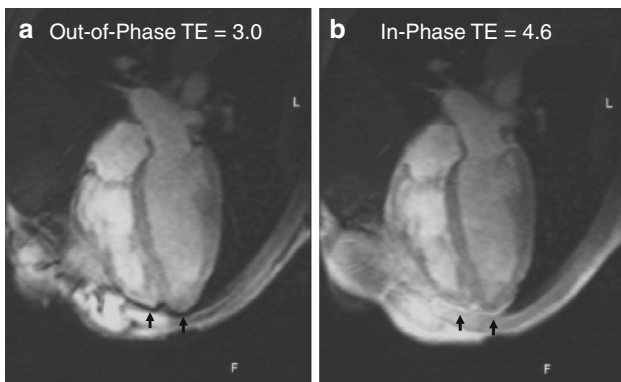


FIGURE 17.9. Images from two cine gradient echo series with different echo times showing a four-chamber view of the heart acquired at 1.5 T. The echo time in (a) is 3.0 ms which is close to the out-of-phase echo time at 1.5 T (2.3 ms). There is a signal void at the interface between the pericardial fat layer and the surrounding water-based tissue (arrows). Image (b) is acquired with an in-phase echo time (4.6 ms) and shows the pericardial fat layer as a bright signal (arrows).

value of the field to either increase (*paramagnetic*) or decrease (*diamagnetic*). Most soft tissues are diamagnetic, but there are significant differences between soft tissue and air, bone, and venous blood (deoxyhemoglobin). Artifacts related to magnetic susceptibility appear when there are two or more tissues or substances that cause a localized change in the magnetic field, effectively creating a small local magnetic field gradient, thus contributing to T_2^* relaxation. This causes local de-phasing of the transverse magnetization. For spin echo sequences, the de-phasing is reversed by the 180° refo-cusing pulse so that it has a negligible effect on the image. For gradient echo pulse sequences, however, the de-phasing causes local signal loss. This signal loss is commonly seen at the boundary between two tissues with different magnetic susceptibilities, or within tissues such as trabecular bone which contains many interfaces within a single voxel.

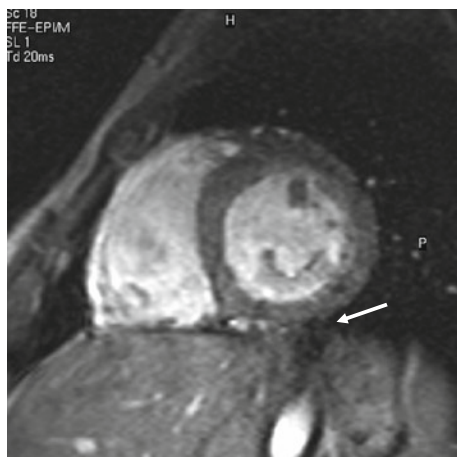


FIGURE 17.10. A short-axis image taken from a Cine Gradient Echo-Echo Planar Imaging (EPI) pulse sequence. Note the signal loss around the great vein (*arrow*) caused by the susceptibility effect of deoxygenated blood.

The signal loss caused by magnetic susceptibility effects increases with increasing echo time as it is a T2* relaxation effect. The effect is particularly marked at tissue-air interfaces around the lungs or bowel and around venous blood in the great veins around the heart. T2*-weighted gradient echo techniques such as echo planar imaging are particularly affected by this (Fig. 17.10).

17.8 Metallic Artifact

The presence of metal, such as clips used in surgery, sternal wires, and heart valves with metallic components, create what is effectively an extreme case of magnetic susceptibility artifact. The local field distortion caused by metal causes de-phasing of the transverse magnetization over a volume that is typically much greater than the size of the implant. The artifact appears as a large signal void on images acquired using gradient echo based techniques. Images acquired using spin echo based methods will have smaller voids with bright

“arc-shaped” artifacts where the magnetization has been partially refocused in the distorted field by the 180° refocusing pulse. In both cases, the size of artifact can be minimized by selecting the shortest possible echo time. In severe cases, the magnetic field distortion also causes significant localized geometric distortion of the image (Fig. 17.11).

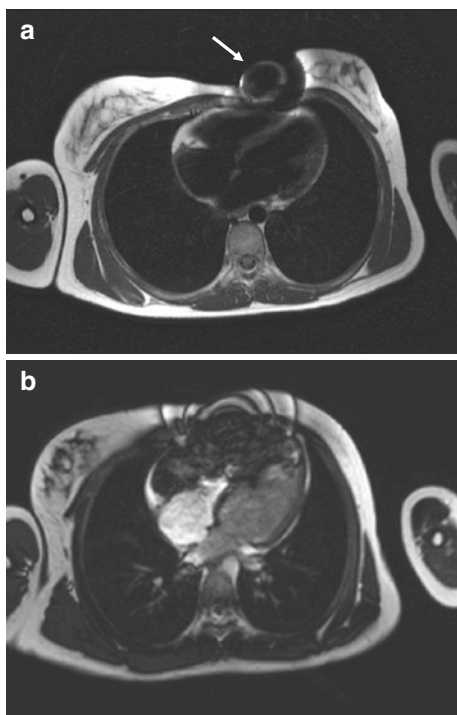


FIGURE 17.11. Two axial images acquired from a patient with a Reveal device implanted in the chest wall. The Black-Blood turbo Spin Echo image (**a**) shows an area of signal loss within the anterior chest wall, containing a bright “ring” artifact where the 180° pulses have refocused some of the signal within the distorted magnetic field. The balanced SSFP image (**b**) shows an area of signal loss that extends into the anterior heart. Note the dark fringes within the subcutaneous fat of the anterior chest wall. This is a characteristic appearance of balanced SSFP pulse sequences in the presence of an inhomogeneous magnetic field. The fringe pattern is indicative of the shape of the magnetic field distortion.

17.9 Radiofrequency Interference Artifacts

Interference can originate from outside the MR environment if the rf shield is damaged or the rf room door is left open (see Sect. 2.1). It can also originate from inside the MR examination room if a piece of electronic equipment that is not MR compatible is taken inside the rf shield, or if the MR equipment itself is faulty.

There are two main kinds of interference: Continuous interference may appear as a line or band of noise across the image in the phase encoding direction (Fig. 17.12a). This is usually caused by bringing non-MR compatible electrical equipment into the exam room, but may also be caused by MR system faults.

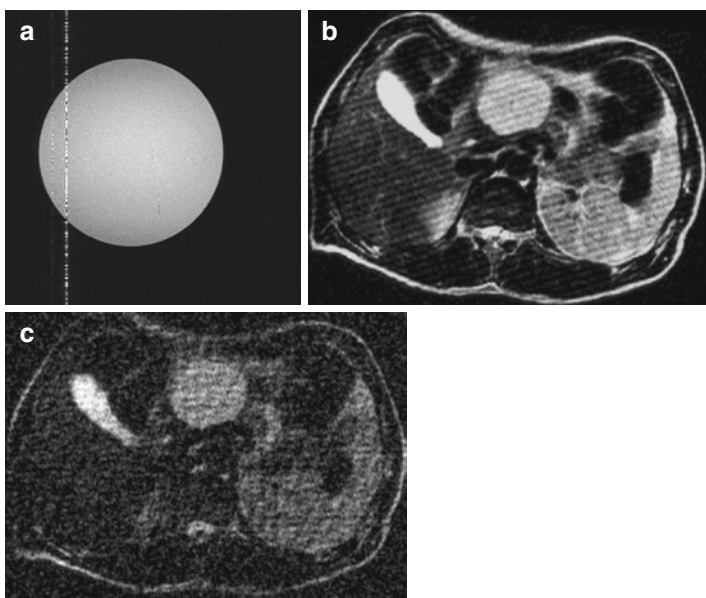


FIGURE 17.12. Examples of artifacts caused by rf interference. (a) An image of a test object showing continuous interference at two frequencies, (one weak, one strong). (b) An abdominal image showing interference from a single interference spike and (c) multiple noise spikes.

An electrical spike (noise spike) generates interference that appears on the image as parallel stripes at any angle across the whole image (Fig. 17.12b). Several spikes will add multiple stripe patterns, giving a herringbone appearance (Fig. 17.12c). These may be caused by faulty MR equipment, very low humidity in the exam room, faulty light bulbs, or even nylon clothing worn by the patient, producing discharges of static electricity.

Summary

- Discusses the causes of the following common image artifacts:
 - Image aliasing in the phase encoding direction
 - Image aliasing with Parallel Imaging
 - Ghosting due to respiratory motion
 - Ghosting due to pulsatile blood flow
 - Flow-related signal loss (flow jets)
 - Chemical Shift Artifact (Spin Echo)
 - Chemical Shift Artifact (Gradient Echo) and In-Phase and Out-of-Phase Imaging
 - Magnetic Susceptibility effects
 - Metal Artifacts
 - Radiofrequency Interference (continuous and noise spikes)
- Remedies and examples are given where appropriate.
- The technique of flow compensation is explained

Part II

How CMR

is Performed

Chapter 18

The Basics of a CMR Study

Sven Plein

18.1 The Referral

A good referral is a key prerequisite for a clinically useful CMR study, providing relevant clinical background information, placing the scan in the appropriate context, and allowing the CMR department to optimally plan the examination ahead of time (e.g., the acquisition protocol, scan duration, special requirements such as sedation). The referral is also an important first step in the safety screening by identifying patients with potential contraindications to MR imaging. All too often, request forms are filled out poorly or incompletely. A well-designed request form will help to ensure that all relevant information is provided.

The request form should include information about

1. Patient demographics
2. Patient height and weight – to identify patients who might not fit in the scanner
3. Possible absolute or relative contraindications to CMR
4. Information on allergies especially to MR contrast media
5. Pregnancy status – although pregnancy is not an absolute contraindication to CMR, a discussion about benefits and potential risks is necessary
6. Results of other imaging tests – this is paramount to provide clinical context

7. Relevant clinical information – to define the clinical questions
8. Information on renal function – see Section 18.3.2.3 below
9. Presence of arrhythmia (it is usually recommended to rate/rhythm control these patients before the CMR scan, unless urgent)
10. The clinical questions to be answered by the CMR study – surprisingly many CMR referrals do not state a clinical question. CMR is a highly versatile imaging test and the scan protocols will vary depending on the clinical indication.

An example of a recommended referral form is given in Fig. 18.1.

Key Points

The CMR Referral Form

- Is key to a clinically useful study
- Can identify patients who may be unsuitable for CMR
- Should contain detailed clinical information and formulate specific clinical questions

Tips and Tricks for Referrals

- In patients with poorly controlled arrhythmia (such as atrial fibrillation), consider deferring referral for CMR until rhythm and/or rate are controlled.
- In obese patients, it is useful to note weight AND height to determine if they are likely to fit in the magnet bore.
- Claustrophobia is not necessarily a contraindication to CMR. Inform the department so that special arrangements (scanning prone or sedation) can be made in advance.
- If the patient has any implanted medical devices, indicate type, model, and year of implantation on the referral form. This saves time on the day of the examination and may avoid the patient being canceled.

Referral form for Cardiovascular Magnetic Resonance scan**Institution details**

Patient Name: _____ Date of Birth: _____

Address: _____ Identification Number: _____

Height: _____ Weight: _____

MRI uses a very strong magnetic field. Some metal objects may interfere with the scanner or be potentially dangerous. Metal in the orbits can lead to blindness. Some MR contrast agents may cause problems in advanced renal failure. Please tick if the patient has:

- | | |
|--|---|
| <input type="checkbox"/> Pacemaker/Implanted defibrillator | <input type="checkbox"/> Pregnancy |
| <input type="checkbox"/> Any implants | <input type="checkbox"/> Allergies |
| <input type="checkbox"/> Metal in eyes (consider orbital x ray) | <input type="checkbox"/> Reaction to MR contrast agents |
| <input type="checkbox"/> Asthma | <input type="checkbox"/> Claustrophobia |
| <input type="checkbox"/> Aneurysm clip | <input type="checkbox"/> brain surgery |
| <input type="checkbox"/> Arrhythmia | |
| <input type="checkbox"/> Renal failure (Result of latest Creatinine _____) | eGFR: _____) |

Clinical details:

Details of other investigations:

ECG: _____

Echocardiogram: _____

Nuclear Perfusion scan: _____

CT scan: _____

Coronary angiography: _____

Specific clinical question(s) this scan should answer:

FIGURE 18.1. Typical CMR referral form.

18.2 Indications for CMR

CMR has become a highly versatile imaging modality with a wide range of clinical indications. These range from assessment of congenital heart disease to the phenotyping of cardiomyopathies and diagnosis of and risk stratification in ischemic heart disease and vascular applications. The currently accepted

indications for CMR are published with their level of evidence in a paper by the ESC.¹ In this book, we will make reference to this publication in the disease-specific chapters in Part III.

The 10 Most Common Indications for CMR

1. Congenital heart disease – initial assessment and follow-up
2. Diseases of the aorta – especially aneurysm and coarctation
3. Assessment of cardiac volumes and function
4. Cardiomyopathy – in particular ARVC, DCM, HCM, and myocarditis
5. Viability assessment – for example post MI
6. Ischemia detection
7. Pericardial disease
8. Cardiac tumors
9. Course of anomalous coronary arteries
10. Heart valve disease

18.3 Contraindications/Safety

CMR, like all MR imaging, is a comparatively safe and harmless imaging procedure that is noninvasive and does not involve the use of harmful ionizing radiation. However, a CMR scanner produces a very strong magnetic field (>10,000 times the strength of the Earth's magnetic field!). The scanner's magnetic and other forces can have important biological effects on patients and health care workers. Therefore, strict procedures have to be observed in the CMR environment to avoid injury or death. At least 15 reports of patient deaths due to MR scanning have been published, mostly associated with pacemakers and other implanted devices, but also include a case in which an oxygen cylinder caused fatal injuries to a child in an MR scanner. Much more frequent than fatal incidents are device malfunctions, burns from wires and injuries from

ferromagnetic projectiles. It is important to remember that the scanner's magnetic field is *always on*, even if the scanner is not in operation, and that the magnetic field extends beyond the physical outline of the scanner.

It is therefore essential that

- Patients undergo a thorough and effective safety assessment and screening procedure before entering the MR environment.
- Patients with contraindications are identified and do not enter the MR scanner room or its fringe field (which are both contained within a controlled area).
- Health care workers involved in MR imaging understand the risks associated with MRI and that this understanding is regularly assessed and documented.
- The institution ensures that procedures and guidelines are in place to control access to the MR environment and to prevent personal items and other potentially problematic objects being brought into the scanner room.

18.3.1 Screening

As outlined above, information on potential contraindications to MR or special circumstances such as pregnancy, disability, or metallic foreign bodies should be obtained from the referral form. This preliminary screening helps to ensure efficient running of the CMR list and allows patients to be listed for further investigations e.g., orbital X-ray imaging ahead of their appointment.²

Upon arrival in the CMR department, patients need to complete a detailed safety questionnaire, in communication with a trained healthcare worker. If required they may need to be accompanied by an interpreter. The patient must not be taken into the controlled area and the examination should not proceed if the safety form cannot be filled in. In unconscious patients, information may need to be obtained from relatives, the family physician, the attending clinical team, and the case notes. An example for a screening form is given in Fig. 18.2.

PRE-MRI PROCEDURE SCREENING FORM**MR Facility**

Date ____ / ____ / _____ MR# _____

Name _____ Height _____ Weight _____

Last name

First name

M.I.

Birthdate _____ Social Security # _____ / _____ / _____

Address _____ City _____

State____ Zip Code_____ Phone (H)(_____) (W)(_____) _____

Physician's name & address _____

1. Have you ever had surgery or any other invasive procedures? Yes No

If yes, please list:

Type: _____ Date: _____ / _____ / _____

Type: _____ Date: _____ / _____ / _____

2. Have you had any previous studies? Yes No If yes, please list below.

Body part	Date	Facility/Location
MRI:	/ /	_____
CT/Computed Tomography:	/ /	_____
X-Ray:	/ /	_____
Ultrasound:	/ /	_____
Nuclear Medicine:	/ /	_____

3. Have you ever:

- worked as a machinist, metal worker, or in any profession or hobby grinding metal?
- had an injury to the eye involving a metallic object (e.g., metallic slivers, shavings, or foreign body)?
- been injured by a metallic foreign body (e.g., bullet, BB, buckshot, or shrapnel)?

Yes No If yes, please describe: _____

4. Are you pregnant, experiencing a late menstrual period, or having fertility treatments? Yes No

5. Are you breast feeding? Yes No 6. Date of last menstrual period: _____ / _____ / _____

7. Are you taking oral contraceptives or receiving hormone treatment? Yes No

8. Are you currently taking or have recently taken any medication? Yes No
If yes, please list: _____

9. Do you have anemia, diseases affecting your blood, history of kidney disease or seizures? Yes No
If yes, please describe: _____

10. Do you have drug allergies? Yes No If yes, please list: _____

11. Have you ever had asthma, an allergic reaction, respiratory disease, or a reaction to a contrast medium used for an MRI or CT exam? Yes No If yes, please describe: _____

FIGURE 18.2. Screening form (From *J Magn Reson Imaging*, 2000;12:92).

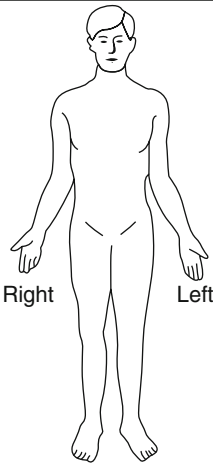
18.3.2 Contraindications to CMR Scanning

The contraindications to CMR scanning are equivalent to contraindications for general MR imaging. The CMR scanner can have the following effects that may endanger patients or staff in the magnet room:

Some of the following items may be hazardous to your safety and some can interfere with the MRI examination. Please check the correct answer for each of the following.

- Yes No Cardiac pacemaker
- Yes No Implanted cardiac defibrillator
- Yes No Aneurysm clip
- Yes No Carotid artery vascular clamp
- Yes No Neurostimulator
- Yes No Insulin or infusion pump
- Yes No Implanted drug infusion device
- Yes No Spinal fusion stimulator
- Yes No Cochlear, otologic, or ear implant
- Yes No Ear tubes
- Yes No Prosthesis (eye/orbital, penile, etc.)
- Yes No Implant held in place by a magnet
- Yes No Heart valve prosthesis
- Yes No Artificial limb or joint
- Yes No Other implants in body or head
- Yes No Electrodes (on body, head or brain)
- Yes No Intravascular stents, filters, or coils
- Yes No Shunt (spinal or intraventricular)
- Yes No Vascular access port and/or catheters
- Yes No Swan-Ganz catheter
- Yes No Transdermal delivery system (Nitro)
- Yes No IUD or diaphragm
- Yes No Pessary or bladder ring
- Yes No Tattooed eyeliner or eyebrows
- Yes No Body piercing(s)
- Yes No Metal fragments (eye, head, ear, skin)
- Yes No Internal pacing wires
- Yes No Aortic clips
- Yes No Venous umbrella
- Yes No Metal or wire mesh implants
- Yes No Wire sutures or surgical staples
- Yes No Harrington rods (spine)
- Yes No Metal rods in bones, joint replacements
- Yes No Bone/joint pin, screw, nail, wire, plate
- Yes No Hearing aid (*Remove before scan*)
- Yes No Dentures (*Remove before scan*)
- Yes No Breathing or motion disorders
- Yes No Claustrophobia
- Yes No Other: _____

Please mark on the figure below, the location(s) of any implants or metal inside or on your body.



Please remove all metallic objects before MRI including: keys, hair pins, barrettes, jewelry, watch, safety pins, paperclips, money clip, credit cards, coins, pens, belt, metal buttons, pocket knife, & clothing with metal in the material.

YOU ARE REQUIRED TO WEAR EARPLUGS OR EARPHONES DURING THE MRI EXAMINATION.

_____/_____
Signature of Person Completing Form

_____/_____
Date

Form Completed by: Patient Relative: _____
Name & relationship to patient

Physician or other: _____
Name & relationship to patient

To Be Completed By MRI Department	Medical Record number: _____	Completed by: _____
Procedure: _____	Clinical History: _____	

FIGURE 18.2. (continued).

- Missile effects:** The scanner will attract any ferromagnetic objects with enormous force. This force is higher the closer one gets to the magnet bore. Non-MR-compatible metallic objects like scissors or oxygen cylinders can become deadly missiles.

2. *Displacement:* Metallic objects in the body such as shrapnel, aneurysm clips, etc., may be moved by the magnetic field and cause injury.
3. *Internal devices:* The magnetic field can have torque effects on implanted active devices such as cardiac pacemakers or insulin pumps, causing them to change their settings or malfunction.
4. *Heating effects:* During scanning, the radiofrequency field can cause heating of devices, cables, and wires that are either adjacent to the patient (e.g. non-MR-compatible ECG cables) or implanted (e.g. pacing wires), with the potential to cause serious burns.

18.3.2.1 Medical Devices

The most common reason why a patient cannot undergo an MR scan is the presence of a non-MR-compatible implanted device. Thousands of medical devices are in use that contain ferromagnetic materials and may therefore be potentially unsuitable for MR scanning, making it impossible to give a meaningful representation of this subject in a textbook. There are large databases that contain information on the MR compatibility of many medical devices (for example www.mri-safety.com) and manufacturers will usually have relevant safety information about their devices. A joint statement has summarized the MR safety of cardiovascular devices.³

It is essential that at the time of referral, detailed information is given about the exact specifications of any implanted device or material in a patient, including model specification and implant date, as the MR compatibility of devices can differ between models and editions. Since 2005, a new classification for MR compatibility is used, proposed by the American Society for Testing and Materials International. This classification distinguished between “MR safe,” “MR conditional,” and “MR unsafe” devices. Many devices fall into the category of “MR conditional,” which means that the device is safe under certain conditions (see Chap. 2).

18.3.2.2 Heating Effects

As outlined in Sect. 18.1, MR systems generate high-frequency radiofrequency (RF) pulses to create the MR signal. These electrical currents can be concentrated in conducting materials within the RF field resulting in heating. Conducting material of certain geometrical shapes such as loops of wire of tens of centimeters are particularly liable to heating effects. Other conducting materials like iron oxide-based pigments in tattoos may also warm up during the MR scan. Several steps can be taken to prevent excessive heating and possible burns in association with MR procedures, including ensuring that there are no unnecessary metallic objects contacting the patient's skin, preventing skin-to-skin contact points and the formation of "closed loops" of conducting materials, and using only electrically conductive materials that are MR safe. It is extremely important that the MR staff who operate the MR system have appropriate training in the safe positioning of the patient, cabling and monitoring transducers.

18.3.2.3 Contrast Agents and Nephrogenic Systemic Fibrosis

The safety of MRI contrast agents is tested in clinical trials and they have very few side effects. The variations in the side effects and possible contraindications are similar to x-ray contrast media, but are very rare. In general, the chance of an adverse reaction increases with the quantity of the MRI contrast medium and also with the osmolarity of the compound.

Recently, concerns have arisen about the association between MR contrast media and a condition called nephrogenic systemic fibrosis (NSF) or nephrogenic fibrosing dermopathy. This is a rare condition that leads to fibrosis of the skin, but in the later stages can involve joints, eyes, and internal organs and can be fatal. It is now assumed that this reaction occurs in patients with advanced renal failure, in particular those undergoing hemodialysis, in whom clearance

of gadolinium-based contrast agents is delayed. To date, no cases have been reported in patients with normal renal function. NSF also seems to depend on the specific gadolinium chelate, with non-ionic linear agents such as gadodiamide (Omniscan), gadobenate dimeglumine (MultiHance), gadopentetate dimeglumine (Magnevist), and gadoversetamide (OptiMARK) being particularly associated with NSF. It is assumed that these agents release Gd³⁺ ions in the body, leading to a toxic effect in patients with advanced renal failure who have reduced clearance of these ions. The European Medicines Agency has classified the gadolinium-containing contrast agents in three groups:

- Safest with a cyclical structure: Dotarem, Gadovist, and ProHance
- Intermediate safety with an ionic linear structure: Magnevist, MultiHance, Primovist, and Vasovist.
- Least safe with a linear non-ionic structure: Omniscan and OptiMARK

And further:

- In patients with an estimated glomerular filtration rate (eGFR) of less than 30 mL/min: Omniscan, Magnevist and OptiMARK are currently contraindicated.
- For an eGFR of between 30 and 60 mL/min, these agents may only be used with caution.

In the United States, the US Food and Drug Administration introduced a class ban and warned about the use of gadolinium-based contrast agents in patients who have reduced renal function. This is a rapidly evolving topic and new guidance can be expected to become available during the lifetime of this book. It is therefore recommended that the reader seeks up-to-date information from sources such as the European Medicines Agency and the US Food and Drug Administration.

18.3.2.4 Performing Stress Examinations in CMR

If stress studies are to be performed, an additional level of safety consideration needs to take place. Hemodynamic monitoring of patients with an MR-compatible blood pressure machine needs to be available. Heart rate has to be monitored either from the scanner display or a stand-alone MR-compatible physiological monitoring station. Medication must be available in the department to reverse the potential side effects or complications of pharmacological stress agents. Emergency recovery procedures of patients from the MR environment must be in place and rehearsed. Arrangements for resuscitation in an appropriate area outside the magnet room must be made. Staff need to be trained in basic and advanced life support. Further details on stress CMR studies can be found in Chap. 27.

18.3.2.5 Other Safety Issues

Other safety concerns are related to the acoustic noise of the scanner and the cryogenic liquids. The noise generated by the switching gradient fields of the MRI scanner is an important occupational hazard and European guidelines regulate exposure to noise as well as magnetic field exposure. Hearing protection must be available to patients and should be worn by staff who have to work in the magnet room on a regular basis during the scanning procedure (e.g., when supervising stress perfusion scans). The gradient fields also generate a rapidly switched magnetic field (Chap. 1). At high switching rates associated with some of the faster MR pulse sequences, this may cause peripheral nerve stimulation. The gradient switching rate is therefore carefully monitored and limited by the MR system. In the near future, occupational exposure to this type of time-varying magnetic field may be limited in Europe by The Physical Agents Directive, (Directive 2004/40/EC). Due to become law in 2012, this could effectively

prevent staff from working in the gradient field which will be particularly problematic for MR-guided interventional procedures, but the recommendations remain under revision.

The large volume of liquid helium used to cool the superconducting magnet has the potential to present an asphyxiation hazard if it were to rapidly boil off, caused by a fault condition within the magnet cooling system (known as a magnet quench). In practice, such a spontaneous “quench” is a rare event and is most likely to occur during magnet installation or servicing. In the event of a quench the exhaust gas should be safely vented to the outside atmosphere through a vent pipe (quench pipe). Only if the quench pipe fails would patients and staff be at risk. It is possible to initiate a quench deliberately should it be necessary to switch off the magnet quickly in an emergency.

Key Messages for CMR Safety

MRI is very safe, but there are important health and safety considerations:

- The magnetic field requires careful screening of patients for contraindications to prevent injuries
- The magnetic field is *always* on, even if no scans are performed
- If in doubt whether a device/implant is MR safe – check www.mrisafety.com
- Some MR contrast agents should be avoided in renal failure, but MR contrast agents in conventional doses are NOT nephrotoxic

Common Devices that are NOT Contraindications for MR Imaging (Considered as “MR Conditional”)

- Most metallic heart valves
- Intracoronary stents

- Prosthetic joints etc.
- Sternal wires
- Dentures
- Cardiac “hole” closure devices

Common Devices that are ABSOLUTE Contraindications to CMR

- Most pacemakers
- Implanted cardioverter/defibrillators
- Insulin pumps
- Metal foreign bodies in the eye

18.4 Setting Up a CMR Study

18.4.1 Equipment

In addition to the basic equipment of a general purpose MR scanner, performing cardiac MR examinations requires some additional software and hardware. The MR vendors offer software packages that provide the functionality (such as ECG gating) and pulse sequences needed for CMR studies. In addition, physiological monitoring is required, i.e., ECG monitoring (ideally on a screen in the MR room as well as in the control room), MR-compatible blood pressure monitoring with remote activation from the control room and an oxygen saturation monitor. A power injector should be used to administer contrast agents for perfusion studies. If stress studies are to be performed, several additional requirements should be met.

- Emergency medication should be available on site. This includes all basic emergency drugs such as adrenaline and atropine, as well as specific medication for pharmacological stress studies: aminophylline, inhaled bronchodilators, intravenous beta blockers, and nitrates.

- A suitable resuscitation area needs to be identified that is close to but separate from the magnet room. This should hold a resuscitation trolley and a defibrillator, access to emergency medication, high flow oxygen, and suction.

18.4.2 ECG Signals

In order to allow ECG gating and ECG triggering (see Sects. 13.3 and 13.4), which are essential for almost all CMR acquisitions, a reliable ECG trace must be obtained. This is complicated by the fact that the MRI environment interferes with the ECG in many ways and that the potential risk of heating from ECG electrodes needs to be considered. The static, gradient, and RF electromagnetic fields of the CMR scanner all distort the ECG. In addition, the so-called magneto-hydrodynamic effect occurs when a conductive fluid such as blood flows in the presence of a strong static magnetic field and induces a biopotential. This effect typically distorts the T-waves of the received ECG. Further distortion can occur with respiration, in particular if the electrode skin contact is poor.

As a consequence of these difficulties, manufacturers have developed specialized algorithms that maximize the received ECG signal and filter out some of the described interferences. In addition, special electrodes and leads have been developed for use in the MRI environment that reduce the risk of heating and optimize signal reception. Most CMR systems now use fiber-optic or wireless ECG transmission. Manufacturers also recommend optimal positioning of the ECG electrodes. With these specialized tools, reliable ECG signals can be obtained in virtually all patients. Still, at times repositioning of ECG electrodes is required to obtain an optimal signal. Often, the effects of the magnetic field can only be fully appreciated once the patient is positioned in the isocenter of the magnet, making repositioning of electrodes a small challenge. This is particularly the case at higher field strengths (e.g., 3 T), where all of the effects described above are more prominent than at 1.5 T.

Despite all the improvements in ECG technology, it has to be emphasized that the ECG obtained in the MR environment cannot be used as a diagnostic tool (e.g., monitoring ST segment deviation as a sign of ischemia): this is particularly relevant when CMR stress studies are performed.

18.4.3 Patient Preparation

- Following the completion of the screening form, patients will usually be asked to change into hospital clothing to ensure that no metallic objects are inadvertently brought into the scanner room. They should then be shown the CMR scanner and introduced to its basic operation. Most CMR studies are performed in the supine position, but sometimes patients are positioned prone (e.g., ARVC protocols or in case of claustrophobia). Often, a knee support is provided to improve patient comfort.
- If required, intravenous cannulae are inserted for administration of contrast and stress agents. This can be performed outside the scanner in a preparation area.
- Next, MR-compatible ECG electrodes are placed on the patient's chest (see notes above). A good ECG tracing is essential for a high-quality CMR study and care should be taken to optimize the signal.
- The phased-array receiver coil is placed on the front of the chest. The coil designs vary widely between vendors.
- Frequently a respiratory motion sensor is placed on the anterior chest wall.
- A blood pressure cuff should be placed on the patient for stress studies. Consideration needs to be given to which side the cuff is placed relative to contrast injection sites.
- Headphones and, if required, earplugs are provided. The headphones are also used for communication with the patient from the control room and often to play music to the patient. Remember, a CMR scan can take an hour and patients get bored!

- It should now be explained to the patient that the scan is about to begin and what to expect. Mention that the scanner is noisy when it acquires images and that this is perfectly normal. Explain breath-holding instructions you will use and consider a practice run while the patient is outside the magnet bore.

Tips and Tricks for ECG Positioning

1. Use only ECG electrodes that are recommended by MR manufacturers
2. Follow manufacturer's recommendation for positioning of electrodes
3. Ensure good skin contact of electrodes by shaving chest hair where necessary and prepare skin with specialized abrasive gels
4. When repositioning electrodes, test effects in the magnet bore
5. Test the stability of the signal during respiration
6. Avoid forming loops with ECG leads that could induce heating.

18.4.4 Commencing the Scan

The patient is now moved into the magnet bore. Be careful not to injure the patient as the table slides into the bore and that cables do not get trapped. Consider asking the patients to close their eyes as they move into the scanner to reduce the sensation of claustrophobia. The area of interest (usually the heart) is placed in the isocenter of the magnet where signal uniformity is highest. All scanners have automatic guidance systems to position the patient. For cardiac studies, this means that the chest is in the middle of the scanner and the head usually remains within the scanner bore. Patients may find this claustrophobic, in which case removing a pillow or offering eye cover may help.

References

1. Pennell DJ, Sechtem UP, Higgins CB, et al. Clinical indications for cardiovascular magnetic resonance (CMR): Consensus panel report. *Eur Heart J.* 2004;25:1940–1965.
2. Sawyer-Glover A, Shellock FG. Pre-MRI procedure screening: recommendations and safety considerations for biomedical implants and devices. *J Magn Reson Imaging.* 2000;12(1):92–106.
3. Levine GN, Gomes AS, Arai AE, et al. Safety of magnetic resonance imaging in patients with cardiovascular devices: an American Heart Association scientific statement from the Committee on Diagnostic and Interventional Cardiac Catheterization, Council on Clinical Cardiology, and the Council on Cardiovascular Radiology and Intervention: endorsed by the American College of Cardiology Foundation, the North American Society for Cardiac Imaging, and the Society for Cardiovascular Magnetic Resonance. *Circulation.* 2007;116:2878–2891.

Chapter 19

Components of CMR Protocols

John P. Greenwood

Key Points

1. CMR protocols are made up of a number of core components, carefully selected to highlight and/or differentiate specific pathological features.
2. CMR therefore allows a multiparametric approach to cardiovascular imaging.
3. One must be aware of how to plan and perform these core components so that image quality can be optimized.

19.1 Introduction

Cardiovasclar magnetic resonance (CMR) has become a fundamental technique for the evaluation of cardiovascular disease. With improvements in both hardware (e.g., coils) and software (pulse sequences) CMR image acquisition has now become very fast, often just requiring short breath-holds of only a few seconds. With an ever-growing range of pulse sequences it is now possible to perform detailed examination of the cardiovascular system both anatomically and functionally. This ability to undertake a multiparametric approach to diagnosis is one of the unique strengths of CMR.

This chapter will take you step-by-step through each of the commonly used components that are used in everyday clinical CMR protocols. For each component, there will be a brief description of the pulse sequence, how it is planned/optimized, an example image, and finally tips and tricks for the novice. These individual components will be referred to frequently in **Part III** of this book, where a disease-orientated approach to CMR imaging will be presented.

19.2 Localizing Images and Simple Planning

Localizer or scout scans are the first part of any imaging protocol. Using either a gradient or spin echo technique (see Chap. 11), a set of low-resolution images are acquired in the three standard orthogonal planes, sagittal, coronal, and transverse (Fig. 19.1). These images are acquired during free breathing

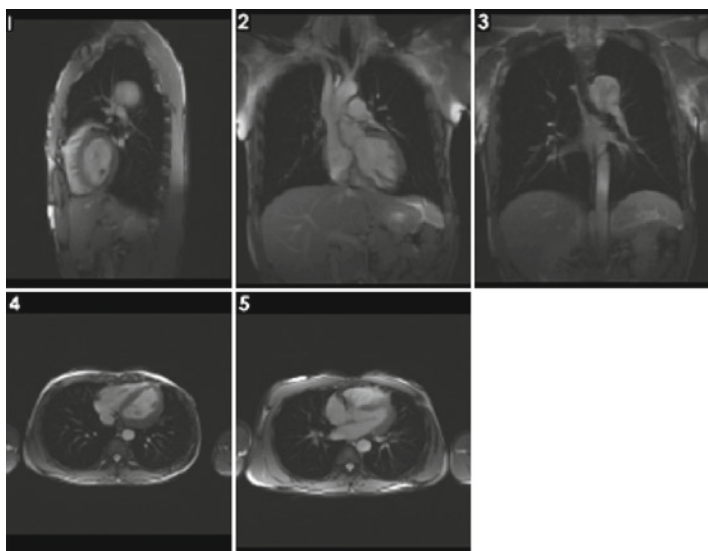


FIGURE 19.1. Localizer scans demonstrating the three standard imaging planes (sagittal, coronal, and transverse).

and are not gated to the electrocardiogram (ECG) (so they are prone to artifacts). This first image set is used to confirm that the patient is positioned correctly on the table (with the heart in the isocenter of the magnet), the RF receiver coil is correctly positioned, and the appropriate array coil elements are turned on. These basic images can also be used to help plan the position and orientation of future standard imaging planes.

The next step for most imaging protocols is to acquire a trans-axial spin echo or gradient echo stack, from the level of the diaphragm to just above the aortic arch, often at low resolution, and planned from the coronal and sagittal localizer images (Fig. 19.2).

The resultant stack of images is then used to plan the main cardiac axes. There are several ways to derive the standard views and we present the approach we follow: Choose a mid ventricular image to plan the vertical long axis (VLA) cine acquisition by orientating an orthogonal slice along the long axis of the left ventricle (LV) (Fig. 19.3, *orange line*), bisecting the mitral valve and the apex (not necessarily completely parallel to the septum).

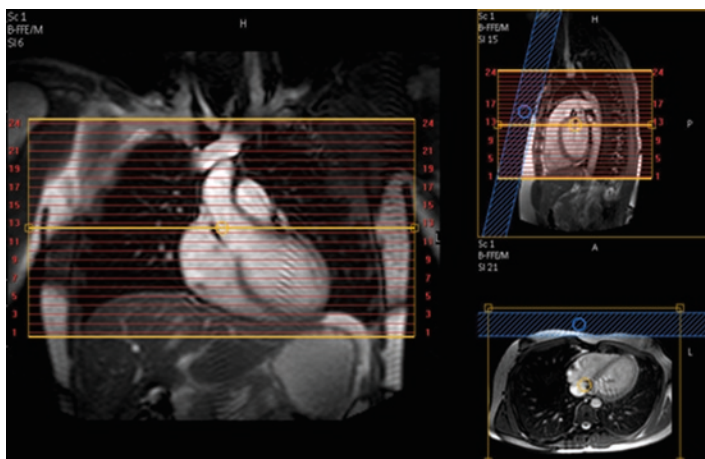


FIGURE 19.2. Planning of the trans-axial stack (yellow box) from coronal and sagittal localizers.

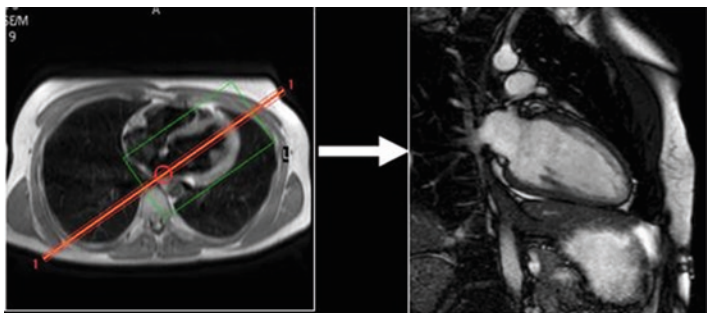


FIGURE 19.3. Planning of the VLA cine from the trans-axial T1-weighted image (orange line).

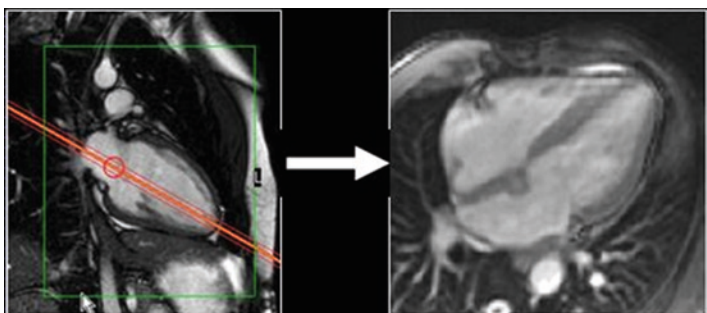


FIGURE 19.4. Planning of the HLA cine from the VLA cine (orange line).

Using the end-diastolic phase of the VLA cine acquired in the previous step, plan the next slice orthogonal to this, bisecting the mitral valve and apex to produce a horizontal long axis (HLA) cine image (Fig. 19.4).

To plan the true short axis (SA) cine, use the VLA and HLA cines just acquired, and plan the next slice(s) parallel to the atrioventricular (AV) ring (Fig. 19.5).

Finally, to plan the true 4-chamber (4ch) geometry, use the VLA and SA cine images just acquired, and plan the next slice through the apex and the maximum lateral dimensions of both ventricles, avoiding the left ventricular outflow tract (LVOT) (Fig. 19.6).

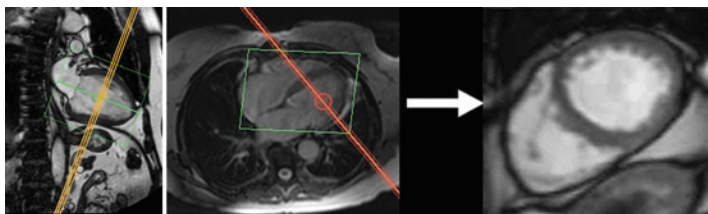


FIGURE 19.5. Planning of the SA cine from the VLA and HLA cine images.

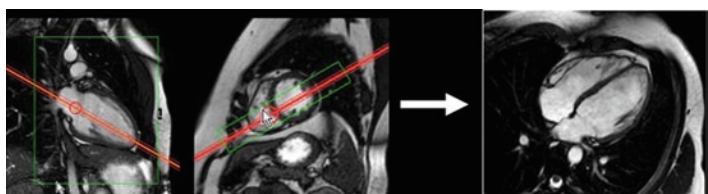


FIGURE 19.6. Planning of the 4ch cine from the VLA and SA cine images.

It is now just one final simple step to plan a full LV SA cine stack for quantitative analysis of LV and right ventricle (RV) volumes and ventricular mass. Use the end-diastolic frames from the VLA and 4ch cines to plan the first slice through the AV groove seen on both views. Then acquire parallel slices, typically 7-mm slice thickness with a 3-mm gap (or 8 + 2 mm or 10 + 0 mm) until you have covered the entire ventricle (Fig. 19.7).

It is now possible to complete a simple functional assessment of the LV and RV by examining the left and right ventricular outflow tracts (LVOT and RVOT). Using the end-diastolic frame from the basal slice of the SA stack, rotate the next orthogonal imaging plane so that it passes through the aortic valve and up into the ascending thoracic aorta. This can be confirmed on the trans-axial stack. This will produce an LVOT cine which is equivalent to the parasternal long axis view on echocardiography (Fig. 19.8). A second LVOT view (LVOT coronal) can be piloted perpendicular to the initial LVOT view (Fig. 19.9).

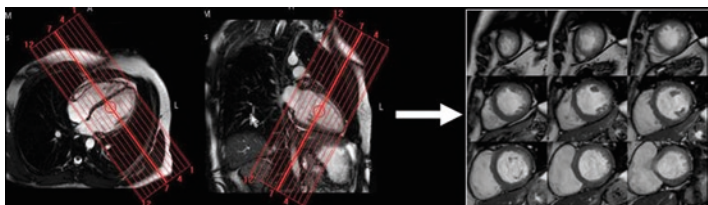


FIGURE 19.7. Planning of the LV SA cine stack (typically 10–12 slices) from the VLA and 4ch cine images.

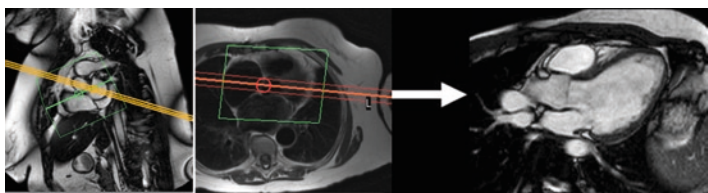


FIGURE 19.8. Planning of the LVOT view.

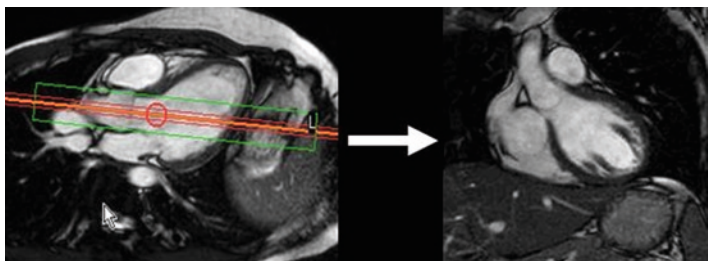


FIGURE 19.9. Planning of the LVOT coronal view from the original LVOT cine image.

To get the RVOT view, use the trans-axial T1-weighted black blood (BB) stack and plan a sagittal plane directly through the main pulmonary artery, checking by scrolling through the slices that it also passes through the pulmonary valve and cavity of the RV (Fig. 19.10).

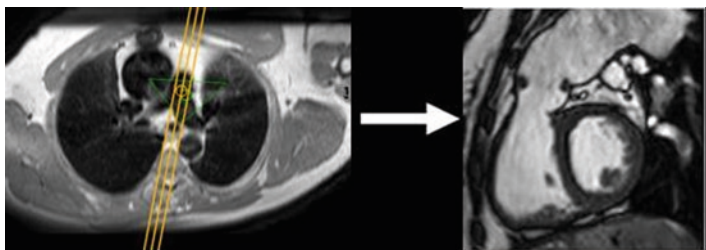


FIGURE 19.10. Planning of the RVOT view from the original transaxial T1-weighted stack.

19.2.1 Interactive Planning

All vendors now offer software that allows planning of these standard imaging planes in an interactive mode that uses real-time cine acquisition (Sect. 16.8) to provide instant feedback on chosen imaging planes. The defined planes can then be saved for use in subsequent imaging protocols. New tools are also being tested that perform these tasks semi-automatically based on anatomical landmarks in an attempt to simplify CMR scanning.

19.3 Anatomical and Morphological Imaging

Spin echo imaging is one of the most basic and commonly applied pulse sequences used in all forms of general MR imaging. As seen in Chapter 16, there are many different variations that can be applied to the basic spin echo pulse sequence, either to accelerate the acquisition (Sect. 15.1) or to produce T1-weighted and T2-weighted images (Sect. 16.4). Different body tissues have different T1 and T2 relaxation times due to the different molecular environments of the hydrogen nuclei (Sect. 5.1). Because fat has very constant T1 and T2 values it is often used as a reference tissue. On T1-weighted images, fat has very high signal intensity, muscle has intermediate signal intensity, and blood has low signal intensity. On T2-weighted images, tissues with high water

content (e.g. cysts, effusions) have the highest signal intensity. A particular advantage of spin echo sequences are their relative insensitivity to local magnetic field inhomogeneity, produced, for example, by metallic implants such as sternal wires, prosthetic valves and arterial stents.

19.3.1 T1-Weighted (*Black Blood*) Imaging

T1-weighted spin echo sequences provide excellent tissue contrast between the myocardium and adjacent structures (e.g., epicardial fat or intra-cavity blood). As such they are a fundamental part of morphological cardiac imaging and are also used for tissue characterization (e.g., tumor assessment). One important feature of spin echo images is that blood flowing rapidly through the image plane will appear dark (black), whereas slow-flowing or stationary blood will have some residual signal. This can produce characteristic artifacts that can catch out the uninitiated (See [Sect. 12.1](#)). The use of Black Blood preparation schemes reduces this tendency (See [Sect. 12.2](#)).

For high-resolution T1-weighted images free from artifact, it is usual to acquire 1 or 2 slices per breath-hold. This can be performed as a stack of contiguous images (typically 8–10-mm thick to get adequate signal-to-noise ratio (SNR)) in any slice orientation depending on the anatomical structure of interest. Although they are ECG-triggered, the resultant image is from a single time point approximately midway through the cardiac cycle. Thus it is not ideal to make measurements of vascular structures from static T1-weighted images, as they are not acquired at end-diastole.

T1-weighted spin echo sequences can also be performed using a frequency-selective fat suppression technique (spectral presaturation inversion recovery (SPIR), fat saturation (Fat SAT), or chemical selective saturation pulse (CHESS)) to produce a “fat suppression” image ([Sect. 16.2](#)). This can be useful to help in tissue characterization (e.g., the identification of a lipoma) or to delineate abnormal presence of fat within a tissue (e.g., fatty infiltration of the myocardium in ARVC). Frequency-selective fat suppression is now widely used in CMR imaging ([Fig. 19.11](#)).

To further aid tissue characterization, T1-weighted imaging is often repeated after the administration of a gadolinium-based contrast agent. This can be particularly useful in highlighting infiltrative or inflammatory myocardial disease. The presumed cause of the increased signal intensity in the pathological area is a combination of increased inflow (hyperemia), altered interstitial contrast kinetics (capillary leakage and edema), and diffusion into cells (necrosis) (Fig. 19.12).

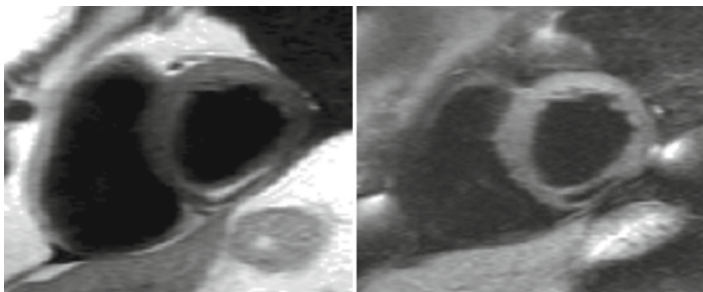


FIGURE 19.11. T1-weighted spin echo SA images, with and without fat suppression. In the first image fat is “bright” in the inferior wall, and in the second image the signal from fat has been suppressed so that it appears “black”; thus the presence of intra-myocardial fat is confirmed.

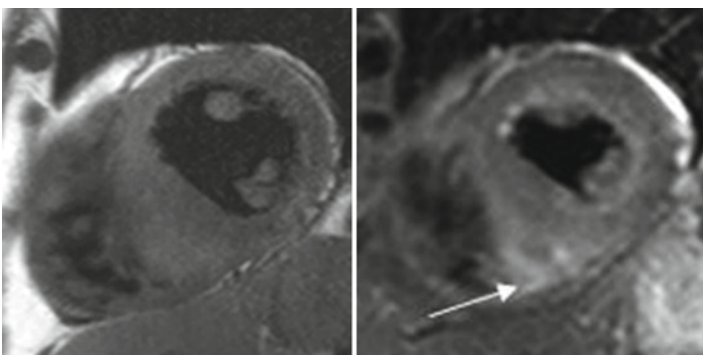


FIGURE 19.12. T1-weighted spin echo images pre- and post contrast showing increased signal intensity in the “mass lesion” in the inferior septum (arrow).

Tips and Tricks

- Generally scan in diastole when there is less cardiac motion and a large amount of blood in the LV.
- If the patient is poor at breath-holding, only acquire one slice per breath-hold or try a respiratory navigator.
- Adjust the trigger delay so that in combination with the TI, the Black Blood preparation and the data acquisition both occur when the heart is in a similar position.
- If there is loss of signal from the basal region of the RV, LV, or septal wall, increase the thickness of the Black Blood inversion pulse.
- Note that the Black Blood inversion time (TI) on Siemens systems is called the “TR.”

19.3.2 T2-Weighted (Black Blood) Imaging

T2-weighted MR imaging has become established in the diagnosis of a number of cardiac inflammatory conditions, in particular acute myocarditis and myocardial infarction (Fig. 19.13). This in part relates to the known correlation between T2 relaxation times and myocardial water content; the higher the water content, the greater is the signal intensity on T2-weighted images. However, T2-weighted imaging is hampered by the requirements for relatively long breath-holds (producing respiratory motion artifacts) and low SNRs. This is because in order to increase the TR as required for T2-weighting, data acquisition is performed only on every second or third heart beat. Increasing the slice thickness can improve signal and SNR, but the trade-off is a reduction in spatial resolution. There are also issues regarding the choice of surface coils or body coils to receive the image: with the former there is a progressive loss of signal moving away from the surface coil, leading to a drop in the sensitivity of

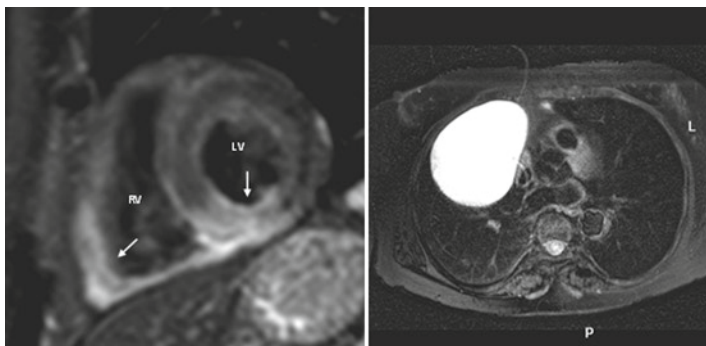


FIGURE 19.13. (a) T2-weighted triple IR SA image demonstrating marked edema in the inferior wall of the LV and RV. (b) T2-weighted trans-axial image demonstrating the very high signal intensity seen in a fluid-filled pericardial cyst.

T2-weighted imaging to detect edema in the posterior LV; with the latter there is the general issue of low SNR. T2-weighted imaging has been improved by short tau inversion recovery (STIR) techniques, using segmented fast spin echo (FSE) acquisition with dark blood preparation (triple inversion recovery) (see Sect. 16.5).

Edema Module

1. Perform imaging prior to contrast administration.
2. Body coil should be used or alternatively functional surface coil intensity correction algorithms.
3. A shorter breath-hold is required with segmented FSE imaging (double inversion recovery).
4. Adjust readout to mid-diastole.
5. Slice thickness should be at least 10 mm.
6. Slice thickness of the dark blood pre-pulse should be greater than the longitudinal shortening of the LV.

Tips and Tricks

- T2-weighted imaging must be performed prior to contrast administration.
- Aim for a slice thickness of at least 10 mm to ensure good SNR.
- The slice thickness of the dark blood pre-pulse should be greater than the longitudinal shortening of the LV.

19.3.3 *T2* Relaxometry*

CMR has become a standard clinical technique for the quantitation of cardiac and liver siderosis (iron loading), both for diagnosis and disease/treatment monitoring. Iron has very strong paramagnetic properties, and deposits will considerably shorten the decay constant $T2^*$ as a result of increased inhomogeneity in the magnetic field. $T2^*$ is typically quantified using a single breath-hold spoiled gradient multi-echo $T2^*$ sequence (or modified black blood sequence with blood signal suppression using a double inversion recovery pulse combined with a gradient multi-echo sequence).

A single mid-ventricular SA slice is acquired using the above bright blood or black blood sequence (the latter may be more reproducible). From this, using dedicated software (e.g., Thalassemia Tools, CMRtools, Cardiovascular Imaging Solutions, London) a region of interest (ROI) can be planimetered in the inter-ventricular septum, and the signal intensity for each image is plotted against the echo time (TE) to give a decay curve, from which $T2^*$ can be derived after solving the equation $y = Ke^{-TE/T2^*}$ (Fig. 19.14). The same pulse sequence is also performed in a trans-axial orientation at the level of the liver, and the same software used to plot the liver decay curve, and hence derive the liver $T2^*$ value. There are now well-established normal ranges for liver and cardiac iron loading, such that this has now become the preferred technique for guiding chelation therapy in cardiac/liver iron-loading conditions.

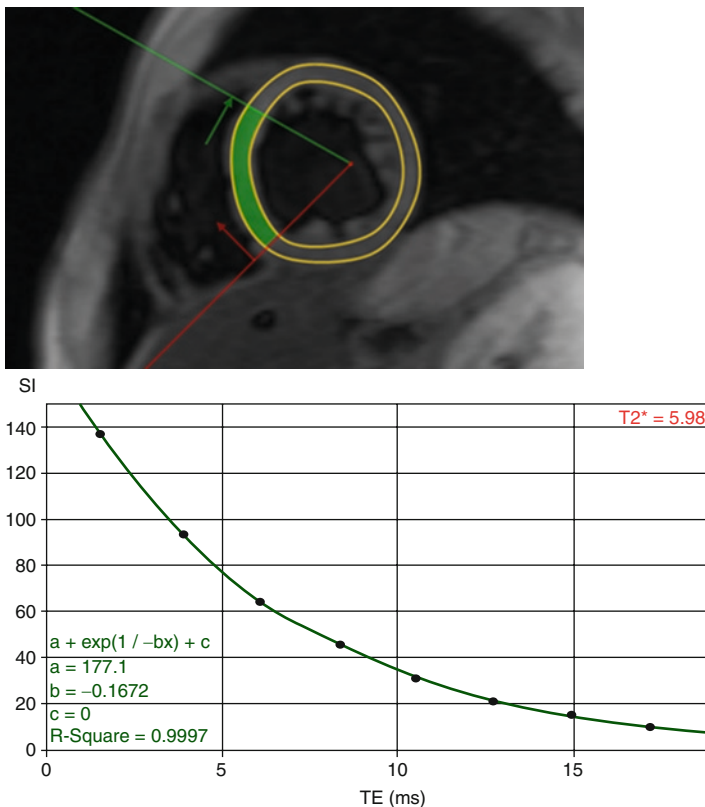


FIGURE 19.14. ROI placed in the inter-ventricular septum and the corresponding decay curve in a patient with cardiac iron loading.

T2* Module

1. T2* quantitation is now a standard CMR technique for disease monitoring and guiding chelation therapy in cardiac iron-loading conditions.
2. Use a single breath-hold, multi-echo, T2* sequence (gradient echo or modified black blood sequence).

3. Acquire a single mid-ventricular slice (and a single trans-axial slice of the liver). Ensure good patient breath-holding by coaching, as the scan duration is quite long.
4. Repeat the scan if there is respiratory artifact as this will compromise quantitation.

Tips and Tricks

- Make sure the septum is of good image quality as this is where the ROI for quantitation is placed.
- If not, repeat scan with strict breath-hold instructions to avoid respiratory motion artifacts.
- Position the transverse liver slice at a location so as to avoid large hepatic vessels so that an ROI can be easily defined in the liver tissue.

19.4 Cine Imaging (Including Real-Time Cine Imaging)

Many different pulse sequence approaches are used for rapid cine imaging which will depend in part on the local availability of the MR system manufacturer. Cine imaging is performed using gradient echo pulse sequences; examples include turbo gradient echo (TGE) and balanced steady-state free precession (SSFP) techniques (see Sects. 13.5 and 16.8). Images are typically acquired during short breath-hold periods (although it is also possible to perform acquisition during free breathing, but respiratory motion artifacts will spoil image quality). To account for cardiac motion during the cardiac cycle, ECG triggering, ECG gating, or real-time imaging is required (see Chaps. 13 and 18).

ECG triggering is the most basic form of cardiac synchronization and can be used in almost all forms of CMR image acquisition (see Sect. 13.3). The QRS complex of the ECG is

detected and then after a short delay the pulse sequence is initiated. In this way, over repeated cardiac cycles an image is formed at a particular time point in the cardiac cycle. If the delay time after the QRS complex is varied, the different time points within the cardiac cycle can be imaged, and in this way a cine image can be built up, usually from a minimum of 15–20 different time points or phases. The other commonly used cardiac synchronization technique is retrospective gating (see Sect. 13.4). This involves repeating the sequence at a constant repeat time over many R–R intervals. After all the data have been acquired, the information is sorted according to where it was collected from within the cardiac cycle. The advantages of this technique are that variations in the heart rate can be corrected for (retrospectively), and that more of the cardiac cycle can be acquired (i.e., late-diastole, which can be difficult from a prospective gating technique).

19.4.1 Real-Time Cine Imaging

Most real-time imaging techniques are just faster versions of SSFP or TGE cine sequences. Methods such as parallel imaging and half Fourier imaging are part of the approach used to accelerate the acquisition (Sects. 15.4 and 15.5). To gain a sufficient level of acceleration, so that all data can be acquired in real time (i.e., a full set of images every single heart beat) typically requires sacrifices in both spatial and temporal resolution. Temporal resolution can be as low as 50–70 ms with a spatial resolution of $\sim 3 \times \sim 3$ mm (reconstructed). Although this generally does not satisfy the requirements for good-quality cine imaging, the advantage is that ECG triggering is not required and nor is breath-holding. Thus this can be a very useful technique in patients with arrhythmias (e.g., poorly controlled atrial fibrillation) or in those who cannot breath-hold at all (e.g., young children). Furthermore, real-time acquisition can be used to acquire information on dynamic variability of cardiac morphology and function, for example in constrictive pericarditis.

19.4.2 Quantitation

CMR is the most accurate and reproducible method for both LV and RV mass and volume calculations, as it provides a 3D volume dataset avoiding the need for mathematical models and geometric assumptions of the shape of each ventricle. Several commercial software packages are available to perform these calculations. Typically, end-diastolic and end-systolic contours are drawn on each slice of the SA stack. Many software packages provide automatic or semi-automatic algorithms for this task, but not all are reliable. In most cases, outlining only the diastolic and systolic images is sufficient, but all phases need to be tracked if more detailed analysis of ventricular filling and contraction is sought. In the analysis of an LV SA stack, care needs to be taken at the base of the heart, where the left ventricular and left atrial borders may overlap. Within a center, it is essential to define an objective approach to dealing with these partial volume effects. In many centers, slices are considered to be within the LV if the blood volume is surrounded by 50% or more of ventricular myocardium. Importantly, the most basal slice and its shape typically differ between diastole and systole because of the longitudinal shortening of the heart, which needs to be considered when outlining LV contours. Towards the apex of the LV, trabeculations within the LV cavity are typically excluded from the LV wall and the papillary muscles are planimetered separately. Once all slices are planimetered, the end-diastolic volume (EDV), end-systolic volume (ESV), stroke volume (SV), ejection fraction (EF%) and mass for both the LV and RV can be calculated by the analysis software using the summation of disks method (Fig. 19.15). For the calculation of RV volumes many centers prefer a cine stack acquired in the trans-axial orientation. For the purposes of reporting ventricular volumes and mass, it is important to use pulse sequence-specific normal ranges as there may be a systematic difference between traditional fast, segmented k-space, gradient echo (TGE), and the balanced SSFP techniques (see Table 19.1). The cine data sets can also be used to derive

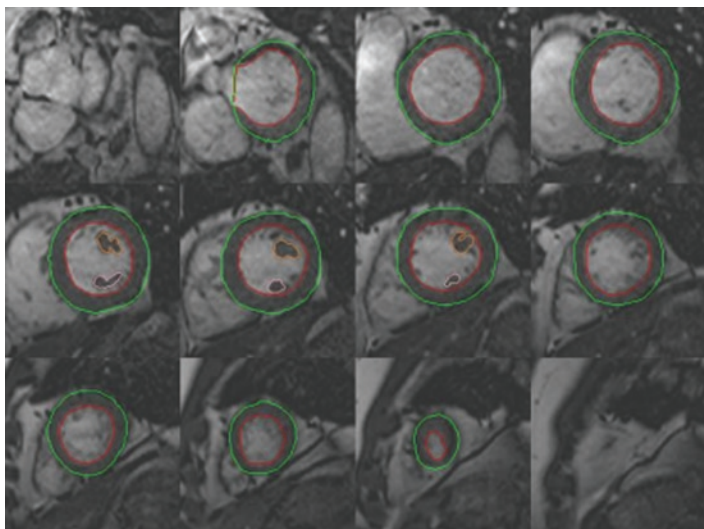


FIGURE 19.15. Multi-phase multi-slice SSFP SA cine stack showing endocardial (red), epicardial (green), and papillary muscle (orange and pink) contours at end-diastole.

regional contractile function. SA sections can be divided into segments and their diastolic to systolic thickening and inward motion calculated from segmental endocardial and epicardial contour displacement.

LV Function Module

1. Use SSFP pulse sequence (parallel imaging as required).
2. Acquire VLA, 4-ch, SA, and LVOT cine images.
3. Plan the SA stack from the mitral valve plane through the apex; slice thickness 6–8 mm, with 2–4-mm inter-slice gaps to equal 10 mm.
4. Keep temporal resolution ≤ 45 ms between phases.
5. Acquire LVOT cines in two orthogonal planes.

TABLE 19.1. Normal ranges for SA orientation (two standard deviations above and below the mean) for TGE and SSFP sequences, with adjustment to BSA and height.

	TGE		SSFP	
	Male	Female	Male	Female
LV EDV (ml)	84–221	84–162	102–235	96–174
LV EDV/BSA (ml/m ²)	45–104	48–94	53–112	56–99
LV EDV/HT (ml/m)	50–122	54–97	60–130	61–104
LV EF%	57–74	58–76	55–73	54–74
LV Mass (g)	108–211	82–132	85–181	66–114
LV Mass/BSA (g/m ²)	60–96	47–77	46–83	37–67
LV Mass/HT (g/m)	65–115	50–80	51–100	41–69
RV EDV (ml)	95–226	71–164	111–243	83–178
RV EDV/BSA (ml/m ²)	50–106	42–93	58–114	48–103
RV EDV/HT (ml/m)	56–124	45–99	66–133	52–108
RV EF%	47–68	51–72	48–63	50–70

LV, left ventricle; RV, right ventricle; EDV, end-diastolic volume; ESV, end-systolic volume; SV, stroke volume; EF, ejection fraction; BSA, body surface area; HT, height

RV Function Module

1. Use SSFP pulse sequence (parallel imaging as required).
2. Acquire trans-axial cine stack from the level of the diaphragm to the pulmonary artery bifurcation.

3. To assess subtle RV wall motion abnormalities it can help if the slice thickness is kept at 6–8 mm, with no inter-slice gap.
4. Keep temporal resolution ≤ 45 ms between phases.
5. Long axis images should include an RV VLA view aligned with tricuspid valve inflow and an RV outflow.
6. Acquire a tract view.

Tips and Tricks

- If it is necessary to shorten breath-hold times, reduce the number of slices or phases (and increase “turbofactor”) acquired for each breath-hold (Sect. 16.8), reduce spatial resolution or use parallel imaging.
- Segmented k-space gradient echo techniques (e.g., turbo field echo (TFE), TurboFLASH) are more flow/velocity-sensitive than SSFP sequences, and so may be useful for the evaluation of valvular pathology or shunts (Sect. 17.5).
- Remember that the heart contracts towards the apex in systole so that usually at least one basal slice is lost.
- Use the movie function of the analysis software to check position of contours.

19.5 Myocardial Tagging

Myocardial tagging is a CMR technique that allows the visualization of intra-myocardial contraction (see Sect. 16.10). It is typically performed using a breath-hold, ECG-gated, spoiled gradient echo technique (although SSFP pulse sequences may permit better tag-line contrast and reduced tag-line fading). Triggered from the ECG R wave, radiofrequency and gradient pulses are applied that saturate or “tag” the tissue magnetization in a linear or grid-like pattern. These

alternate bands of saturation/desaturation persist for a short period of time, typically through systole and into early diastole (Fig. 19.16). Different techniques have been used to generate tagged images, such as spatial modulation of magnetization (SPAMM), complementary spatial modulation of magnetization (CSPAMM), which improves tag persistence, and delays alternating with nutations for tailored excitations (DANTE). More recently, full 3D data sets of tagged images have been acquired allowing full cardiac coverage, as opposed to conventional single 2D slices.

Analysis of tagged images can either be by simple visual interpretation or by quantitative software techniques. At present, routine clinical applications of tagged images are limited to visual analysis. Quantitative techniques are particularly time-consuming and are currently a focus of research.

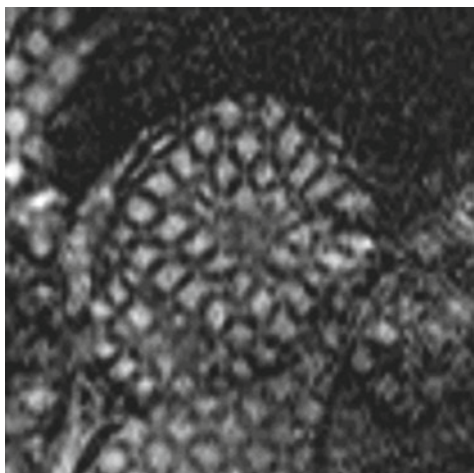


FIGURE 19.16. Myocardial tagged cine image (in SA) showing deformation of the tagging grid during systole.

Tagging Module

1. Scout imaging as per LV structure and function module.
2. Choose line tagging or grid tagging pattern.
3. Choose slice orientation from cine study.
4. Acquire data in breath-hold.

Tips and Tricks Tagging

- Linear tags are more useful if you are interested in contraction of the RV free wall; grid tags are well suited to the study of the LV.
- Linear tag orientation is usually by personal choice as is tag-line spacing.
- Acceleration techniques used to shorten the breath-hold time are the same as for cine imaging.
- Use a low flip angle to reduce tissue saturation and prolong the tagging pattern throughout the cardiac cycle.

19.6 Phase Contrast Velocity Encoding

Techniques for measuring blood flow have greatly enhanced the utility of CMR (analogous to Doppler measurements by echocardiography). The unique advantage of CMR is that in addition to measuring accurately the velocity at pixel locations in any imaging plane, the area of the vessel of interest is also measured simultaneously. This allows volume of flow to be measured. This is particularly useful for calculating the regurgitant fraction through a leaking valve or for comparing left and right heart cardiac outputs to assess cardiac shunting.

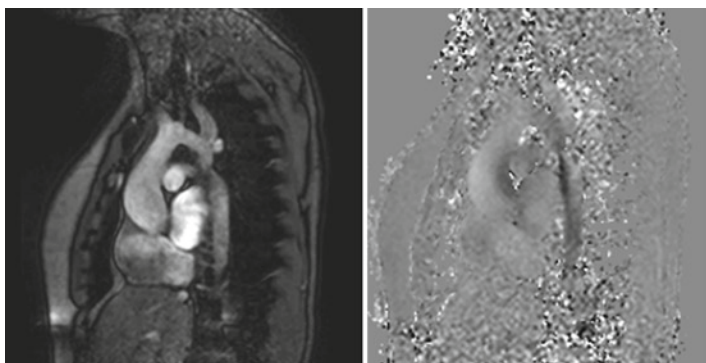


FIGURE 19.17. Magnitude and phase images acquired from the thoracic aorta showing a high velocity jet (dark) in the descending thoracic aorta associated with aortic coarctation.

A phase-contrast acquisition is made up of two acquisitions with different flow sensitivities that produce the images in magnitude (i.e., anatomical) and in phase (quantitative for flow direction and velocity) (Fig. 19.17 and Sect. 16.9). An appropriate encoding speed (velocity encoding (VENC)) must be chosen by the operator before running the sequence so as to avoid aliasing errors from high-velocity flow measurements. This can either be predicted by an experienced operator, or a short breath-hold acquisition can be performed with a particular VENC and the image checked afterwards for aliasing. If this occurs, the VENC is increased by an appropriate amount. This type of sequence is typically performed during free breathing (as many cardiac cycles are needed); cardiac gating is retrospective, with continuous gradient echo acquisition and phase encoding changes for each R wave.

Phase-contrast images are analyzed off-line using commercial software (or the vendor-supplied workstation). The vessel of interest is manually planimetered at each phase of the cardiac cycle to correct for motion and change in diameter of the vessel lumen between systole and diastole. From this the absolute forward and reverse flow volumes can be calculated as well as the peak forward low velocity (Fig. 19.18).

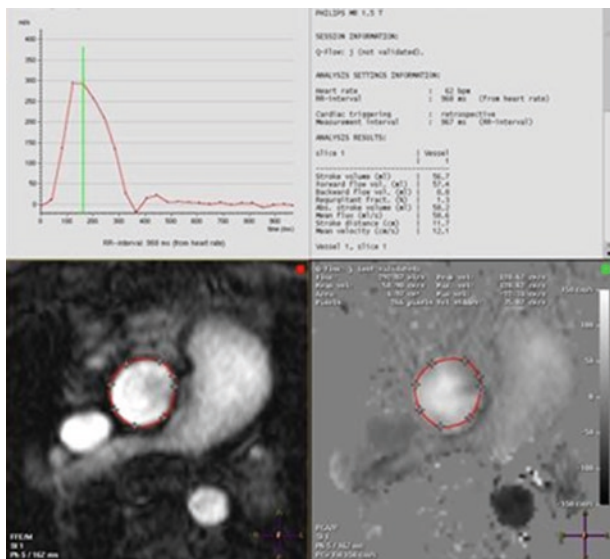


FIGURE 19.18. Post-processing software showing the magnitude and phase images acquired transverse to the thoracic aorta. Contours have been drawn around the ascending thoracic aorta and a volume–time curve plotted showing aortic flow (volume and direction) throughout the cardiac cycle.

Phase-Contrast Velocity-Encoding Module

1. Choose the appropriate imaging plane (orthogonal to expected direction of flow). Consider orthogonal acquisitions to define peak velocity.
2. Set required direction of flow.
3. Choose appropriate VENC (start with 150 ms for normal systemic flow and 100 ms for right-sided flow. Adjust in pathological situations).
4. Choose between free breathing and breath-hold techniques. For flow/volume calculations use a free-breathing phase-contrast acquisition; a breath-hold acquisition is acceptable if only peak velocity is required.

Tips and Tricks Velocity-Encoded Imaging

- Do not set the VENC too high above the maximum predicted velocity, otherwise error will be introduced (ideally it should be within 25% of the true peak velocity).
- Always check that you have set the correct direction of flow to be measured, whether you are scanning in-plane or through-plane.
- For peak velocity measurements always make sure that the true jet axis has been well defined and perform in-plane imaging using this geometry. Ideally a thin slice should be acquired and the field of view rotated so that it is orthogonal to the direction of flow. Make sure there is adequate temporal resolution so that velocity is not underestimated (e.g., for free-breathing acquisition use 30 phases; for breath-hold use 20–25 phases).

19.7 Contrast-Enhanced MR Angiography (Excluding Coronary Arteries)

MR angiography has become a widely accepted technique for the evaluation of vascular abnormalities in all areas of the body. It has many advantages over x-ray angiography in that it is minimally invasive (no arterial access required), uses safer contrast agents (non-iodinated), and is free of ionizing radiation.

The technique involves a peripheral venous bolus injection of gadolinium-based contrast agent which shortens the T1, providing increased vascular signal, avoidance of blood signal saturation, and better turbulent flow imaging. Typical pulse sequences are fast 3D spoiled gradient echo sequences, with short TR and a short TE ([Sects. 8.5 & 13.5](#)). A parallel

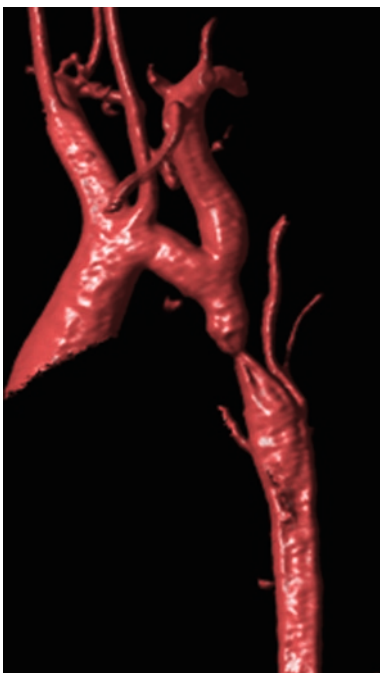
imaging technique can be used to speed up the image acquisition duration. A 3D acquisition is used to obtain high spatial resolution and a good SNR, and the imaging volume can be acquired in any desired orientation. The sequence does not require ECG triggering (so is unaffected by arrhythmias) and can be performed in a single breath-hold (20+s).

To obtain a high image quality as standard, it is important to have the correct timing between intravenous contrast injection and image acquisition. Central filling of k space ([Chap. 7](#)) needs to occur at the moment of peak intravascular contrast, otherwise if too late there is the risk of contamination by the venous signal. The optimal timing between contrast injection and imaging can be determined in several ways:

- Test bolus technique: injection of a small dose of contrast (2 mL) and saline flush (20 mL) whilst acquiring a 2D gradient echo slice through the ROI every 1–2 s. The contrast arrival time can then be calculated visually and used for the main acquisition.
- Automatic triggering: this involves monitoring signal intensity in a large voxel in the vascular territory of interest. The arrival of the contrast produces a sharp increase in signal intensity which is used to automatically trigger the 3D gradient echo sequence.
- Time-resolved contrast-enhanced magnetic resonance angiography (ce-MRA): This technique is independent of the exact contrast arrival time. Rapid collection of successive 3D data sets is performed immediately after contrast injection (10 mL, 3–5 mL/s), such that at least one is timed at the arterial phase after contrast injection. With this technique multiple vascular phases are acquired (arterial, tissue perfusion, and venous).

Sophisticated post-processing software is now available to allow viewing of the 3D data set from any desired angle/orientation. Maximum intensity projections and surface-rendered image projections ([Fig. 19.19](#)) can be manipulated off-line to display specific vascular anatomical features.

FIGURE 19.19. Surface-rendered image of the thoracic aorta showing a tight aortic coarctation.



MR Angiography Module

1. Prepare contrast infusion pump with contrast agent and flush.
2. Define 3D target region; unlike most other CMR applications, a very large volume is usually selected.
3. Define required timing of acquisition (arterial or venous).
4. Determine best timing parameters for data acquisition (pre-bolus or automatic triggering).
5. Perform a dummy acquisition.
6. Perform acquisition with contrast administration.

Tips and Tricks MR Angiography

- Make sure that your chosen timing technique ensures that the centre of k space is acquired at the same time as the bolus of contrast arrives in the vessel of interest.
- Ensure that when you plan the volume it covers the whole area of interest including any collateral or aberrant vessels (if unsure you could acquire a “dummy” scan without contrast to check the positioning of the volume).

19.8 Myocardial Perfusion CMR

Assessment of myocardial blood flow using contrast-enhanced dynamic first-pass myocardial perfusion CMR is a rapidly increasing clinical application. Perfusion studies are performed to interrogate the vascularity of cardiac and extracardiac masses and, predominantly, to detect myocardial reduced perfusion reserve as occurs in coronary artery disease and cardiomyopathies. For the detection of reduced myocardial perfusion reserve, perfusion imaging needs to be combined with either physiological or pharmacological stress. Although performed in some centers, physiological exercise is not practical in the MR environment and coronary vasodilator (e.g., adenosine) stress is the primarily used pharmacological stress agent. Under conditions of maximal hyperemia (vasodilatation), regions of myocardium supplied by a stenotic artery will demonstrate hypoperfusion during first-pass imaging.

The optimal imaging sequence for stress perfusion MR is open to debate and therefore individual choice generally

comes down to local experience/preference. The three most commonly used methods are described below, with some potential advantages and disadvantages of each (see also Sect. 16.11):

1. Spoiled gradient echo ([Sect. 13.5](#))
 - Short time between radiofrequency pulses so lower flip angles must be used, which can lead to lower SNR and contrast-to-noise ratio (CNR) relative to other sequences.
 - Relatively long acquisition time per image, which limits the maximum heart rate at which perfusion imaging may be performed. Can be combined with acceleration techniques such as parallel imaging to speed up image acquisition.
2. Balanced steady-state free precession (bSSFP) ([Sect. 13.5](#))
 - Highest CNR of all three sequence types
 - Sequence type most prone to artifacts
3. Hybrid echo planar imaging (EPI) ([Sect. 13.5](#))
 - Multiple data lines acquired per radiofrequency pulse
 - Potentially higher flip angles than gradient echo, which can translate into a higher CNR
 - Shorter acquisition time per image, allowing imaging at higher heart rates than gradient echo
 - Similar level of artifacts to gradient echo

In all three cases, T1 contrast is introduced by the use of a magnetisation preparation pulse ([Sect. 16.11](#)) (saturation pulse). Whatever pulse sequence is chosen, ideally it should permit the acquisition of at least three SA slices (apical, mid, and base), every heart beat, with an in-plane spatial resolution of less than 3 mm (to minimize “dark rim” artifacts) ([Fig. 19.20](#)).

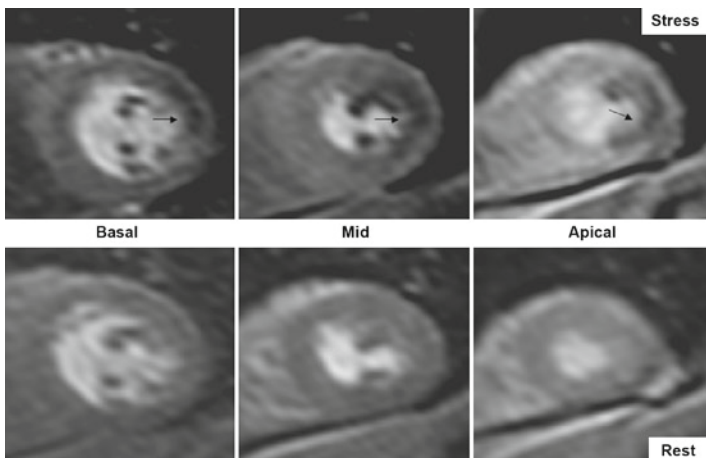


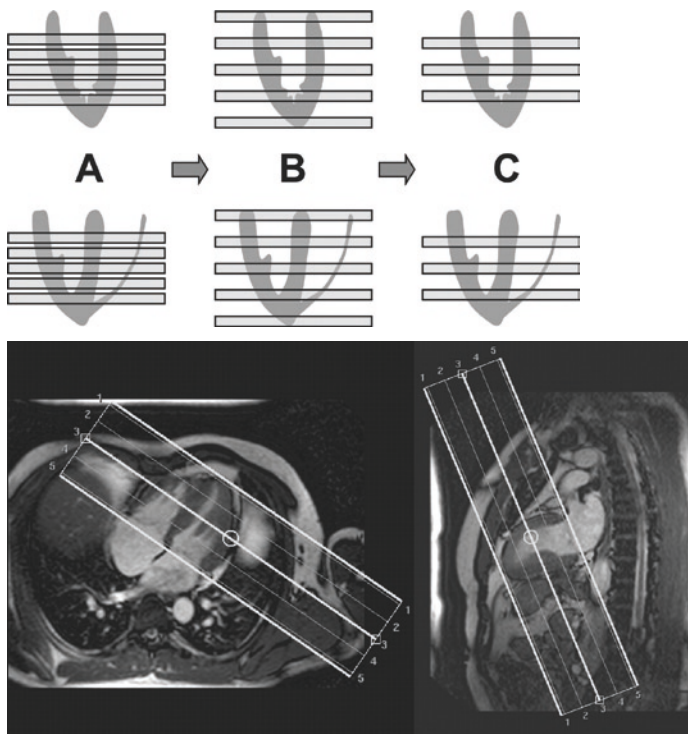
FIGURE 19.20. First-pass MR perfusion study. Three slices are acquired during adenosine stress (*upper row*) and at rest (*lower row*). A lateral wall perfusion defect is demonstrated at stress (arrows), but no abnormality is seen at rest. Coronary angiography revealed subtotal occlusion of a large obtuse marginal branch of the circumflex artery.

19.8.1 Reproducible Planning of Three Short Axis Slices

It is important to position the three SA slices correctly. If they are too basal, the LVOT will appear in the slice and make some segments uninterpretable. If they are too apical, then you will only image the apical cap. In addition, if serial studies are planned it is important to “individualize” the slice positioning for that patient so that future studies can be performed in exactly the same location. The “3 of 5” technique allows this to be achieved.

The “3 of 5” Technique

1. Use the 4-ch and VLA localizer views for planning. Advance both of these scans into end-systole (maximal LV contraction).
2. Plan *five* 10-mm-thick SA slices (Stage A).
3. Alter slice gap to achieve coverage from the mitral valve plane to the apex of the LV cavity (Stage B).
4. Reduce the number of slices to *three*, leaving optimally positioned apical, mid, and basal slices (Stage C).



Perfusion Module

1. Scout imaging as per LV structure and function module
2. Saturation-recovery imaging with gradient echo-echo planar (GRE-EPI) hybrid, GRE, or SSFP readout
3. Parallel imaging, twofold acceleration, if available
4. Readout temporal resolution ~100–125 ms or shorter as available
5. SA view imaging (at least three slices per heartbeat); preferably obtain data every heart beat
6. Slice thickness 8–10 mm; in-plane resolution <3 mm
7. Contrast is given (0.05–0.1 mmol/kg, 3–7 mL/s) followed by at least 30 mL saline flush (3–7 mL/s)
8. Breath-hold starts during early phases of contrast infusion before contrast reaches the LV cavity
9. Image for 40–50 heartbeats, by which time contrast has passed through the LV myocardium

19.8.2 Dark Rim Artifact

The “dark rim artifact” is a common abnormality seen during perfusion imaging. A number of factors contribute to its existence, including magnetic susceptibility effects, Gibbs ringing, cardiac motion, and spatial resolution. It may mimic a subendocardial perfusion defect in its location but has certain characteristics that allow it to be differentiated from a genuine perfusion defect (Fig. 19.21):

- The artifact is usually most intense when signal intensity reaches a peak in the LV cavity. As this is before the arrival of contrast in the myocardium, it cannot be attributed to a blood supply issue.
- The artifact is generally short-lived, often lasting only 5–10 dynamic frames in duration.
- The location of the artifact is often determined by the pulse sequence design. If a consistent design is used for all of the studies, the experienced observer will learn to recognize where the artifact occurs and not misread it as a perfusion abnormality.

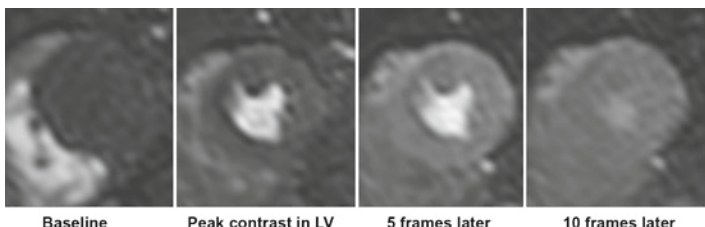


FIGURE 19.21. A typical subendocardial dark rim artifact is seen in the septal wall of a healthy volunteer. Characteristically, it is of maximal intensity when contrast levels peak in the LV cavity and fades as contrast enters the myocardium.

19.8.3 Interpretation of CMR Myocardial Perfusion Images

MR perfusion images may be assessed by either visual or semi-quantitative/fully quantitative means. In a clinical setting, visual assessment is generally preferred, as this requires no additional post-processing.

19.8.3.1 Visual Assessment

As all CMR perfusion sequences are T1-weighted to maximize the signal generated by a gadolinium-based contrast agent, the principles of visual assessment are identical irrespective of the pulse sequence design used. Contrast agents shorten T1 and so increase signal intensity. If the coronary blood supply is normal, the myocardium should develop a homogeneous grey appearance after first pass. However, where there is a functionally significant obstruction to myocardial blood flow, the entry of a contrast agent will be impaired. This manifests as a darker area, “a perfusion defect,” in the poorly perfused myocardium.

Perfusion should be assessed and recorded in accordance with the 17-segment American Heart Association model. However, a three-SA slice acquisition strategy will not provide views of segment 17 (true apex), so typically

only 16 segments are reported. Perfusion defects should be graded according to their transmurality. Stress perfusion images should be compared with late gadolinium enhancement (LGE; +/- rest perfusion images if acquired) to identify inducible ischemia, infarction, artifacts, and normal areas of perfusion.

19.8.3.2 Quantitative/Semi-Quantitative Assessment

The first pass of contrast into the myocardium can be assessed objectively by semi-quantitative and fully quantitative means. However, this is a time-intensive process which currently lends itself better to research rather than to normal clinical practice.

1. Contours are drawn around the epicardial and endocardial surfaces of the left ventricular myocardium and an area of interest is drawn within the LV cavity using a dedicated software package (Fig. 19.22).

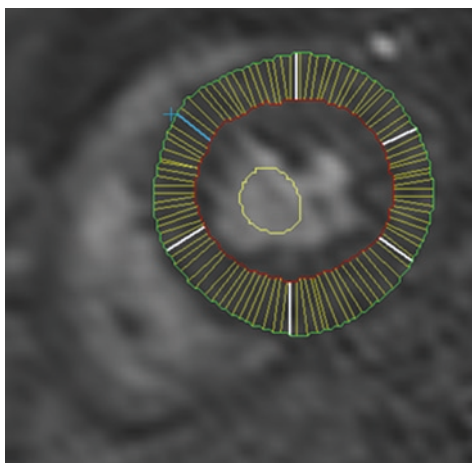


FIGURE 19.22. Perfusion contours. Epicardial (green), endocardial (red), and LV blood pool (yellow) contours are drawn on each phase of every slice of both the rest and stress perfusion images to allow an objective assessment of first-pass myocardial perfusion.

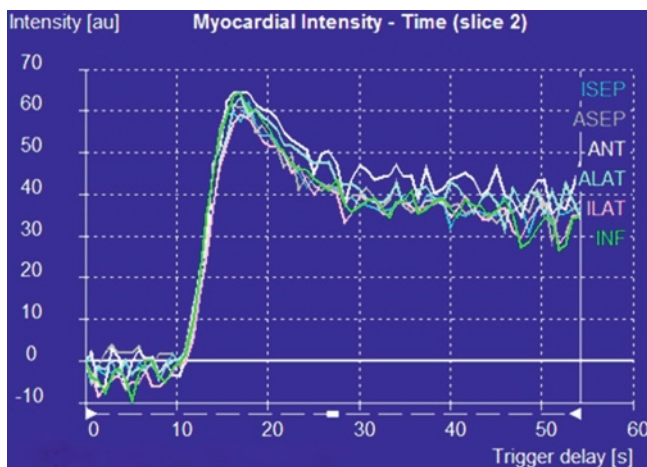


FIGURE 19.23. First-pass CMR myocardial perfusion curve from a normal individual. Each colored line represents the signal intensity/time profile in a different myocardial segment, as indicated by the legend on the right-hand side of the graph.

2. The myocardium is divided into six segments and the signal intensity in each region is calculated.
3. A graph of signal intensity versus time can be generated for each myocardial segment and for the LV blood pool (Fig. 19.23).

A semi-quantitative assessment of perfusion is undertaken by calculating the myocardial perfusion reserve index (MPRI). This is undertaken as follows:

1. The maximal upslope of the signal intensity-time curves for the myocardium and left ventricular blood flow is calculated by the software using a “line of best fit.”
2. The myocardial upslope at stress and rest is divided by the corresponding LV blood pool upslope, to correct for differences in the arterial input function at stress and rest.
3. The MPRI is then calculated by dividing the corrected upslope value at stress by the value at rest. This value correlates with myocardial blood flow but does not represent absolute flow.

It is also possible to use the signal intensity profiles to estimate absolute myocardial blood flow in mL/g/min. Several model-dependent or model-independent analysis methods have been proposed, but are rarely used in clinical routine.

Tips and Tricks

- Always run a “dummy” scan to ensure correct slice positioning and that there are no parallel imaging (wrap) artifacts. Ensure on the dummy scan that triggering really does occur every single heartbeat; if necessary reposition the ECG and repeat the dummy.
- When the heart rate is too high (e.g., during stress) switch to alternate heartbeat acquisition (some systems may do this automatically).
- Keep the field of view as small as possible (without wrap) to maximize in-plane spatial resolution.
- Angle the field of view so that it is parallel to the anterior chest wall to minimize the chance of getting wrap.
- Make sure that both intravenous (IV) lines are patent and that 3-way taps are opened correctly and all lines are attached before you start.
- Make sure you know what to do in the event of serious arrhythmia or complications during stress perfusion imaging.

19.9 Early and Late Gadolinium Enhancement

Following animal and clinical validation in the late 1990s, this technique has become established as one of the most fundamental in CMR clinical practice. Often referred to as delayed enhancement imaging (or delayed hyper-enhancement imaging), it is used principally for the detection of irreversible myocardial damage (infarction or fibrosis) typically seen in ischemic, infiltrative (e.g., sarcoid, amyloid), and other forms of cardiomyopathy (e.g., dilated cardiomyopathy (DCM,

hypertrophic cardiomyopathy (HCM), and Fabry's disease). The technique is also used as an adjunct to tissue characterization, for example imaging of tumors and their differentiation from simple thrombus (see Chap. 25).

As the name suggests, this technique involves the use of a gadolinium-based IV contrast agent. The gadolinium is bound to a chelate so as to avoid toxicity (e.g., gadolinium diethylene triamine penta-acetic acid (Gd-DTPA)), which limits its distribution to the extracellular space. As cell membrane integrity is preserved in normal and viable myocardium, the extracellular space is minimal, such that the volume of distribution of gadolinium is small and hence there is no contrast enhancement of living myocardium. The sharp demarcation of myocardial necrosis by LGE relates to the increased concentration of contrast material within necrotic tissue. The disruption of cell membranes in acute myocardial infarction allows gadolinium to passively diffuse into the intracellular space. This increases the distribution volume of gadolinium and, in combination with slower washout kinetics, leads to relative hyper-enhancement compared to normal myocardium, which can be detected in the late washout phase. However, LGE also highlights chronic myocardial infarction and this is thought to be due to accumulation of gadolinium in the collagen matrix of the infarcted tissue.

Gadolinium shortens T1 relaxation and therefore increases the signal intensity on T1-weighted images. The contrast between normal myocardium and infarcted tissue should be optimized by manually setting the TI delay so that normal myocardium appears black and infarcted myocardium is bright white. This can be determined by performing a "Look locker" or "TI scout" sequence. Most commonly a 2D segmented inversion recovery (IR) gradient echo sequence is used, timed to readout at mid-diastole (to reduce motion artifact), with a single slice acquired per breath-hold (see Sect. 16.6). For a more rapid assessment (but lower spatial resolution) a 3D acquisition can be used to cover the entire LV in a single (but longer) breath-hold. A more recent alternative is the phase-sensitive IR-GRE (PSIR) sequence, which avoids the need for precise "nulling" of normal myocardium (Fig. 19.24). The practicalities of performing early gadolinium enhancement (EGE) and LGE imaging are described below.

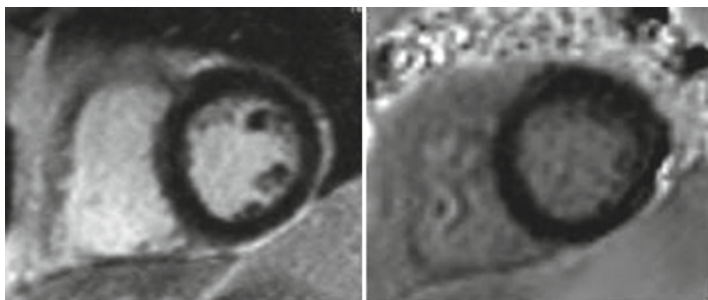


FIGURE 19.24. Mid-ventricular SA LGE images from the same patient showing the standard 2D IR-GRE sequence and the PSIR sequence.

19.9.1 *Protocol for Early and Late Gadolinium Enhancement Imaging*

1. Administer a bolus IV injection of gadolinium-based contrast agent at a dose of 0.1–0.2 mmol/kg.
2. For the EGE technique (detection of microvascular obstruction or intra-cardiac thrombus), imaging is performed immediately after contrast administration (and usually no later than 5 min) with a fixed long TI, often 400–500 ms. Typically images are acquired in the VLA, SA, and 4ch orientations. This produces images whereby normal myocardium has an intermediate signal intensity (grey) and areas of microvascular obstruction or thrombus appear black as contrast has not been able to permeate into them due to their lack of blood supply (Fig. 19.25).
3. For the LGE technique, imaging typically starts at around 10 min post contrast injection. For this to be performed correctly the optimal TI to “null” the signal from normal myocardium must be determined. This can be done by performing a “Look Locker” or “TI scout” sequence. This is a breath-hold sequence whereby a series of images are acquired, each with a progressively longer TI. These images can then be examined by the operator to decide which TI

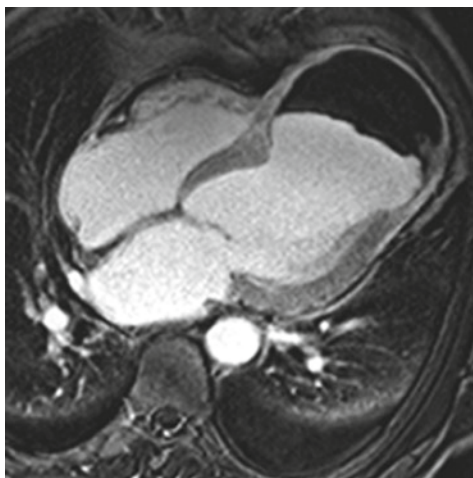


FIGURE 19.25. EGE image acquired in the 4ch orientation showing intermediate signal intensity (grey) in normal myocardium and a large apical thrombus (black).

depicts normal myocardium as black, i.e., nulled (Fig. 19.26).

4. A full stack of SA slices is then usually acquired using this TI. As the TI for correct myocardial “nulling” changes with time, typically the TI is increased by 10–15 ms before the VLA and 4ch slices are acquired. The Look Locker TI scout can be repeated at any point if the chosen TI appears to be incorrect. The technique of LGE applied according to this convention produces images whereby normal myocardium appears black and areas of infarction or fibrosis appear white (hence the well-used phrase “*white is dead*”).

Early and Late Gadolinium Enhancement Module

1. Use 2D-segmented IR GRE imaging during diastolic standstill.
2. Same views as for cine imaging (SA, VLA, 4-ch).

3. In-plane resolution ~1.4–1.8 mm.
4. For EGE, image immediately after contrast with a set TI of 440 ms.
5. For LGE wait 10 min after gadolinium injection (0.1–0.2 mmol/kg). Note: The delay may be shorter than 10 min if lower doses are used.
6. TI set to null normal myocardium (use a T1 scout or Look Locker sequence). Alternative is to use fixed TI with a phase-sensitive sequence.
7. Readout is usually every other heartbeat but could be modified to every heartbeat in the setting of bradycardia, and every third heartbeat in the setting of tachycardia.

Tips and Tricks

- When acquiring LGE images, help in determining the optimum TI can be gained from the performance of a “Look Locker” or “TI scout” sequence.
- Once determined, the correct TI for “nulling” of normal myocardium slowly changes over time; therefore every couple of minutes the TI needs to be increased by 10–15 ms.
- Images should generally be acquired in mid- or late-diastole to minimize cardiac motion artifact.
- Saturation ([Sect. 16.1](#)) bands can be applied across the spinal column and the anterior chest wall to reduce ghosting artifacts across the heart.
- If you are not sure whether there is an artifact or true abnormality on an image, “phase swapping” (i.e., changing the phase encoding direction) and repeating the scan should always be performed.
- Using a respiratory navigator and performing the scan during free breathing can help in those few patients who cannot perform an adequate breath-hold.
- Acquiring the images during every second or third heartbeat can help if there are problems with arrhythmia (e.g., atrial fibrillation).

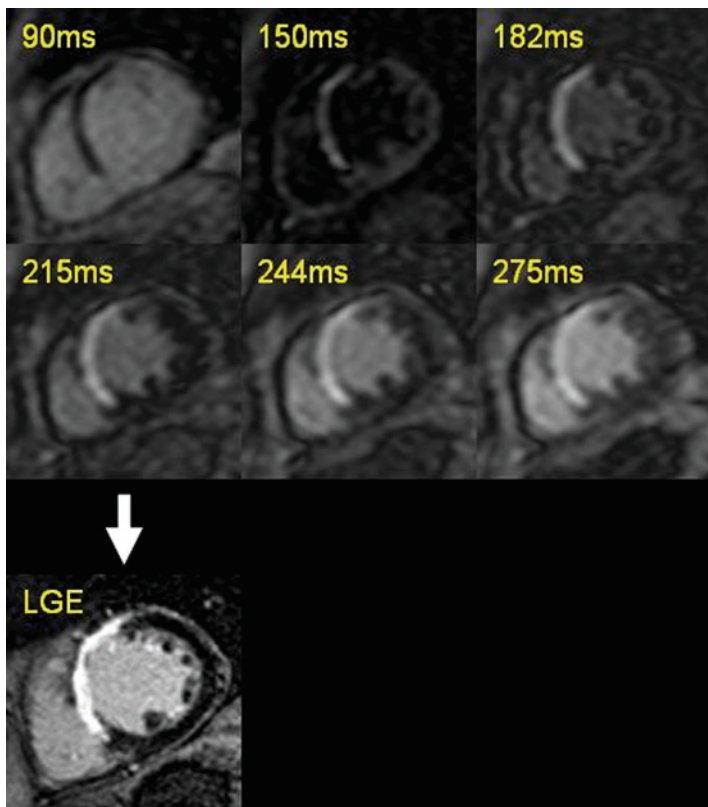


FIGURE 19.26. A typical “Look locker” sequence with increasing TIs. This patient had suffered an anterior MI. The normal myocardium appeared “nulled” (i.e., blackest) with a TI of 215 ms and this produced clear demarcation of the infarction (white appearance of the anterior wall and septum) on LGE imaging.

19.10 Coronary Artery Imaging

Although techniques for coronary MR angiography have improved over the last 10 years, it is still fundamentally limited by low spatial resolution and problems with cardiac and respiratory motion. As such this technique has really only limited clinical applications in the setting of ischemic

heart disease. Perhaps its main clinical use is in the detection and determination of aberrant coronary arteries and their anatomical course, for which CMR is the investigation of choice (due accuracy in classification and lack of ionizing radiation).

There are a variety of techniques available for coronary artery imaging by CMR, which will be summarized into two broad types:

1. “*Whole Heart Technique*” – a 3D volume of the heart is acquired from transverse slices at isotropic spatial resolution. Data can be reformatted off-line in any desired plane using post-processing software.
2. “*Targeted Technique*” – left and right coronary arteries are imaged separately using a smaller 3D volume specifically adapted for each coronary artery.

In general, a *navigator-gated free-breathing technique* is preferred (see [Sect. 16.7](#)). This method has the benefit of allowing much longer acquisitions with subsequently better SNR and resolution. This is the preferred method in the vast majority of patients, assuming a regular breathing pattern can be achieved. It is possible to acquire a 3D data set in a long breath-hold, especially when using multichannel coil arrays and parallel imaging. However, the achievable spatial resolution and SNR are limited.

19.10.1 Whole Heart Technique

- Perform a 4-ch cine acquisition with 50 phases (for coronary artery motion tracking). *Tip* – use a parallel imaging technique to reduce breath-hold duration.
- Perform a low-resolution 3D coronary survey. Position a “navigator” on the dome of the right hemi-diaphragm, approximately two thirds into the liver. Coverage should include the inferior border of the heart up to the pulmonary artery bifurcation ([Fig. 19.27](#)). Set “longest trigger delay” for optimal diastolic imaging. Then check for “navigator efficiency” ([Fig. 19.28](#)).

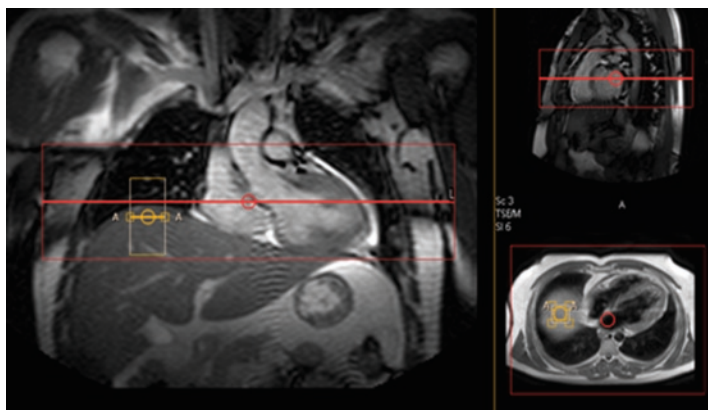


FIGURE 19.27. Coronal image showing the acquisition volume (red box) and the correct positioning of the respiratory navigator (orange box) in relation to the diaphragm.

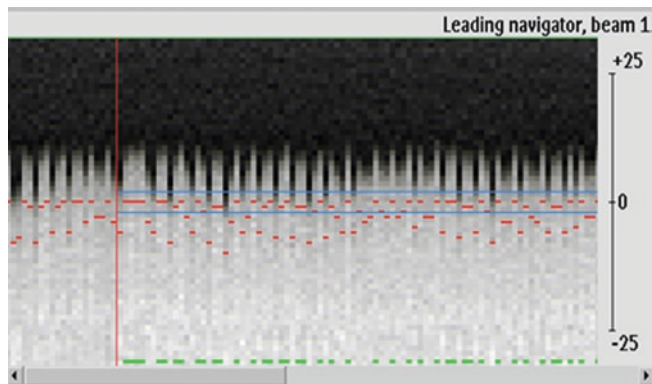


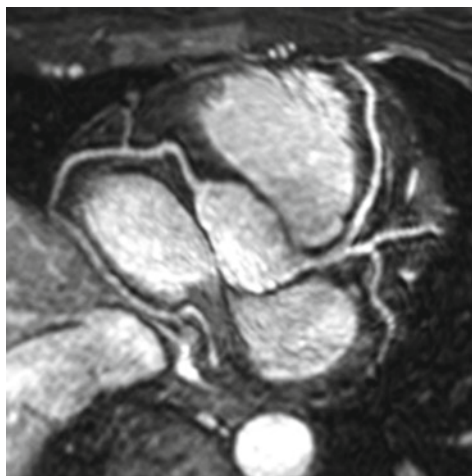
FIGURE 19.28. Screen grab from the scanner showing the motion of the lung-diaphragm interface during free breathing. Data is only 'accepted' for reconstruction when it is acquired within the narrow acceptance window (blue lines) - i.e. at a consistent point within the respiratory cycle, thus reducing the effect of respiratory motion on the cardiac image.

- If poor:
 - Practice breathing patterns with the patient.
 - Reposition the navigator to avoid vascular structures or fat planes below the diaphragm.
- Whilst the coronary survey is being acquired, scroll through the phases of the 4-ch cine and note the time points in the cardiac cycle when each coronary artery is stationary. Note that this is different for the left coronary artery (LCA) and the right coronary artery (RCA).
- Note the stationary overlap range for the LCA and RCA (see example in Fig. 19.29). The optimal timing range for imaging the LCA and RCA in this example is between 550 and 900 ms. If the overlap between the LCA and RCA is small (<50 ms), a timing range suited to the more important artery is selected. Remember, the left artery is usually more difficult to image and therefore timings chosen should favor imaging of the LCA.
- To plan a 3D whole-heart acquisition adjust the number of slices to cover left ventricular apex to pulmonary artery bifurcation by checking coverage on the 3D coronary survey images. Select a “trigger delay” that corresponds to, or slightly after, the start point of the optimal timing range. Adjust the “shot” or “acquisition” duration to fit in the optimal timing range (best results are obtained below 100 ms). Reduce the rectangular field of view (RFOV) to reduce the scan time. The resultant 3D coronary data set can be manually reformatted to delineate the course of individual coronary arteries (Fig. 19.30).

	Left Coronary	Right Coronary	Over-lap Range
Early Diastole	550ms	500ms	From ~ 550ms
Late Diastole	1100ms	900ms	Up to ~ 900ms

FIGURE 19.29. Example of coronary artery rest periods.

FIGURE 19.30. Reformatted 3D coronary MRA data set using SoapBubble™ software.



19.10.2 Targeted Technique

This technique relies on the patient being able to perform a reasonably long breath-hold. Perform a low-resolution 3D coronary survey as described above. Then use the “3-Point Plan Scan” facility to plan the optimal imaging plane for either LCA or RCA imaging. Typically points are placed at the ostium, mid vessel, and at the distal vessel. If the whole of the LCA needs to be imaged in a single acquisition, the points will need to be chosen in both the left anterior descending artery (LAD) and the left circumflex artery (LCx) (Figs. 19.31 and 19.32).

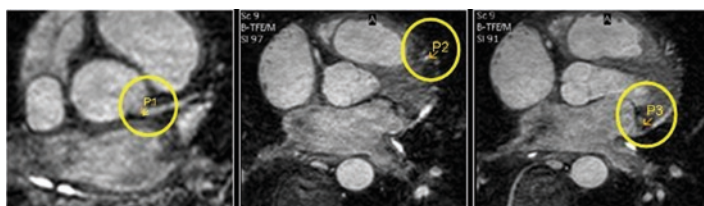


FIGURE 19.31. The targeted technique: LCA using “3-Point Plan Scan. Point 1 – origin of left main stem; Point 2 – mid-distal portion of LAD; Point 3 – mid-distal portion of LCx.



FIGURE 19.32. The targeted technique: RCA using “3-Point Plan Scan.” Point 1 – origin of RCA; Point 2 – mid portion of RCA; Point 3 – distal portion of RCA.

Coronary Artery Imaging Module

1. Repeat HLA with high temporal resolution (50 phases) to accurately determine quiescent period of RCA.

Navigator-gated, 3D, free-breathing, MRA sequence:

2. Trans-axial slices spanning from level of proximal main pulmonary artery down to the middle of the right atrium (entire cardiac coverage if desired). Slice thickness 1–1.5 mm; acquired spatial resolution in-plane of 1.0 mm or less.
3. Slices – typically 50–80, as needed to encompass vessels of interest.
4. Adjust trigger delay and acquisition window according to observed coronary artery rest period.
5. Parallel acquisition preferred; navigator placed over the right hemi-diaphragm.
6. Optional – consider contrast to increase vessel conspicuity.

Optional:

7. Breath-hold techniques if poor image quality or if navigators are unavailable or are of poor quality.
8. T2-prepared sequence may be useful.

Tips and Tricks

1. If no rest period between systole and diastole is seen, repeat high temporal resolution 4ch cine scan at the correct cardiac frequency and reassess for rest periods. Hint: timings are more accurate when this is performed just before the actual coronary artery acquisition. Consider cine scan during free breathing if heart rate changes during breath-hold. Correct input of the heart rate (for the 4ch cine) ensures that the full cardiac cycle is captured to allow accurate identification of the rest periods.
 2. Still no rest period seen. Solution 1: Check for early rest period during systole and scan with a tight window (<50 ms). It is sometimes possible and necessary to scan during systole if there is a short natural rest period. A short acquisition duration is necessary to avoid blurring.
 3. Still no rest period seen in systole or diastole. Solution 2: Select longest trigger delay and scan with a tight window (<50 ms). In some cases there are no natural coronary artery “rest periods” in the cardiac cycle. Scanning at the longest trigger delay with a short acquisition duration is a compromise that may be useful in some cases.
 4. Heart rate is 90 bpm or above. The solution is to scan with the tightest scan window possible. This will minimize blurring of the coronary arteries and due to the high heart rate, the scan will be completed in a faster time.
- Remember:
 - Coronary blurring occurs with the slightest movement.
 - Keep scan times to a sensible limit.
 - Higher spatial resolution equals longer scan times.
 - Longer scan times can lead to more patient movement.

Chapter 20

Anatomy by CMR

Charles Peebles

20.1 Cross-sectional Anatomy

A basic understanding of the anatomy is a prerequisite for performing and interpreting a CMR examination. A detailed discussion of cardiac anatomy is beyond the scope of this text but this section will provide an introduction to the essentials of cardiac and thoracic anatomy as applied to CMR.

One of the strengths of MRI is the unique ability to acquire images in any cross-sectional plane. Whilst this allows visualization of complex structures in the optimal orientation it does demand a three dimensional understanding of relevant anatomy.

The standard imaging planes are axial, coronal, and sagittal. All CMR examinations will include a localizing scan which uses these orientations. In addition most studies will also obtain a stack of images, usually in an axial plane, as a prelude to planning the specific views along the cardiac axis. These images are often acquired with a “black blood” sequence. Figures 20.1, 20.2, and 20.3 demonstrate standard anatomy in the axial, coronal, and sagittal planes, respectively. Axial images are conventionally viewed as though from the feet and ordered from top to bottom. Coronal images are viewed as though from the front and ordered front to back. Sagittal images are viewed as from the patients left side and ordered right to left.

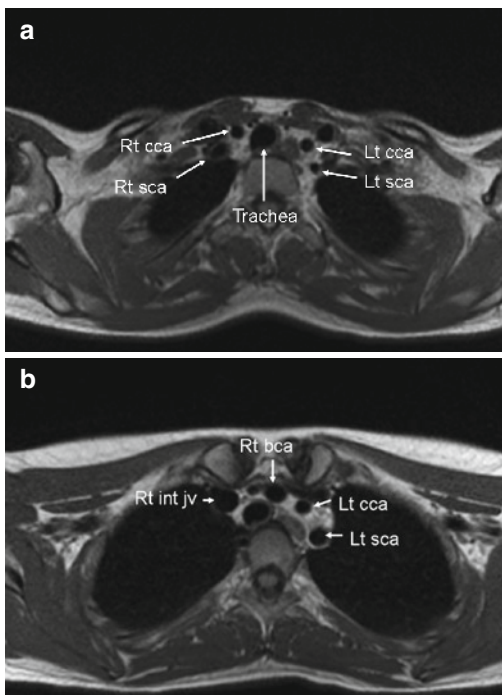


FIGURE 20.1. Axial black blood images. Rt cca, right common carotid artery; Rt sca, right subclavian artery; Lt cca, left common carotid artery; Lt sca, left subclavian artery; Rt int jv, right internal jugular vein; Rt bca, right brachiocephalic artery; SVC, superior vena cava; Ao, aorta; rmb, right main bronchus; lmb, left main bronchus; lpa, left pulmonary artery; rpa, right pulmonary artery; mpa, main pulmonary artery; lupv, left upper pulmonary vein; llpa, left lower pulmonary vein; rupv, right upper pulmonary vein; rtbim, right bronchus intermedius; lca, left coronary artery; LAA, left atrial appendage; lltb, left lower lobe bronchus; RAA, right atrial appendage; rca, right coronary artery; rvot, right ventricular outflow tract; lad, left anterior descending coronary artery; cx, circumflex coronary artery; llpv, left lower pulmonary vein; ct, crista terminalis; LA, left atrium; lvot, left ventricular outflow tract; RA, right atrium; RV, right ventricle; LV, left ventricle; pap m, papillary muscle; TV, tricuspid valve; mb, moderator band; IVC, inferior vena cava; PV, pulmonary valve.

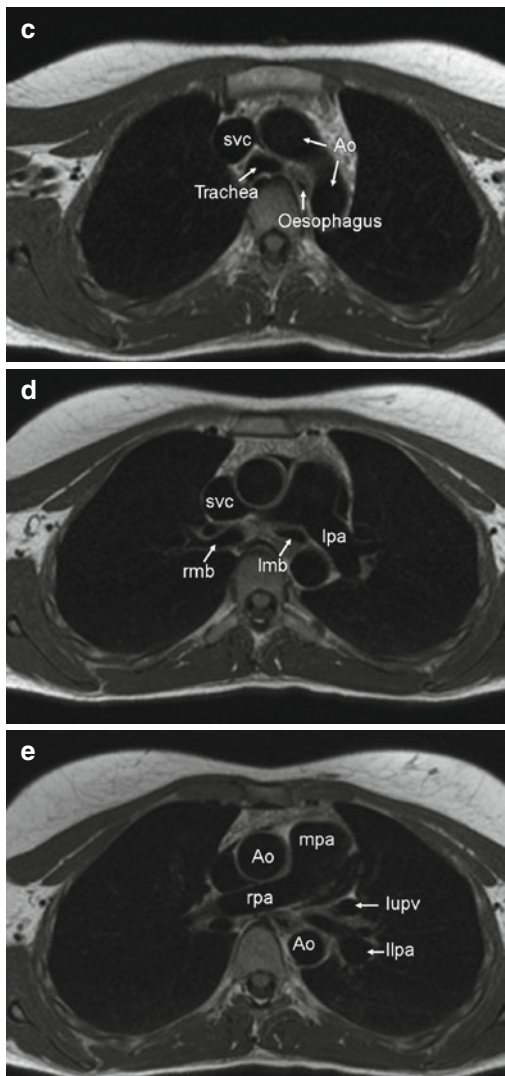


FIGURE 20.1. (continued).

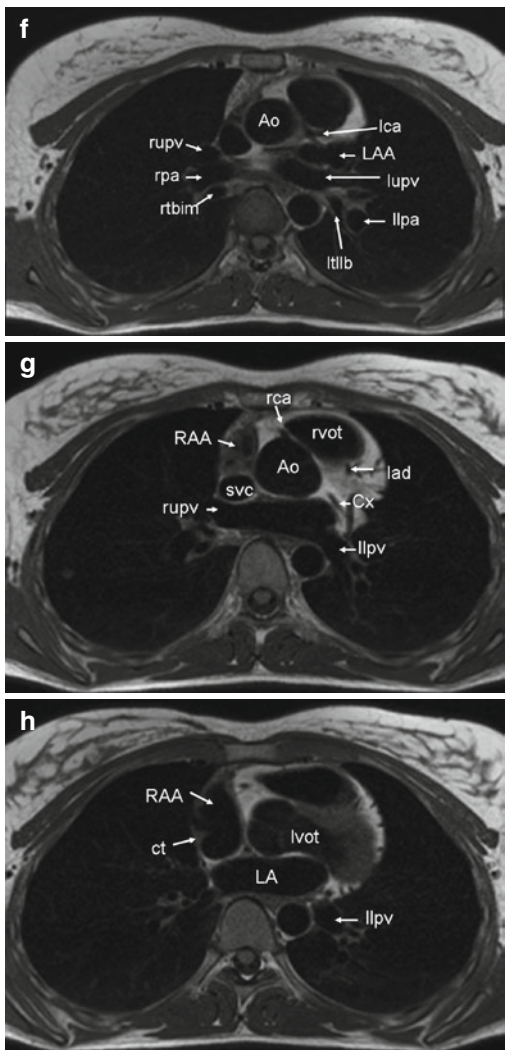


FIGURE 20.1. (continued).

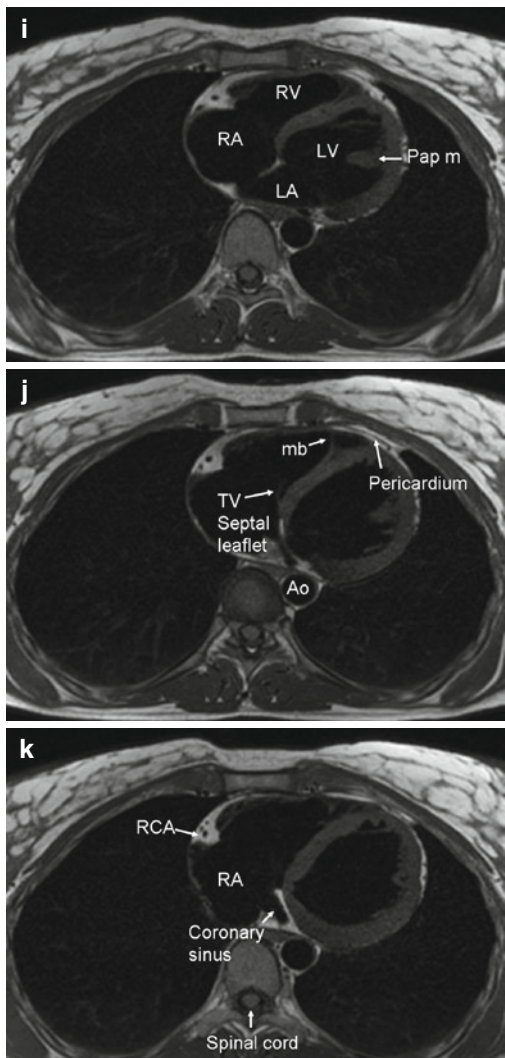


FIGURE 20.1. (continued).

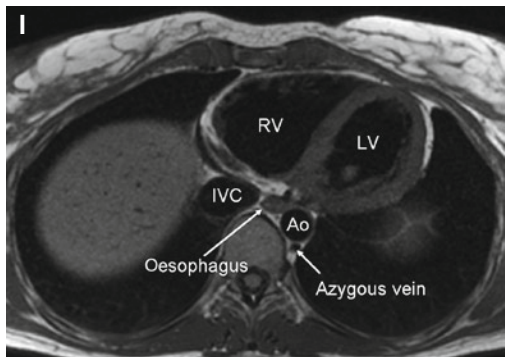


FIGURE 20.1. (continued).

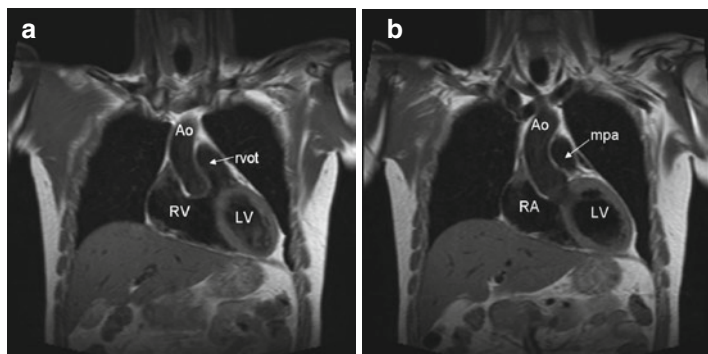


FIGURE 20.2. Coronal black blood images. Lt sca, left subclavian artery; Rt int jv, right internal jugular vein; Rt bca, right brachiocephalic artery; SVC, superior vena cava; Ao, aorta; rmb, right main bronchus; lmb, left main bronchus; lpa, left pulmonary artery; rpa, right pulmonary artery; mpa, main pulmonary artery; lupv, left upper pulmonary vein; llpv, left lower pulmonary vein; rupv, right upper pulmonary vein; lca, left coronary artery; rvot, right ventricular outflow tract; llpv, left lower pulmonary vein; LA, left atrium; lvot, left ventricular outflow tract; RA, right atrium; RV, right ventricle; LV, left ventricle; mv, mitral valve; IVC, inferior vena cava.

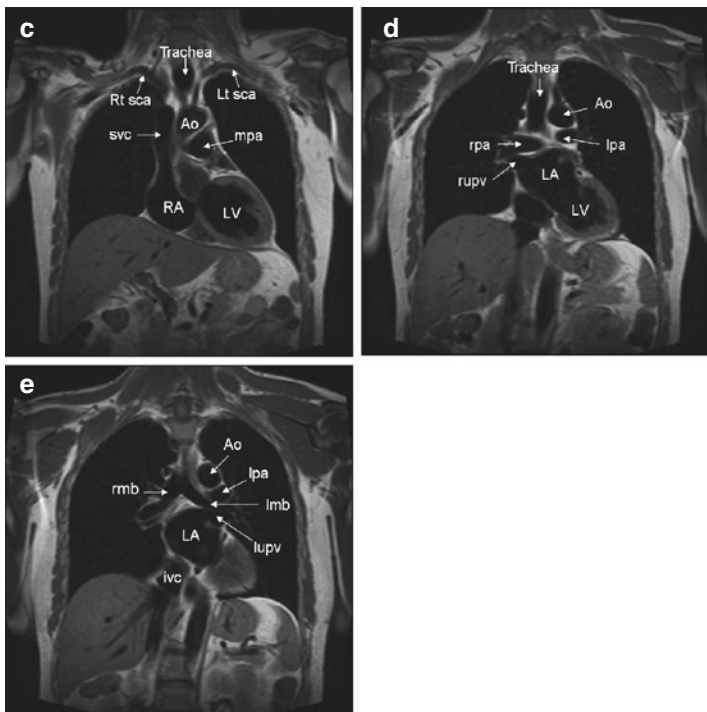


FIGURE 20.2. (continued).

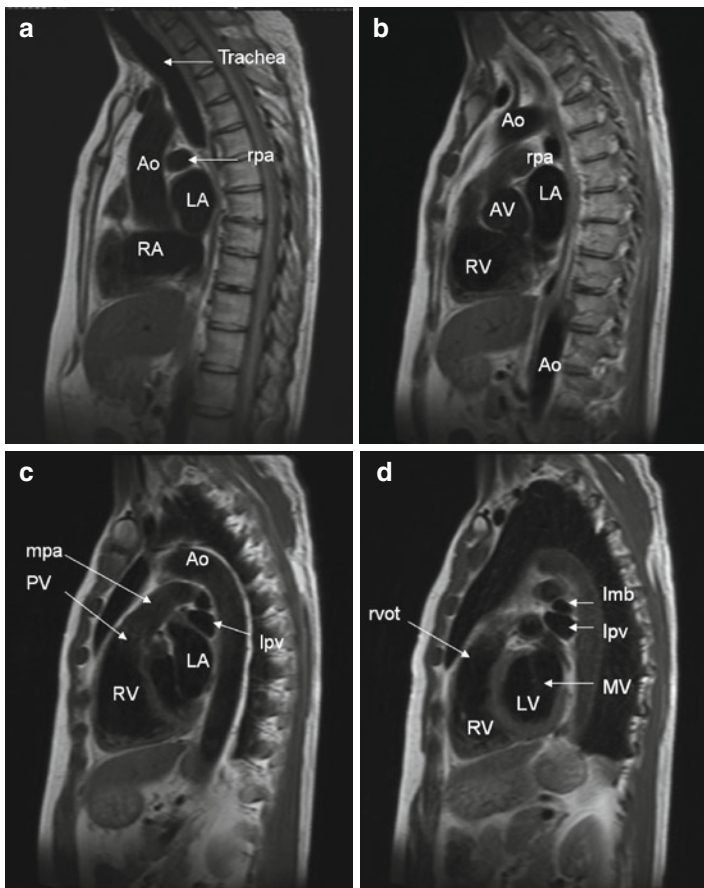


FIGURE 20.3. Sagittal black blood images. SVC, superior vena cava; Ao, aorta; rmb, right main bronchus; lmb, left main bronchus; lpa, left pulmonary artery; rpa, right pulmonary artery; mpa, main pulmonary artery; rpv, right pulmonary vein; rvot, right ventricular outflow tract; llpv, left lower pulmonary vein; LA, left atrium; lvot, left ventricular outflow tract; RA, right atrium; RV, right ventricle; LV, left ventricle; TV, tricuspid valve; MV, mitral valve; IVC, inferior vena cava.

20.2 Customized Views

The variable orientation of the heart and great vessels within the thorax necessitates further imaging in specific planes to allow accurate and reproducible assessment of the cardiac structures. These customized views are largely comparable with the echocardiographic views of the heart and great vessels and are planned from the axial images obtained earlier in the examination. They are generally designed to assess the intracardiac structures and because of their complex obliquities in a number of planes can cause confusion if looking at extra cardiac structures.

20.3 Comparison with Other Imaging Modalities

Echocardiographic imaging planes resemble the customized CMR views. Cardiac CT acquires an axial stack of data, which then during post-processing can be reformatted in any plane comparable to CMR.

Tips and Tricks

1. If unsure about anatomy always scroll up and down through the image stack following the relevant structure – this will almost always answer the question.
2. When acquiring the scan images always obtain views in orthogonal planes if there is a difficult anatomical question to be answered.
3. Three-dimensional data sets such as MR angiograms will often give optimal anatomical views particularly of great vessels and extracardiac structures.
4. On black blood images, it can be difficult to differentiate between air-containing (bronchi) and fluid-filled (blood vessels) structures. Compare with bright blood (cine) images in cases of uncertainty.

Chapter 21

The CMR Report

Sven Plein

A typical CMR study generates hundreds of images and consists of many different image types. Reporting a CMR study, therefore, requires a comprehensive and structured approach.

21.1 A Structured Approach to Reporting a CMR Study

In this chapter an outline of a structured approach to reporting a CMR study is given. This is complemented by indication-specific suggestions for reporting in **Part III** of this book (Clinical indications for CMR).

1. Identify the key clinical questions from the referral letter.
2. Review if possible original data from relevant related procedures such as echocardiography or angiography.
3. Identify the correct CMR study on the patient database by checking patient name, date of birth, unique identification number, and study date.
4. Check that all CMR data are available for reporting.
5. Take note of any particular circumstances affecting the CMR study (such as ECG-gating problems, arrhythmia, breath holding problems, etc.).
6. Start the data review by gaining an overview of the gross cardiovascular anatomy. This overview can use localizer or other data that cover the largest section of the heart and

great vessels. A stack of axial black blood or cine images is an ideal source. This overview can be quick or may need to be more detailed, for example, in patients with congenital heart disease. It is useful to focus on the vascular morphology and connections and the extracardiac findings separately. Every CMR report should include an assessment of

- a. The connection of the great vessels and heart chambers
 - b. Global LV and RV dimensions and function
 - c. The pericardium
 - d. Any other incidental findings (e.g., valve regurgitation)
 - e. Incidental extracardiac findings. However, when reporting potential extracardiac findings, recognize and indicate in your report that CMR images are optimized for the cardiovascular system and not for a diagnostic assessment of abnormalities outside of the cardiovascular system.
7. Depending on the specific indication now look at the acquired data in a logical order. For example, in a study indicated for assessment of myocardial ischemia, one might want to assess the components of the scan in the following order:
- a. Global and regional LV function from cine images
 - b. Presence and extent of scar from late gadolinium-enhanced images
 - c. Presence and extent of inducible ischemia outside scar from stress perfusion images
 - d. If applicable, comparison of stress with rest perfusion images to identify artifacts.
8. Relating to the scan indication and any previous imaging reports, an overall summary and conclusion(s) should complete the report. Be mindful that this is the part of the report that referring clinicians will often read first – or indeed the only part they will read at all. Thus be sure to include all relevant information, while keeping the content concise. Be sure to answer specifically the clinical questions in the referral letter.
9. Images or Bull's eye plots may be added to the report to illustrate specific findings.

In Part III of this book, specific additional items that should be reported on for particular CMR indications are listed.

21.2 The Report

The Society of Cardiovascular Magnetic Resonance has published guidelines for reporting of CMR examinations.¹ The recommendation is that the report includes information pertaining to

- a. Site and equipment information
- b. Patient demographics
- c. Indications for study
- d. Study performance
- e. Cardiovascular imaging features of the examination
- f. Concluding statements that synthesize the study results into a comprehensive diagnosis that can be used for planning therapy or determining prognosis.

Figure 21.1 shows a sample CMR report.

<u>Cardiovascular Magnetic Resonance Report</u>	
Cardiac MRI Unit	Anywhere
Patient details: Name: Anthony Nonymous	Patient ID: 111111
Date of Birth: 01/01/1901	Gender: male
Height: 175cm	Weight: 80kg
CMR Study: Date of Procedure: 01/01/2010	Time of Procedure: 10:00am
Personnel involved in procedure: A. Consultant, B. Radiographer	
Scanner details: Vendor 1.5T, 6 element cardiac coil	
<i>Primary indication for test:</i>	
Previous anterior MI in 2001, now recurrent chest pain, ?ischaemia	
<i>Listing of sequences used:</i>	
<ul style="list-style-type: none"> • Non-contrast T1 weighted dark blood (axial stack) • Cine SSFP imaging • Adenosine stress and rest first pass perfusion • Late gadolinium enhancement 	
<i>Contrast agent:</i>	Magnevist, 24ml, i.v. right antecubital fossa.
<i>Stress agent:</i>	Adenoscan, 140mcg/kg/min for 5 minute, i.v., left dorsal hand vein.
<i>Haemodynamics:</i>	BP rest: 130/80mmHg, HR rest: 60bpm, BP stress: 140/80, HR stress: 73bpm.
CMR findings: <i>General findings:</i>	The patient was unable to hold his breath during the stress perfusion study, so that image quality was impaired. No other problems encountered. The gross vascular anatomy and connections are normal.
<i>Specific findings:</i>	The left ventricle is dilated, with a LVEDD of 68mm (measured in the ap direction at the tip of the papillary muscles). Global LV systolic function is mildly impaired. Volumetric measurements by summation of discs from a SAX stack are as follows: EDV: 228ml, ESV: 114ml, SV: 114ml, EF 50%. Indexed to BSA: The mid anterior and basal anterior and septal segments are hypokinetic, all other segments are normokinetic.
	Late gadolinium enhanced images demonstrate transmural (>75%) infarction of the mid anterior and basal anterior and septal segments. All other segments are viable.
	Adenosine stress provoked marked symptoms of chest tightness. The first pass perfusion images show an extensive perfusion defect in all anterior and septal segments.
Summary:	<ol style="list-style-type: none"> 1. Dilated LV with impaired systolic function and EF of 50% 2. Transmural anterior myocardial infarction in the mid anterior and basal anterior and septal segments 3. Inducible peri-infarct ischaemia in the LAD territory in 4 segments.
Dr. MR Expert, 01.01.2010	

FIGURE 21.1. Sample CMR report (Modified from the SCMR recommendation in Ref. [1]).

Reference

1. Hundley WG, Bluemke D, Bogaert JG, et al. Society for Cardiovascular Magnetic Resonance guidelines for reporting cardiovascular magnetic resonance examinations. *J Cardiovasc Magn Reson.* 2009;11(1):5.

Part III

Clinical Indications

for CMR Imaging

Chapter 22

Diseases of the aorta

Andrew M. Crean

The Role of CMR in Aortic Disease

1. To establish the location, size and patency of the aorta and its major branches
2. To assess the aortic wall and its components
3. To demonstrate inflammatory, vasculitic or atherosclerotic lesions
4. To follow noninvasively chronic aortic disease (e.g., type B dissection) and the postoperative aorta (e.g., following coarctation repair)

CMR Protocol in Aortic Disease

1. Anatomy module (see Section 19.3.1) (page X)
2. Flow module where relevant (see Section 19.6) (page X), for example, dissection, coarctation, and valvular lesions
3. MRA module (See Section 19.7)
4. Post-contrast T1-weighted imaging module where relevant, for example, arteritis
5. Special views – e.g., sagittal oblique SSFP imaging of aorta “candy cane view”
6. LV function module (Section 19.4)
7. Cine imaging of aortic valve

22.1 Introduction

Thoracic aortic disease is one of the commonest indications for performing a CMR study. The technique is particularly suited to examination of the aorta since it facilitates a wide field of view which – when employed in magnetic resonance angiography – allows the entire length of the vessel to be studied (Fig. 22.1). The lack of ionizing radiation is a distinct advantage also since many of the conditions for which MR is employed are chronic and will require multiple examinations over an individual's lifetime. Importantly, CMR provides anatomical and functional information about the aorta and in addition allows assessment of associated pathologies such as aortic valve disease and left ventricular function.

22.2 CMR versus Other Imaging Modalities

CT is the main competing imaging modality for assessment of the aorta. The main advantage of CT over CMR is the faster acquisition speed. In most acute presentations, CT is, therefore,

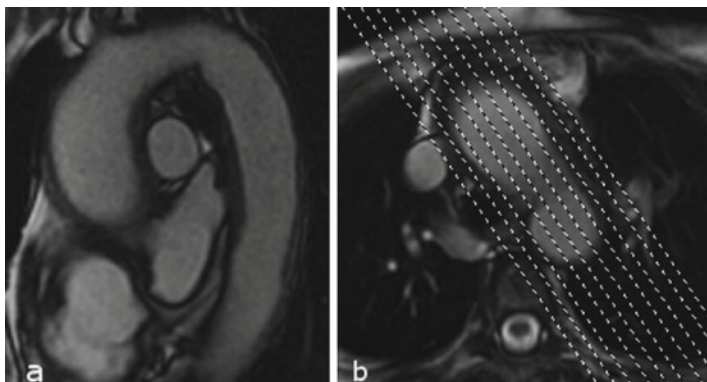


FIGURE 22.1. “Candy cane view” of the aorta (a). A useful sagittal oblique projection in which to perform cine imaging or MRA. Multiple slices are acquired parallel to the long axis of the aortic arch as shown (b).

the method of choice. The main reason for choosing CMR in an acute setting is if CT results are equivocal, exposure to ionizing radiation is a particular concern or CT is unavailable. The main role of CMR is the longitudinal follow-up of congenital and acquired diseases of the aorta, where radiation exposure is a more prominent concern. Echocardiography can assess the proximal aorta, but is not usually a sufficient test for aortic assessment.

22.3 CMR in the Assessment of Aortic Atherosclerosis and Dissection

Atherosclerosis is the dominant cause of mortality in the western world, largely from coronary arterial disease. However, there are a number of pathological manifestations of aortic atherosclerosis, which also account for significant morbidity and mortality. The entities of penetrating atherosclerotic ulcer (PAU), acute intramural hematoma (IMH), and acute aortic dissection are intertwined pathologically, yet have relatively individual CMR appearances.

22.3.1 Acute Intramural Hematoma

This condition is regarded as a *forme fruste* of aortic dissection. The initiating event is believed to be a spontaneous rupture of one of the vasa vasorum within the media of the aortic wall. The clinical presentation is similar to that of a standard aortic dissection (although often without differential BP if the great vessels are uninvolves). The resulting collection of blood is readily appreciated as localized, circumferential aortic wall thickening on either SSFP or black blood imaging (Fig. 22.2a). However, the majority of these cases are diagnosed by CT since this modality is readily available out of hours and the scan time much shorter – a major safety consideration with a potentially unstable patient. It is also one of the few conditions in which CT provides a degree of tissue characterization

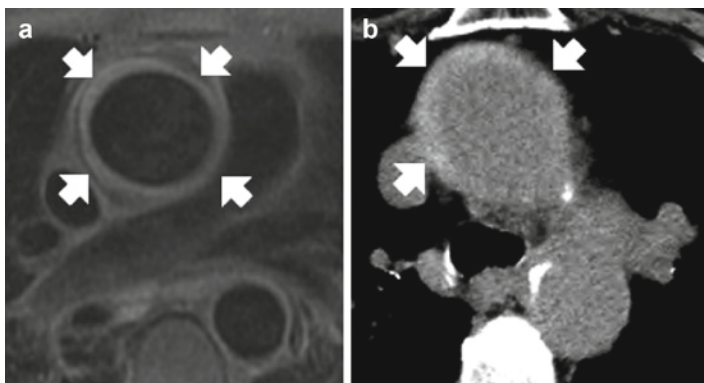


FIGURE 22.2. Acute intramural hematoma. Double inversion recovery MR image (**a**) shows circumferential thickening of the ascending aorta. This appearance is nonspecific and may also be seen in active vasculitis. However, non-contrast acute CT image (**b**) demonstrates a crescentic ring of increased density compared to the aortic lumen – this is due to the presence of hematoma in the aortic wall and confirms the diagnosis of IMH.

(usually the sole province of MR) (Fig. 22.2b). The main role of CMR, therefore, is to follow up the acute lesion to ensure that it stabilizes/resolves and that progression to chronic dissection does not occur.

22.3.2 Penetrating Atherosclerotic Ulcer

This entity often occurs on the background of generalized atherosclerosis and may also be a precursor to dissection. Just as in the coronary tree, the reason some plaques erode and fissure and some do not remains obscure. CMR readily identifies the site of focal erosion into the media (Fig. 22.3a), defines the extent of the abnormal collection, and identifies any associated thrombus formation. Volume-rendered imaging displays only the enhanced portion of an MR angiogram and aortic thrombus may be missed if only an early angiographic phase is acquired (Fig. 22.3b and c).

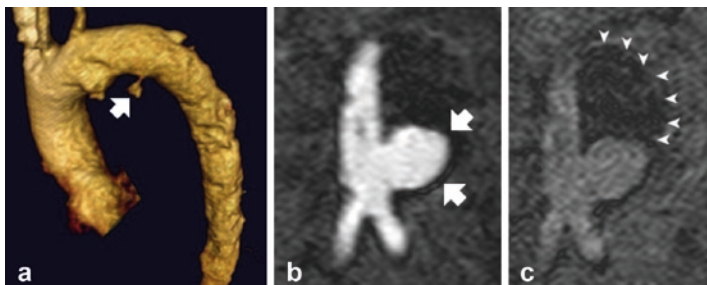


FIGURE 22.3. Penetrating atherosclerotic ulcer. (a) A volume-rendered reconstruction of a thoracic aortic MRA demonstrates a focal collection of contrast (arrow) beyond the arterial lumen. Note also the marked irregularity of the descending thoracic aorta due to widespread atherosclerosis. (b) A different patient with PAU and a large atherosclerotic ulcer which has transformed into a pseudoaneurysm (arrows) is clearly seen above the aortic bifurcation on this arterial phase MRA. A second venous phase (c) permits better visualization of the associated thrombus within the aneurysm cavity (arrowheads).

22.3.3 Aortic Dissection

For reasons given above the diagnosis of acute aortic dissection is appropriately more often sought by CT imaging (although CMR is equally accurate). However, if CMR is performed acutely the principal aim is to confirm the diagnosis and establish whether there is ascending aortic involvement (Stanford Type A) since this usually predicates immediate surgery. Ancillary signs – other than the presence of an intimal flap – include pericardial effusion and aortic valvular regurgitation. Identification of extension into head and neck vessels also pre-warns the surgeon that hemi-arch replacement may be indicated.

CMR is ideally suited to the follow up of chronic aortic dissection. The main points to encompass in the examination are shown in Table 22.1.

Acute CT imaging is often performed and reported in a necessarily hurried manner prior to transfer of the patient to

TABLE 22.1. Principal points to address in the CMR follow-up of aortic dissection.

Extent of dissection
Head and neck vessel involvement
Renal involvement – differential perfusion between the 2 kidneys in the venous phase of angiography suggests arterial compromise by dissection flap
Mesenteric involvement
Extension into the legs
Relative luminal size
Partial, complete or no thrombosis of false lumen
Progressive enlargement of the false lumen
Follow-up of surgical repair of type A dissection i.e., any evidence of new dissection in the non-replaced native portion (common in Marfan syndrome)?

a cardiothoracic center. On occasion, outside studies are not archived onto the tertiary center image vault. It is therefore vital that the first MR is thorough and answers all of the questions listed. Magnetic resonance angiography (MRA) should *always* be performed on the first occasion. *This is ideally done in the sagittal oblique plane to minimize coverage, allow for thinner slices, and maximize spatial resolution.* Follow up imaging can reasonably be performed without gadolinium contrast if axial or sagittal oblique cine imaging of the aorta is substituted (Fig. 22.4).

22.4 Aortic Aneurysm

Weakening of the medial layer of the aortic wall leads to progressive fusiform or focal enlargement of the aorta over time. Several congenital disorders, most importantly Marfan disease, are associated with life-threatening progressive dilatation and rupture. Susceptible individuals require close monitoring at least every 2 years whilst the aorta remains of normal size and more frequently once enlargement is established. A sinus of

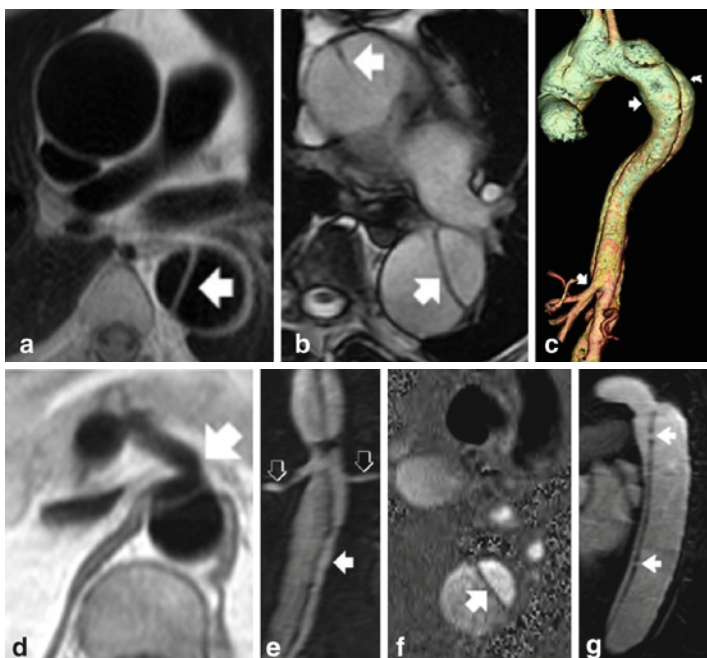


FIGURE 22.4. Dissection imaging. Either black blood (a) or cine imaging (b) may be used to identify dissection flaps (arrows). A volume rendered MRA (c) is a visually attractive method of demonstrating both true lumen (straight arrow) and false lumen (curved arrow) as well as the origin of major branch vessels – in this example the mesenteric vessels arise from the true lumen (oblique arrow). Thin slice axial imaging (different patient) also allows evaluation of vessel origin – here the celiac trunk arises from the smaller more anterior true lumen (d). Contrast MRA (e) demonstrating origin of both renal arteries (black arrows) from true lumen (white arrow). Phase velocity mapping of the descending thoracic aorta (f) demonstrates faster flow and thus a more intense white in the true lumen (arrow). Sagittal reconstruction from an MRA (g) demonstrates several fenestrations (arrows) in the intimal flap allowing exchange of blood between true and false lumens.

Valsalva measurement greater than 5.5 cm is an indication for root replacement in most institutions (less if pregnancy is anticipated). Examples of the predisposing conditions for aneurysm formation are given in Table 22.2 and Fig. 22.5.

Patients with unoperated but dilating aortic aneurysms are a source of considerable clinical anxiety. This should not be unduly heightened by inaccurate or inappropriate measurements of the aorta. The advantage of using a cine sequence for this is that the maximum diameter can be tracked throughout the cardiac cycle and, thus, subsequent examinations may be easily compared for genuine change. An MRA is less ideal for comparative measurements since it is usually performed ungated and as such represents the pulsating aorta averaged over multiple cardiac phases. Nevertheless, an MRA should be part of every initial assessment and ought to be repeated if the aneurysm is significantly enlarging since a volume render of this data set is often the most effective method of “accelerating” surgical assistance. When an MRA is performed, reconstructed double oblique imaging planes should be used to ensure accurate aortic dimensions are reported.

As with aortic dissection, MRA may miss sizeable aortic thrombus layering within an aneurysm unless a second acquisition is performed in the early venous phase following the initial contrast bolus.

TABLE 22.2. Conditions which predispose to aortic aneurysm formation.

Conditions in which aortic aneurysm may occur

Familial

Atherosclerotic

Congenital, e.g., Marfan, Tetralogy, bicuspid aortic valve, Sinus of Valsalva aneurysm

Postinfective, e.g., endocarditis, syphilis

Postsurgical, e.g., coarctation with subclavian flap repair

Vasculitic, e.g., SLE

Valvular, e.g., aortic stenosis

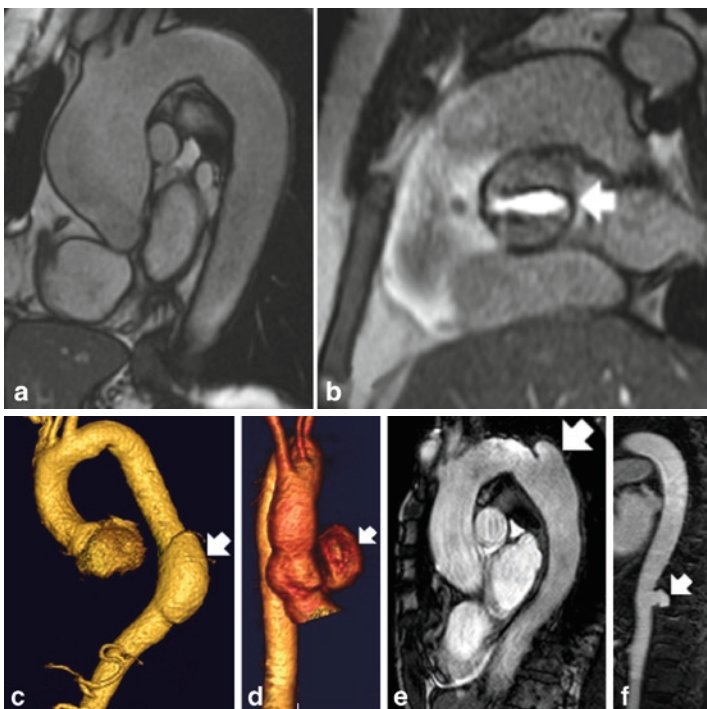


FIGURE 22.5. Examples of aortic aneurysm formation. Fusiform dilation of the ascending aorta (a) may occur as an aortopathy secondary to bicuspid aortic valve (b). Aneurysm following PAU (c). Aneurysm secondary to infective endocarditis (d). Aneurysm arising at site of previous subclavian flap patch repair of coarctation (e). Aneurysm arising due to aortic vasculitis – SLE in this example (f).

Key Points CMR in Aortic Disease

1. CMR is the method of choice for diagnosis and follow-up of non-acute aortic disease
2. All aortic imaging for an individual patient should be performed at a single center to allow for reproducible techniques and measurements
3. Optimum assessment results from a combination of anatomical and cine imaging

Tips and Tricks

- Always perform a second breath held venous phase MRA after the initial arterial phase study (free data set without re-injection)
- Standardize protocols so that the same technique, imaging plane, and slice thickness are used for each follow-up examination to facilitate meaningful comparison
- In an MR intolerant, restless or needle-phobic patient, a sagittal oblique cine acquisition (“candy cane view”) of the aorta provides 90% of the necessary information in approximately 15 min from start to finish.

CMR Report in Aortic Disease

Report dimensions (measured in diastole from cine image or MRA) of:

- a. Aortic annulus
- b. Sinuses of Valsalva
- c. Sinotubular junction
- d. Ascending and descending diameters at the level of the pulmonary artery.

Comment on:

- a. Position of aorta (right or left-sided)
- b. Sinotubular effacement
- c. Tortuosity of aorta
- d. Aortic atherosclerosis: location, mobility, extent, and estimate %-stenosis
- e. Aortic aneurysm: size, morphology, location, relation to branch vessels, presence of mural thrombus, visceral compressive effects, presence of periaortic, mediastinal, pericardial, or pleural fluid
- f. Aortic dissection: classification type, intimal flap, location of tear, areas of communication, size and extent of the true and false lumens, presence of mural thrombus or blood in false lumen, branch vessel involvement, presence of periaortic, mediastinal, pericardial, or pleural fluid
- g. Inflammatory diseases of the aorta: aortic wall thickness, multispectral appearance on different pulse sequences, contrast enhancement pattern, branch vessel involvement, presence of periaortic, pleural, or pericardial fluid
- h. Aortic flow: direction and magnitude of flow (if available)
- i. Associated aortic valvular stenosis or regurgitation

Chapter 23

Cardiomyopathies

Daniel Messroghli and Sven Plein

23.1 General Overview

In 1995, the World Health Organization (WHO) defined five classes of cardiomyopathies: Dilated cardiomyopathy (DCM), hypertrophic cardiomyopathy (HCM), restrictive cardiomyopathy, arrhythmogenic right ventricular cardiomyopathy (ARVC), and unclassified cardiomyopathies. According to the more recent scientific statement on “contemporary definitions and classification of the cardiomyopathies” published in 2006 by the American Heart Association (AHA)¹, cardiomyopathies are “a heterogeneous group of diseases of the myocardium associated with mechanical and/or electrical dysfunction that usually (but not invariably) exhibit inappropriate ventricular hypertrophy or dilatation and are due to a variety of causes that frequently are genetic. Cardiomyopathies either are confined to the heart or are part of generalized systemic disorders, often leading to cardiovascular death or progressive heart failure–related disability.”¹ This new definition acknowledges the wide range of myocardial diseases, some of which are primary (predominantly involving the myocardium), others secondary (due to a systemic disease affecting other organs).

CMR has emerged as the most powerful clinical imaging tool to detect and differentiate cardiomyopathies, except for those that primarily cause electrical rather than morphological changes of the heart (e.g., Brugada Syndrome). CMR is also the most sensitive method to screen family members of

affected individuals. While it is impossible to cover all cardiomyopathies in this text, the CMR features of the most common primary and secondary disorders will be discussed.

General CMR approach to the patient with suspected cardiomyopathy:

With the exception of ARVC, CMR protocols for patients referred for evaluation of cardiomyopathy should contain the following elements:

1. Anatomy module (Section 19.3.1)
2. LV function module (Section 19.4)
3. Late Gadolinium Enhancement (LGE) module (Section 19.9.1)

Further additions to the protocol and specific findings are discussed in the disease specific sections below.

CMR Protocol in DCM

1. Anatomy module (Section 19.3.1.)
2. LV function module (Section 19.4)
3. Edema module (Section 19.3.2)
4. LGE module (Section 19.9.1)

23.2 Dilated Cardiomyopathy (DCM)

23.2.1 *Introduction*

DCM represents a heterogeneous group of disorders characterized by a dilated LV with impaired systolic function in the absence of coronary artery disease (CAD) and other non-myocardial causes of dilatation such as valvular heart disease. A family history of sudden cardiac death or congestive heart failure at an early age is common in genetic forms, while a history of chronic alcohol abuse might be suggestive of an ethanol-induced form. However, in the clinical setting, patient

and family history can be unclear and the etiology remain inconclusive. A residual state of subclinical myocarditis has been considered as a potential mechanism for dilatation in such cases.

23.2.2 CMR versus Other Imaging Modalities in DCM

CMR is the most accurate test for the measurement of left and right ventricular volumes and function. Echocardiography can be unreliable in the setting of abnormally shaped ventricles. CMR is therefore recommended for baseline volumetric measurements. Cine CMR can also delineate mitral valve annulus dimensions and combined with phase contrast velocity encoded imaging can be used to measure mitral regurgitant fraction (see Chap. 20). LGE-CMR is uniquely able to detect myocardial scar from (often silent) myocardial infarction, a common differential diagnosis of DCM with important implications on patient management. LGE-CMR may also be used to guide lead placement in resynchronization therapy, in particular by avoiding areas with transmural scar. Similar information may be obtained from SPECT or in the future cardiac CT, but CMR is at present the most reliable test for identifying scar. In many cases, CMR can detect midline scar especially in the interventricular septum. The presence of scar indicates adverse prognosis and may be an important predictor of arrhythmic complications.²

The Role of CMR in DCM

1. Confirm DCM morphology
2. Provide precise measurement of LV dimensions and EF
3. Exclude ischemic etiology
4. Exclude acute problem: signs of myocardial edema?
5. Risk assessment: Arrhythmogenic substrate?

23.2.3 Findings on CMR

- Global LV dilation, wall thinning, reduction of systolic function
- No myocardial edema
- Diffuse hyperenhancement on LGE, most frequently as “midwall sign”
- Concomitant dilation of RV and atria
- Mitral valve regurgitation secondary to LV dilation
- Pleural effusions (decompensated heart failure)

23.2.4 Differential Diagnosis

- Acute (active) myocarditis: Diffuse or focal myocardial edema on T2-weighted images, patchy hyperenhancement predominantly of subepicardial origin in the inferolateral wall on LGE images
- Chronic myocarditis: Hyperenhancement on LGE as in acute myocarditis, without signs of edema
- CAD: Regional rather than global wall motion abnormalities, subendocardial or transmural hyperenhancement on LGE that can be assigned to a coronary territory

Tips and Tricks

- DCM patients are rarely good breath holders. Use parallel imaging techniques to keep the breath hold times short for cine imaging
- If regional findings occur (marked regional wall motion abnormalities, subendocardial or transmural hyperenhancement) consider unrecognized CAD or thromboembolic myocardial infarction

Key Points of CMR in DCM

1. CMR can be used to differentiate acute myocarditis from the more chronic forms of DCM
2. LGE (presence of midwall sign) adds prognostic value to exam

23.2.5 Case Example

A 52 year male presented with heart failure. Cardiac investigations revealed normal coronary arteries and no significant valvular disease. CMR images showed a dilated left ventricle (LV end diastolic diameter 83 mm). Cine images showed globally impaired LV function with an ejection fraction of 13%. LGE images suggested midwall enhancement (see Fig. 23.1) consistent with a diagnosis of DCM.

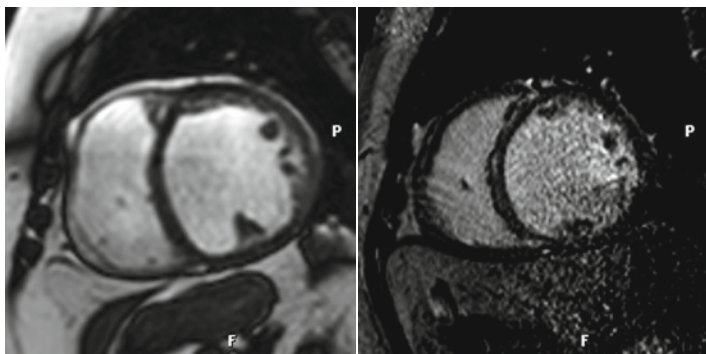


FIGURE 23.1. 49 year old patient presenting with symptoms and signs of heart failure. The left figure is a diastolic of a cine CMR scan showing a dilated LV. The right sided image shows the corresponding LGE-image with mild septal enhancement typical for DCM.

CMR Report in DCM

Report dimensions of:

- a. LV: EDV, ESV, SV, EF (all corrected for BSA), end-diastolic diameter
- b. RV: EDV, ESV, SV, EF (all corrected for BSA)
- c. Dimension of atria

Presence and severity of valvular regurgitation

Presence, location, and extent (circumferential and transmural) of scar

Presence of any abnormal vascular connections/shunts

23.3 Hypertrophic Cardiomyopathy (HCM)

CMR Protocol in HCM

1. Anatomy module (Section 19.3.1)
2. LV function module (Section 19.4) (consider tagging)
3. LVOT cines (Section 19.2)
4. Velocity encoded imaging in LVOT plane (Section 19.6)
5. LGE module (Section 19.9.1)

23.3.1 *Introduction*

HCM is a familial disease where genetic defects lead to malformation of contractile proteins such as troponins. While microscopic studies reveal myocardial disarray, the most prominent macroscopic feature is asymmetric hypertrophy, most frequently involving the septum. Narrowing of the left ventricular outflow tract (LVOT) or circular hypertrophy of mid portion of the LV can lead to LVOT or intracavity obstruction (hypertrophic obstructive cardiomyopathy = HOCM), with hemodynamic consequences similar to those

seen in valvular aortic stenosis. Clinical signs include malignant ventricular arrhythmias and heart failure (initially diastolic dysfunction in the early stages progressing to systolic dysfunction later), with an increased risk of syncope in obstructive forms.

23.3.2 CMR versus Other Imaging Modalities

The diagnosis of HCM is usually made by echocardiography. However, sometimes the differential diagnosis of HCM versus concentric LVH can be difficult, in particular if image quality is suboptimal. In addition, early changes of HCM, for example, in relatives of affected individuals, may be missed on echocardiography. CMR is, therefore, commonly requested for inconclusive cases. CMR can clarify the diagnosis by providing high quality cine images, accurate quantitative measurement of myocardial thickness, and clear depiction of LVOT morphology. In addition, typical patterns of replacement fibrosis may be seen with LGE-CMR, which cannot be identified with any other imaging modality.³

The Role of CMR in HCM

1. Confirm HCM morphology
2. Assess LVOT or intracavity obstruction
3. Assess myocardial fibrosis for risk stratification
4. Follow-up therapeutic effects of septal ablation in obstructive forms
5. Family screening

23.3.3 Findings on CMR

- Asymmetric hypertrophy of LV with different patterns (e.g., septal form, apical form)
- RV involvement

- LVOT obstruction with or without SAM phenomenon (mitral regurgitation caused by systolic anterior movement of the anterior leaflet of the mitral valve due to jet effects of blood leaving the narrowed LVOT)
- Abnormal contraction of the hypertrophied segments
- Intracavity obstruction
- Intramyocardial fibrosis

23.3.4 Differential Diagnosis

- Other conditions leading to (concentric) LVH: athletic training, arterial hypertension, aortic stenosis, cardiac involvement in amyloidosis
- Fabry's disease: causes typical hyperenhancement in the inferolateral segments that can be midwall and patchy.

Tips and Tricks

- Typical locations of hyperenhancement on LGE images are the insertion points of the RV to the LV
- Presence of hyperenhancement on LGE images might be associated with adverse prognosis
- Presence of hyperenhancement and abnormal contraction on tagged cine images are suggestive of HCM rather than LVH

Key Points of CMR in HCM

1. Frequent referral for evaluation of LVH
2. LGE might be able to identify high-risk patients
3. LV and LVOT obstruction can be quantified without provocative tests

23.3.5 Case Example

A 75 year female with HOCM diagnosed 8 years ago was referred for CMR for follow-up of LVOT obstruction. Six months earlier she had suffered from decompensated heart failure, and therapeutic microsphere embolization of a septal coronary artery had been performed in order to reduce LVOT obstruction (pre-interventional pressure gradient at rest on echocardiography: 160 mmHg). While there was some relief of symptoms, the patient still reported significant dyspnea on moderate exertion (NYHA II to III) and occasional episodes of chest pain (Figs. 23.2–23.7).

The area of therapeutic infarction appears to be located too apical to fully reduce LVOT obstruction in this patient. The location of the therapeutic infarct site on the RV side of the septum (as in this case) is common even in cases with successful reduction of LVOT obstruction.

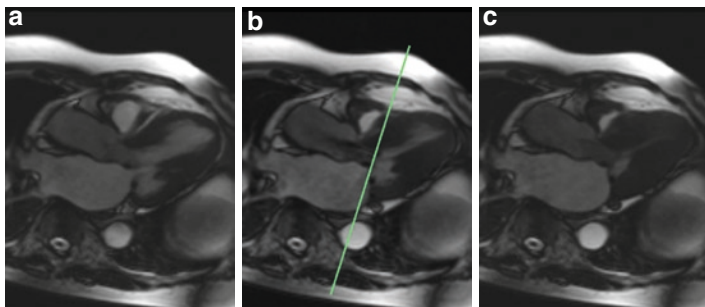


FIGURE 23.2. Cine 3 chamber view demonstrating asymmetric hypertrophy of the septum, LVOT obstruction with turbulent flow and SAM phenomenon causing mitral regurgitation. (a) End-diastole, (b) mid-systole, and (c) end-systole.

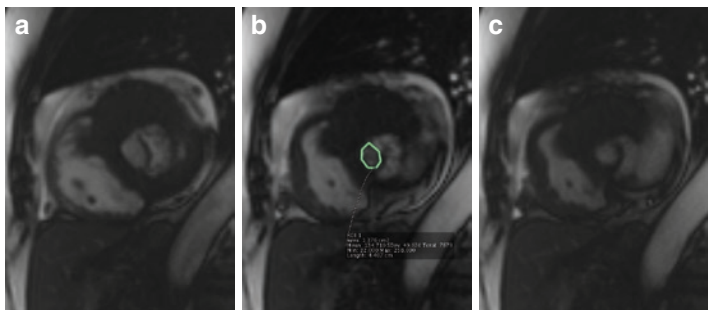


FIGURE 23.3. Cine images of the LVOT perpendicular to the turbulent jet (positioning: see line in mid-systolic image of Fig. 23.2). The opening area of the LVOT is still reduced to 1.4 cm^2 . (a) End-diastole, (b) mid-systole, and (c) end-systole.

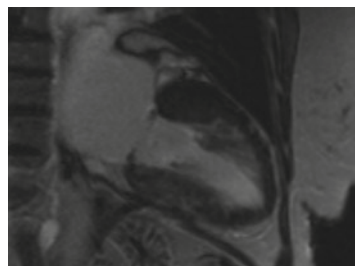


FIGURE 23.4. LGE 2 chamber view demonstrating patchy (*inferior*) and spotty (*anterior*) areas of hyperenhancement corresponding to myocardial fibrosis. In contrast to CAD, hyperenhancement is not based at the subendocardium and is less “bright”.

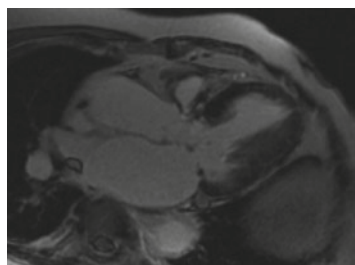


FIGURE 23.5. LGE 3-chamber view without major signs of fibrosis.

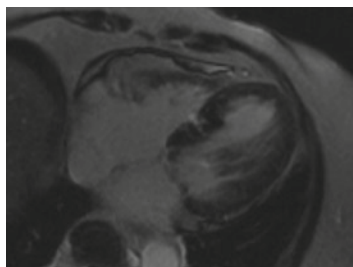


FIGURE 23.6. LGE 4-chamber view showing bright area of hyperenhancement in the mid-cavity level of the septum. This area was not present on pre-interventional images (not shown here) and represents the infarction induced by embolization of the septal artery.

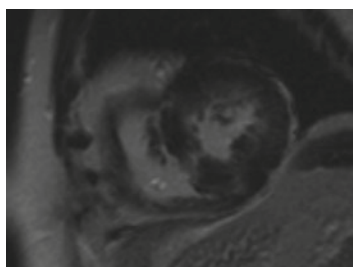


FIGURE 23.7. LGE short-axis view with hyperenhancement at the anterior and inferior insertions of the RV (typical for HCM) and in the inferior part of the septum (caused by therapeutic embolization).

CMR Report in HCM

Report dimensions of:

1. LV: EDV, ESV, SV, EF
2. LV mass
3. Thickness and function of myocardial segments
Presence of LVOT obstruction
Presence of SAM and mitral regurgitation
Presence of replacement fibrosis on LGE-CMR

23.4 Arrhythmogenic Right Ventricular Cardiomyopathy (ARVC)

CMR Protocol in ARVC

1. Anatomy module (Section 19.3.1)
2. LV function module (Section 19.4)
3. RV function module (axial SSFP cines, RVOT cines) (Section 19.4)
4. T1-weighted black blood images (Section 19.3.1) in axial orientation
5. Same acquisition with fat suppressions
6. Proven ARVC: LGE module in same orientations as above. Consider T1 nulling for RV (Section 19.9.1).

23.4.1 Introduction

In contrast to other cardiomyopathies, ARVC is a familial disease that primarily affects the right ventricle. Clinical presentation is usually malignant arrhythmia or sudden cardiac death, equally affecting both sexes most frequently during the fourth decade. If patients survive these events, the disease might proceed toward heart failure. In later stages, the LV is usually also affected with varying degrees of LV dysfunction. From a cellular point of view, ARVC is a disease of the binding proteins that link the myocardial cells. Initially normal myocardium is infiltrated/ replaced by fibrofatty tissue.

In 1994, the task force of the Working Group Myocardial and Pericardial Disease of the European Society of Cardiology and of the Scientific Society and Federation of Cardiology published a consensus statement, which listed criteria that should be used for the diagnosis of ARVC.⁴ According to this statement, two major, one major and two minor, or four minor criteria from five sections (history, imaging, pathology, ECG, and rhythm) are necessary to establish the diagnosis ARVC, each section being allowed to contribute a maximum of one major and one minor criterion (Table 23.1).

TABLE 23.1. Task force criteria for diagnosis of ARVC in *Index Cases*.

1. Family history

MAJOR

Familial disease confirmed at necropsy or surgery

MINOR

Family history of premature sudden death (<35 years of age) due to suspected ARVC

Family history (clinical diagnosis based on present criteria)

2. ECG depolarization/conduction abnormalities

MAJOR

Epsilon waves or localized prolongation (>110 ms) of QRS complex in right precordial leads (V1–V3)

MINOR

Late potentials on signal-averaged EKG

3. ECG repolarization abnormalities

MINOR

Inverted T waves in right precordial leads (V2 and V3) in people >12 years of age and in absence of right bundle branch block

4. Arrhythmias

MINOR

Sustained or non-sustained left bundle branch block-type ventricular tachycardia documented on EKG or Holter monitoring or during exercise testing

Frequent ventricular extrasystoles (>1,000/24 h on Holter monitoring)

5. Global or regional dysfunction and structural alterations

MAJOR

Severe dilatation and reduction of right ventricular ejection fraction with no or mild left ventricular involvement

Localized right ventricular aneurysms (akinetic or dyskinetic areas with diastolic bulging). Severe segmental dilatation of right ventricle

(continued)

TABLE 23.1. (continued).

MINOR

Mild global right ventricular dilatation or ejection fraction reduction with normal left ventricle

Mild segmental dilatation of right ventricle

Regional right ventricular hypokinesia

6. Tissue characteristics of walls

MAJOR

Fibro fatty replacement of myocardium on endomyocardial biopsy

23.4.2 CMR versus Other Imaging Modalities

CMR is the optimal imaging modality for assessment of the right ventricle and has a very important role in the diagnosis and follow-up of ARVC and for screening of relatives. However, the ability of CMR to detect fatty infiltration of the RV free wall on T1-weighted images wall has been overestimated and was previously over-reported. It is now recognized that fatty infiltration is very difficult to conclusively identify and if present is usually associated with other clear abnormalities, for example, of contractile function. The ascent of LGE-CMR has added a further component to the CMR study of ARVC, which many centers now favor over T1-weightted imaging. It has to be recognized that ARVC cannot be diagnosed by CMR alone according to the Task Force criteria, and also that a normal CMR study does not exclude the presence of early “concealed” ARVC.⁵ CT can show typical abnormalities in ARVC, but is not currently a first line investigation.

The Role of CMR in ARVC

1. Assess task force criteria (imaging section) for ARVC
2. Follow-up of patients with established ARVC
3. Assessment of fibrofatty infiltration/replacement
4. Assessment of LV involvement

23.4.3 Findings on CMR

- Major criteria: Severe dilatation and reduction of RV ejection fraction with no (or only mild) LV impairment; localized RV aneurysms (akinetic or dyskinetic areas with diastolic bulging); severe segmental dilatation of the RV
- Minor criteria: Mild global RV dilatation and/ or ejection fraction reduction with normal LV; mild segmental dilatation of the RV; regional RV hypokinesia
- Additional features: Signs of fibrofatty replacement/ infiltration (not part of the diagnostic criteria!)
- Thinning of LV wall, reduction of LV function, fibrofatty replacement/ infiltration of LV myocardium

There is wide variance to RV morphology in healthy subjects. For example, relative end-systolic bulging of a thin but contractile region of the RV free wall adjacent to the moderator band can be a normal finding and basal short axis cines may give the impression of inferior wall dyskinesis due to normal through-plane motion. At the same time, ARVC is a rare disease. Therefore, CMR reports should always remain descriptive, and the diagnosis ARVC should never be based on CMR findings alone but rather be established using the combination of criteria recommended by the ESC task force.

- CMR has the ability to visualize fat with high sensitivity. However, it should be kept in mind that evidence of fat is not a recognized imaging criterion for the detection of ARVC. Therefore, reporting should not over-emphasize on the presence or absence of fat on CMR.
- Presence of hyperenhancement on LGE images might be associated with impaired prognosis
- Presence of RV dilatation and impairment of RV function are often early imaging markers of disease.

23.4.4 Differential Diagnosis

- Normal variant
- RV dilation due to other cardiac condition (pulmonary hypertension, pulmonary valve stenosis, atrial septal defect).

Tips and Tricks

- Since the RV wall is a very thin structure (~3 mm) even in normal subjects and since abnormalities might occur focally, high in-plane spatial resolution and thin slices without inter-slice gap should be used.
- If there are no wall motion abnormalities or dilation of the RV seen on the RV function module, significant findings are very unlikely and the RV morphology module might be skipped in order to reduce scan time.
- Hypokinesia at the insertion of the moderator band is a common finding in normals and should not be classified as pathologic.
- In patients who are able, scanning should be performed in the prone position in order to optimize image quality of the RV.
- Ventricular arrhythmia is a frequent finding in patients referred for ARVC and might severely affect image quality. In such cases, pretreatment with antiarrhythmic drugs should be discussed with the referring physician.

Key Points of CMR in ARVC

1. Frequent referral but rare disease
2. Diagnosis cannot be based on imaging criteria alone
3. Interest should be focused on functional abnormalities of the RV

23.4.5 Case Example

A 65 year female was referred with palpitations. There was no family history of cardiac arrhythmia or sudden cardiac death. A 24 h ECG recorded multiple episodes of non-sustained ventricular and supraventricular tachycardia. On echocardiography, enlargement and impaired function of the RV was noted. A CMR study was requested to further assess RV morphology and function (Figs. 23.8–23.11).

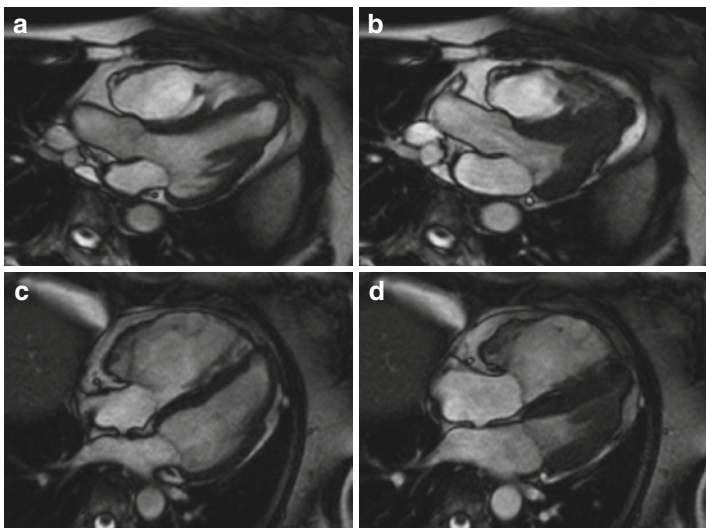


FIGURE 23.8. Standard long-axis cine images showing enlargement and severe functional impairment of the RV. The LV is of normal size and function (EF 69%) except for the lateral apex, where there appears to be depression of the myocardium by bulky epicardial fat. (a) 3 cv, end-diastole, (b) 3 cv, end-systole, (c) 4 cv, end-diastole, and (d) 4 cv, end-systole.

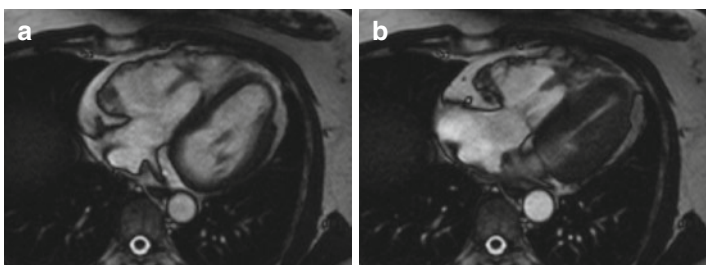


FIGURE 23.9. Axial cine images at two different levels demonstrating marked enlargement of the RV ($260 \text{ mL} = 156 \text{ mL/m}^2$), impairment of global RV function (EF 27%), segmental aneurysm of the RV wall, and fatty infiltration of the lateral wall of the LV. Quantification of RV parameters was done using a full set of axial cine images covering the entire RV (not shown here). (a) End-diastole, (b) end-systole, (c) end-diastole, and (d) end-systole.

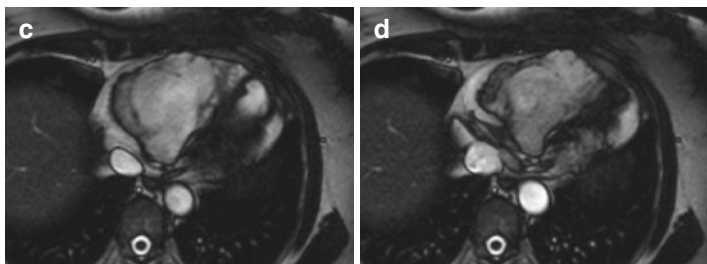


FIGURE 23.9. (continued).

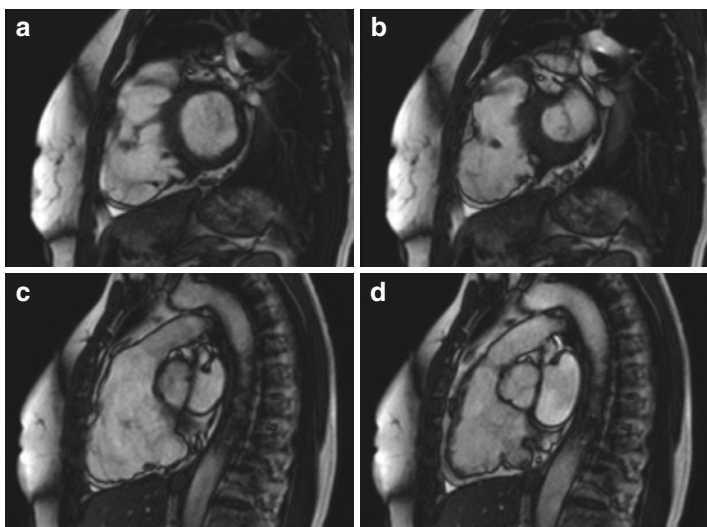


FIGURE 23.10. Sagittal cine images at two different levels. The RV wall appears irregular and is dyskinetic in its anterior part. (a) End-diastole, (b) end-systole, (c) end-diastole, and (d) end-systole.

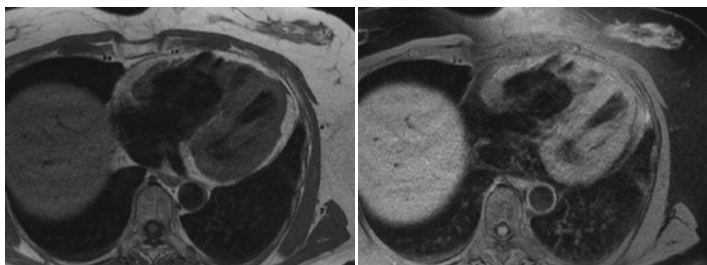


FIGURE 23.11. Axial T1-weighted fast spin-echo images without (*left*) and with (*right*) fat suppression. In the aneurysmal part of the anterior RV wall, there is severe thinning of the RV myocardium. The lateral apex of the LV appears infiltrated/replaced by epicardial fat. There is also a fatty streak within the basal interventricular septum.

According to the task force criteria, this patient fulfilled two major criteria for ARVC (note that a maximum of only one major and one minor criterium from an imaging technique can be allowed according to the task force rules). Together with other clinical and ECG criteria, the diagnosis of ARVC with LV involvement was made and the patient received an internal cardioverter/defibrillator (ICD).

CMR Report in ARVC

Identify major and minor criteria associated with ARVC:

- Global right ventricular performance (RVEF)
- RV dilation
- Location of regional RV wall motion abnormalities (infundibulum, body or apex of right ventricle).

When acquired, comment on:

- Fatty infiltration of the right ventricle
- Occurrence of fibrosis by LGE

23.5 Left Ventricular Non-Compaction Cardiomyopathy (LVNC)

CMR Protocol in LVNC

1. Anatomy module (Section 19.3.1)
2. LV function module (Section 19.4)
3. Resting first pass perfusion in long-axis plane (Section 19.8.1)
4. LGE module (Section 19.9.1)

23.5.1 *Introduction*

LVNC is a congenital disease where the fetal process of compaction of the initially spongy myocardium is incomplete. Severe forms have been described as a frequent cause of early cardiac death in infants; its adult form has only been recognized recently with the technical advances in cardiac imaging. In the past, most cases might have been misdiagnosed as LV hypertrophy due to poor image quality of early echocardiographic machines. Clinically, patients might present with congestive heart failure, malignant arrhythmia, or thromboembolic complications such as stroke.

23.5.2 *CMR versus Other Imaging Modalities*

LVNC is usually first suspected on a transthoracic echocardiogram. Echo contrast agents can be given to improve the diagnosis. However, LVNC is a difficult diagnosis to make and CMR may be requested for clarification because of its superior image quality. Cardiac CT may be used as an alternative investigation if CMR is contraindicated.⁶

23.5.3 *Role of CMR in LVNC*

- Confirm diagnosis
- Detect myocardial fibrosis
- Detect LV thrombus

23.5.4 Findings on CMR

- Hyper-trabecularization of the LV and thinning of the compact wall, particularly in apical segments
- LV dilation, reduced LV function
- Myocardial fibrosis
- LV thrombus

23.5.5 Differential Diagnosis

- HCM
- DCM
- Chronic myocardial infarction
- Normal variant.

Tips and Tricks

- In contrast to echocardiography, where a ratio of 2.0:1 of trabecula diameter versus compact wall thickness on *end-systolic* images is used as cut-off to make the diagnosis of LVNC, a ratio of 2.3:1 on *end-diastolic* images has been proposed for CMR. In either case, some normal subjects without signs or history of LVNC fulfill these criteria; so far it is not known whether these findings have any clinical value in these subjects or not.
- Hyperenhancement on LGE images has been found in a number of, but not all cases, of LVNC. It is postulated that these cases represent severe or late forms of the disease.

Key Points of CMR in LVNC

1. CMR can identify hyper-trabecularization that might have been underdiagnosed (taken for LV hypertrophy) in the past
2. Using quantitative standards (trabecula – compact ratio of 2.3:1) alone might lead to overdiagnosis of LVNC

23.5.6 Case Example

A 39 year female was referred with a 5 year history of recurrent syncope. There was no family history of arrhythmia or sudden cardiac death. Holter monitoring documented repeated episodes of non-sustained ventricular tachycardia. Echocardiography raised the suspicion of LVNC, but was not conclusive due to poor acoustic windows (Figs. 23.12 and 23.13).

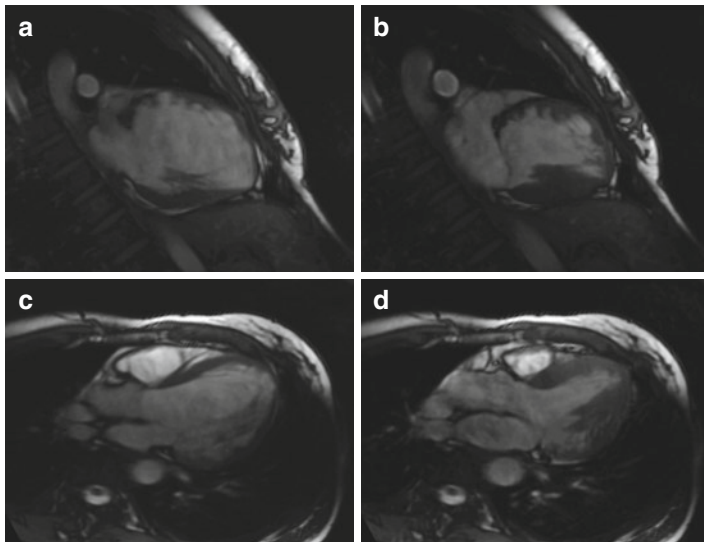


FIGURE 23.12. Cine images. The compact LV wall is thin and irregularly shaped. There is excessive non-compaction/hyper-trabecularization within the LV cavity. As a result, the LV wall appears “spongy.” The ratio of non-compact to compact to wall thickness at end-diastole was 4.1:1. (a) 2-chamber view end-diastole, (b) 2-chamber view end-systole, (c) 3-chamber view end-diastole, (d) 3-chamber view end-systole, (e) 4-chamber view end-diastole, (f) 4-chamber view end-systole, (g) short-axis end-diastole, and (h) short-axis end-systole.

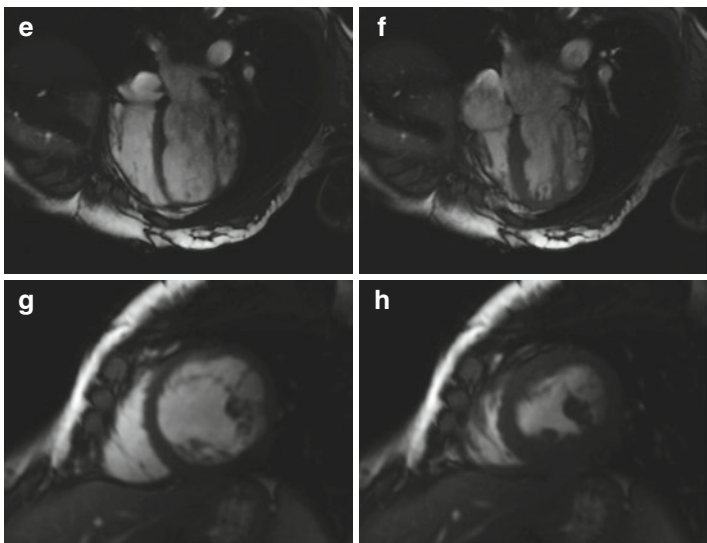


FIGURE 23.12. (continued).

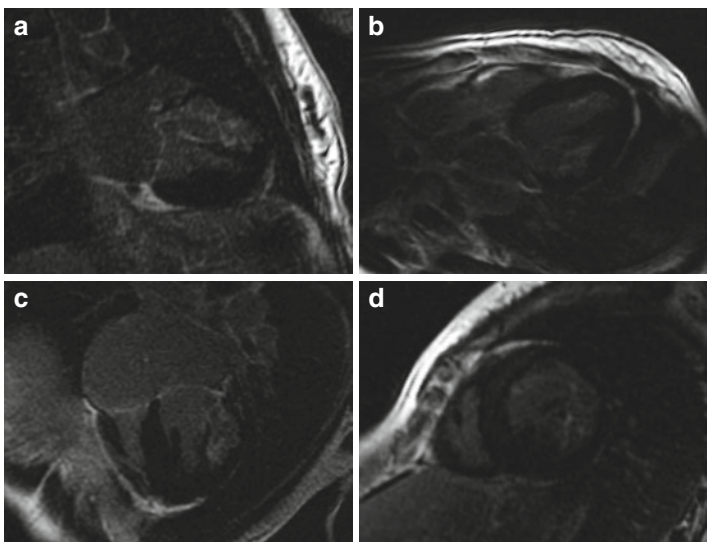


FIGURE 23.13. LGE images. While some of the non-compact parts of the LV show thin lines of hyperenhancement, none of the normal compact parts of the LV wall do. (a) 2-chamber view, (b) 3-chamber view, (c) 4-chamber view, and (d) short-axis.

CMR ruled out CAD (no subendocardial fibrosis), DCM (irregular LV wall, hyper-trabecularization) and myocarditis (no patchy or subepicardial hyperenhancement) as the causes of LV dilation and impairment of LV function, and established the diagnosis of LV non-compaction cardiomyopathy. The patient received heart failure therapy, was given an ICD, and anticoagulated.

CMR Report in LVNC

LV volumes and function

RV volumes and function

Location of any abnormal segments

Ratio of trabeculated versus compacted myocardium

23.6 Inflammatory Diseases: Myocarditis

CMR Protocol in Myocarditis

1. Anatomy module (Section 19.3.1)
2. LV function module (Section 19.4)
3. Edema module (Section 19.3.2)
4. LGE module (Section 19.9.1)

23.6.1 *Introduction*

Myocarditis is an inflammatory disease of the myocardium caused by viral infection and subsequent immunological response, with onset of symptoms (chest pain, arrhythmia, heart failure, and fatigue) typically starting several days to 6 weeks after a respiratory or gastrointestinal tract infection. While subclinical involvement of the myocardium is frequent

and self-limiting, symptomatic myocarditis can lead to lethal arrhythmia and/or severe reduction of LV function especially if protection of the myocardium by pharmacological (ACE inhibitors, beta blockers) and physical (rest) measures is not initiated and maintained adequately. Acute myocarditis might be accompanied by (global) ST changes on ECG and elevation of troponin, creatine kinase and C-reactive protein levels.

23.6.2 CMR versus Other Imaging Modalities

CMR is the currently best imaging modality to confirm a suspected diagnosis of myocarditis. Echocardiography can detect regional or global wall motion abnormalities, but CMR has the additional ability to detect focal inflammation and scarring. CMR is commonly requested in patients presenting with acute chest pain and raised myocardial biomarkers, but normal X-ray coronary angiograms. In these patients CMR can very accurately confirm or exclude the presence of myocardial infarction, which may have arisen from the rupture of a minor atherosclerotic plaque. This distinction has obvious implications for the management of patients with secondary prevention medication. In many patients, CMR can also identify characteristic positive features of myocarditis.⁷ In only approximately 1/3 of patients with troponin-positive chest pain, but normal coronary angiography, can no conclusive answer be given by CMR. CMR is therefore widely regarded as a “must” in patients with suspected acute myocarditis.

Role of CMR in Myocarditis

- Confirm diagnosis
- Assess presence of “inflammation”
- Assess pericardial involvement
- Follow-up LV function

23.6.3 Findings on CMR

- Hyperenhancement on LGE images (not confined to specific coronary territory; typically subepicardial or intramural; less bright than myocardial infarction; most frequently in the infero-lateral wall)
- Myocardial edema (not confined to coronary territory; might be used as marker for acute process)
- Impairment of LV function
- Impairment of RV function
- Pericardial effusion

23.6.4 Differential Diagnosis

- Thromboembolic myocardial infarction (subendocardial or transmural hyperenhancement on LGE images assigned to coronary territory)
- Dilated cardiomyopathy (global thinning of LV; differentiation between chronic myocarditis and DCM often impossible)
- Tako-Tsubo cardiomyopathy (apical ballooning or “inverted” pattern = basal ballooning; full recovery of LV function within 5–14 days)
- Other inflammatory diseases with myocardial involvement (e.g., sarcoidosis, systemic lupus erythematosus: no history of recent infection; additional noncardiac symptoms).

23.6.5 Case Example

A 28 year male presented to the emergency department with acute chest pain. He had also suffered from diarrhea for the last 3 days. On the ECG, there was ST elevation in leads I, II, V4–V6. Blood tests showed elevated troponin T, creatine kinase, WBC, and CRP values. Coronary artery disease was

Tips and Tricks

- Most severe cases present with hyperenhancement in the acute stage. If present, hyperenhancement is usually less bright than in myocardial infarction and might shrink or even disappear in some cases over time
- LGE imaging might be used to guide myocardial biopsy
- At first presentation, systolic function might not be impaired even in the presence of severe clinical symptoms and extensive myocardial lesions as demonstrated by LGE. Nevertheless, these patients should not be allowed to exercise, and should be considered for ACE inhibitors +/- beta blockers in order to avoid deterioration of LV function
- For research purposes, additional CMR techniques (early gadolinium enhancement¹³, global T2 ratio, T1 mapping, etc.) might be considered

Key Points CMR in Myocarditis

1. CMR is the only noninvasive tool that is able to detect myocardial injury in the course of myocarditis
2. The presence of hyperenhancement on LGE images has a high specificity for a severe course of the disease
3. The presence of focal myocardial edema might be used as a marker for ongoing inflammatory activity

excluded by X-ray coronary angiography. Initial study, 2 days after onset of cardiac symptoms (Figs. 23.14–23.16).

The patient remained asymptomatic and after 1 month was re-studied by CMR (Figs. 23.17 and 23.18). Regional wall motion abnormalities had resolved and ejection fraction improved to 63% (images not shown).

The initial CMR study excluded thromboembolic infarction and demonstrated multiple myocardial lesions typical

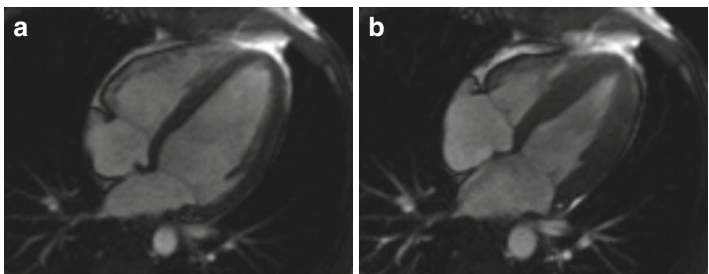


FIGURE 23.14. Cine 4-chamber view at (a) end-diastole and (b) end-systole showing apical anterolateral wall motion abnormality; ejection fraction is mildly reduced (52%).

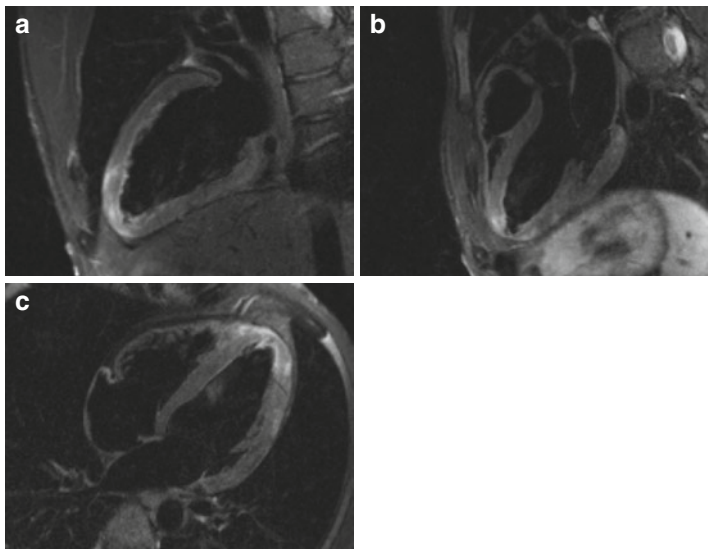


FIGURE 23.15. STIR images demonstrating apical myocardial edema. (a) 2-chamber view, (b) 3-chamber view, and (c) 4-chamber view.

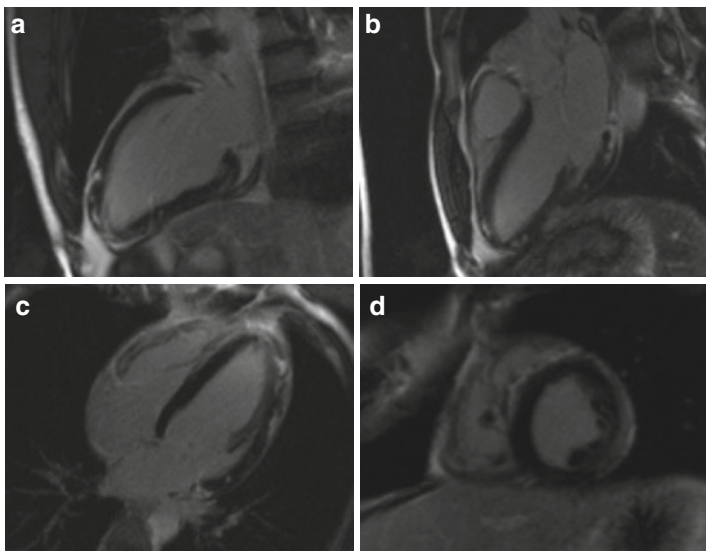


FIGURE 23.16. LGE images showing multiple areas of hyperenhancement in apical, anterolateral, and inferolateral regions. The lesions are predominantly seen in the subepicardial layer. Despite this there is no pericardial effusion (which would indicate concomitant pericarditis). (a) 2-chamber view, (b) 3-chamber view, (c) 4-chamber view, and (d) short-axis view.

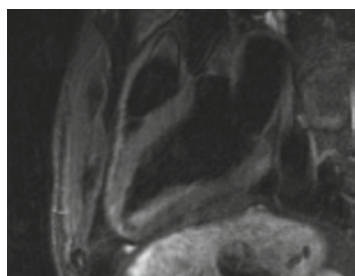


FIGURE 23.17. Re-study after 1 month. STIR 3-chamber view with only small residual apical spot of myocardial edema. *Note:* there is intracavity (not myocardial) hyperintensity adjacent to the inferolateral wall caused by insufficient blood suppression due to slow flow (normal finding).

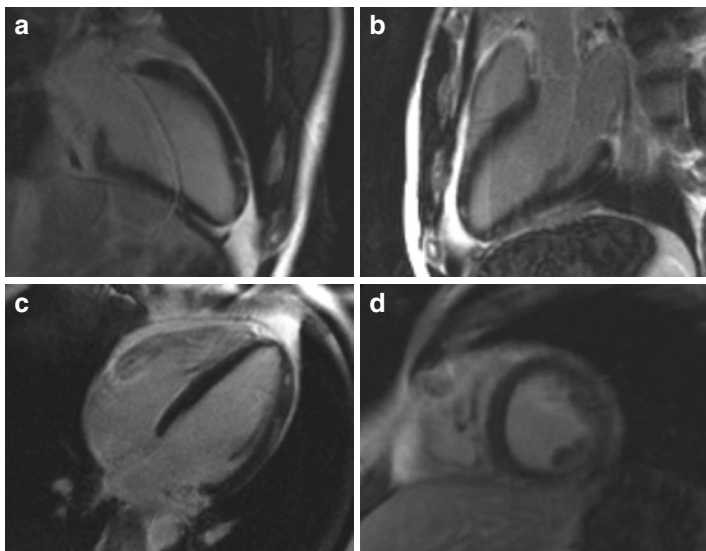


FIGURE 23.18. LGE images still show myocardial lesions, which appear smaller. (a) 2-chamber view, (b) 3-chamber view, (c) 4-chamber view, and (d) short-axis view.

of viral myocarditis. The follow-up study demonstrated regression of inflammatory activity, improvement in ventricular function, and a reduction of lesion size during therapy.

CMR Report in Myocarditis

Presence and location of edema

Presence and location of hyperenhancement on LGE

Regional and global LV function

Pericardial effusion or hyperenhancement

23.7 Inflammatory Diseases: Sarcoidosis

CMR Protocol in Sarcoidosis

1. Anatomy module (Section 19.3.1)
2. LV function module (Section 19.4)
3. Edema module (Section 19.3.2)
4. LGE module (Section 19.9.1)

23.7.1 *Introduction*

Sarcoidosis is a granulomatous systemic disease most frequently involving lung and skin. Cardiac involvement is a rare (~5%) but a severe complication, which requires immunosuppressive therapy in order to prevent malignant arrhythmia and heart failure.⁸

23.7.2 *Findings on CMR*

The Role of CMR in Sarcoidosis

- Confirm cardiac involvement
- Assess inflammatory activity and response to treatment
- Follow-up LV function

- Hyperenhancement on LGE images
- Elevated relative enhancement index on early gadolinium enhancement images
- Impairment of LV function

- Pericardial effusion
- Mediastinal lymphadenopathy

23.7.3 Differential Diagnosis

- Other inflammatory diseases of the myocardium (e.g., myocarditis, systemic lupus erythematosus)
- Myocardial infarction (subendocardial or transmural hyperenhancement on LGE images assigned to coronary territory).

Tips and Tricks

- Hyperenhancement is usually intramural, spotty, and can be almost as pronounced as in myocardial infarction.
- Lesions presenting as hyperenhancement usually respond to immunosuppressive treatment.
- Pure cardiac sarcoidosis is a rare condition. Hilar or mediastinal lymphadenopathy can be pronounced and is often visible on scout images.

Key Points CMR in Sarcoidosis

LGE can be used to detect focal myocardial lesions that might disappear on follow-up after medical treatment.

23.7.4 Case Example

A 31 year male with known pulmonary sarcoidosis developed acute chest pain accompanied by ST elevation in leads I and aVL and elevated levels of troponin T and creatine kinase.

Initially, he had been hospitalized for painful skin lesions and fever. Initial CMR on the day of onset of chest pain (Figs. 23.19–23.21).

Follow-up study after treatment with prednisolone (100 mg/d) and resolution of chest pain (Figs. 23.22–23.24).

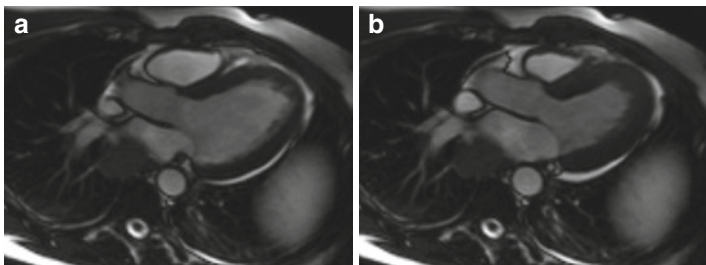


FIGURE 23.19. Long-axis cine images in 3-chamber orientation. There is mild impairment of global LV function (EF 47%) with pronounced wall motion abnormalities. There is a small pericardial effusion (max. 4 mm). A large retrocardiac mass is visible adjacent to the left atrium. (a) 3-chamber view end-diastole and (b) 3-chamber view end-systole.

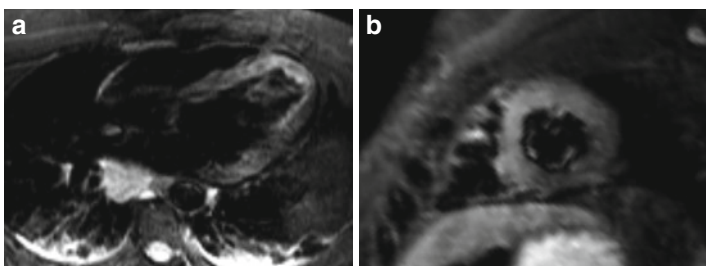


FIGURE 23.20. STIR images revealing myocardial edema (hyperintensity) of the apical anterior and septal wall. (a) 3-chamber view and (b) apical short axis.

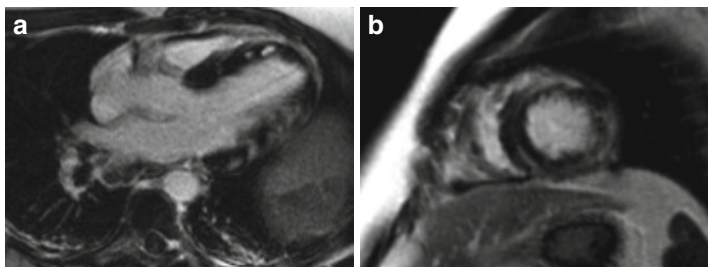


FIGURE 23.21. LGE images showing multiple intramyocardial, almost transmural myocardial lesions (hyperenhancement). (a) 3-chamber view and (b) apical short axis.

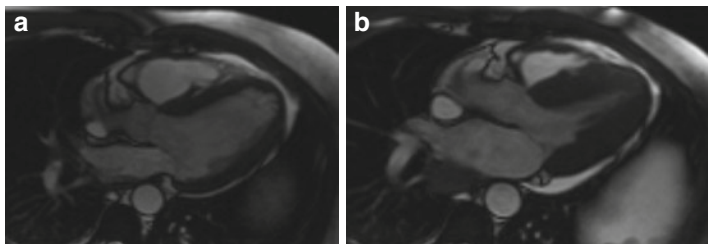


FIGURE 23.22. Follow-up study. Cines show full recovery of LV function. The mediastinal mass is no longer detectable. (a) Diastole and (b) systole.

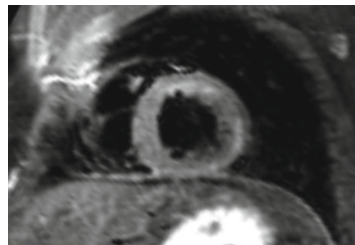


FIGURE 23.23. Apical short-axis STIR image without new signs of myocardial edema.

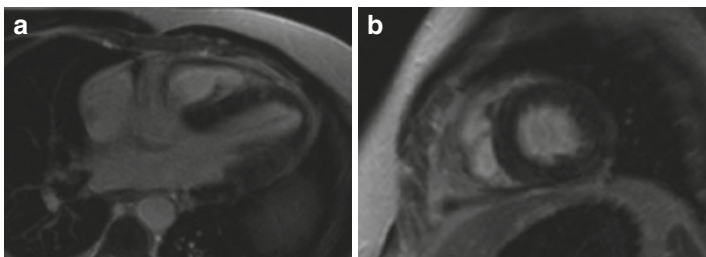


FIGURE 23.24. LGE images: The myocardial lesions are still detectable but are significantly smaller and appear less hyperintense. (a) 4cv and (b) apical short axis.

In summary, CMR detected acute cardiac involvement of sarcoidosis initially and showed good response to steroid therapy on follow-up studies.

CMR Report in Sarcoidosis

Comment on:

- Mediastinal or hilar abnormalities (lymphadenopathy)
- Myocardial granulomas on LGE
- LV/RV function

23.8 Inflammatory Diseases: Vasculitis (Churg–Strauss Syndrome)

CMR Protocol in Churg–Strauss Syndrome

- a. Anatomy module (Section 19.3.1)
- b. LV function module (Section 19.4)
- c. Edema module (Section 19.3.2)
- d. LGE module (Section 19.9.1)

23.8.1 *Introduction*

Churg–Strauss Syndrome is an autoimmune disease affecting small and medium size vessels, including the microcirculation of the myocardium in the later stages of disease.

The Role of CMR in Churg–Strauss Syndrome

- Accurately assess cardiac function
- Confirm cardiac involvement

23.8.2 *Findings on CMR*

- Circular subendocardial hyperenhancement on LGE images⁹

Tips and Tricks

- Hyperenhancement in Churg–Strauss Syndrome rarely affects more than 50% of the wall thickness

Key Points CMR in Churg–Strauss Syndrome

LGE images reveal circular subendocardial hyperenhancement

23.8.3 Differential Diagnosis

- Multiple myocardial infarctions.

23.8.4 Case Example

A 70 year male was hospitalized for dyspnea at rest (NYHA IV). A CXR showed pulmonary edema and large bilateral pleural effusions. Blood tests yielded elevated creatine and eosinophilia. p-ANCA was negative. Echocardiography revealed moderate LV dilatation and severely impaired global LV function (EF 22%). CMR was performed after drainage of the left pleural effusion (Fig. 23.25).

Because of the atypical distribution of hyperenhancement (subendocardial location not typical for DCM; non-regional distribution and severely impaired LV function despite non-transmural lesions not typical for CAD), cardiac involvement of vasculitis was suspected and a CT scan of the chest was performed, which showed multiple small pulmonary infiltrations. Lung biopsy confirmed Churg–Strauss Syndrome.¹⁰

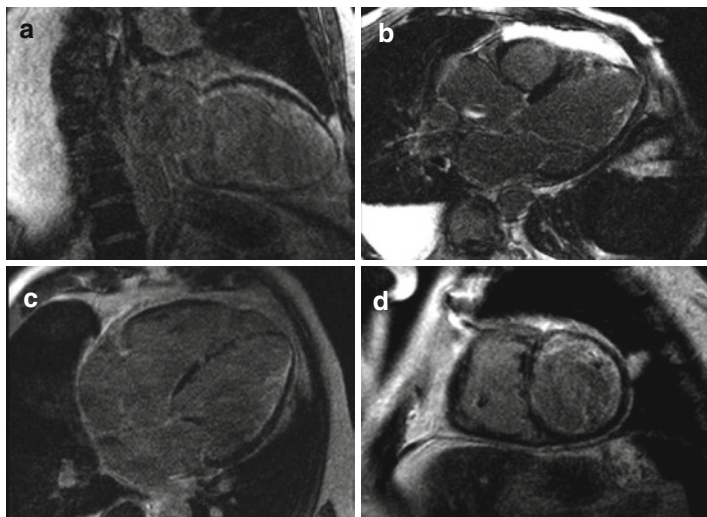


FIGURE 23.25. LGE images. There is subendocardial hyperenhancement that is not confined to a typical coronary territory. There is a persistent large right-sided pleural effusion. **(a)** 2-chamber view, **(b)** 3-chamber view, **(c)** 4-chamber view, and **(d)** short axis.

CMR Report in Churg–Strauss Syndrome

Comment on:

- LV/RV function
- Presence and extent of scar on LGE

23.9 Infiltrative/Storage Diseases: Amyloidosis

CMR Protocol in Amyloidosis

1. Anatomy module (Section 19.3.1)
2. LV function module (Section 19.4)
3. Edema module (Section 19.3.2)
4. LGE module (Section 19.9.1)

23.9.1 *Introduction*

Amyloidosis is a systemic disorder where abnormal proteins are produced and deposited in different tissues causing multiorgan damage. While some forms progress slowly, cardiac involvement implies a worse prognosis, with a median survival time of 6 months after diagnosis.¹⁰

The Role of CMR in Amyloidosis

- Accurately assess cardiac function
- Confirm cardiac involvement
- Assess pericardial effusion

23.9.2 *Findings on CMR*

- Blurry, inhomogeneous suppression of myocardial signal and dark blood on LGE images
- Restrictive configuration of the heart: small ventricles, large atria
- Concentric LV hypertrophy
- Pericardial effusion

- Pleural effusions
- Hypertrophy of atrial septum

23.9.3 Differential Diagnosis

- Other conditions causing LV hypertrophy: arterial hypertension, hypertrophic cardiomyopathy, aortic stenosis: Diagnosis based on pattern of LGE. In addition, the amyloid heart tends to have impaired global and longitudinal contraction patterns and the LA and RA are typically enlarged.
- Other conditions causing restrictive pattern: other storage disease: These differential diagnoses cannot usually be made by CMR as the findings are nonspecific.

Tips and Tricks

- In patients where LGE “doesn’t seem to work” despite proper technical procedures, amyloidosis should be considered
- If amyloidosis is suspected, a first set of LGE images should be acquired early (i.e., 3–5 min) after the application of contrast agent, which might demonstrate an epicardial – endocardial signal gradient
- Cardiac involvement without hyperenhancement is possible but rare
- Cardiac involvement is usually accompanied by pericardial and pleural effusions
- Hypertrophy of the atrial septum is only present in ~20% of cases
- If available, T1 mapping techniques can be used to document increased global gadolinium uptake of the myocardium

Key Points of CMR in Amyloidosis

1. CMR is able to detect cardiac amyloidosis with high sensitivity and specificity
2. Myocardial behavior on LGE images in amyloidosis is different from any other pathology. It is, however, not specific and other infiltrative diseases need to be considered.
3. Biopsies in amyloidosis can be negative, so if CMR findings are highly suggestive of infiltration, repeat biopsies, using CMR as a guide to areas worst affected.

23.9.4 Case Example

A 71 year female was hospitalized for decompensated biventricular heart failure and renal insufficiency. Echo revealed severely impaired LV function and aortic stenosis. She was referred to CMR for evaluation of the aortic valve (Figs. 23.26–23.29).

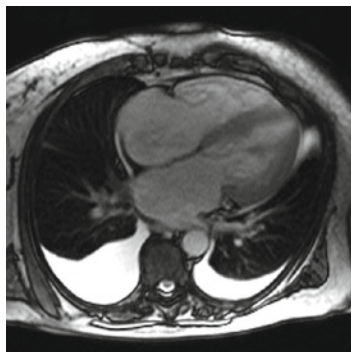


FIGURE 23.26. Localizer and subsequent images show bilateral pleural effusions and mild pericardial effusion (image quality is reduced due to tachyarrhythmia).

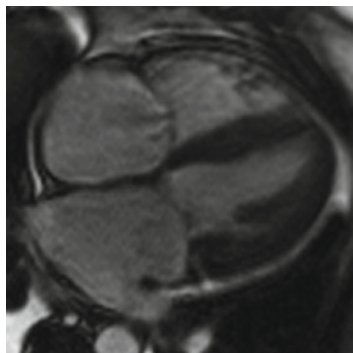


FIGURE 23.27. Systolic cine 4-chamber view showing restrictive configuration of heart chambers (small ventricles, large atria), LV hypertrophy, pericardial effusion, and tricuspid insufficiency.

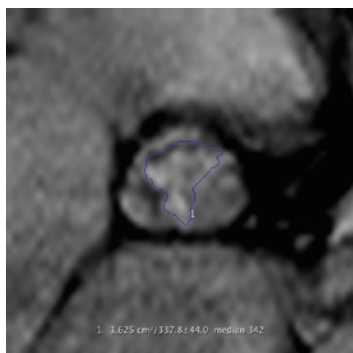


FIGURE 23.28. Planimetry of the opening area of the aortic valve revealed mild aortic valve stenosis (1.6 cm^2).

The CMR report excluded aortic stenosis as cause of decompensation and raised the suspicion of cardiac involvement by amyloidosis. Subsequently, blood tests and rectal biopsy revealed AL amyloidosis. 8 weeks later, the patient was re-admitted to hospital after resuscitation from cardiac arrest.

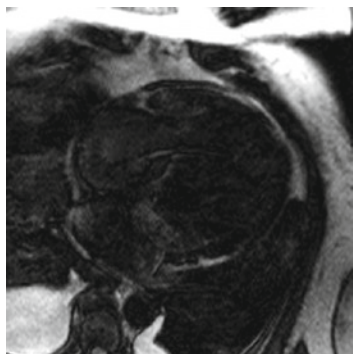


FIGURE 23.29. LGE 4-chamber view with inhomogeneous suppression of myocardium and dark blood.

CMR Report in Amyloidosis

Comment on:

- Global and regional LV/RV function
- Comment on longitudinal shortening
- Size of left/right atrium
- Thickness of interatrial septum
- Valve regurgitation
- Enhancement pattern on LGE
- Extracardiac findings (pericardial/pleural effusion)
- Consider assessment of diastolic function

23.10 Infiltrative/Storage Diseases: Siderotic Cardiomyopathy

CMR Protocol in Siderotic Cardiomyopathy

- a. Anatomy module (Section 19.3.1)
- b. LV function module (Section 19.4)
- c. T2* imaging (Section 19.3.3)

23.10.1 *Introduction*

Chronic iron overload, for example, caused by repetitive blood transfusions for hematological disorders such as thalassemia major, can lead to siderotic cardiomyopathy, characterized by myocardial iron deposition. Cardiac involvement can cause congestive heart failure and arrhythmia, and indicates poor prognosis.

23.10.2 *CMR versus Other Imaging Modalities*

CMR has a unique role in the management of iron loading disease. CMR has been shown to be able to reproducibly quantify myocardial iron content and the degree of iron loading directly correlates with outcome. Similar information cannot be provided by other imaging modalities. For this reason CMR is becoming an irreplaceable tool for management of siderotic cardiomyopathy.¹¹

The Role of CMR in Siderotic Cardiomyopathy

- Confirm cardiac involvement
- Risk stratification
- Accurately assess cardiac function
- Follow-up of iron loading during chelation therapy

23.10.3 Findings on CMR

- Reduced T2* values (<20 ms) in septal myocardium
- Reduced T2* values (<20 ms) in liver tissue
- Reduced LV function
- LV hypertrophy

23.10.4 Differential Diagnosis

- Cardiac amyloidosis
- Other storage disease.

Tips and Tricks

- If other myocardial diseases are considered, a LGE module should be added to the protocol
- T2* should be assessed in the septal wall since this is the region where susceptibility artifacts are rare (in contrast to the inferolateral wall where they are common due to the proximity to the great cardiac vein)
- Patients can have myocardial iron overload without hepatic iron overload and vice versa.

Key Points CMR in Siderotic Cardiomyopathy

1. T2* mapping can be used to detect and quantify iron overload of the heart and liver

23.10.5 Case Example

A 68 year female presented with progressive dyspnea on exertion. Since the patient had received multiple blood transfusions in the past 40 years for hemolytic anemia due to pyruvate kinase deficiency, iron overload of the heart was suspected and the patient was sent for CMR (Figs. 23.30–23.33).

As a result, CMR confirmed moderate cardiac and liver iron overload.

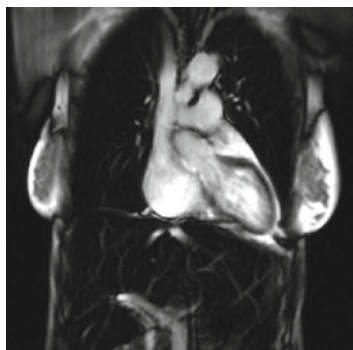


FIGURE 23.30. Coronal scout image shows large hypointense liver.

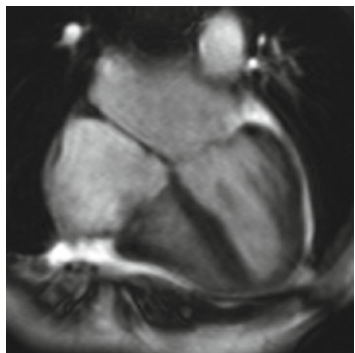


FIGURE 23.31. Systolic cine 4-chamber view with dilated atria (image quality is suboptimal due to atrial fibrillation and poor breath hold capacity of the patient). LV function was mildly reduced (EF 46%) with global hypokinesia.

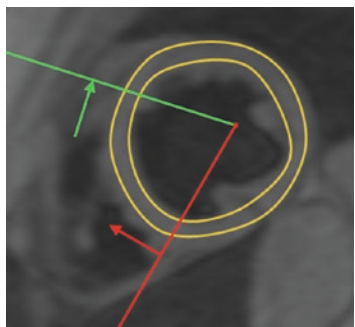


FIGURE 23.32. Mid-cavity short-axis T2* measurement of the heart. Mean T2* in septal myocardium was 10 ms (normal: >20 ms).

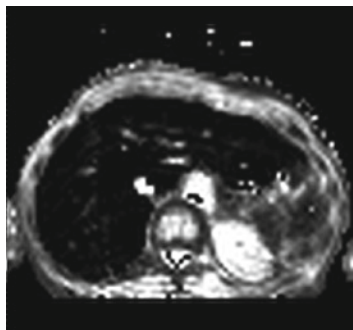


FIGURE 23.33. Axial T2* map of the liver (scale: 0–50 ms). Mean hepatic T2* was 2 ms.

CMR Report in Siderotic Cardiomyopathy

Comment on:

- LV/RV function and mass
- T2* values of heart and liver

23.11 Tako-Tsubo Cardiomyopathy

CMR Protocol in Tako-Tsubo Cardiomyopathy

- a. Anatomy module (Section 19.3.1)
- b. LV function module (Section 19.4)
- c. Edema module (Section 19.3.2)
- d. LGE module (Section 19.9.1)

23.11.1 *Introduction*

In Tako-Tsubo cardiomyopathy, an episode of massive emotional or physical stress to the patient leads to an acute condition mimicking acute coronary syndrome, while coronary arteries are typically normal/unobstructed in these patients. In its typical form, function of the apical and mid-cavity portions of the LV are initially severely impaired (“apical ballooning”), resembling the shape of a traditional Japanese vessel used to catch octopus (“Tako-Tsubo”). It is believed that this acute disease is a “toxic” reaction to excessive levels of catecholamines.¹²

23.11.2 *CMR versus Other Imaging Modalities*

The suspicion of Tako-Tsubo cardiomyopathy usually arises in the cardiac catheter laboratory at the time of primary angioplasty or on an early “post-infarct” echocardiogram. The main imaging features of this syndrome are characteristic and do not require CMR imaging. However, CMR adds to the diagnosis in uncertain cases, and can on occasions identify unexpected myocardial infarction despite angiographically normal coronary arteries.

The Role of CMR in Tako-Tsubo Cardiomyopathy

- Confirm diagnosis
- Rule out myocardial infarction
- Rule out myocarditis
- Follow-up functional recovery
- Detect complications

23.11.3 Findings on CMR

- Typical pattern of functional impairment: apical ballooning or inverted pattern (mid-ventricular ballooning with basal and apical hyperkinesias).
- Quick restoration of LV function: significant amelioration within 5 days, full recovery within 10–14 days after onset.
- Myocardial edema in the area of wall motion abnormality
- Lack of hyperenhancement on LGE images
- LVOT obstruction due to bulging of the basal septum caused by impaired contraction pattern of the LV; reversible with recovery of LV function
- Complications similar to those in acute myocardial infarction: rupture of the LV or papillary muscles

23.11.4 Differential Diagnosis

- Thromboembolic or vasospastic myocardial infarction: these will show subendocardial or transmural hyperenhancement attributable to a coronary artery territory; no immediate recovery of LV function.
- Acute myocarditis: may show subepicardial or intramural hyperenhancement; usually more gradual recovery of LV function.

Tips and Tricks

- While typical cases do not exhibit any hyperenhancement on LGE images, there have been reports of cases of histologically proven Tako-Tsubo cardiomyopathy that did show infarct-like hyperenhancement. Given the disastrous histopathological damage that has been documented in a large series of “classic” cases, these findings are not surprising and it rather seems remarkable that there are not more of them. If hyperenhancement is present, the differentiation of Tako-Tsubo from thromboembolic infarction relies on the distribution pattern of the myocardial injury (confined to a coronary territory) and might even be impossible in some cases.

Key Points CMR in Tako-Tsubo Cardiomyopathy

CMR is the best imaging technique to differentiate Tako-Tsubo from thromboembolic myocardial infarction and acute myocarditis.

23.11.5 Case Example

Six hours after the funeral of her husband, an 83 year female was admitted with acute chest pain, ST elevation in anterior leads, and elevated troponin T. X-ray coronary angiography found only minor CAD without a culprit lesion. CMR was performed the next day (Figs. 23.34–23.36).

Follow-up on echocardiography one week later confirmed LV function had returned to normal.

Diagnosis: Apical ballooning syndrome or Tako-Tsubo cardiomyopathy.

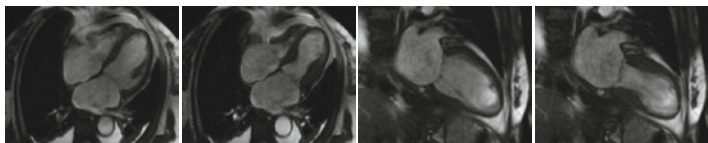


FIGURE 23.34. Cine images showing apical ballooning. Ejection fraction is 41%. There are bilateral pleural effusions indicating acute heart failure.

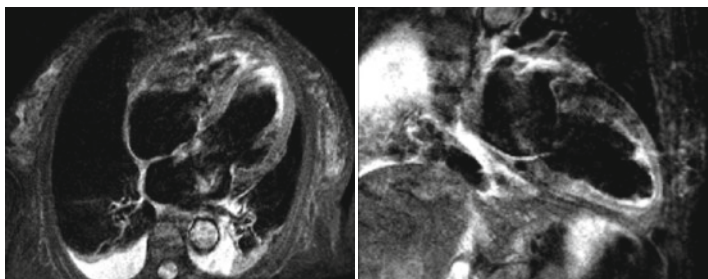


FIGURE 23.35. STIR images in 2-chamber (*left*) and 4-chamber views (*right*). There is mild apical hyperintensity of the myocardium (in addition to intra-cavity hyperintensity given by normal slow-flow phenomena).

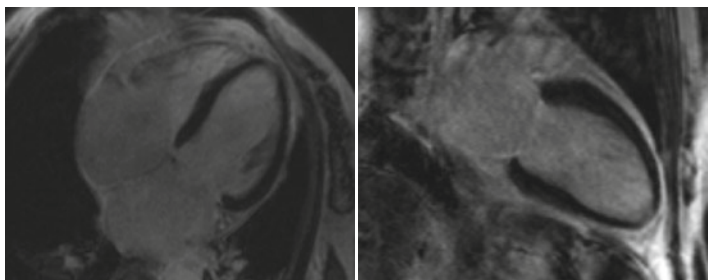


FIGURE 23.36. LGE images without signs of myocardial necrosis or scarring.

CMR Report in Tako-Tsubo Cardiomyopathy

LV/RV volumes and function

Presence and pattern of regional wall motion abnormalities, edema and LGE

References

1. Maron BJ et al. Contemporary definitions and classification of the cardiomyopathies: An American Heart Association Scientific Statement From the Council on Clinical Cardiology, Heart Failure and Transplantation Committee; Quality of Care and Outcomes Research and Functional Genomics and Translational Biology Interdisciplinary Working Groups; and Council on Epidemiology and Prevention. *Circulation.* 2006;113(14):1807–1816.
2. Assomull RG et al. Cardiovascular Magnetic Resonance, Fibrosis, and Prognosis in Dilated Cardiomyopathy. *J Am Coll Cardiol.* 2006;48(10):1977–1985.
3. Moon JC et al. The histologic basis of LGE cardiovascular magnetic resonance in hypertrophic cardiomyopathy. *J Am Coll Cardiol.* 2004;43(12):2260–2264.
4. McKenna WJ et al. Diagnosis of arrhythmogenic right ventricular dysplasia/cardiomyopathy. Task Force of the Working Group Myocardial and Pericardial Disease of the European Society of Cardiology and of the Scientific Council on Cardiomyopathies of the International Society and Federation of Cardiology. *Br Heart J.* 1994;71(3):215–218.
5. Tandri H et al. MRI of arrhythmogenic right ventricular cardiomyopathy/dysplasia. *J Cardiovasc Magn Reson.* 2004;6(2):557–563.
6. Petersen SE et al. Left ventricular non-compaction: insights from cardiovascular magnetic resonance imaging. *J Am Coll Cardiol.* 2005;46(1):101–105.
7. Mahrholdt H et al. Cardiovascular magnetic resonance assessment of human myocarditis: a comparison to histology and molecular pathology. *Circulation.* 2004;109(10):1250–1258.

8. Smedema J-P et al. Evaluation of the accuracy of gadolinium-enhanced cardiovascular magnetic resonance in the diagnosis of cardiac sarcoidosis. *J Am Coll Cardiol.* 2005;45(10):1683–1690.
9. Petersen SE, Kardos A, Neubauer S. Subendocardial and papillary muscle involvement in a patient with Churg-Strauss syndrome, detected by contrast enhanced cardiovascular magnetic resonance. *Heart.* 2005;91(1):e9.
10. Maceira AM et al. Cardiovascular magnetic resonance in cardiac amyloidosis. *Circulation.* 2005;111(2):186–193.
11. Anderson LJ et al. Cardiovascular T2-star (T2*) magnetic resonance for the early diagnosis of myocardial iron overload. *Eur Heart J.* 2001;22(23):2171–2179.
12. Wittstein IS et al. Neurohumoral features of myocardial stunning due to sudden emotional stress. *N Engl J Med.* 2005;352(6):539–548.
13. Friedrich MG, Strohm O, Schulz-Menger J, Marciniak H, Luft FC, Dietz R. Contrast media-enhanced magnetic resonance imaging visualizes myocardial changes in the course of viral myocarditis. *Circulation.* 1998;97:1802–1809.

Chapter 24

Pericardial Disease

Charles Peebles

24.1 Pericardial Effusion

CMR Protocol in Pericardial Effusion

1. Anatomy module including T1 and T2 weighting (Section 19.3)
2. LV function module (Section 19.4)
3. Targeted sequences depending on findings, for example, tumor protocol, valve imaging, real-time dynamic respiratory cine.
4. Late Gadolinium Enhancement module (Section 19.9.1)

24.1.1 *Introduction*

The etiology of pericardial effusions is varied and can be broadly divided into transudates, exudates, hemorrhage, and chyle. A full review of the causes of pericardial fluid is beyond the scope of this text. The role of imaging is to identify the effusion, assess its physiological significance and, if possible, diagnose the cause. Exudative processes tend to be associated with more complex effusions and greater pericardial inflammation, transudates conversely are generally simpler. Cross-sectional imaging has a specific role in assessing the extracardiac structures to identify malignancy and other systemic diseases.

24.1.2 CMR versus Other Imaging Modalities

Echocardiography remains the primary investigation for diagnosis of pericardial effusions but is susceptible to both false negative and positive results due to the presence of loculated fluid, poor acoustic windows, or adjacent pleural fluid. CMR demonstrates the whole of the pericardium, as well as the surrounding structures, making it an ideal tool for secondary imaging.

The functional significance of a pericardial effusion is also primarily assessed by clinical and echocardiographic examination. CMR provides similar information to echo regarding compromise to RV and RA filling but is advantageous if acoustic windows are poor or difficult to interpret.

24.1.3 Findings on CMR

The pericardial space normally contains a trace of pericardial fluid (<30 mL), which may be observed on CMR. There are no absolute CMR criteria for differentiating a physiological effusion from a pathological one but as a guideline a pericardial width of >4 mm is considered abnormal. An effusion measuring >5 mm anterior to the RV is likely to be a moderate volume (100–500 mL). Most effusions show a gravitational distribution being deepest posterolateral to the left ventricle.

24.1.3.1 Black Blood Images (Spin Echo Sequence)

It is important to initially scan the whole thorax when imaging a pericardial effusion. This will usually be performed with a fast black blood sequence and the intention is to identify extracardiac pathology such as lung tumors, lymph nodes, pleural effusions, etc. Echocardiography provides little or no information about the extracardiac structures and this is a major advantage for CMR. Computed tomography (CT) fulfills a similar role but provides more detail relating to the lungs as well as the abdomen. CT and MRI are thus complementary and both may well

TABLE 24.1. Typical CMR appearances of pericardial effusions.

	T1 signal (SE)	Cine appearances and signal intensity (b-SSFP)	
Transudate	↓	Simple	↑
Exudates	↓↑	Complex	↓↑
Hemorrhage	↓↑	Complex	↓↑
Chylous	↑↑	Simple	↑

be indicated. In practice, CT is generally used if there is a strong suspicion of underlying malignancy while MRI is favored if functional information is required.

In principle T1 characteristics of the fluid can give an indication of the nature of the effusion (see Table 24.1). In practice the signal return from the fluid is more influenced by flow voids and loculation than by pure T1 effects. A more useful finding is the complexity of the effusion and degree of pericardial thickening and enhancement – transudates tend to be simple with little pericardial inflammation while exudates and hemorrhage are complex with greater pericardial thickening.

24.1.3.2 CINE Imaging (b-SSFP)

Pericardial fluid generally appears as high signal on b-SSFP techniques, comparable to pleural effusions (if these should be present). Loculation and soft tissue stranding is well visualized as areas of mixed or reduced signal within the fluid effusion.

As with echocardiography the size of the effusion has a limited relationship with the physiological consequences, being more related to the duration and rate of accumulation of fluid. CMR criteria for functionally important effusion are similar to echocardiography; diastolic compression of the RV free wall, early systolic collapse of the RA, distortion of the LV and RV morphology, and potentially paradoxical interventricular septal motion during inspiration (ventricular coupling – more commonly seen in constrictive pericarditis).

24.1.3.3 Targeted Sequences

Depending on the initial findings further sequences may be indicated:

1. Pericardial inflammation – linear high signal with T1-weighted gadolinium-enhanced images.
2. Tumor – first pass perfusion, T1-weighted post-gadolinium images, myocardial delayed enhancement, myocardial tagging.
3. Myocardial disease – additional tissue characterization sequences (T1/T2/STIR), myocardial delayed enhancement.

The Role of CMR in Pericardial Effusion

1. CMR is useful in confirming the presence and size of a pericardial effusion if doubt exists on echo (particularly if loculated).
2. CMR may identify the cause of a pericardial effusion or give indications as to the etiology.
3. CMR provides functional information about the hemodynamic consequences of the effusion.
4. CMR is complementary to other imaging modalities.

24.1.4 Case Example

A 65 year old lady presented with increasing breathlessness on exertion and swollen ankles. She had a long history of Rheumatoid arthritis. An Echo suggested a pericardial effusion but this was not well visualized so an MRI was requested.

Following pericardial drainage the effusion was found to be an exudate and was rheumatoid factor positive. She was diagnosed with constrictive-effusive pericarditis and required a surgical pericardial window followed by pericardectomy (Figs. 24.1–24.3).

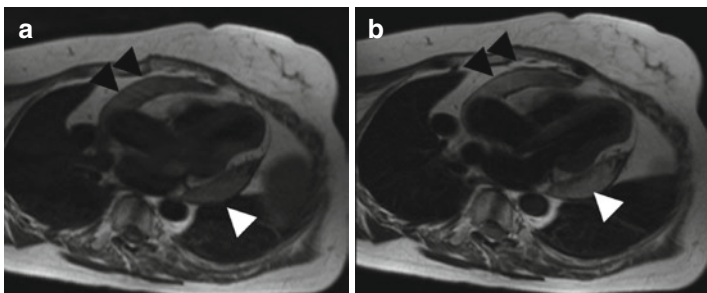


FIGURE 24.1. (a) T1 TSE image in a 3-chamber view shows an intermediate signal pericardial effusion (*arrow heads*). (b) T2-weighted image in the same position again showing an intermediate signal (*arrow heads*). The signal intensity suggests a proteinaceous effusion/exudate rather than a simple transudate, which should be lower signal on T1 images.

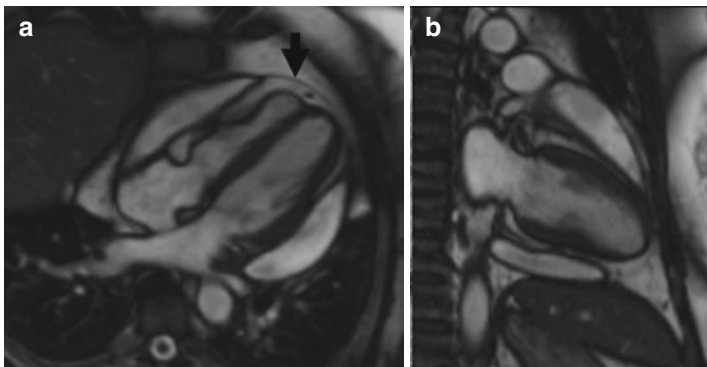


FIGURE 24.2. (a) 4-Chamber cine image showing a loculated pericardial effusion anterior to the RV and posterior to the LV. The RV chamber is distorted and compressed suggesting that the effusion is hemodynamically significant. Normal pericardium is seen over the apex (*arrow*). (b) 2-Chamber cine image. The loculated effusion has a similar distribution to Fig. 24.3a. (c) Short axis cine. The effusion is circumferential and has a typical high signal on SSFP images. Epicardial fat (*arrow*) is easily visualized.

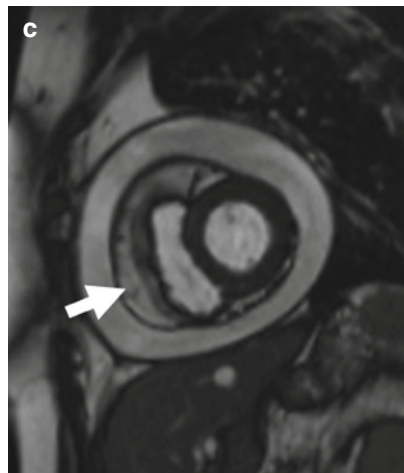


FIGURE 24.2. (continued).

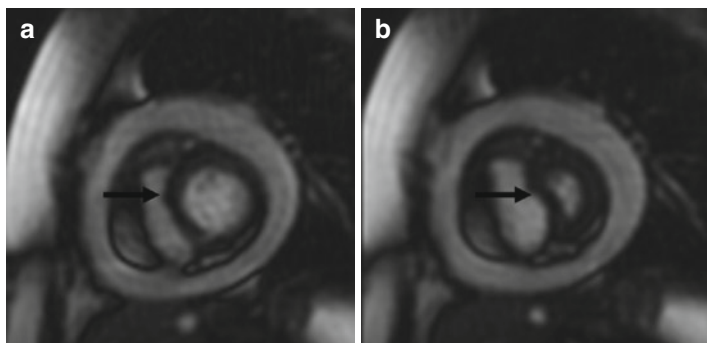


FIGURE 24.3. (a) Real-time short axis cine image taken during expiration shows a normal interventricular septal position (arrow). (b) Real-time short axis cine image taken from the same cine loop during early inspiration. There is clear septal displacement to the left side confirming a constrictive physiology.

Tips and Tricks

Cine images usually show pericardial effusions as high signal, if a pleural effusion is present the signal will often be similar on cine images but differ on TSE sequences.

CMR Report in Pericardial Effusion

Morphology (descriptive)

1. Pericardial thickness: describe as local or circumferential and list thickness measurements
2. Pericardial effusion: presence and extent

Ventricular parameters

1. LV volumes (see Chap. 20, page XXX)
2. Ventricular wall motion:
 - Systolic wall motion
 - Septal motion during normal respiration and breath holding.
3. Presence or absence of atrial inversion

Late Gadolinium Enhancement in RV, LV and pericardium

Key points CMR in Pericardial Effusion

1. Useful adjunct to echo
2. Gives functional and anatomical information
3. May identify or indicate the cause

24.2 Constrictive Pericarditis

CMR Protocol in Constrictive Pericarditis

1. Anatomy module including T1 and T2 weighting (Section 19.3)
2. LV function module (Section 19.4)
3. Targeted sequences depending on findings, for example, real-time dynamic respiratory cine, tagging, mitral valve flow.

24.2.1 *Introduction*

Constrictive pericardial disease is the end result of a number of inflammatory, infective, or malignant processes involving the pericardium causing a constrictive physiology. Usually this is associated with macroscopic thickening of the visceral and/or parietal pericardium, which may become adherent to the myocardium and regularly calcifies (particularly if tuberculous in origin). Constrictive pericarditis may, however, be associated with a pericardial effusion (effusive-constrictive pericarditis) or a normal thickness pericardium. Generally, it is a progressive and chronic condition but may be acute or rarely transient.

The physiological consequence of pericardial constriction is reduced ventricular diastolic filling. Ventricular filling pressures therefore increase in a similar way to restrictive cardiomyopathy, the main differential diagnosis. In constrictive pericarditis, however, the pericardial volume becomes fixed creating competition for diastolic filling between the ventricles – ventricular coupling or interdependence. The end result is preferential RV filling during inspiration (when negative intrathoracic pressure encourages systemic venous return), and preferential LV filling during expiration (when positive intrathoracic pressure encourages pulmonary venous return).

The MRI sequela of this is the paradoxical displacement of the interventricular septum to the left side during early inspiration and normalization during expiration. Ventricular coupling is not seen in restrictive cardiomyopathy.

24.2.2 CMR versus Other Imaging Modalities

The primary role of cross-sectional imaging in patients with signs and symptoms suggestive of constrictive pericarditis or restrictive cardiomyopathy is to identify pericardial thickening. The presence of thickened pericardium in the appropriate clinical context effectively differentiates constrictive pericarditis from restrictive cardiomyopathy and allows planning of pericardial stripping. Echocardiography is relatively poor at visualizing the pericardium and hence cross-sectional imaging is superior. CT demonstrates the pericardium well and has the advantage of being very sensitive to pericardial calcification. CMR, as well as showing the pericardium, has a much greater ability to provide functional information to support the diagnosis of constriction. CT and CMR are therefore often complimentary, particularly in the difficult diagnostic case.

24.2.3 Findings on CMR

24.2.3.1 Pericardial Thickening

The normal pericardium is seen over the RV free wall and the atrioventricular and interventricular grooves where there is abundant surrounding fat. The pericardium is usually pencil thin except over the diaphragmatic reflections. A thickness of >4 mm on spin echo sequences is generally considered to be pathological. Pericardial thickening is often patchy and may in some cases be absent.

Cine images readily differentiate pericardial effusion from thickening but tend to overestimate the thickness.

24.2.3.2 Indirect Signs of Constrictive Physiology

1. Distortion of RV and LV shape. The RV in particular may be flattened and tubular. This is best demonstrated with Cine imaging.
2. Atrial dilatation (in the absence of ventricular dilatation).
3. IVC and SVC dilatation (reflecting elevated filling pressures).
4. Pericardial adhesions between the thickened pericardium and the epicardial surface of the myocardium. This may be highlighted by tagged cine imaging demonstrating loss of the normal slippage of the pericardium over the myocardium.
5. Ventricular coupling. Paradoxical diastolic interventricular septal motion during early inspiration. This is best seen with a real-time cine sequence during deep breathing.

Tips and Tricks

Use real-time dynamic respiratory sequence in several short axis views and a 4-chamber view. The 4-chamber view demonstrates the whole length of the interventricular septum, the paradoxical septal motion often being limited to one part of the septum. The short axis views show the diaphragmatic position clearly, allowing assessment of the respiratory phase. Obtaining several short axis views samples the septum at a number of levels.

The Role of CMR in Constrictive Pericarditis

1. CMR identifies pericardial thickening.
2. CMR provides functional information that may support or indicate constrictive physiology.
3. CMR helps exclude restrictive cardiomyopathy.
4. CMR is complementary to other imaging modalities.

24.2.4 Case Example

This 80 year old man presented with a history of increasing exertional breathlessness and upper abdominal pain. An Echocardiogram suggested reduced RV function and diastolic dysfunction. He was referred for an MRI scan which diagnosed constrictive pericarditis. He subsequently underwent pericardectomy and has made a full recovery (Figs. 24.4–24.8).

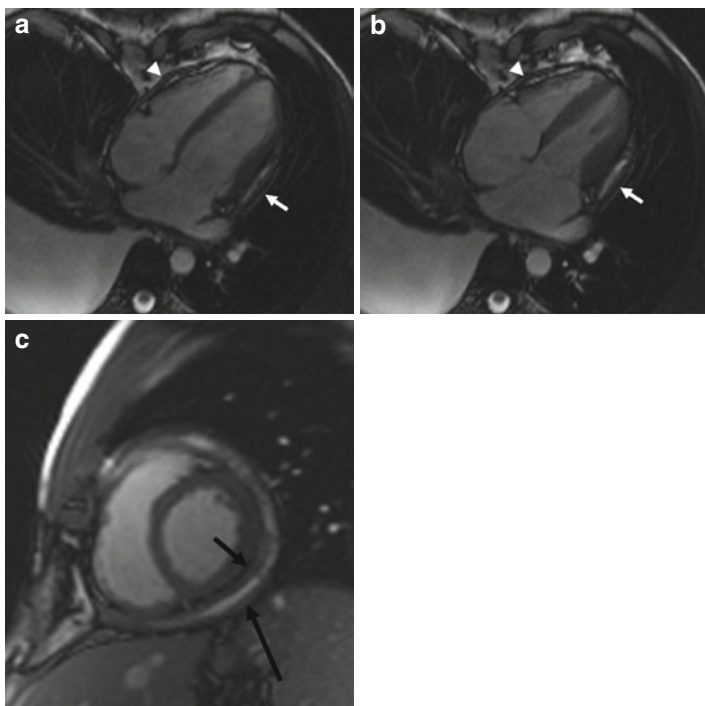


FIGURE 24.4. Four-chamber cine image in diastole (a) and systole (b). There is pericardial thickening over the lateral wall with a trace of pericardial fluid (white arrow). There is further pericardial thickening anterior to the RV (arrow head). There is subtle distortion of the LV free wall during diastole and bi-atrial dilatation – features suggesting a constrictive physiology. Note the substantial simple right pleural effusion. (c) Short axis cine image showing thickened parietal (long black arrow) and visceral (short black arrow) pericardium separated by a thin pericardial effusion.

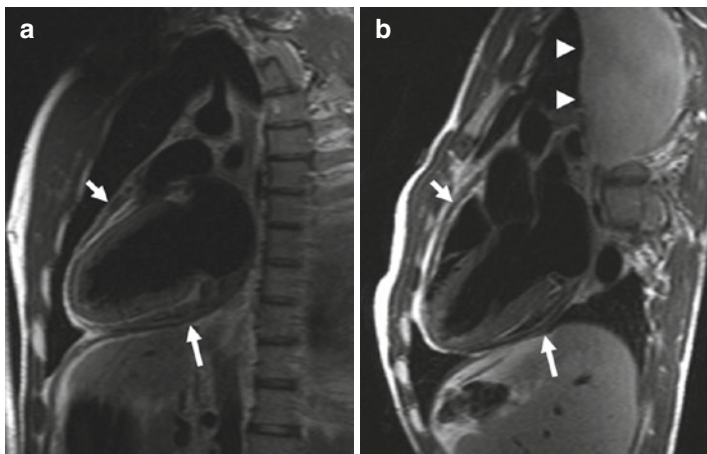


FIGURE 24.5. T1-weighted TSE image in a 2-chamber plane (**a**) and T2-weighted image in the 3-chamber plane (**b**) showing diffuse pericardial thickening (*arrows*) sparing the apex. This measures up to 1 cm in thickness. Note is made of the pleural effusion (*arrowhead*).

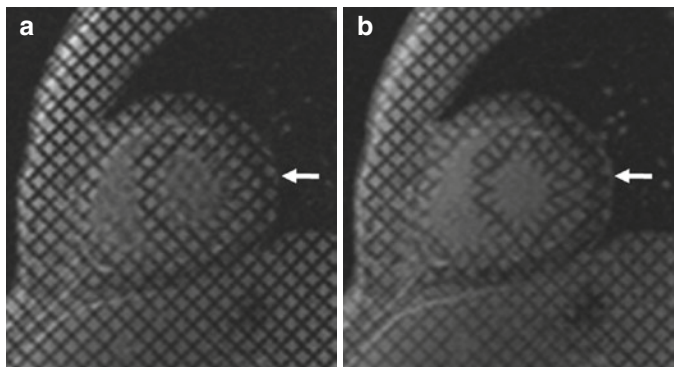


FIGURE 24.6. Myocardial-tagged image in the short axis plane at end-diastole (**a**) and end-systole (**b**). There are adhesions between the pericardium and the myocardium over the lateral wall demonstrated on the images as failure of “slippage” of the tag lines between the myocardium and pericardium during the cardiac cycle (in the region of the *arrows*).

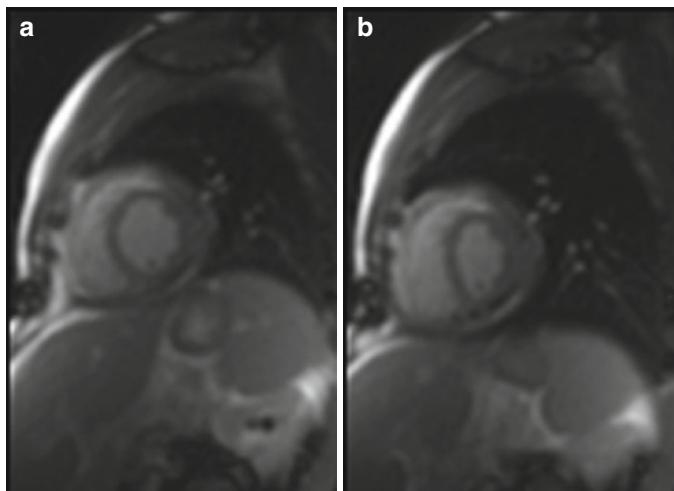


FIGURE 24.7. Two diastolic images taken from a real-time dynamic respiratory sequence. During expiration (a) the interventricular septal contour is normal, during inspiration there is subtle flattening of the septum indicating abnormal ventricular coupling. This finding is useful for differentiation between restrictive cardiomyopathy and constrictive pericarditis (see fig. 24.4 for a more dramatic example).

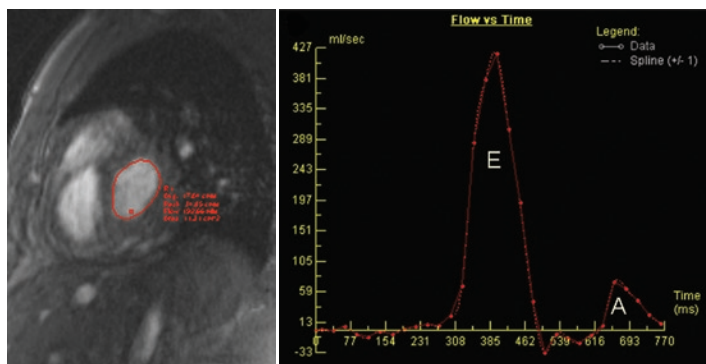


FIGURE 24.8. Phase contrast flow mapping of the mitral in-flow shows a pronounced E wave with rapid deceleration time and a small A wave. This indicates a restrictive or constrictive physiology. Respiratory variation would be seen in constriction but CMR does not have the ability to demonstrate this due to the need for breath hold acquisition or respiratory averaged images.

CMR Report in Pericardial Constriction

Morphology (descriptive)

1. Pericardial Thickness: describe as local or circumferential and list thickness measurements
2. Pericardial effusion: presence and extent

Ventricular parameters

1. LV volumes (see Chap. 20)
2. Ventricular wall motion:
 - Systolic wall motion
 - Septal motion during normal and dynamic respiration
3. Presence or absence of atrial inversion

Late Gadolinium Enhancement in RV, LV and pericardium

Key Points CMR in Constrictive Pericarditis

1. Identification of thickened pericardium in the appropriate clinical context is diagnostic of constriction
2. CMR gives indirect physiological information that may support the diagnosis
3. Pericardial constriction may be present with a normal pericardial thickness or patchy thickening
4. CMR is complimentary to CT, echo, and cardiac catheterization

24.3 Pericardial Tumors

CMR protocol in pericardial tumors

1. Anatomy module including T1 and T2 weighting. Images should cover the whole thorax (Section 19.3)
2. LV function module (Section 19.4)
3. Myocardial tagging (Section 19.5)
4. First pass perfusion imaging (Section 19.8.1)
5. T1-weighted post-contrast images
6. Late gadolinium enhancement module (Section 19.9.1)

24.3.1 Introduction

Pericardial tumors are divided into primary and secondary lesions. The commonest are the secondary lesions with breast cancer, lung cancer, or hematological tumors being the most frequent.

Primary pericardial tumors are rare, the commonest being mesothelioma (not associated with asbestos exposure) followed by sarcomas and intrapericardial teratomas. Pericardial tumors tend to cause complex pericardial effusions but may encase the pericardium and result in constrictive physiology. The volume of tumor in pericardial metastasis may be small and not macroscopically visible.

Tumors in the lung and mediastinum may directly invade the pericardium and CMR has a useful role in identifying such invasion and staging thoracic malignancies.

24.3.2 CMR versus Other Imaging Modalities

Echocardiography remains the initial investigation for most patients with pericardial tumors as the presentation is often that of pericardial effusion. If there is a suspicion of tumor clinically or on other imaging modalities a CMR is likely to

be the next imaging modality. Its excellent soft tissue differentiation and large field of view make it an ideal tool to identify pericardial tumor and delineate its origin and extent. CT has a complementary role although is less versatile at dynamic imaging or multiplanar imaging. CT is, however, more robust in identifying other thoracic lesions including lung primaries, pulmonary metastases, and mediastinal nodes, all of which may be instrumental in making a definitive diagnosis.

Having identified a pericardial tumor, attention turns to delineating its extent and the presence of local invasion. CMR is ideal for this and using the full range of imaging sequences can also provide useful information about the nature of the lesion and its physiological consequences. Coronary angiography may be needed, if surgical resection is considered, to identify distortion/invasion of the coronaries although CT and MRI will provide adequate information in most cases.

24.3.3 Findings on CMR

The whole of the thorax should be imaged in patients with suspected pericardial tumors to identify primary lesions, other secondaries and mediastinal nodes.

24.3.3.1 CINE Imaging (b-SSFP)

Standard cine images will identify a pericardial effusion if present and also show areas of thickened pericardium. This alone may be enough to confirm a pericardial mass or pericardial deposits as well as extra-pericardial tumors invading the pericardium.

Most pericardial tumors will show similar signal to the myocardium but greater heterogeneity of the tumor and slight increase in signal will usually allow differentiation. Tethering and/or invasion of the adjacent myocardium or great vessels are generally easily identified and are an indicator of malignancy. Well-defined or encapsulated lesions are more likely to be benign.

Cine images provide additional direct or indirect information about the physiological consequences of the tumor (see the sections on pericardial effusion and constriction).

24.3.3.2 Myocardial Tagging

Tagging may help to differentiate tumor (which is non-contractile) from myocardium, and subsequently indicate the extent of myocardial invasion.

24.3.3.3 Black Blood Images (TSE)

Characterization of tumors is difficult although differentiation of benign and malignant lesions can be indicated by well-defined/encapsulated margins versus soft tissue invasion, respectively. Lipomas can be positively identified by their fat content on T1- /T2-weighted TSE images and fat suppressed sequences. Most soft tissue tumors will have similar signal characteristics to myocardium although increased tissue edema may be manifest by slight increase in signal on T2 weighting.

24.3.3.4 First-Pass Perfusion Imaging

Both primary and secondary pericardial tumors will show some degree of enhancement on first pass perfusion imaging. Enhancement on first pass perfusion imaging helps to confirm the presence and extent of the tumor and differentiate it from hematoma or complex effusion.

24.3.3.5 Post-Contrast T1 TSE and Delayed Enhanced Images

As indicated above most soft tissue tumors will display some contrast enhancement and delayed contrast wash-out. T1 TSE images early following contrast may show heterogeneous enhancement in the tumor as will delayed inversion recovery sequences. These findings help confirm the presence

and extent of tumor but give little information regarding the pathological diagnosis.

The Role of CMR in Pericardial Tumors

1. CMR identifies and delineates focal pericardial masses.
2. CMR demonstrates extracardiac tumors invading the pericardium and is useful in staging mediastinal and thoracic tumors.
3. Excellent soft tissue differentiation allows accurate assessment of extent of pericardial tumors and invasion of adjacent structures.
4. CMR may provide useful tissue characterization, for example, lipoma.
5. CMR provides additional functional information.

24.3.3.6 Case Example 1

A 61-year-old man presented with a three week history of shortness of breath, dry cough, chest tightness, and orthopnea. Having been previously fit he was now breathless on climbing one flight of stairs. Examination primarily showed evidence of right-sided failure with raised JVP and swollen legs. Echocardiogram showed a large pericardial effusion and on pericardiocentesis 2 L of blood stained fluid was drained.

The patient was transferred to our institution with the drain in situ and a repeat echocardiogram suggested a pericardial clot. CMR imaging helped to clarify the anatomical findings. The patient underwent surgical resection of the lesion, which on histology was a synovial sarcoma (Figs. 24.9–24.13).

24.3.3.7 Case Example 2

This 35 year old man presented with a large anterior mediastinal mass closely applied to the pericardium. CMR was used

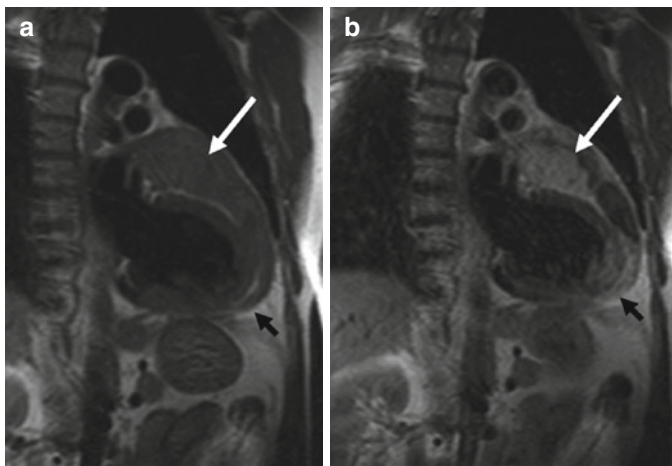


FIGURE 24.9. T1-weighted TSE pre- and post-gadolinium in a 2-chamber view. Pre-contrast (a) there is 4×6 cm soft tissue mass (white arrow) arising from the pericardium with more diffuse pericardial thickening elsewhere (black arrow). The mass appears not to involve the myocardium with preservation of the epicardial fat. Post-contrast (b) the mass enhances (white arrow) and becomes differentiated from the adjacent pericardial thickening.

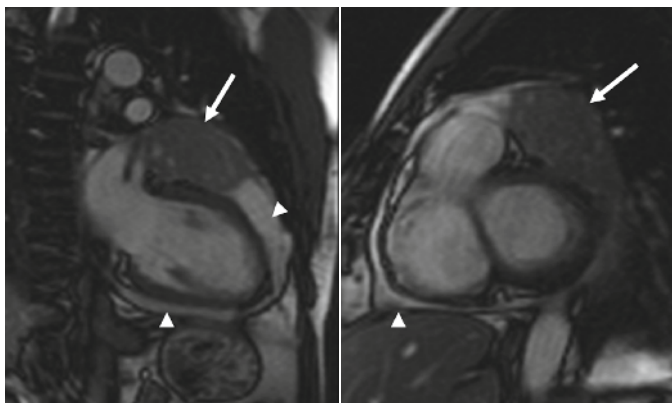


FIGURE 24.10. Cine SSFP 2-chamber and short axis views. The soft tissue mass (white arrows) seems to arise from the pericardium with normal myocardial signal and motion. The fat around the interventricular groove and LAD is preserved. The pericardial effusion has homogeneous high signal (arrow heads).

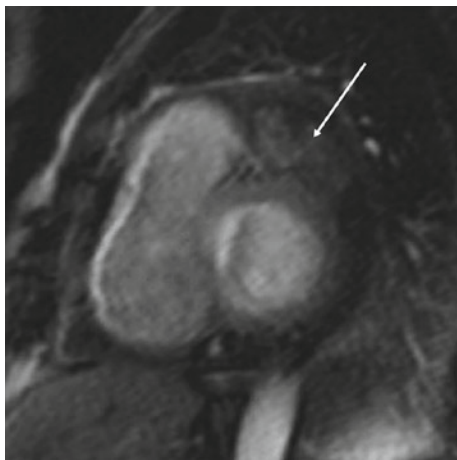


FIGURE 24.11. First-pass perfusion study. An arterial phase image from a first-pass perfusion study shows heterogeneous enhancement of the mass (arrow). This effectively precludes a pericardial hematoma and makes a soft tissue tumor the most likely diagnosis.

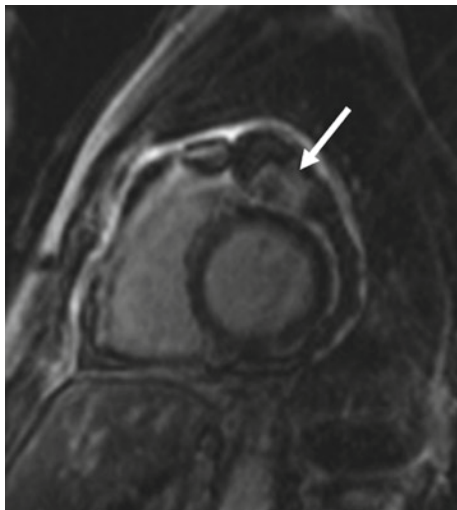


FIGURE 24.12. TSE inversion recovery delayed enhanced image. There is patchy high signal within the lesion. The myocardium remains of normal low signal. This is a nonspecific finding but again helps to exclude a hematoma.

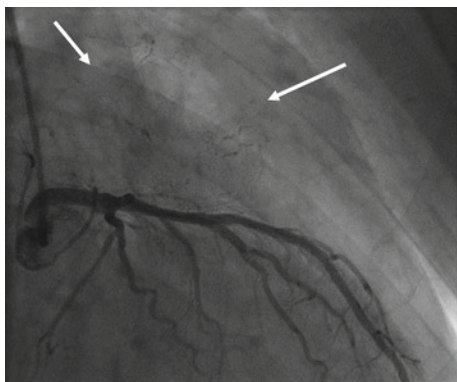


FIGURE 24.13. Angiogram. The coronary angiogram shows normal coronaries with capillary filling of the soft tissue lesion (*arrows*).

to assess myocardial invasion. The tumor was a thymic carcinoma and was resected. As the CMR demonstrates the tumor invaded the pericardium but could be removed from the myocardium and coronary arteries. CMR is a powerful tool for staging mediastinal tumors prior to surgery (Fig. 24.14).

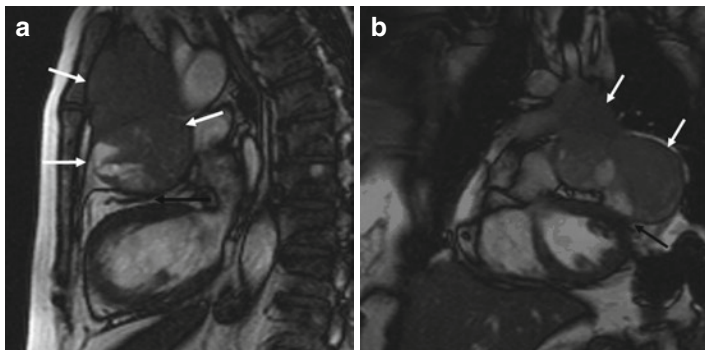


FIGURE 24.14. (a) Coronal Cine image. The large heterogeneous anterior mediastinal mass is well demonstrated (*white arrows*) and appears to invade the pericardium (*black arrows*). Although the epicardial fat is effaced the myocardium is not obviously involved. (b) Sagittal Cine image. In this plane the tumor abuts the pericardium and distorts the Left anterior descending coronary artery although does not clearly invade it. There is again no tumor invasion of the myocardium.

CMR Report in Pericardial Tumors

1. Location (pericardial, myocardial, valve relationship, chamber relationship)
2. Size (cross-sectional dimensions)
3. T1 signal intensity (homogeneous, heterogeneous, hyper-, iso-, or hypointense to myocardium/or chest wall-specify reference tissue)
4. T1 fat sat images signal intensity (if performed, homogeneous, heterogeneous, hyper-, iso-, or hypointense to myocardium/or chest wall-specify reference tissue)
5. T2 signal intensity (homogeneous, heterogeneous, hyper-, iso-, or hypointense to myocardium/or chest wall-specify reference tissue)
6. STIR signal intensity
7. Perfusion pattern (if perfusion performed)
8. Late gadolinium enhancement pattern on static/delayed images (if gadolinium administered)
9. Relationship to myocardium/pericardium, mediastinum
10. Margins (e.g., smooth, irregular, infiltrating, pediculated)
11. Cine CMR appearance (pedunculated, motion with myocardium/pericardium)
12. Myocardial function (if performed, qualitative or quantitative as appropriate)
13. Pericardial abnormalities if present (pericardial thickness should be reported along with determination of the presence or absence of a pericardial effusion)

Key Points CMR in Pericardial Tumors

1. Useful for identifying primary and secondary pericardial tumors
2. Useful for assessing pericardial involvement from other mediastinal or lung tumors
3. Accurate tumor characterization is usually not possible and requires histological confirmation

24.4 Congenital Abnormalities of the Pericardium

CMR Protocol in Congenital Abnormalities of the Pericardium

1. Anatomy module including T1 and T2 weighting (Section 19.3)
2. LV function module (Section 19.4)
3. Targeted sequences depending on findings, for example, first pass perfusion (Section 19.5 and 19.8.1) tagging.

24.4.1 Introduction

Pericardial cysts are caused by embryonic remnants of pericardium, which become fluid filled. They generally lie adjacent to the pericardium but may rarely be intrapericardial. If they communicate with the pericardium they are termed diverticulae, but usually they are separate. Approximately 70% are located in the right cardiophrenic angle and 20% on the left. The majority of patients are asymptomatic and present coincidentally following a chest X-ray with a right paracardiac mass. Occasionally patients present with symptoms from complications such as pressure effects or secondary infection.

Pericardial defects or agenesis are congenital abnormalities that often pass unnoticed. Part of, or all of the pericardium fails to develop, possibly as a result of vascular insufficiency during pericardial embryogenesis. One third of cases are associated with other cardiac malformations and the condition is more common in males. Complete agenesis is rare (9%) and is considered benign as symptoms are uncommon. Partial defects are more common and are generally over the left heart (70%). They may result in herniation of cardiac structures through the defect with potential strangulation or compromise of the herniated structure, for example, the left atrial appendage. Cases of coronary compromise have

been described. Repair of partial pericardial defects has therefore been recommended.

24.4.2 CMR versus Other Imaging Modalities

CMR is used to confirm the position and nature of cystic lesions around the heart, which have been identified by CXR or Echocardiography. Likewise, pericardial defects can be demonstrated on CMR if there is a radiological or clinical suspicion, but are more commonly incidental findings.

Additional physiological information can be gained if there is compression or distortion of an adjacent cardiac chamber or vessel.

24.4.3 Findings on CMR

Pericardial cysts are fluid-filled thin walled lesions usually abutting the pericardium. The fluid is a transudate and as such appears simple on MRI with low T1 signal, high T2 signal, and high signal on SSFP sequences. Occasionally, the cyst will contain proteinaceous fluid and show higher T1 signal. They are generally round and well defined but may conform to surrounding structures as they are under low pressure, indeed they may change shape during respiration. Occasionally, they become tense and distort or compress the adjacent intrapericardial structures with significant hemodynamic consequences, particularly if the cyst itself is intrapericardial. The main differential is from other paracardiac masses and this is usually straightforward given the simple cystic nature of the lesion and the location.

Pericardial defects are identified by absence of the normal pericardium and a subsequent change in the normal cardiac contour. The heart may shift leftward or specific chambers may herniate through the defect. Likewise, paracardiac structures that are normally separated from the heart may lie in direct contact with heart and create abnormal contours, such

as the lung extending into the aorto-pulmonary window. In clinical practice these defects are rarely seen.

The Role of CMR in Congenital Abnormalities of the Pericardium

1. CMR identifies the normal pericardium and pericardial defects.
2. CMR demonstrates and characterizes cystic lesions relating to the pericardium.
3. CMR is complementary to other imaging modalities.

24.4.4 Case Example

This patient presented following an abnormal CXR as part of a health screening assessment. He has no symptoms of cardiac disease (Figs. 24.15–24.17).

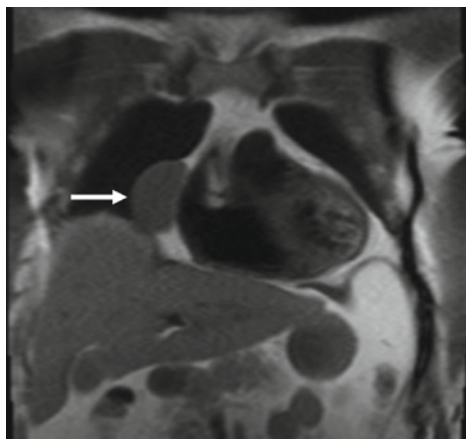


FIGURE 24.15. Coronal HASTE image. A pericardial cyst is demonstrated in the typical position (*white arrow*).

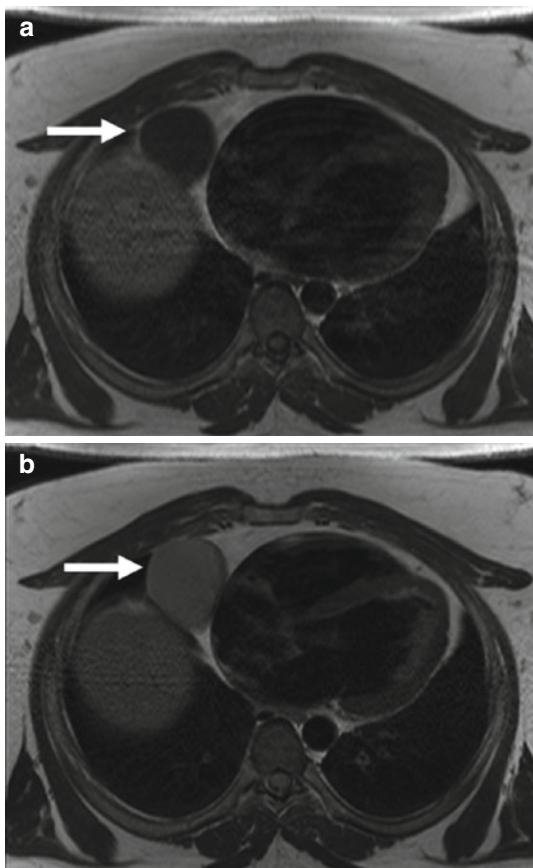


FIGURE 24.16. TSE images in an axial plane with T1 (**a**), T2 (**b**), and Fat suppressed (**c**) weighting, respectively. The cyst (*white arrow*) is well defined and abuts the pericardium. It is low signal on T1-weighted images, intermediate signal on T2 weighting and high signal on T2-weighted fat-suppressed images consistent with a simple transudate.

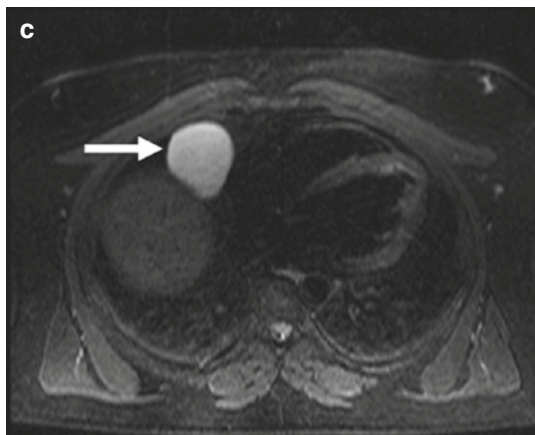


FIGURE 24.16. (continued).

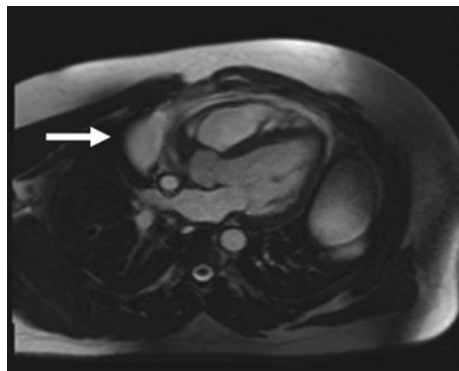


FIGURE 24.17. Three-chamber cine image (SSFP). The pericardial cyst (arrow) shows high signal without septations. There is no distortion of the adjacent cardiac structures.

CMR Report in Congenital Pericardial Abnormalities

1. Morphology of the abnormality
2. Appearance on different CMR image types
3. Associated pathologies

Key Points: CMR in Congenital Pericardial Abnormalities

1. Used to confirm the typical cystic nature and location of pericardial cysts.
2. Excludes other causes of paracardiac mass lesions.
3. Identifies congenital pericardial absence or pericardial defect.
4. Demonstrates any functional consequence of pericardial abnormality.

Chapter 25

Cardiac Masses

John P. Greenwood

The Role of CMR in the Diagnosis of Cardiac Masses is

1. To confirm or refute the presence of a mass identified on CXR or Echo
2. To establish the tumor location, size and relationship to surrounding cardiac structures
3. To assist with tissue characterization
4. To determine extracardiac involvement
5. To guide surgical intervention

CMR Protocol for Cardiac Masses

1. High-resolution trans-axial BB T1-weighted stack, diaphragm to aortic arch (Section 19.2)
2. Cine imaging in all standard planes and additional targeted planes (Section 19.2)
3. In two optimized orthogonal planes:
 - a. BB T1w with fat suppression (Section 19.3.1)
 - b. BB T1w pre and post contrast (Section 19.3.1)
 - c. T2w (Section 19.3.2)
- d. 1st pass myocardial perfusion imaging (Section 19.8)
- e. Early and Late Gadolinium Enhancement imaging (Section 19.9)

25.1 Introduction

Cardiac magnetic resonance (CMR) imaging is an important technique for the evaluation of a suspected cardiac mass. CMR imaging offers a larger field of view, multi-planar imaging, and superior tissue contrast compared to echocardiography. With recent improvements in MR pulse-sequence technology, tissue characterization is possible by comparing the T1 and T2 values of the mass to a reference tissue (Table 25.1). Thus CMR is an important imaging modality for the assessment of any suspected cardiac or paracardiac mass

TABLE 25.1. CMR tissue characteristics of common cardiac tumors (compared to normal myocardium).

Tumor	T1W spin echo	T2W spin echo	Post contrast
Myxoma	Intermediate SI ^a	High SI	Hyperintense
Lipoma	High SI (like fat)	Intermediate SI	Nonspecific
Fibroma	Intermediate SI	Low SI	Hyperintense
Rhabdomyoma	Intermediate SI	High SI	Nonspecific
Hemangioma	High SI ^a	High SI	Hyperintense
Angiosarcoma	High SI ^a	High SI ^a	Hyperintense
Lymphoma	Low-intermediate SI	High SI	Hyperintense ^a
Pericardial cyst	Low SI	Highest SI	Nonspecific
Thrombus	Low-high SI ^b	Low-high SI ^b	No enhancement

^a May be heterogeneous with areas of lower and higher signal intensity, depending on vascularity, necrosis, and calcification

^b Signal intensity varies according to age (fresh thrombus usually high SI on T1W and T2W, older thrombus usually low SI on T1W and T2W spin echo imaging, SI = Signal Intensity)

as it can determine tumor size, location, relationship to other cardiac structures, invasion into the pericardium, or extracardiac spread (e.g., invasion into the great vessels), which is vital for any proposed surgical planning. Serial CMR studies can also be performed for monitoring tumor regression after surgical resection or chemotherapy.

Tumors of the heart can be either primary or secondary, the former of which can be either benign or malignant (Table 25.2). Primary cardiac tumors are very rare with a quoted prevalence of between 0.001 and 0.3% in autopsy series. Approximately 75% of primary cardiac tumors are benign. Secondary cardiac tumors occur with a frequency of 30–50 times that of primary malignant cardiac tumors. Benign primary cardiac tumors tend to be well circumscribed and homogeneous, do not invade local structures, and tend not to be associated with pleural or pericardial effusions. The most common primary malignant cardiac tumors are the various sarcomas and lymphomas. Unfortunately, due to the small numbers studied and their variable presentation, reliable tissue differentiation by CMR is still not possible.

A CMR scan is usually performed after a transthoracic echocardiogram has identified an abnormality and further characterization is required. For example, CMR can provide detailed information on extracardiac involvement, lesion vascularity, and tissue characterization. With the advent of cardiac CT, comparable anatomical information can be obtained

TABLE 25.2. Primary cardiac tumors in adults.

Benign (~70%)	Malignant (~30%)		
Myxoma	30%	Angiosarcoma	9%
Lipoma	10%	Rhabdomyosarcoma	5%
Papillary fibroelastoma	10%	Mesothelioma	4%
Fibroma	4%	Fibrosarcoma	3%
Rhabdomyoma	7%	Lymphoma	2%
Hemangioma	3%		

from this modality, but CMR is still important due to its ability to provide additional functional information.

25.2 Benign Cardiac Tumors

25.2.1 *Myxoma*

This is the most common primary cardiac tumor, accounting for ~30% of all cardiac masses and half of all benign tumors. Myxomas typically present between the third and sixth decades of life, more commonly in women, and whilst 20% may be asymptomatic, the classic triad of symptoms relate to obstruction, constitutional symptoms, and the effects of embolization.

Pathologically myxomas are typically solitary, are located in the left atrium (75%), and are heterogeneous containing cystic areas, hemorrhage, necrosis, and calcification. On CMR imaging, myxomas appear spherical and often the pedunculated point of attachment to the endocardial surface can be identified on cine imaging. On spin-echo images, myxomas are characterized by an intermediate (similar to myocardium), but heterogeneous signal intensity due to their complex architecture. On T2-weighted imaging, myxomas may show marked increased signal intensity, whilst after contrast, there may be moderately high contrast enhancement mixed with non-enhancing areas which are cystic or necrotic (Fig. 25.1).

25.2.2 *Lipoma*

The second most common benign cardiac tumor is lipoma, which is typically solitary, encapsulated, and well circumscribed. Lipomas can arise subepicardially (25%), subendocardially (50%), or from the myocardium and arise most commonly from the right atrium or left ventricle. On CMR lipomas are characterized by high signal intensity on T1 weighted imaging, slightly less signal on T2 imaging, and a marked reduction in signal intensity on T1-weighted imaging when a fat saturation

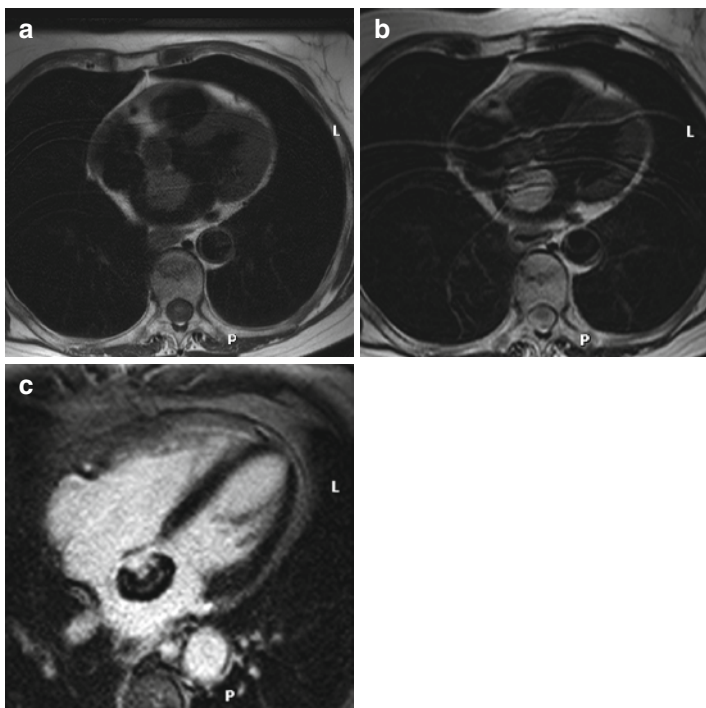


FIGURE 25.1. Eighty-four-year-old female presenting with syncope and embolic phenomena. CMR characteristics of a left atrial myxoma: (a) T1-weighted black blood image in axial orientation showing an oval mass in the left atrium. (b) T2-weighted imaging using the same geometry. (c) LGE image confirming the heterogeneous nature of the lesion.

prepulse is used (compare appearance to that of subcutaneous fat). They do not enhance following the administration of contrast (Fig. 25.2).

Lipomatous hypertrophy is a non-encapsulated fatty infiltration, typically seen in the inter-atrial septum and is usually contiguous with the epicardial fat, but spares the fossa ovalis.

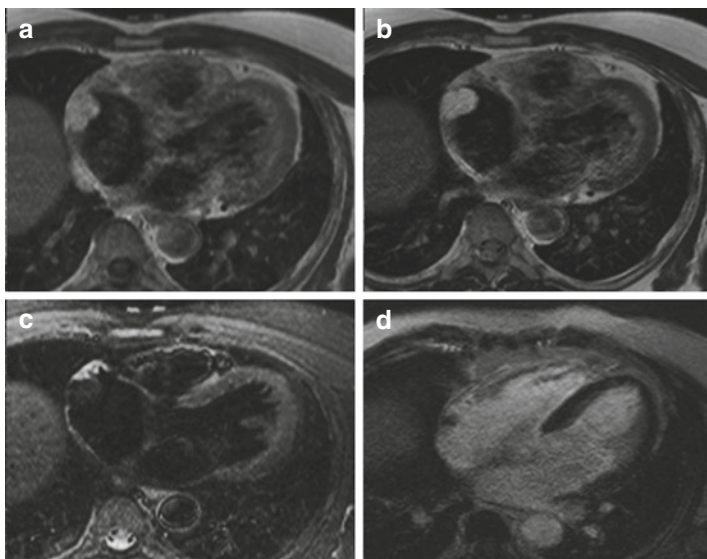


FIGURE 25.2. Forty-five-year-old female presenting with palpitations. CMR features of a lipoma in the right atrium demonstrated by: (a) T1-weighted black blood image in transaxial plane. (b) T2-weighted black blood imaging. (c) T1-STIR (fat suppression prepulse). (d) LGE image confirming no contrast uptake into the lesion. (Images courtesy of G. McCann, Leicester).

25.2.3 Papillary Fibroelastoma

These represent the third most common benign cardiac tumor, typically occurring on the valves (90%) as a frond-like structure. They are generally not visualized well by CMR due to their small size and high mobility.

25.2.4 Fibroma

These are congenital tumors that typically first present in young adult life. Fibromas are usually solitary and located within the ventricular myocardium (LV more frequently than

RV). The tumor typically exerts a local “mass” effect and is frequently associated with malignant ventricular arrhythmias. On CMR, fibromas appear homogeneous, well demarcated, and solitary. On T1-weighted imaging, they appear isointense compared to normal myocardium and skeletal muscle; on T2-weighted imaging, they appear hypointense. Using the late gadolinium enhancement technique 10–15 min after contrast, fibromas characteristically show hyperenhancement (Fig. 25.3).

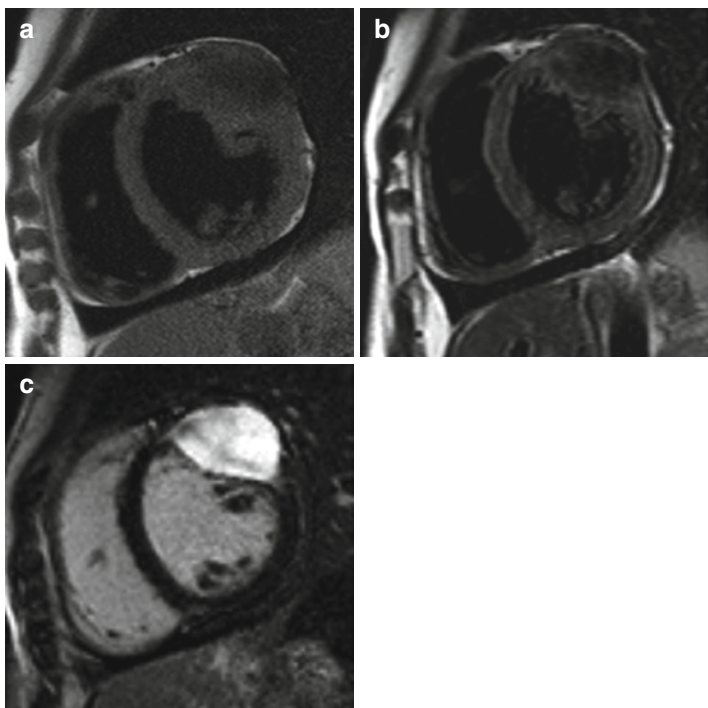


FIGURE 25.3. Thirty-two-year-old female presenting with palpitations. CMR features of a fibroma demonstrated by: (a) T1-weighted black blood image in short axis. (b) T2-weighted black blood imaging. (c) LGE image confirming hyperenhancement confined to the lesion.

25.2.5 *Rhabdomyoma*

These tumors typically present in the first year of life and are often associated with a diagnosis of tuberous sclerosis. They arise in the ventricular myocardium (LV>RV), may be multiple, and are well circumscribed but not encapsulated. On CMR rhabdomyomas appear homogeneous and isointense on T1-weighted imaging and hyperintense on T2-weighted imaging compared to normal myocardium.

25.2.6 *Hemangioma*

Arteriovenous hemangiomas are rare accounting for 5–10% of benign cardiac tumors. They are typically solitary, non homogeneous and found in the LV or RV. They typically show increased signal intensity on T1-weighted images pre-contrast; after contrast they are hyperintense due to their vascular nature.

25.3 Malignant Cardiac Tumors

25.3.1 *Sarcoma*

This group represents approximately 95% of primary malignant cardiac tumors and includes angiosarcomas, leiomyosarcomas, fibrosarcomas, liposarcomas, and osteosarcomas. Angiosarcomas are the most common of this group, typically arise in the RA, and are irregular or nodular. They often infiltrate into the cardiac chambers or extend along the pericardium. Due to their associated hemorrhage and necrosis, on CMR they appear heterogeneous with areas of increased signal intensity on T1- and T2-weighted images. After contrast they continue to appear heterogeneous with areas of signal enhancement (Fig. 25.4). Other sarcomas are rare and beyond the scope of this text.

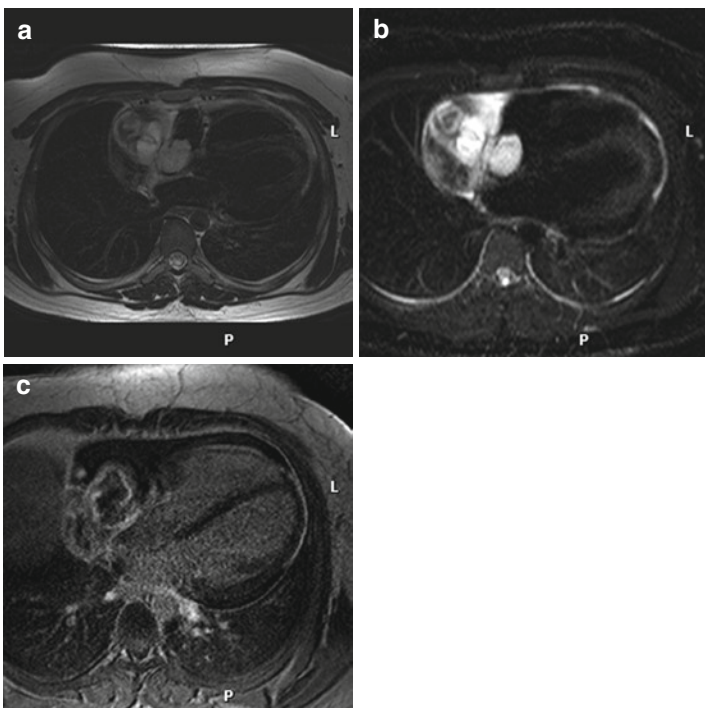


FIGURE 25.4. Twenty-five-year-old male presenting with clinical features of tamponade. CMR imaging features included: (a) T1-weighted black blood imaging transaxially showing large heterogeneous mass compressing the right atrium and invading through the wall into the right atrial cavity. (b) T2-weighted images and (c) LGE images confirmed the heterogeneous nature of the tumor.

25.3.2 Lymphoma

Primary cardiac lymphomas are very rare, but postmortem studies have documented cardiac involvement in up to 25% of patients with lymphoma. On CMR they appear isointense or hypointense on both T1- and T2-weighted imaging

compared to normal cardiac muscle. After contrast they appear heterogeneous and may have a central necrotic core.

25.3.3 Metastatic Tumors

Metastatic spread to the heart is most commonly associated with lung cancer, breast cancer, lymphoma, and melanoma. Spread to the heart may be by direct invasion, and by hematological or lymphatic spread. Transvenous spread can also occur, for example, via the IVC in the case of hepatic or renal tumors. Typically metastases tend to have low signal intensity on T1-weighted images, appear brighter on T2-weighted images, and enhance after contrast. Melanoma is the exception which appears bright on T1-weighted imaging due to the paramagnetic metals bound by melanin.

25.4 Other Masses and Tumors

25.4.1 Thrombus

This is one of the most common causes of an intracardiac mass and is typically found in the LA in association with chronic AF or mitral valve disease, or in the LV in association with myocardial infarction. The CMR appearances are variable depending on age of the thrombus; fresh thrombus appears bright on T1- and T2-weighted imaging, older thrombi typically have lower signal intensity on T2-weighted images. After contrast administration, intra-cavity thrombus appears very dark on both the early and late gadolinium enhancement images (Fig. 25.5).

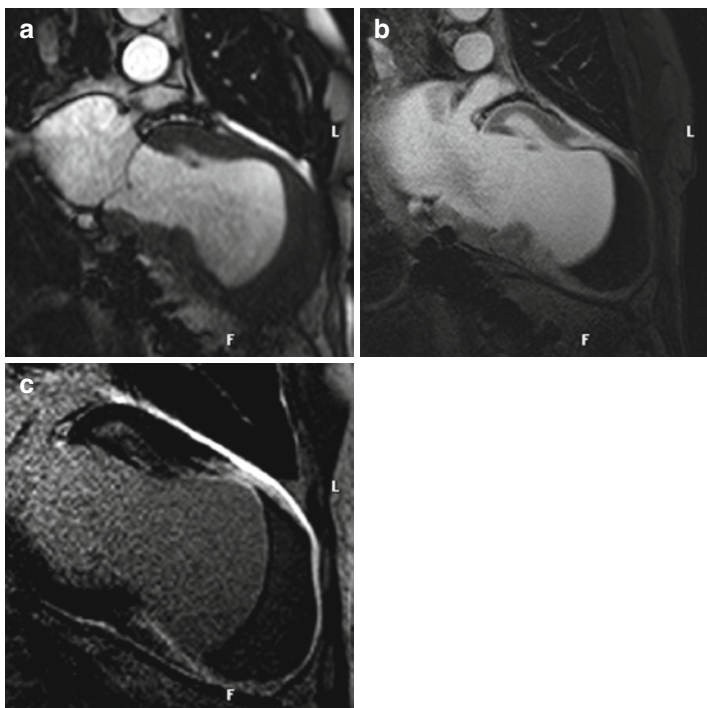


FIGURE 25.5. Sixty-five-year-old male presented with worsening heart failure. (a) SSFP cine imaging in the VLA orientation showed a large antero-apical aneurysm which appeared to be lined with thrombus. (b) Early gadolinium enhancement and (c) LGE images in the VLA orientation confirmed the presence of thrombus (very dark area at the apex).

25.4.2 Cysts

Pericardial cysts are usually located in the right pericardiophrenic angle and are often discovered incidentally on CXR or by echocardiography. Usually the patient is asymptomatic unless the cyst exerts a local compressive effect. The cyst is usually filled with clear fluid and on CMR they characteristically appear very bright on T2-weighted imaging (Fig. 25.6).

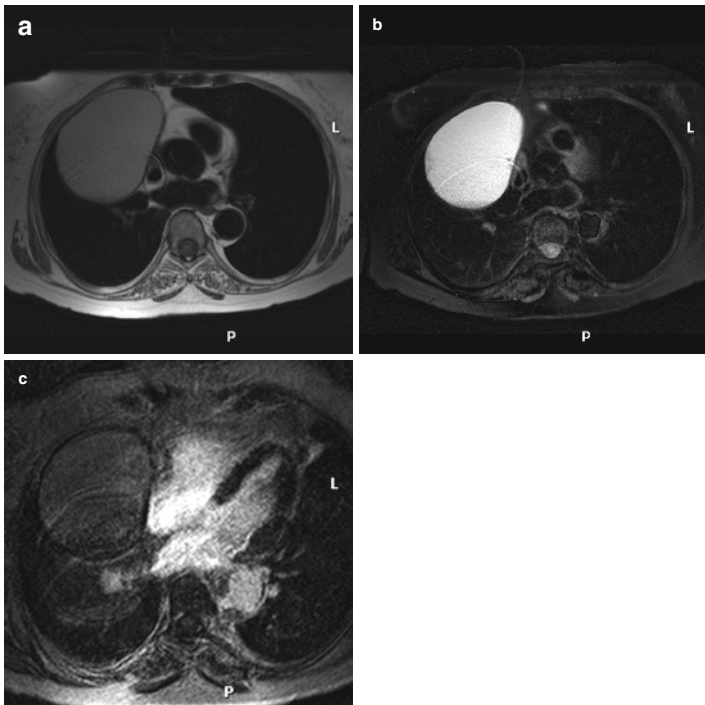


FIGURE 25.6. Seventy-one-year-old female presented with shortness of breath and a large mass lesion seen on the CXR and echocardiogram. CMR features included: (a) T1-weighted black blood imaging showing large well-demarcated lesion exerting local compression of the right hilum, right atrium, and SVC. (b) T2-weighted imaging showing very high signal intensity from the fluid-filled cyst. (c) LGE image shows no contrast uptake.

25.4.3 Pseudotumors

Not infrequently, normal intracardiac structures or remnants can be mistaken for a tumor e.g., crista terminalis, Thebesian valve, Eustachian valve, or a Coumadin ridge. Other structures outside the heart can also give ‘cause for concern’ such as prominent coronary sinus, AV malformations, and left-sided SVC. With its large field of view and high spatial resolution CMR can rapidly characterize these structures.

Tips and Tricks

1. Identify the lesion on multi-slice, multi-phase cine imaging in at least two orthogonal planes.
2. For tissue characterization always perform multiple pulse sequence acquisitions (e.g., BB T1-weighted sequences with and without a fat saturation prepulse, BB T2-weighted imaging, and late gadolinium enhancement imaging) using the same planning geometry.
3. First-pass myocardial perfusion imaging can be extremely helpful in the determination of vascularity.

Key Points: CMR in Diagnosis of Cardiac Masses

1. CMR is the principal modality for the diagnosis and follow-up of intracardiac tumors.
2. CMR allows detailed assessment of tumor location and its involvement of other cardiac/extracardiac structures to assist with surgical planning.
3. Very small, highly mobile masses (e.g., valvular vegetations) may be best visualized by echocardiography.
4. Whilst CMR can provide information on tissue characterization, it cannot give a histological diagnosis and thus further assessment (e.g., biopsy) may be required.

Standard CMR Report for Cardiac Masses

1. Location (pericardial, myocardial, valve relationship, chamber relationship)
2. Size (in three cross-sectional dimensions)
3. Signal intensity on T1, T1 fat, T2 and STIR images (homogeneous, heterogeneous, hyper, iso- or hypointense to myocardium or chest wall (specify reference tissue))
4. Relationship to myocardium/pericardium, mediastinum
5. Margins (e.g., smooth, irregular, infiltrating, pediculated)
6. Cine CMR appearance (pedunculated, motion with myocardium/pericardium)

Optional (if performed)

7. Perfusion pattern
8. Late gadolinium enhancement pattern

Further Readings

1. Sparrow PJ, Kurian JB, Jones TR, Sivananthan MU. MR imaging of cardiac tumors. *Radiographics*. 2005;25:1255–1276.
2. Hoffmann U, Globits S, Frank H. Cardiac and paracardiac masses. *Eur Heart J*. 1998;19:553–563.
3. Chiles C, Woodard PK, Gutierrez FR, Link KM. Metastatic involvement of the heart and pericardium: CT and MR imaging. *Radiographics*. 2001;21:439–449.

Chapter 26

Valvular Heart Disease

Amedeo Chiribiri

CMR Protocol in Valvular Heart Disease

1. LV structure and function module (see Section 19.4)
2. Cine images specific to individual valves:
 - a. Aortic valve: LVOT views, coronal view, and in-plane view of valve (Section 19.2)
 - b. Mitral valve: LVOT view, VLA view, and in-plane view of valve (Section 19.2)
 - c. Pulmonary valve: RVOT views and in-plane view of valve (Section 19.2)
 - d. Tricuspid valve: RV long axis view and in-plane view of valve (Section 19.2)
3. Flow measurement perpendicular to the vessel and distal from the edge of valve leaflets (Section 19.6)

Optional

4. Contiguous stack of 5 mm cines aligned with the direction of inflow and transecting the principal line of coaptation to assess valve morphology.
5. Gradient echo/EPI rather than SSFP cine to visualize regurgitant jets

26.1 Introduction

Echocardiography still plays a pivotal role in the evaluation of valvular heart disease. CMR can be useful in case of inadequate echocardiographic examination, in particular for the assessment of valvular regurgitation. The CMR evaluation of valvular heart disease should always include the quantification of lesion severity (quantification of the regurgitation or stenosis), the measurement of the consequences of the valvular defect on the cardiac chambers (volume, mass, and function), and the assessment of valve morphology.

26.2 CMR Versus Other Imaging Modalities

Echocardiography is the principal imaging modality for the assessment of heart valve disease and it is not anticipated that CMR will challenge this role. However, CMR may be useful in specific clinical scenarios, for example when image quality by echocardiography is poor. CMR is also an excellent and more reproducible test for the measurement of chamber volumes and can accurately quantify regurgitant fractions, although the clinical relevance of such CMR-derived measurements remains to be established. In congenital heart disease, assessment of valvular morphology is a routine component of CMR protocols (Table 26.1 and Fig. 26.1).

Role of CMR in Valvular Heart Disease

- Provides accurate measurements of ventricular function and mass (Class I indication)
- Provides accurate measurements of regurgitant blood volume (Class I indication)
- Useful for valve morphology description, particularly to identify bicuspid aortic valve (Class II indication)

TABLE 26.1. Indications for CMR in patients with valvular heart disease.

Indication	Class
1. Valve morphology	
Bicuspid aortic valve	II
Other valves	III
Vegetations	Inv
2. Cardiac chamber anatomy and function	I
3. Quantification of regurgitation	I
4. Quantification of stenosis	III
5. Detection of paravalvular abscess	Inv
6. Assessment of prosthetic valves	Inv

From Clinical indications for CMR: Consensus Panel report. EHJ 2004;25:1940–1965

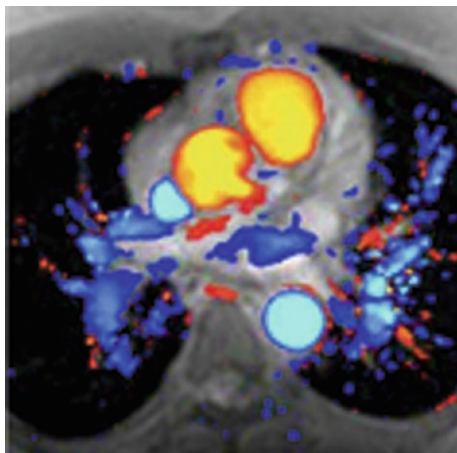


FIGURE 26.1. Phase-sensitive flow sequence with color-encoded reconstruction, showing a systolic frame acquired at the level of the pulmonary artery and of the ascending aorta. Blood flow pulling away from the reader is represented in *yellow-red*; blood flow crossing the image plane towards the reader is represented in *cyan-blue*.

Furthermore, in selected cases CMR can assess the presence of turbulence and the direction of jets, and can provide essential information on concomitant vascular abnormalities.

26.3 Congenital

Bicuspid aortic valve is a frequent congenital abnormality. Cine SSFP or cine turbo gradient echo sequences allow a direct visualization of the shape of the valvular orifice and of the number of cusps. The evaluation is usually possible also in severely calcified valves, using a flow sequence and evaluating the shape of the forward flow.

CMR also allows a complete evaluation of the abnormalities that are usually associated with a bicuspid aortic valve, such as aortic regurgitation and the dilatation of the ascending aorta, and is very useful to obtain repeated measurements during the follow-up of the patient (Fig. 26.2).

In patients with Ebstein anomaly, CMR provides a complete assessment of tricuspid valve displacement, valve morphologic abnormalities, volume and function of the residual RV, and presence and size of an associated interatrial defect.

CMR allows the visualization of the left ventricular outflow tract and a precise differential diagnosis between different types of subaortic stenosis. In patients with hypertrophic

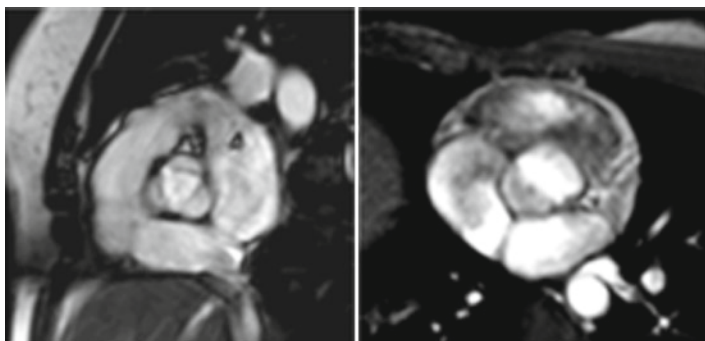


FIGURE 26.2. Tricuspid (*left*) and Bicuspid (*right*) aortic valve.

cardiomyopathy, an eventual systolic anterior movement of the anterior leaflet of the mitral valve (sometimes accompanied by a jet of mitral regurgitation) can confirm the diagnosis of obstruction of the left ventricular outflow tract. CMR is also a valuable tool to identify other causes of obstruction, such as a subvalvular fibrous ridge.

26.4 Regurgitation

CMR is the modality of choice for the evaluation of pulmonary valve regurgitation. Due to the through-plane motion of the pulmonary artery (PA) during the cardiac cycle, care must be taken to avoid the appearance of the right ventricle outflow tract (RVOT) or the right and left branches of the PA in the imaging plane (through-plane) of the flow sequence used to measure the regurgitant fraction. CMR also offers a complete evaluation of the size and function of the right ventricle (RV), of the RVOT, and of the PA.

Patients with known or suspected aortic regurgitation can be fully evaluated with CMR. Flow measurements at the level of the aortic valve allow a reliable measurement of regurgitant fraction. CMR can also provide an accurate measurement of left ventricular (LV) function and mass, and can diagnose associated abnormalities such as bicuspid aortic valve, dilatation of the ascending aorta, or aortic coarctation (Fig. 26.3).

Due to the movement of the atrioventricular valves during the cardiac cycle, a reliable evaluation of the transvalvular blood flow is precluded with bidimensional flow sequences. Mitral regurgitant volume can be indirectly quantified as the difference between LV stroke volume and aortic forward flow or as the difference between LV stroke volume and RV stroke volume in case of normal function of the tricuspid and pulmonary valves. Cine long-axis views (particularly with turbo gradient echo sequences) allow the visualization of the regurgitant jet in the atrial cavities.

New approaches using a moving slice for flow measurement were proposed but are not implemented for clinical use in the majority of the CMR scanners.

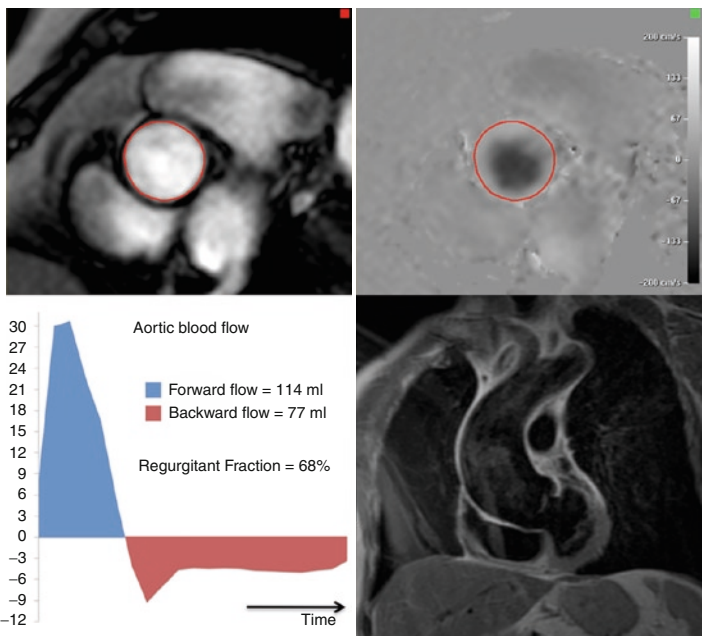


FIGURE 26.3. Aortic regurgitation. Modulus and phase images are reconstructed from a gradient-echo flow sequence (*top, left*, and *right* respectively). Post-processing of the data (*bottom left*) allows an accurate measurement of forward and backward flow across the valve.

In mitral or tricuspid regurgitation, a contiguous stack of thin (5 mm) cine images in the inflow direction and transecting the valve's coaptation line or a stack of cines oriented radially along the long axis of the LV or RV enables assessment of tethering, prolapse, or regurgitation through the different scallops of the valve leaflets (Fig. 26.4).

26.5 Stenosis

CMR can provide useful data for the evaluation of patients with aortic stenosis in whom good echocardiographic images are precluded due to an inadequate acoustic window.

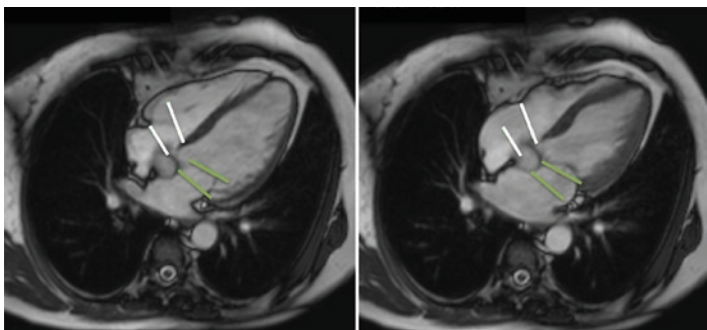


FIGURE 26.4. A 4-chamber view showing the end-diastolic (left) and the end-systolic frame (right). The atrioventricular valves have a marked movement throughout the cardiac cycle (tricuspid valve: white lines; mitral valve: green lines). For this reason the evaluation of transvalvular blood flow is not reliable using a bidimensional flow sequence.

Flow sequences can provide an estimation of the peak and medium pressure gradient across the valve, and a stack of cine sequences (gradient echo or high resolution balanced) provide a direct measurement of the aortic valvular area.

CMR represents a second-line investigation in patients with known mitral stenosis. It allows a precise determination of the atrial size, and of the number and location of the pulmonary veins in those patients undergoing ablation of atrial fibrillation.

As in mitral or tricuspid regurgitation, a contiguous stack of thin (5 mm) cine enables detailed assessment of the morphology of the valve substructures.

In aortic or pulmonary stenosis, CMR can be used to delineate valve morphology, such as fusion of leaflets, and to planimeter valve area. For this, a slightly overlapping stack of cines should be acquired that covers the valve in diastole and systole. Planimetry should be performed on the cross section that delineates the orifice or flow jet most clearly. Alternatively, aortic valve area can be measured by the continuity equation as (Velocity time integral LVOT/Velocity time integral aorta) × Area LVOT (Fig. 26.5).

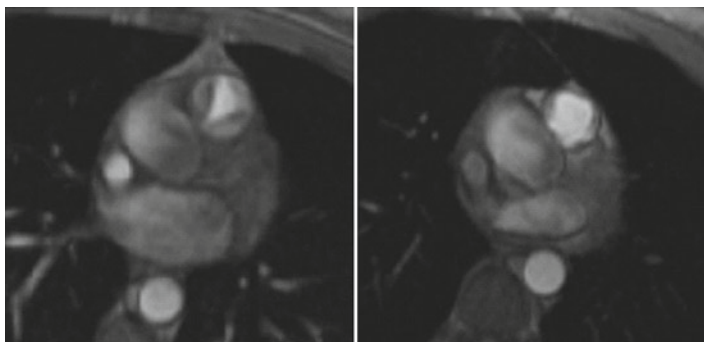


FIGURE 26.5. Pulmonary valve (PV) stenosis. Turbo-gradient echo cine images acquired in short axis at the level of the PV (end-systolic frame). In case of PV stenosis, the opening of the valve is usually incomplete. In this case the shape is triangular (*left*), different from the almost circular shape of a normal PV (*right*).

26.6 Prosthetic Valves

With the exception of the ball and cage Starr-Edwards prosthesis, implanted metallic heart valves are not a contraindication to CMR. Metal parts of the prosthesis create a local artifact that affects the interpretation of the image (Fig. 26.6).

26.7 Vegetations

CMR is less effective than echocardiography in the detection of mobile vegetations of the valvular leaflets. Nevertheless, infective endocarditis is not a contraindication in itself to the CMR examination.

26.8 Paravalvular Abscesses

Just a few cases are described in the literature of paravalvular abscesses identified with CMR. When a paravalvular abscess is suspected, echocardiography is the method of choice to

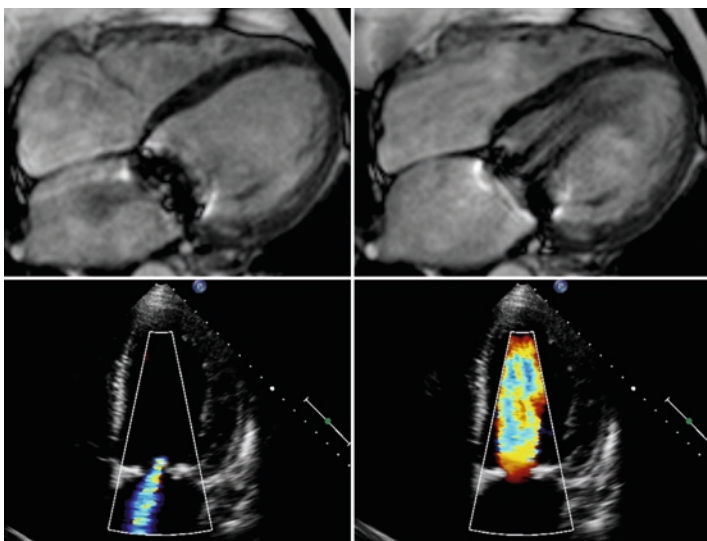


FIGURE 26.6. Example of a dysfunctioning bio-prosthetic valve in mitral position in a patient referred for dyspnea. CMR cine images identified the regurgitant jet in the left atrium (*left image*) and a turbulent diastolic flow towards the left ventricle (*right*). These findings were confirmed with color Doppler echocardiography. The diagnosis of the prosthetic dysfunction was made despite the artifact from the metallic components of the prosthesis.

confirm the diagnosis. In patients with prosthetic valves (particularly for mechanical valves), artifacts and signal loss due to the metallic valve components usually preclude the evaluation of the area surrounding the prosthesis.

Key Points CMR in Valvular Heart Disease

1. CMR is the method of choice for assessment of ventricular function.
2. Patients with prosthetic valves can safely undergo CMR at 1.5 and 3 T, except patients with the old ball and cage Starr-Edwards prosthesis.
3. Determine left and right ventricular stroke volume from cine stacks to measure single valve regurgitation.
4. Mitral regurgitation can be measured by subtracting aortic flow from LV stroke volume.
5. Multiple valve lesions can be assessed from comparison of the aortic and pulmonary diastolic regurgitant flow and the LV and RV stroke volumes.
6. Measure aortic valve area by direct planimetry or continuity equation.
7. Calculate peak mitral valve gradient from peak mitral valve flow.

Tips and Tricks

- During flow measurements, adapt velocity encoding to the actual velocity (the lowest value without aliasing) and use the shortest possible TE.
- The best value for velocity encoding can be estimated from previous echocardiographic evaluations where available or with an iterative approach, increasing the value at each acquisition until an image without aliasing is obtained.
- The software for flow measurement is usually available on the scanner. A quick evaluation of the results of flow sequences to exclude the aliasing artifact is advisable before discharging the patient.
- Arrhythmias can lead to the acquisition of low-quality images and obscure the diagnostic evaluation of the patient. If cardioversion is indicated and feasible, the CMR examination should be postponed unless the patient is in sinus rhythm.

CMR Report in Valvular Heart Disease

- LV and RV dimensions and volumes.
- Morphology of each component of the valve complex (e.g., leaflets, annulus, chordae).
- Presence of any insufficiency or reduced valvular excursion.
- Peak velocity (single value when recorded across semilunar valves or a vessel in cross-section, both early (E) and late (A) peak velocities for atrioventricular valves).
- Forward stroke volume and peak and mean transvalvular gradients.
- Regurgitant volume and fraction.
- Valve area (mention the method of determination).

Chapter 27

Ischemic Heart Disease

Adam Mather, Neil Maredia, and Sven Plein

27.1 Introduction

Cardiovascular magnetic resonance (CMR) offers a wide-ranging assessment of ischemic heart disease (IHD), including:

- Accurate measurement of global and regional myocardial contractile function.
- Detection of myocardial ischemia with either myocardial perfusion imaging during vasodilator stress (akin to nuclear scintigraphy) or wall motion assessment during inotropic stress (akin to stress echocardiography).
- Accurate delineation of the extent of myocardial infarction (MI) and residual viability with late gadolinium enhancement (LGE) to inform revascularization decisions.
- Assessment of contractile reserve during low-dose inotropic stimulation.
- In acute coronary syndromes, identification of myocardium at risk with T2-weighted imaging as well as delineation of infarcted myocardium and infarct characteristics such as microvascular obstruction (MVO) with LGE.
- Direct visualization of coronary anomalies and stenoses with coronary MR angiography.

CMR is thus a highly versatile imaging modality for the diagnosis and management of patients with known or suspected IHD. CMR offers several conceptual advantages over other

current imaging modalities. Compared with nuclear scintigraphy, specific advantages of CMR are its higher spatial resolution, lack of ionizing radiation, and more accurate assessment of left ventricular (LV) function and viability. Compared with echocardiography, image quality by CMR is more consistent and viability assessment by LGE is a unique feature. Compared with cardiac computed tomography (CT), CMR does not expose patients to ionizing radiation and it is more versatile, although coronary CT is superior to coronary CMR.

Although CMR remains less available and less used than nuclear perfusion imaging or stress echocardiography, in many centers it has become an invaluable addition to the available diagnostic tools for the assessment of IHD and in some centers CMR has replaced these tests as a first-line investigation for the detection of IHD. Importantly, the evidence base for using CMR in IHD has steadily increased and studies have demonstrated the prognostic relevance of a normal or abnormal CMR study.

27.2 Stress Myocardial Perfusion Imaging for the Detection of Myocardial Ischemia

CMR Protocol for Stress Perfusion CMR

1. Anatomy module (Section 19.3.1)
2. LV function module (Section 19.4)
3. Myocardial perfusion module “dummy” scan (Section 19.8.1)
4. Myocardial perfusion module during vasodilator stress (Section 19.8.1)
5. Myocardial perfusion module at rest (optional) (Section 19.8.1)
6. LGE module (Section 19.9.1)

27.2.1 Introduction

CMR first-pass myocardial perfusion imaging is used to analyze the flow of blood through the myocardial capillary bed (See Sect. 19.8). Because of autoregulation, which keeps resting myocardial blood flow constant until epicardial coronary stenoses becomes critical, it is necessary to acquire perfusion data during physiological or pharmacological stress in order to reveal myocardial ischemia. In the ischemic cascade, a perfusion defect is the first manifestation of ischemia, which subsequently leads to wall motion abnormalities, symptoms, and electrocardiogram (ECG) changes. In principle, perfusion assessment is therefore the most sensitive test for ischemia.

Practically, CMR perfusion imaging is usually performed during vasodilator stress, induced by adenosine or dipyridamole. It is important to emphasize that these agents do not usually induce ischemia, but induce maximal vasodilation and thus delineate myocardial perfusion reserve. A “perfusion defect” by first-pass perfusion CMR is therefore usually an area that has reduced perfusion reserve because of epicardial coronary stenosis or microvascular pathology. In specific pathophysiological states such as two-vessel coronary stenosis, myocardial ischemia may occur during vasodilator stress because of coronary steal, but this phenomenon is relatively rare.

CMR provides sufficiently high spatial resolution to delineate subendocardial perfusion, which is much more sensitive to ischemia than the subepicardial layer. The analysis of Myocardial perfusion CMR data in clinical practice is usually visual, by comparing contrast uptake patterns in different parts of the heart, but methods for objective quantitative measurement of myocardial blood flow are available.

27.2.2 Myocardial Perfusion CMR Versus Other Imaging Modalities

The most commonly used method for assessment of myocardial perfusion is nuclear scintigraphy with single photon

emission computed tomography (SPECT) or positron emission tomography (PET). Although based on similar principles, that is, the measurement of myocardial blood flow at rest and during stress, the acquisition and analysis of nuclear scintigraphy and Myocardial perfusion CMR imaging are different in many key areas.

Contrast agents: Contrast agents used for nuclear myocardial perfusion imaging are either potassium analogs that are taken up in perfused myocardium or labeled perfusion molecules such as water. CMR uses gadolinium-based and mostly extracellular contrast agents, which diffuse into the extracellular space.

Data acquisition: In SPECT, data are acquired some time after the administration of the tracer over several minutes. This makes the test susceptible to movement artifacts. In addition, attenuation of signal can lead to diagnostic errors. Myocardial perfusion CMR assesses the first myocardial passage of the contrast agent. This requires very rapid data acquisition with the associated technical challenges. It also means that unlike SPECT or PET, myocardial perfusion CMR does not usually cover the entire heart.

Spatial resolution: The acquired voxel size in SPECT is around 10 mm, in PET around 6 mm, and in CMR 3 mm or better. The higher spatial resolution of CMR may improve the detection of subendocardial ischemia and multi-vessel disease, when balanced ischemia can pose a diagnostic challenge in SPECT analysis.

Ionizing radiation: Both PET and SPECT expose patients to considerable doses of ionizing radiation, in the order of 10 mSv (with a wide variation depending on the isotope used, patient size, and other variables).

In particular, because of its higher spatial resolution and lack of ionizing radiation, CMR is widely regarded as the potentially superior test for myocardial perfusion assessment. However, SPECT and PET are much more mature imaging modalities and the evidence base for SPECT in particular is much larger than for CMR. To date, direct comparisons between the two modalities are sparse and mainly small single-center studies have been published, showing

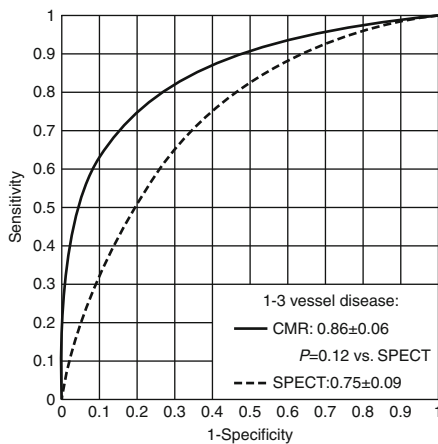


FIGURE 27.1. Comparison of diagnostic accuracy of myocardial perfusion CMR imaging with SPECT showed no significant difference in the area under the receiver-operating characteristic curve (Reproduced from¹⁵).

comparable diagnostic accuracies. Only one larger multi-center trial in 234 patients compared the performance of first-pass perfusion cardiac MR with SPECT and found that CMR was not inferior to SPECT for the detection of IHD (Fig. 27.1). Two larger studies are due to report soon (MR-IMPACT 2: over 500 patients and CEMARC: 750 patients). Until these larger studies have reported, it cannot be conclusively stated whether CMR may be a viable or superior alternative to SPECT or PET for assessment of myocardial perfusion.

Myocardial perfusion can also be assessed with contrast echocardiography, but to date there has been no comparison between CMR and echocardiography.

27.2.3 Diagnostic Performance

A 2007 meta-analysis of myocardial perfusion CMR showed an overall sensitivity of 91% and specificity of 81% for the

detection of coronary artery disease by CMR perfusion analysis, using x-ray coronary angiography as the reference standard.¹ (By comparison, a meta-analysis of nuclear SPECT in 2004 showed sensitivity rates in the region of 90% and specificity rates between 75% and 80%).² The results of larger comparative studies of SPECT and CMR perfusion imaging are awaited (Fig. 27.2).

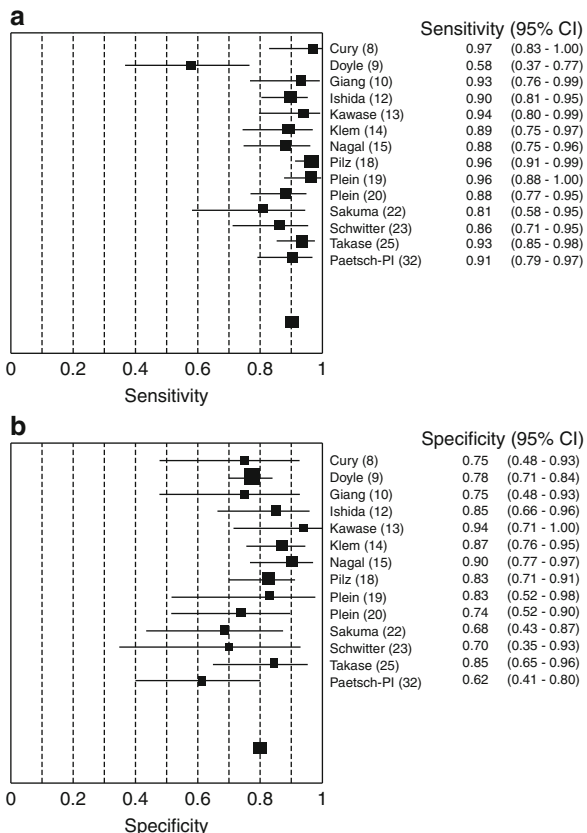


FIGURE 27.2. Meta-analysis of diagnostic performance of adenosine first-pass CMR perfusion imaging from 24 studies (1,516 patients). Perfusion imaging demonstrated a sensitivity (**a**) of 0.91 and specificity (**b**) of 0.81 (Reproduced from¹).

27.2.4 Prognostic Performance

Myocardial perfusion CMR imaging can be used to reliably determine a patient's prognostic risk over the subsequent 2 years. Following a normal CMR perfusion study, the cumulative event rate over the first 2 years has been shown to be 0.7%,³ which is similar to that following a normal SPECT study (Fig. 27.3).

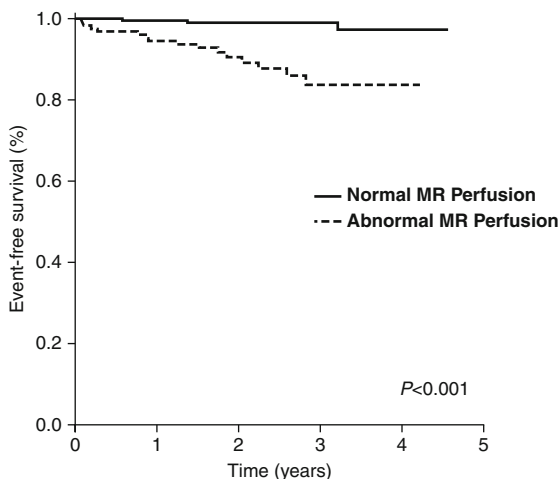


FIGURE 27.3. A normal MR perfusion study portends a low prognostic risk over a number of years (Reproduced from³).

The Role of Myocardial Perfusion CMR in IHD

1. Detect reduced myocardial perfusion reserve as a marker of ischemia.
2. Combine perfusion assessment with cine and viability assessment.
3. Indications:
 - a. Detect IHD in patients with intermediate risk
 - b. Second-line test if other investigations have been inconclusive
 - c. Identification of culprit lesions to guide revascularization

27.2.5 How to Perform a Myocardial Perfusion CMR Study

Important: Instruct patients in the invitation letter to refrain from caffeine (coffee, tea, caffeinated beverages or foods, e.g., chocolate, caffeinated medications), theophylline, and dipyridamole for 24 h prior to the examination. Caffeine is a competitive analog of adenosine and can thus reduce the response to vasodilator stress. Some centers also ask patients to refrain from smoking and beta-blockers prior to vasodilator stress testing.

1. Scout imaging to plan a true short axis (SA) view of the LV.
2. Plan perfusion imaging.

Before starting adenosine, run a “dummy” perfusion sequence (*without contrast*), assessing for:

- a. Presence of artifact. Move/increase field of view (FOV) if necessary.
 - b. Satisfactory vectorcardiogram (VCG) triggering. Change lead position if needed.
 - c. Patient compliance with breathing commands. We ask patients to hold their breath in end-expiration during the first pass of contrast, taking shallow breaths after that should they be unable to hold their breath for the entire scan duration.
3. Consider removing patient from magnet bore to improve monitoring. Commence intravenous (iv) infusion of stress agent (adenosine is administered at 140 mcg/kg/min), monitoring:
 - a. VCG for arrhythmia.
 - b. Patient for symptoms. Reassure as necessary.
 - c. Blood pressure. Check at 2 min into adenosine infusion.
 4. While the adenosine infusion continues, the perfusion scan is commenced. A power injector is used to deliver an iv bolus of contrast agent (typical infusion rate 3–7 mL/s) and a subsequent saline flush (typically 15–30 mL at the same rate). The patient is instructed to hold their breath in expiration from the moment contrast enters the right ventricle (RV). Imaging should continue for 40–50 cardiac cycles, to ensure that the entire first pass of contrast is observed. The dose of contrast to be delivered may be between 0.05 and 0.1 mmol/kg, according to local protocols.

5. Rest perfusion is performed a minimum of 15 min after the stress perfusion study, using identical slice geometry and scan settings as the stress perfusion sequence.

In most instances, the above protocol will be performed as part of a larger comprehensive IHD study as outlined in Fig. 27.4. The comprehensive protocol has superior overall accuracy than any of its individual components for the detection of IHD.⁴ Importantly, it was also shown that omission of (potentially time-consuming) coronary artery imaging did not reduce the diagnostic accuracy obtained by a combination of the remaining three components.

Vasodilator Stress Agents

Adenosine

- Most widely used agent for stress perfusion imaging
- Produces coronary artery vasodilatation – preferentially dilating non-stenosed vessels
- Very short half-life (<10 s)
- Adverse events easily reversed by cessation of infusion
- Can demonstrate perfusion abnormalities (reduced perfusion reserve) without inducing myocardial ischemia

Dipyridamole

- Longer half-life
- More frequently requires aminophylline administration in event of adverse effects
- Mechanism of action, side effects, and contraindications similar to adenosine

Vasodilator Agents in Development

- Selective A² adenosine receptor agonists (e.g., regadenoson, binodenosan)

- Similar vasodilatory action to adenosine but potentially lower side effect profile

Side effects

Severe side effects are extremely rare and adenosine is therefore a very suitable agent for pharmacological stress in the MR environment. Side effects include:

- Dyspnea
- Wheezing
- Chest heaviness
- Facial flushing
- Atrioventricular (AV) nodal block

Contraindications⁵

- Known hypersensitivity to adenosine
- Second- or third-degree AV nodal block
- Reversible airways disease
- Sinus bradycardia (heart rate (HR) < 45 bpm)
- Systemic arterial hypotension (<90 mmHg)

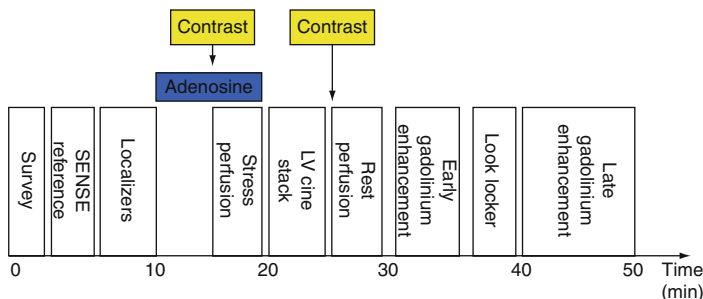


FIGURE 27.4. A comprehensive IHD protocol, which can be performed in less than 50 min in most patients. Depending on the dose of contrast used for stress and rest perfusion studies, an additional “top-up” of contrast may be delivered after rest perfusion imaging in order to achieve a total dose of 0.15–0.2 mmol/kg prior to LGE imaging.

27.2.6 Safety Considerations

The administration of any form of stress in the MR environment requires particular consideration for patient and staff safety. ECG monitoring is limited because of magneto-electrical effects. Therefore, ST segment changes that might occur during myocardial ischemia cannot be reliably detected. Heart rhythm monitoring is possible, but p-waves cannot be detected reliably, so lower-grade AV conduction block may not be recognized and higher-grade AV block is only evident because of changes in ventricular rate. It is therefore essential to monitor patients' symptoms very closely and respond to symptoms quickly. Furthermore, resuscitation within the magnetic field is limited and it is usually impractical for the hospital's resuscitation team to enter the magnet room. An efficient evacuation procedure to a safe and suitable resuscitation environment close to the magnet room has to be in place and must be regularly practiced. Finally, staff involved in stress testing must be trained in basic and advanced life support.

Safety Considerations

- A physician should always be present to supervise stress CMR studies
- A resuscitation protocol must be in place *and practiced regularly*
- Contraindications to specific stress agents should be identified and an appropriate agent chosen accordingly

Additional Equipment

- Sphygmomanometer for blood pressure monitoring
- IV infusion pump for administration of pharmacological stressor

If not MR-compatible, devices must be located outside the scan room and connected to the patient via waveguide tunnels through the wall.

- Heart rhythm monitoring (VCG)
- Resuscitation equipment
 - Defibrillator (to be kept *outside* the scan room)
 - Medications for cardiac arrest scenarios and management of arrhythmia
- Other medications
 - IV aminophylline for reversal of vasodilator (particularly if using dipyridamole)
 - Salbutamol inhaler
 - Beta-blocker (esmolol or metoprolol)
 - Glyceryl trinitrate (GTN) spray
- MR-compatible rapid infusion pump for delivery of contrast bolus (most general magnetic resonance imaging (MRI) units will already have one of these)

27.2.7 Analysis of CMR Perfusion Images

In clinical practice, myocardial perfusion CMR data are usually analyzed visually by scrolling through the series of dynamic images. Where there is a physiologically significant obstruction to myocardial blood flow, the entry of contrast agent will be impaired. This manifests as a darker area, “a perfusion defect,” in the poorly perfused myocardium.

A true perfusion defect has the following characteristics:

- Most prominent in the subendocardium
- Occurs in segments that anatomically correlate to a particular coronary artery distribution
- Persists for several RR intervals

As outlined in Chap. 20, endocardial dark rim artifacts can affect CMR perfusion images. Often comparison is made with rest perfusion images and, if available, also LGE images that delineate scar. By using the information from these data, artifacts can usually be identified⁶:

Stress	Rest	LGE	Diagnosis
Positive	Negative	Negative	Inducible ischemia
Positive	Positive	Positive	Infarction
Positive	Positive	Negative	Likely artifact

Perfusion should be assessed and recorded in accordance with the 17-segment American Heart Association (AHA) model.⁷ However, a three SA slice acquisition strategy will not provide views of segment 17 (true apex) and, therefore, only 16 segments may be reported in this instance. Perfusion defects should be graded according to transmurality. Stress perfusion images should be compared with LGE (+/- rest perfusion images – see earlier discussion) to identify inducible ischemia, infarction, artifacts, and normal areas of perfusion (Fig. 27.5).

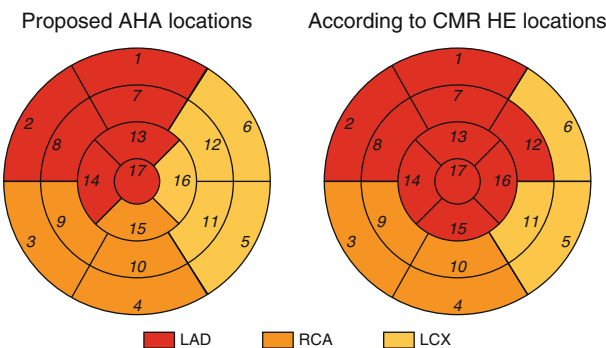


FIGURE 27.5. Distribution of coronary artery supply to the myocardium. The left bull's-eye plot represents the official segmentation proposed by the AHA in 2002.⁷ The right bull's-eye plot is derived from a recent CMR study analyzing the pattern of LGE in patients undergoing primary percutaneous intervention for AMI.¹⁶

Tips and Tricks

- IV cannulae should be inserted into both arms for stress perfusion. Adenosine should be administered through a cannula in the opposite arm to that used for contrast administration. This prevents the interruption of adenosine delivery by the inflation of the sphygmomanometer.
- Patient compliance may be improved by removing them from the magnet bore during the first phase of stress administration.

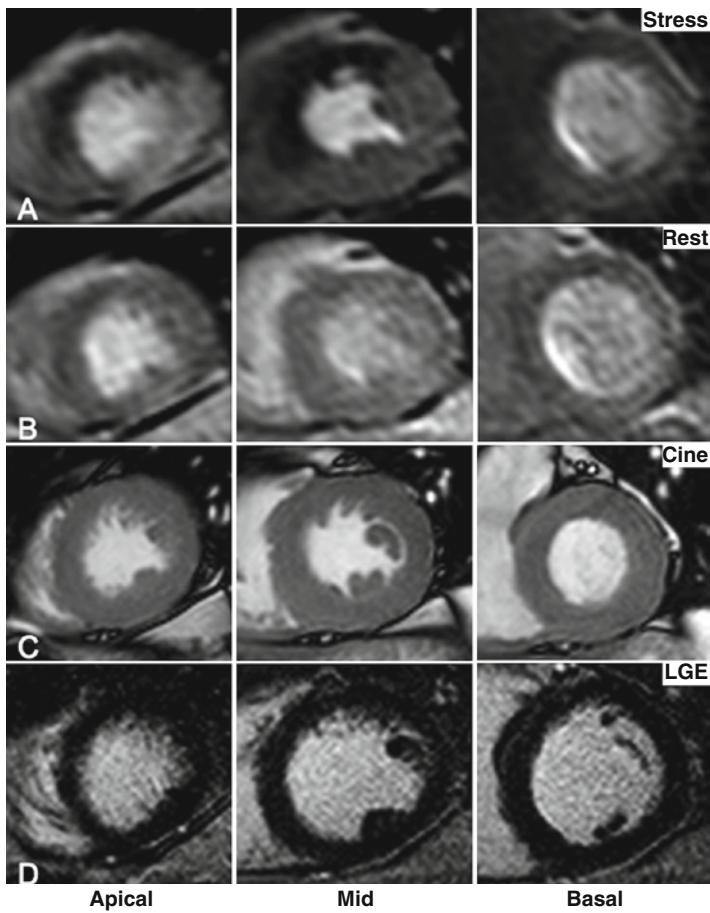
Key Points Myocardial Perfusion CMR in IHD

1. Higher spatial resolution than SPECT and PET
2. Similar diagnostic performance as SPECT and PET
3. Usually combined with cine and scar imaging
4. Safety in MR environment requires special consideration

27.2.8 Case Examples

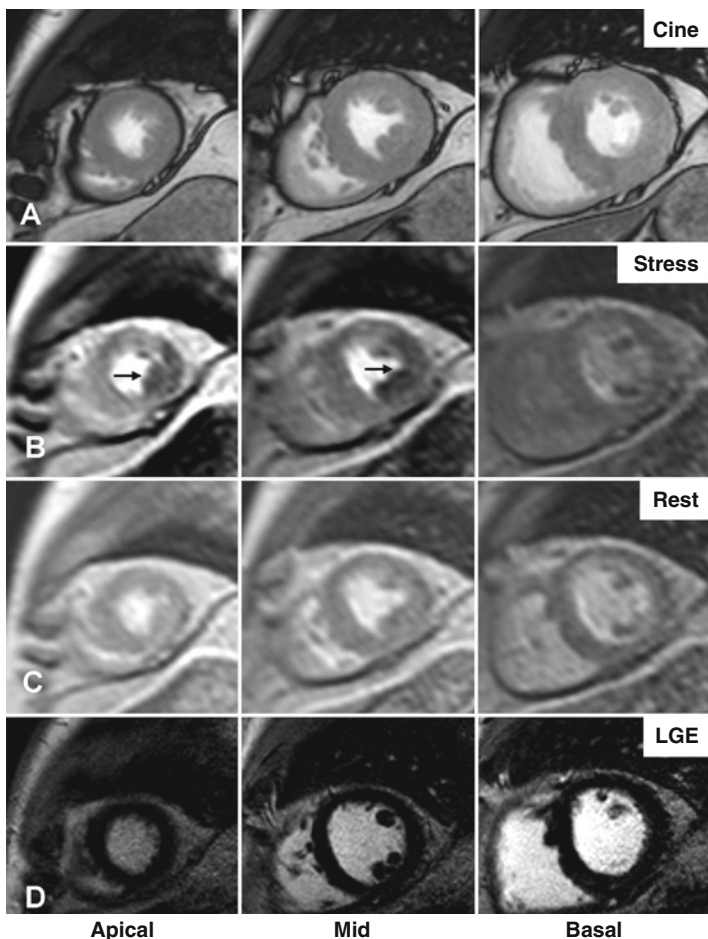
27.2.8.1 Case 1

A 49-year-old gentleman presented with angina. Three-slice adenosine stress perfusion revealed a transmural perfusion defect in the left anterior descending (LAD) artery territory (row A). No defect was seen at rest (row B). Left ventricular systolic function was normal (row C shows the end-systolic cine images). LGE imaging did not reveal any scar (row D). Coronary angiography subsequently demonstrated a severe proximal LAD stenosis.



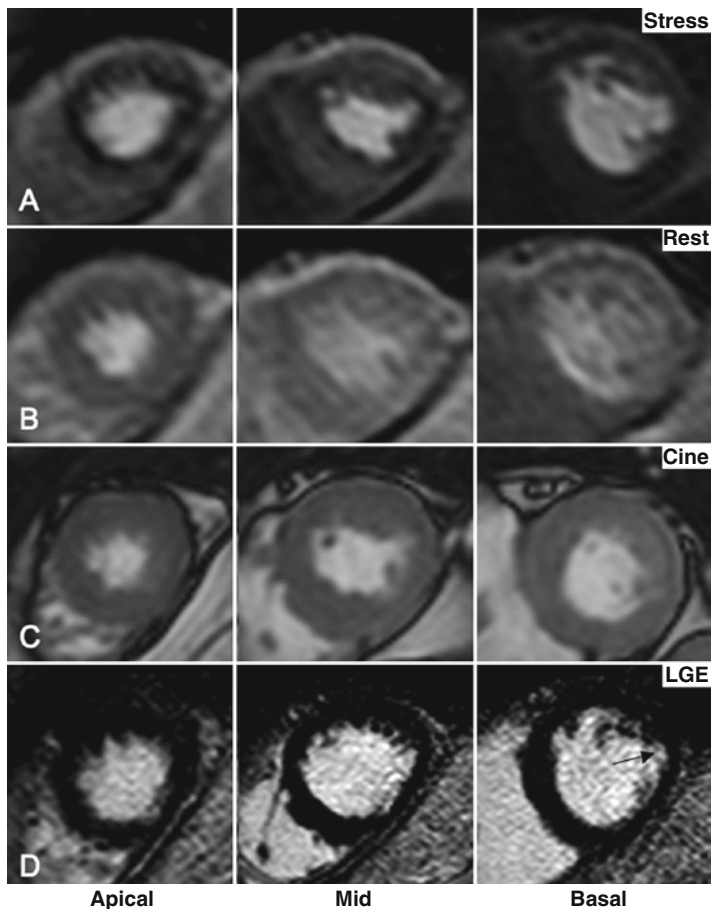
27.2.8.2 Case 2

A 62-year-old male presented with exertional angina. Cine imaging demonstrated normal left ventricular systolic function (row A). Adenosine stress perfusion highlighted a perfusion defect in the lateral wall (row B, see *arrows*). There were no perfusion defects at rest (row C). LGE did not demonstrate any scar (row D). Coronary angiography subsequently revealed a significant stenosis in the circumflex artery.



27.2.8.3 Case 3

A 67-year-old gentleman presented with angina. Perfusion defects were evident in all three coronary artery territories during adenosine stress but absent at rest (rows A and B). LV systolic function was normal (row C shows the end-systolic cine images). LGE imaging showed a small focal lateral subendocardial infarction (row D, *arrow*). Coronary angiography subsequently confirmed severe three-vessel coronary artery disease.



CMR Report for Myocardial Perfusion

- Report global and LV and RV volumes and function.
- Report regional wall motion abnormalities using the AHA segmentation.
- Describe distribution of scar and its transmural extent using the AHA segmentation.
- Describe inducible perfusion abnormalities using the AHA segmentation. Note transmurality of perfusion defect.
- Correlate ischemia and scar.
- If indicated, give an overall assessment of suitability for revascularization based on presence of ischemia in viable myocardium.
- Comment on presence and location of any artifacts.

27.3 CMR Stress Wall Motion Imaging for the Detection of IHD

Dobutamine Stress CMR Protocol

1. Anatomy module (Section 19.3.1)
2. LV function module (Section 19.4)
3. Rest cine images in at least three SA slices and two to three long axis (LA) views (Section 19.2)
4. Start dobutamine and increase at 3-min intervals in increments of 10 mcg/kg/min until target HR [$85\% \times (220 - \text{age})$] is reached
5. Consider adding Atropine to increase HR response
6. Repeat cine images at each stress level
7. Check blood pressure at each stage of the protocol, and monitor ECG throughout
8. View cine loops online as they are being acquired
9. Stop test for new wall motion abnormality, serious side effect, or achievement of peak HR

27.3.1 *Introduction*

The echocardiographic assessment of LV wall motion during stress is now a well-established method of detecting myocardial ischemia. By applying similar techniques using CMR imaging, it is possible to achieve a comparable level of diagnostic accuracy for the detection of IHD.

27.3.2 *CMR Versus Other Imaging Modalities*

Dobutamine stress echocardiography (DSE) and dobutamine stress CMR (DSCMR) are based on the same principle of detecting ischemia through inducible wall motion abnormalities. However, several notable differences between the two tests need to be considered:

Key differences between DSCMR and DSE	
Favoring CMR	Favoring Echo
Higher spatial resolution	Real-time imaging may allow earlier identification of ischemia
Excellent slice reproducibility	ECG ST segment monitoring is possible (not possible using the VCG in CMR)
No reliance on a good “acoustic window” and more reproducible image quality	Bed-side testing permits better interaction with patient and swifter management of complications

A direct comparison of DSE and DSCMR was performed by Nagel et al. in 1999, showing higher sensitivity and specificity for the CMR technique than its echo equivalent. In a subanalysis, the differences in diagnostic accuracy occurred in particular in those studies where image quality by echocardiography was suboptimal. However, it should be noted that many of the DSE studies used in these comparisons did not make use of echocardiographic contrast, which is known to improve the reliability of DSE through improved definition of the endocardial border.

27.3.3 Diagnostic Performance

DSCMR has proven to be an effective method of diagnosing myocardial ischemia. In a 2007 meta-analysis, studies using dobutamine or exercise as the stressor were found to have a sensitivity of 0.85 and specificity of 0.86 for the detection of IHD.¹ By comparison, a pooled analysis of 102 DSE studies found a weighted mean sensitivity of 0.81 and specificity of 0.84.⁸

27.3.4 Prognostic Performance

DSCMR has been shown to have a similar ability to stratify prognostic risk as DSE. The cumulative event rate at 2 years following a normal DSCMR study was 2.6%,³ which is similar

to the 1–3% annual event rate following a normal DSE study (Fig. 27.6).

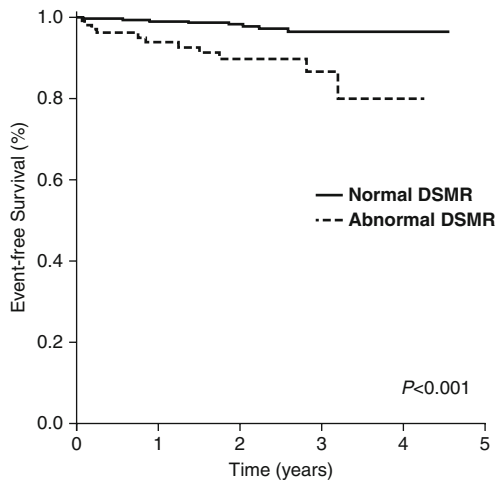


FIGURE 27.6. A normal DSCMR study also portends a low prognostic risk over several years (Reproduced from³).

The Role of Dobutamine Stress CMR

1. Detect myocardial ischemia by inducing wall motion abnormalities.
2. Combine with low-dose dobutamine stress to assess contractile reserve.
3. Indications:
 - a. When perfusion CMR is contraindicated
 - b. Detect IHD in patients with intermediate risk
 - c. Second-line test if other investigations have been inconclusive
4. Identification of culprit lesions to guide revascularization

27.3.5 *Method*

1. Resting LV function is assessed using a full LV cine stack.
2. Three SA slices through the LV are planned using the three of five technique described previously.
3. A horizontal long axis (HLA), a vertical long axis (VLA), and three SA cine slices are acquired at rest and at each increment of the dobutamine stress protocol. A 3-chamber view may be added.
4. IV dobutamine is commenced at 5 or 10 mcg/kg/min. The dobutamine dose is increased every 3 min in increments of 10 mcg/kg/min up to a maximum of 40 mcg/kg/min. Blood pressure should be measured at each stage of the protocol, and continuous VCG monitoring should occur throughout.
5. Uptitration ceases when 85% of the patient's maximum predicted HR is achieved (200 minus age for women, 220 minus age for men). If this is not achieved at a dobutamine dose of 40 mcg/kg/min, IV atropine may be administered in increments of 0.25 mg up to a maximum dose of 2 mg.⁵
6. Reasons for stopping the study prematurely include:
 - New regional wall motion abnormality (view cine loops online as they are being acquired)
 - Arrhythmia
 - Other serious side effects/patient request

27.3.6 *Safety Considerations*

The administration of IV dobutamine is associated with a small but definite risk of inducing ventricular arrhythmias (ventricular tachycardia and ventricular fibrillation) and MI. Arrhythmias occur in approximately 3–4/1,000 cases. Even more than for vasodilator stress myocardial perfusion CMR, careful consideration needs to be given to patient safety prior to commencing a dobutamine stress service. As outlined earlier, these include in particular patient evacuation from the magnet room in case of a complication occurring and the rapid and safe transfer to an appropriate resuscitation environment.

Because ECG monitoring is limited in the magnet room, ischemia detection should be based on immediate review of acquired cine loops at every stress level. The test should be terminated as soon as an inducible wall motion abnormality is identified or other end points reached (as outlined above).

Dobutamine

- β_1 agonist. Beta-blockers should be omitted for 24 h before the test.
- Less preferable for perfusion imaging due to its positive chronotropic effect.
- High HRs may require compromises in slice coverage or image resolution.

Side effects

- Nausea
- Palpitations
- Dyspnea
- Dizziness

Contraindications⁵

- Severe systemic arterial hypertension ($\geq 220/120$ mmHg)
- Unstable angina pectoris
- Significant aortic stenosis (peak valve gradient > 50 mmHg or aortic valve area $< 1 \text{ cm}^2$)
- Complex cardiac arrhythmias including atrial fibrillation
- Hypertrophic obstructive cardiomyopathy
- Myocarditis, endocarditis, pericarditis
- Uncontrolled congestive heart failure

Atropine

Administered when target HR not achieved with maximum dose of dobutamine (see P410)

*Contraindications*⁵

- Narrow-angle glaucoma
- Myasthenia gravis
- Obstructive uropathy
- Obstructive gastrointestinal disorders

27.3.7 Analysis

For each imaging orientation (HLA, VLA, and SA), cine images from each dobutamine increment should be viewed side by side, allowing the effect of stress to be determined. Wall motion may be assessed qualitatively according to the AHA 17 segment model as follows:

1. Normal or hyperkinetic
2. Hypokinetic
3. Akinetic
4. Dyskinetic

A wall motion score index may be calculated by dividing the sum of the wall motion scores by the number of segments assessed. Quantitative assessment of the percentage of wall thickening or strain may also be performed. It should be noted if global LV function does not improve or worsens during stress.

Four typical patterns of wall motion are seen with dobutamine stress:

1. Normal – normal resting myocardial contraction, becoming more vigorous as dobutamine dose increases.
2. Reversible ischemia – contractile function deteriorates as stress increases.
3. Biphasic response – an initial improvement in contractile function is seen with low-dose dobutamine (up to 10 mcg/kg/min) but further increases in stressor dose

lead to a deterioration in contractile function. This response is typical of ischemic “hibernating” myocardium.

4. No response – poorly contracting myocardium at rest, which fails to show any improvement with dobutamine. This is characteristic of non-viable myocardium.

The report should conclude with a summary of myocardial viability and any inducible wall motion abnormalities identified.

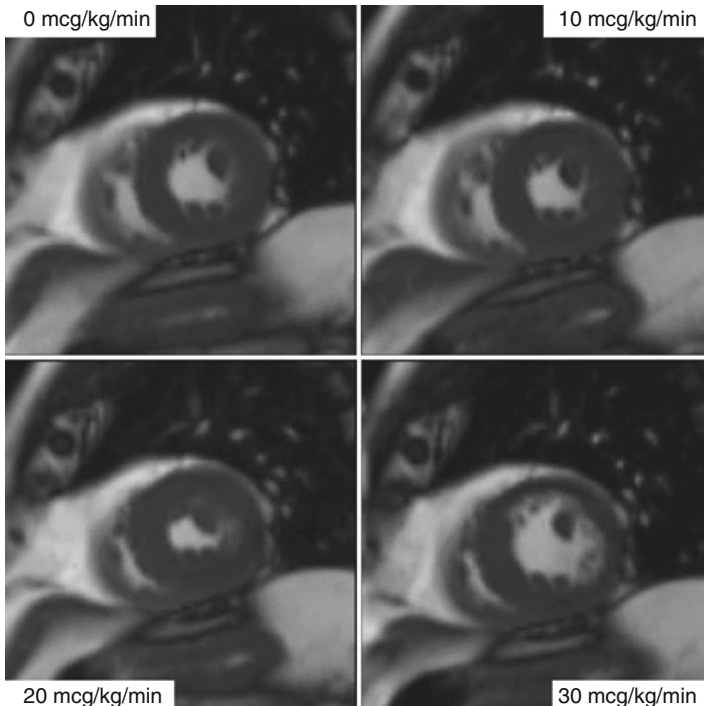
Tips and Tricks

- Dobutamine stress images must be analyzed as they are acquired so that dobutamine may be stopped promptly in the event of a new regional wall motion abnormality as needed as the heart rate increases.
- Adapt the steady-state free precession (SSFP) cine sequence to optimize temporal resolution as needed as the heart rate increases.

27.3.8 Case Example

27.3.8.1 Case 4

End-systolic SA cine images from a DSCMR study. Inducible ischemia was identified by the development of new wall motion abnormalities in the anterior and inferolateral walls at 30 mcg/kg/min of dobutamine. The study was terminated at this point (Images courtesy of Charles Peebles, Southampton).



Dobutamine Stress CMR Report

1. Comment on global LV and RV volumes and function.
2. Comment on resting regional wall motion abnormalities using the AHA segmentation.
3. Comment on improvement of regional wall motion during low-dose stress.
4. Comment on inducible regional wall motion abnormalities using the AHA segmentation.
5. Summarise resting function, contractile reserve, and ischaemia for coronary territories.
6. Provide wall motion index.
7. Comment if global LV function fails to improve during stress.
8. Comment if valvular regurgitation occurs or worsens during stress.

27.3.9 Which Stress Modality Should I Choose?

For most patients, either vasodilator or inotropic stress will be applicable, with a similar level of confidence in the result. The decision as to which to choose often comes down to local preference. However, there are certain situations in which one modality may be preferred:

- Absolute contraindications to a specific stressor agent
- Chronic renal impairment of sufficient severity to preclude the use of contrast agent (see section on NSF). In this situation, DSCMR clearly represents the best option

27.4 CMR for Assessment of Viability

CMR Protocol for Viability Assessment

1. Anatomy module (Section 19.3.1)
2. LV function module at rest (Section 19.4)
3. LGE module (Section 19.9.1)
4. Consider low-dose dobutamine cine imaging in particular if LGE shows 25–75% transmural infarction

27.4.1 *Introduction*

The delineation of myocardial scar and viability in patients with IHD is of great clinical relevance. Contractile abnormalities in IHD can be caused by stunning (if it recovers function spontaneously), hibernation (if it recovers after revascularization), or scar. Myocardial stunning is commonly seen in patients with early reperfusion after coronary artery occlusion. Patients with hibernating myocardium often present with either multi-vessel coronary artery disease and global LV dysfunction or a history of previous MI and infarct scar with associated regional wall motion abnormality. Several studies have shown that revascularization of hibernating myocardium improves clinical outcomes. CMR with LGE has become the gold standard imaging modality for the delineation of MI. CMR can accurately determine the presence, location, and extent of infarcted tissue and assess the likelihood of functional recovery. It is therefore extremely useful in planning coronary arterial revascularization. It is also an important tool in the identification of complications of MI.

27.4.2 *CMR Versus Other Imaging Modalities*

The detection of MI by LGE-CMR has been compared with PET and SPECT. In both comparisons, CMR detected more MI more frequently than nuclear imaging, in particular if the

infarcts were small or limited to the subendocardium. The reason for the higher sensitivity of CMR to detect MI is likely to be its much higher spatial resolution and the direct anatomical correlation. Echocardiography can provide information on myocardial viability through measurements of myocardial thickness, contractile function, and contractile reserve. More recently, contrast echocardiography has also been used to assess viability. There have, however, been no comparisons between echocardiography and CMR.

27.4.3 CMR Methods for Viability Assessment

Cine imaging: MI is first suspected by the observation of myocardial thinning with associated akinesia, as seen on initial cine images. Myocardium that is less than 4 mm thick is unlikely to be viable.

Contractile reserve: Viable myocardium should demonstrate improved contractility in response to a suitable inotropic stimulus. The most widely used method of stimulation is the IV infusion of low-dose dobutamine, up to 10 mcg/kg/min. Dobutamine is a β_1 -receptor agonist and, therefore, patients should avoid beta-blockers for 24 h prior to the CMR scan. Regular blood pressure measurements should also be taken. Side effects of dobutamine include nausea, dizziness, dyspnea, chest pain, and palpitations. Cine imaging in the standard planes should be performed in order to assess wall thickness and contractility with stress.

Late gadolinium enhancement: As outlined in Chap. 3, most gadolinium-based contrast agents in current use are extracellular and extravascular agents that diffuse freely into the interstitial space. Their distribution volume is therefore increased in both acute myocardial infarction (AMI) where cell barriers are destroyed and chronic infarction where myocardial cells are replaced with a fibrotic matrix. In viable myocardium, on the other hand, extracellular space is small and the volume of distribution of gadolinium lower. Several minutes after contrast administration a steady state evolves with larger contrast concentrations in infarcted tissue, which

can be imaged with an appropriate T1-sensitive imaging method – the technique called LGE. LGE due to MI occurs in the perfusion territory of the occluded artery. Occlusion of a coronary artery initiates a process of myocyte necrosis which spreads from the subendocardium to the epicardial borders. Therefore, LGE always extends from the endocardium outwards with infarction (Fig. 27.7). Complete sparing of the endocardial border suggests that the cause of LGE is not infarction.

LGE also occurs in areas of fibrosis and, therefore, the sequence can be used to identify pathologies such as infiltrative cardiomyopathy and myocarditis. If the presence of LGE appears unusual, images should be re-acquired after changing the phase encode direction of the slice (*phase swapping*) in

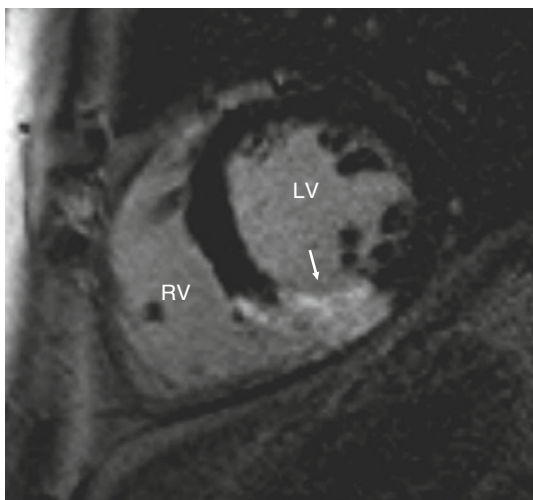


FIGURE 27.7. A 65-year-old male presented with an acute inferior ST-elevation MI. LGE images clearly demonstrated inferior LV infarction with transmural hyperenhancement (white arrow) spreading from the endocardial to the epicardial border.

order to exclude artifacts. If the LGE remains in the same position, then one can assume the abnormality to be genuine.

Functional improvement of stunned myocardium can be predicted by LGE. The likelihood of improvement and complete recovery decreases with increasing transmurality of LGE (Fig. 27.8). As can be seen in the figure, functional recovery is variable in infarction between 25% and 75% transmurality. In such instances, additional low-dose dobutamine imaging may add prognostic information.

LGE can also identify hibernating myocardium prior to revascularization. The likelihood of improvement in contractility after revascularization also reduces with increasing transmural extent of LGE. Dysfunctional myocardium which demonstrates <50% transmural extent of LGE has a high likelihood of functional recovery (Fig. 27.9).

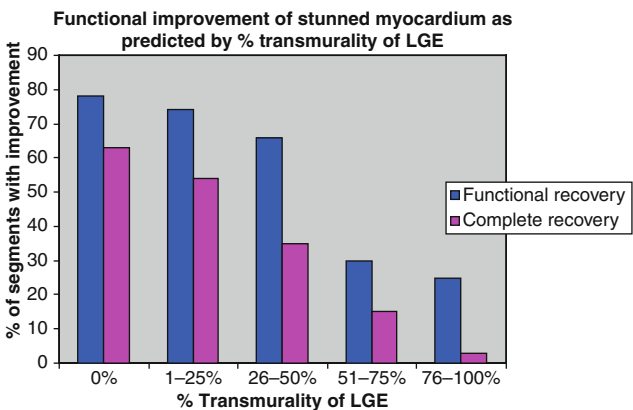


FIGURE 27.8. Graph demonstrating percentage of dysfunctional segments with functional improvement and complete recovery after MI according to transmularity of LGE.¹⁷

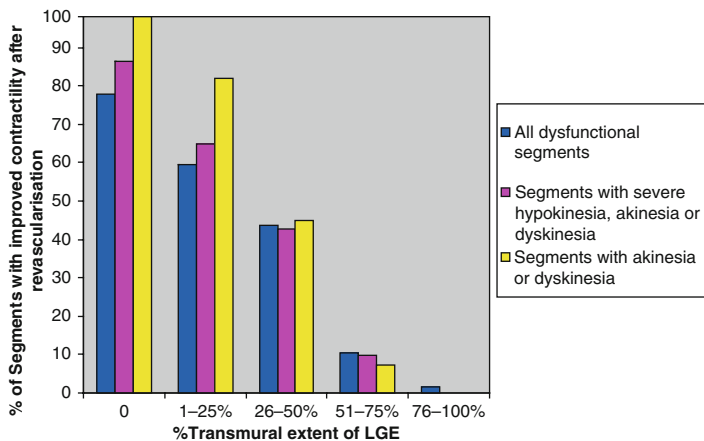


FIGURE 27.9. Graph demonstrating the relationship between the transmural extent of LGE before revascularization and the likelihood of increased contractility after revascularization.¹⁸

The Role of CMR for Viability Assessment

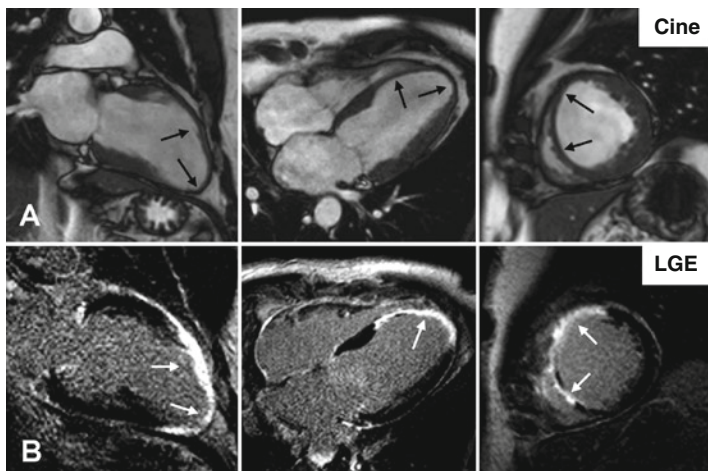
1. Assess global and regional contractile function.
2. Delineate MI and its transmural extent.
3. Determine contractile reserve.
4. Guide revascularization decisions either based on LGE infarct extent or contractile reserve.

27.4.4 Case Examples

27.4.4.1 Case 5

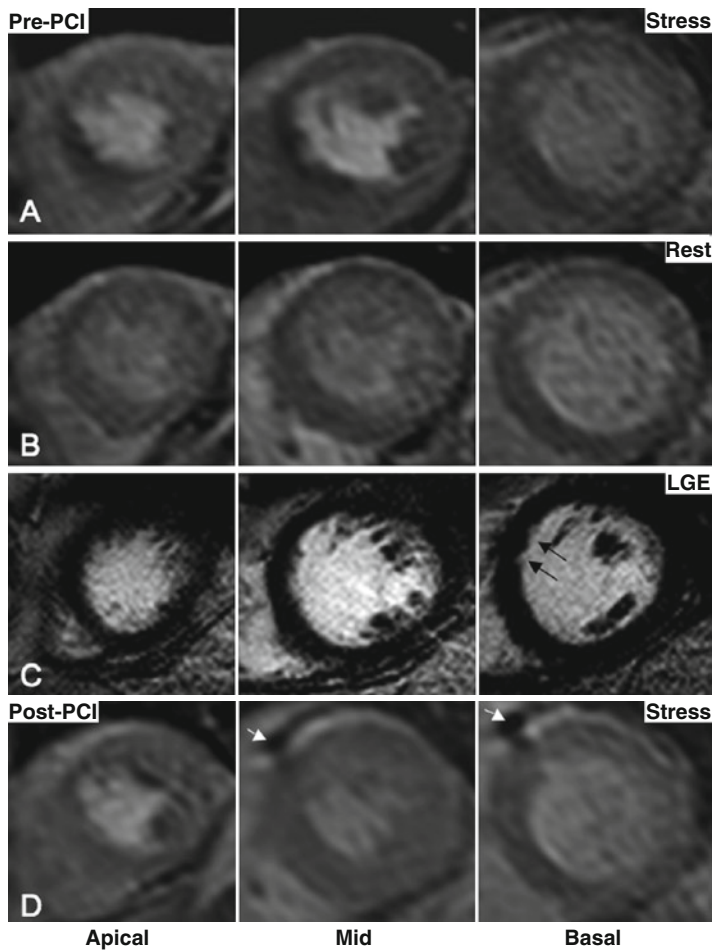
A 54-year-old male presented with breathlessness after suffering an anterior MI. CMR was requested to look for viable myocardium. Cine imaging demonstrated thinned and akinetic myocardium in the anterior wall and apex (row A, see

arrows). LGE showed transmural scar in the anterior wall and apex (row B, see arrows). It was, therefore, concluded that the anterior wall was nonviable.



27.4.4.2 Case 6

A 73-year-old male underwent CMR to look for reversible ischemia and viable myocardium. A reversible perfusion defect was noted in the apical and mid septum (rows A and B). LGE imaging demonstrated minimal scar in the basal septum (row C, arrows). Six months following percutaenous coronary intervention (PCI) to an occluded left anterior descending artery. A repeat CMR scan revealed no defect (row D). Note the prominent artifact arising from the LAD stent (white arrows).



CMR Report for Viability

1. Acquire quantitative measurements of LV volumes and function.
2. Describe regional wall motion abnormality according to the 17-segment model as proposed by the AHA.
3. Describe presence and pattern of LGE according to the 17-segment model. Use >2 SD above the average of normal myocardium as cut-off for infarction. Describe LGE pattern as subepicardial, intramural, subendocardial, or transmural.
4. Provide transmural extent of the LGE as 0%, $\leq 25\%$, 26% to $\leq 50\%$, 51% to $\leq 75\%$, and 76–100%.
5. Report total amount of infarcted tissue (g or % of LV).
6. If available, comment on contractile reserve.

27.5 CMR in Acute Coronary Syndromes

27.5.1 *Introduction*

CMR has the unique ability to characterize a range of pathophysiological effects of AMI. Multi-parametric CMR assessment with cine imaging, T2-weighted imaging, early gadolinium-enhanced (EGE) and LGE acquisition delineates contractile function, myocardial edema, MVO, intracardiac thrombus, and myocardial scar. Many of these parameters have prognostic significance, for example, LV ejection fraction, extent of scar, and presence of MVO. Therefore, CMR can contribute to the risk stratification of patients with AMI and may play an important future role in assessing the efficacy of treatment strategies.

CMR Protocol for Acute Myocardial Infarction

1. Anatomy module (Section 19.3.1)
2. LV function module (Section 19.4)
3. Edema module (Section 19.3.2)
4. EGE/LGE module (Section 19.9.1)

27.5.2 *CMR Versus Other Imaging Modalities*

CMR is the most versatile imaging modality for assessment of AMI. Its main drawback is that CMR scanners are usually remote from cardiology wards and unstable patients will not be suitable for CMR assessment. The role of echocardiography for bedside assessment of AMI is therefore unchallenged by the emergence of CMR. However, stable patients with recent acute coronary syndromes can be safely scanned in a suitable CMR environment and important additional information can be obtained that is not available from other imaging modalities. Although no direct comparisons have been

published in the context of acute infarction or other acute coronary syndromes, CMR is likely to be the most valuable second-line test in their assessment, offering much more information than nuclear imaging studies.

27.5.3 *Methods*

27.5.3.1 Cine and LGE-CMR

The extent of MI is a reliable predictor of clinical outcome and patients with large infarcts and poor contractile function are at substantially higher risk of malignant arrhythmia and heart failure than patients with limited infarction and preserved LV function. CMR is the most accurate test currently available for the measurement of LV function and infarct size, both in the acute, necrotic phase and in the late fibrotic stages of infarction. CMR has therefore become the method of choice in clinical trials assessing the efficacy of therapies in AMI and it is also a very useful test for clinical risk stratification.

27.5.3.2 Edema Imaging for Area at Risk Assessment

Prolonged ischemia triggers an inflammatory response which results in tissue edema. Hence, edema is one of the key features of viable myocardium at risk. T2-weighted CMR sequences are very sensitive to water-bound protons and, therefore, can delineate tissue edema as regions of high signal intensity. T2-weighted CMR has been shown to successfully visualize infarct-related edema (Figure 6) and recent data indicate its clinical applicability for differentiating acute from chronic infarction.⁹ This CMR sequence can also help to diagnose acute myocardial ischemia in the emergency setting.¹⁰ Acute inflammatory conditions such as acute myocarditis may also produce high signal intensity on T2-weighted imaging. However, the distribution of the edema may not be consistent with a coronary artery territory as in the case of acute myocardial ischemia.

27.5.3.3 Myocardial Salvage

The difference between the actual infarct size on LGE and area at risk, or potential infarct size, on T2-weighted CMR is a measure of myocardial salvage. This measure is important because it can be used to determine strategies to optimize management of AMI. Myocardial salvage can be measured by SPECT performed during and after coronary occlusion, but using CMR several days after the index event provides similar estimates of salvage. CMR may therefore become the method of choice for measurements of myocardial salvage.

27.5.3.4 Microvascular Obstruction

MVO occurs early after AMI and represents the angiographic appearance of “no-reflow.” The presence of MVO predicts cardiovascular complications in the first 2 years after AMI and is associated with a significant reduction in event-free survival.¹¹

CMR can be used to look for MVO with EGE. EGE uses the same sequence as LGE but images are acquired in the first 1–5 min after administration of the contrast agent. A fixed inversion time (TI) is usually set to ensure that the myocardium is bright. We recommend a TI of 400–500 ms. MVO appears as black areas within the infarct territory. MVO will be evident on LGE images as black areas within the bright white region of infarcted tissue.

MVO can also be detected on first-pass perfusion imaging. The volume of MVO measured by these three methods may differ because contrast agent diffusion into the MVO reduces its apparent extent over time following contrast injection. Theoretically, first-pass perfusion CMR should be the most accurate method to measure MVO, but this technique has been limited by lower spatial resolution than EGE and LGE as well as incomplete cardiac coverage. A recent study compared these three techniques and concluded that MVO

detected by LGE is the best prognostic marker of LV remodeling and that the contrast-to-noise ratio between the infarct and MVO areas is highest with LGE imaging.¹²

27.5.3.5 Complications of AMI

Ventricular thrombus is a well-recognized complication of AMI. Thrombus tends to occur at the site of scarred myocardium as detected by LGE and often the myocardium in this area appears dyskinetic or aneurysmal on cine imaging. Thrombus is best visualized with EGE images. The blood pool will have high signal intensity due to the contrast agent but the thrombus will demonstrate low signal intensity and will appear as a dark mass in the bright ventricular cavity (Figure 9). Perfusion imaging sequences can also be performed if there is any doubt about the ventricular mass. Thrombus will not take up contrast on perfusion imaging unlike a tumor, which will have a vascular supply. Post-infarction ventricular septal defects (VSDs) can be assessed by cine imaging (Figure 10), which will demonstrate the anatomy of the defect as well as highlight signal loss in the RV due to flow of blood through the VSD. The ventricular SA cine stack can be used to measure the difference in stroke volumes between the LV and RV. This information can then be used to assess the shunt ratio. Shunt ratio can also be calculated from the comparison of Q flow measurements of the pulmonary and systemic circulations.

Tips and Tricks

- T2-weighted images must be acquired before the administration of any contrast agents.
- Thrombus and MVO are best seen on early gadolinium-enhanced images (within 2 min of contrast application) with a fixed TI of 400–500 ms.

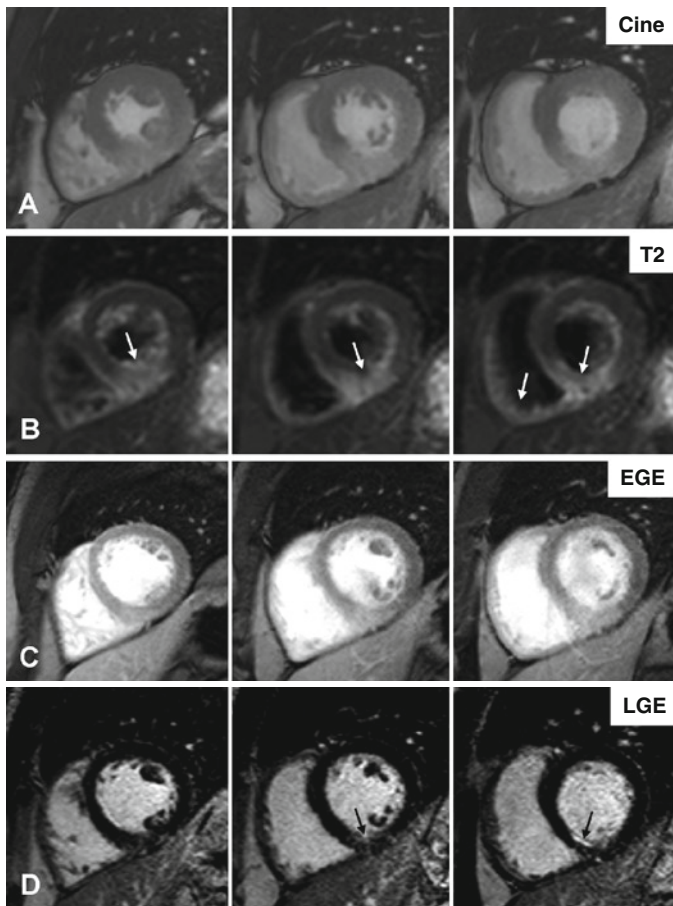
The Role of CMR in ACS

1. Assess global and regional contractile function.
2. Delineate area at risk and myocardial salvage.
3. Provide risk stratification based on assessment of infarct size, LV function, and presence of MVO.
4. Further assess complications of MI such as thrombus or VSD.

27.5.4 Case Examples

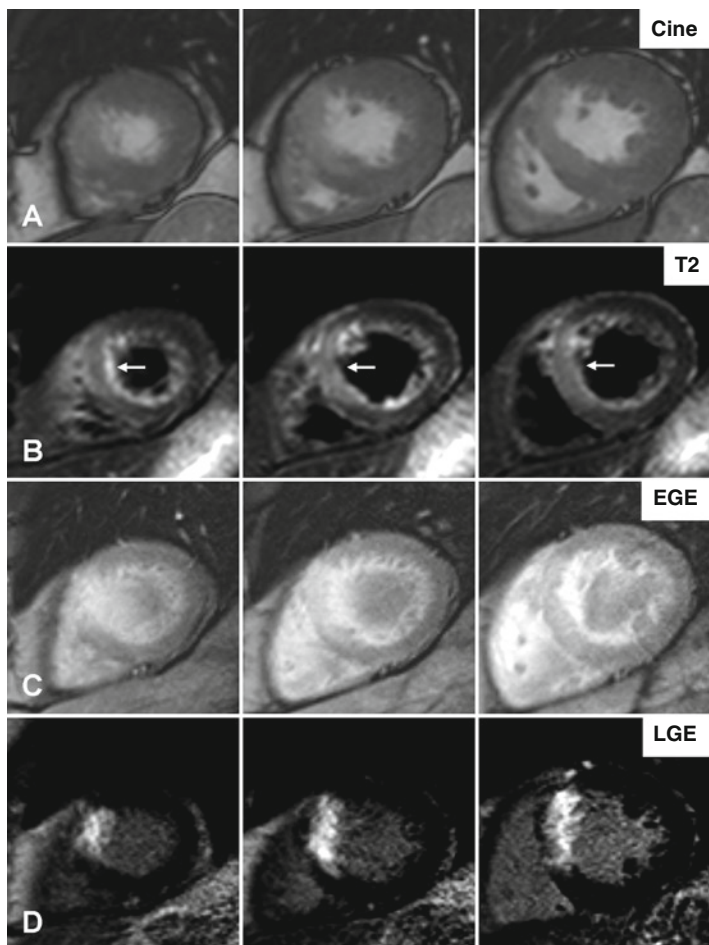
27.5.4.1 Case 7

A 39-year-old male presented with an acute inferior MI successfully treated with primary PCI. Cine imaging demonstrated mild hypokinesia in the inferior wall (row A). T2-weighted imaging highlighted myocardial edema in the inferior walls of both LV and RV (row B, see *arrows*). EGE did not demonstrate any MVO (row C). LGE showed only minimal scar in the inferior wall of the LV (row D, see *arrows*).



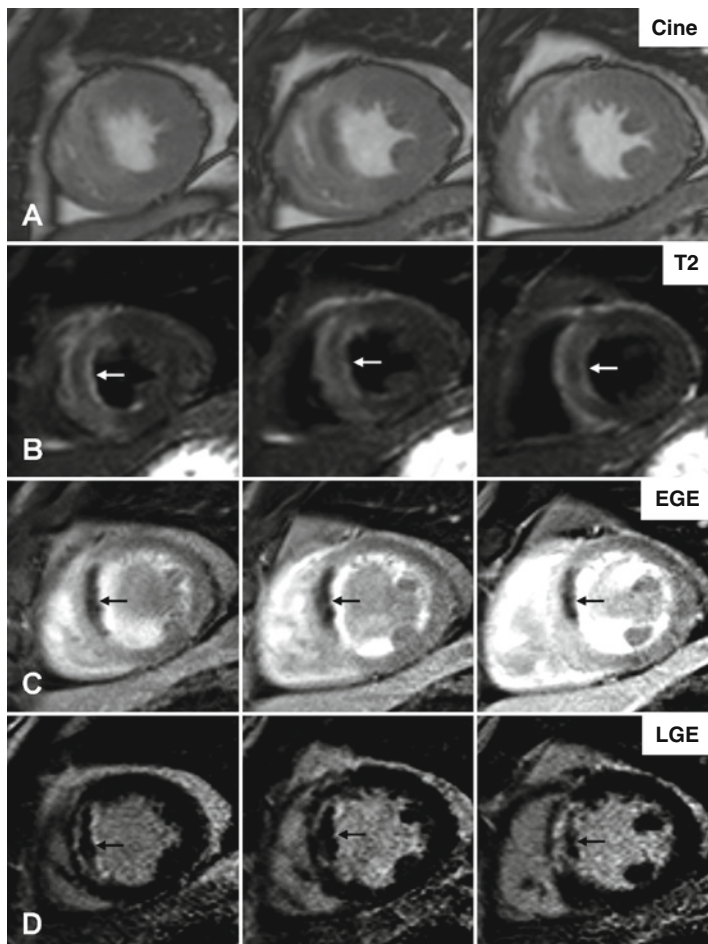
27.5.4.2 Case 8

A 59-year-old male presented with an acute anterior MI and was successfully treated with primary PCI 6 h after the onset of chest pain. Cine imaging demonstrated hypokinesia of the mid-interventricular septum (row A). T2-weighted imaging highlighted myocardial edema in the mid-septum (row B, see arrows). EGE did not demonstrate any MVO or intracardiac thrombus (row C). LGE revealed transmural MI in the mid-septum (row D).



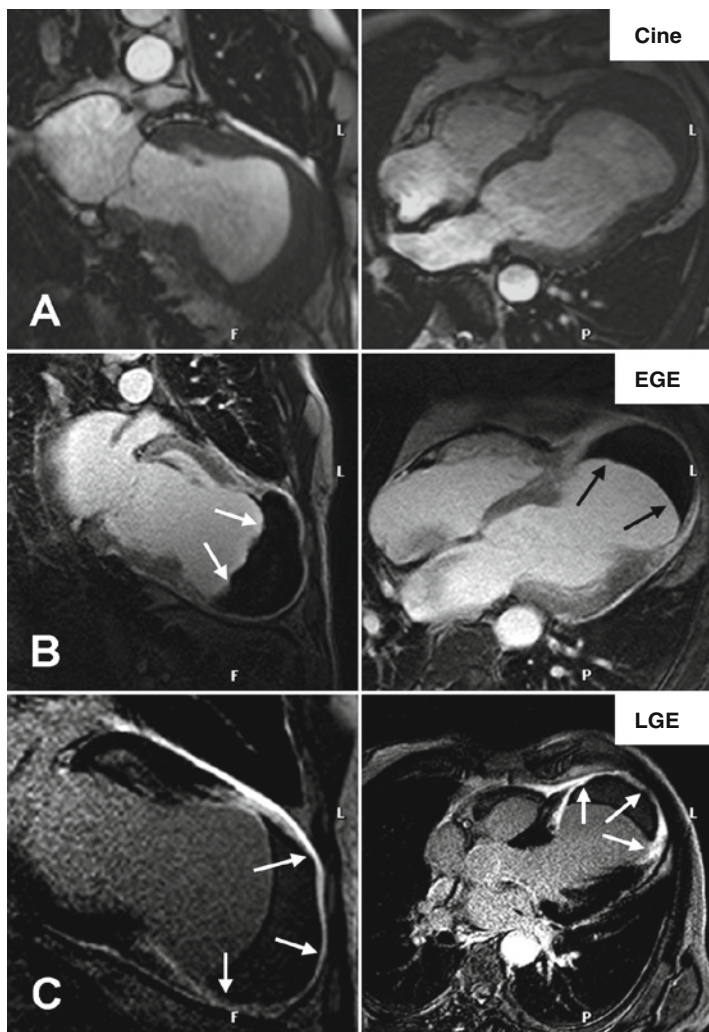
27.5.4.3 Case 9

A 36-year-old male presented with an acute anterior MI and was successfully treated with primary PCI 5 h after the onset of symptoms. Cine imaging demonstrated hypokinesia in the mid-interventricular septum (row A). T2-weighted imaging highlighted myocardial edema in the mid-septum (row B, see *arrows*). EGE demonstrated significant MVO (row C, see *arrows*). LGE confirmed the presence of MVO within an area of infarcted myocardium (row D, see *arrows*).



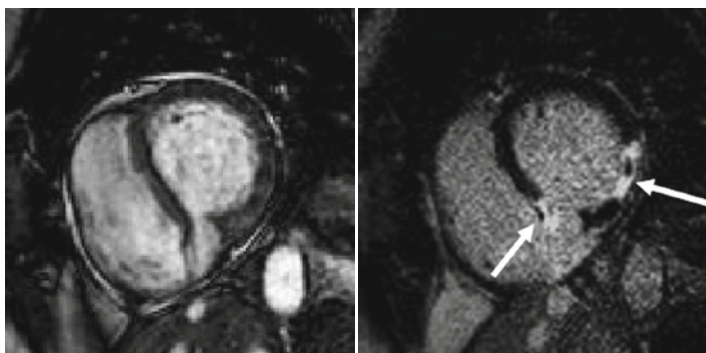
27.5.4.4 Case 10

A 60-year-old male presented with breathlessness after suffering an anterior MI. Cine imaging demonstrated that the LV apex was aneurysmal and akinetic (row A). EGE revealed a large mass of thrombus in the apex (row B, see *arrows*). LGE confirmed the presence of apical thrombus surrounded by transmural scar (row C, see *arrows*).



27.5.4.5 Case 11

A 78-year-old lady presented several days after severe chest pain and ECGs suggested recent inferior MI. (A) SA cine imaging revealed a VSD in the inferior septum. (B) LGE confirmed the VSD within the region of infarcted myocardium and associated MVO.



27.6 Positive Cardiac Enzymes and Normal Coronary Arteries

With the development of increasingly sensitive markers of myocardial necrosis, larger numbers of patients are being labeled as having an acute coronary syndrome and proceeding to coronary angiography. In a small proportion of this group, the coronary arteries are found to be normal, raising questions as to the cause of the biomarker rise. Potential explanations include:

- MI with subsequent recanalization of the artery
- Myocarditis or other cardiomyopathy
- Noncardiac causes

Given its ability to detect MI and edema, CMR represents the ideal method to investigate this patient group. Assomull et al. investigated the use of CMR in a group of 60 patients

with raised troponin levels and normal coronary angiography. They were able to establish a diagnosis in 65% of patients, the details of which are shown in table.¹³

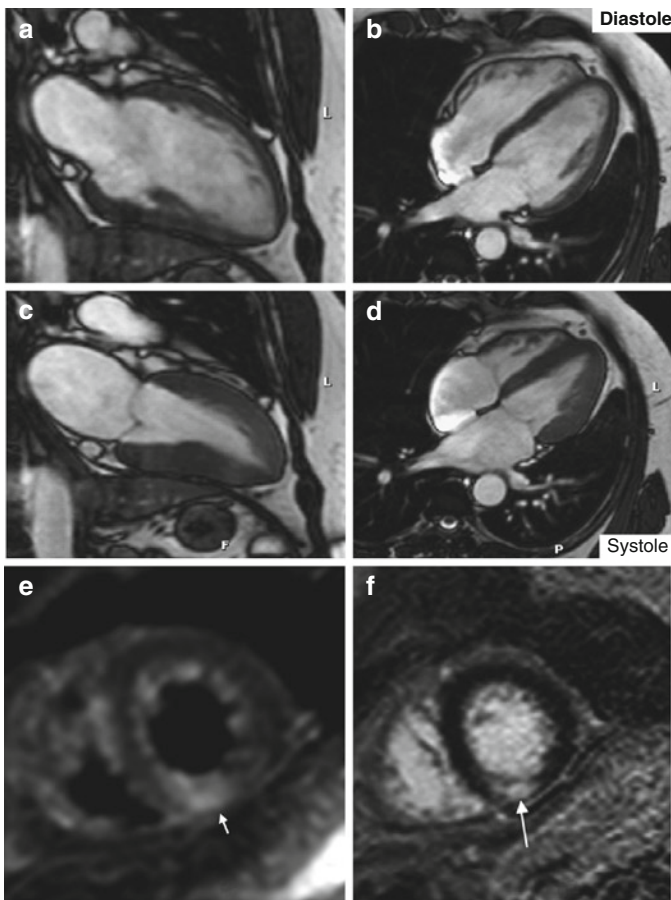
CMR findings	n (%)
Myocarditis	30 (50)
• Acute	19 (31.7)
• Chronic	11 (18.3)
MI	7 (11.6)
Takotsubo cardiomyopathy	1 (1.7)
Dilated cardiomyopathy	1 (1.7)
Normal CMR findings	21 (35)

These impressive results make a strong case for the use of CMR in this clinical situation. It is particularly interesting to note the 11.6% of patients who had evidence of MI at CMR despite normal coronaries at angiography. By identifying this group with CMR, prognostically important secondary prevention therapy could be commenced with confidence.

27.6.1 Example Case

27.6.1.1 Case 12

46-year-old female presenting with a Troponin-positive acute coronary syndrome. Coronary angiography revealed no stenosis. Cine CMR revealed good LV systolic function and T2-weighted imaging transmural edema of the inferior LV wall (*arrow*). LGE imaging revealed a small focal transmural inferior wall infarct. The patient was therefore started on secondary prevention therapy.



27.7 Potential Future Developments

The future of CMR imaging in IHD will be guided by software- and hardware-led refinements of existing CMR techniques, and by the introduction of new methods that will provide a different perspective on the heart.

27.7.1 Hardware Development

The greatest potential for improvement exists in the hardware field, where the introduction of many-element cardiac receiver coils and 3 T scanners has allowed the use of significantly higher degrees of acceleration by parallel imaging, which in turn translates into improved image resolution, with consequent benefits for both CMR perfusion and coronary imaging.

27.7.2 Software Development

From a software perspective, advanced acceleration methods (e.g., $k\text{-}t$ BLAST and T-SENSE) are now allowing higher-resolution perfusion images to be generated using existing hardware. Most of these techniques are also applicable to the more advanced hardware outlined above (Fig. 27.10).

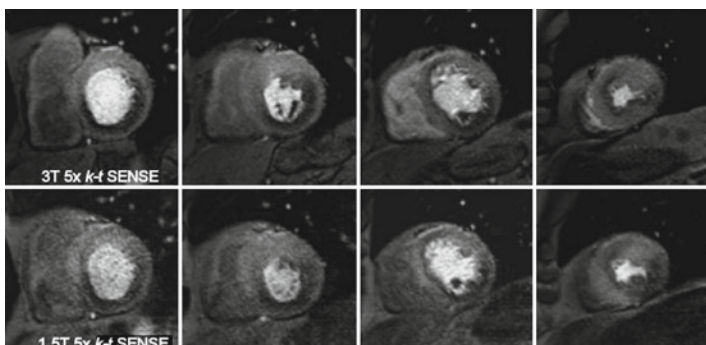


FIGURE 27.10. Myocardial perfusion CMR images of the same patient at 1.5 T and 3 T field strengths, using the advanced acceleration technique, $k\text{-}t$ SENSE. Note the improved image quality at the higher field strength (From¹⁹).

27.7.3 New Methods

27.7.3.1 Noninvasive Arterial Wall Imaging

Intravascular ultrasound (IVUS) is now a widely used, but invasive, method of assessing the characteristics and extent of coronary artery atherosclerosis. There have been several promising reports using black blood MRI to assess vessel wall thickness. However, the spatial resolution of this technique is still significantly less than IVUS and the method is challenging to apply in many patients.

27.7.3.2 Myocardial Perfusion Imaging without Contrast?

There have been some initial investigations into MRI myocardial perfusion imaging using arterial spin labeling (ASL), where arterial water is used as a tracer and gadolinium-based contrast is not therefore required.¹⁴ Although this technique may hold promise for the future, it is not yet a practical proposition for the clinical setting.

27.7.3.3 Targeted (Molecular) Contrast Agents

There is growing interest in the use of targeted contrast agents to help investigate specific disease processes. For example, fibrin-specific agents may be used to highlight ruptured coronary artery plaques, thereby aiding the noninvasive detection of acute coronary syndromes.

Key Points CMR in IHD

- Adenosine myocardial perfusion and dobutamine stress wall motion imaging have similarly high accuracies for the detection of myocardial ischemia.
- The diagnostic accuracy and prognostic value of both techniques is comparable to other noninvasive modalities.
- Comprehensive CMR protocols provide greater information than any other single noninvasive imaging modality alone.
- LGE imaging by CMR is now the reference standard for *in vivo* detection of myocardial scar.
- The extent of myocardial scar on LGE imaging is a good predictor of functional recovery following revascularization.
- T2-weighted imaging may differentiate AMI from chronic MI.
- CMR may be used to detect many IHD-related complications and is an ideal modality for the investigation of patients with chest pain, raised myocardial enzymes, and normal epicardial coronary arteries.

References

1. Nandalur KR, Dwamena BA, Choudhri AF, Nandalur MR, Carlos RC. Diagnostic performance of stress cardiac magnetic resonance imaging in the detection of coronary artery disease: a meta-analysis. *J Am Coll Cardiol.* 2007;50(14):1343–1353.
2. Underwood SR, Anagnostopoulos C, Cerqueira M, et al. Myocardial perfusion scintigraphy: the evidence. *Eur J Nucl Med Mol Imaging.* 2004;31(2):261–291.
3. Jahnke C, Nagel E, Gebker R, et al. Prognostic value of cardiac magnetic resonance stress tests: adenosine stress perfusion and dobutamine stress wall motion imaging. *Circulation.* 2007;115(13):1769–1776.
4. Plein S, Greenwood JP, Ridgway JP, Cranny G, Ball SG, Sivananthan MU. Assessment of non-ST-segment elevation acute coronary syndromes with cardiac magnetic resonance imaging. *J Am Coll Cardiol.* 2004;44(11):2173–2181.

5. Kramer C, Barkhausen J, Flamm S, Kim R, Nagel E. Standardized cardiovascular magnetic resonance imaging (CMR) protocols, society for cardiovascular magnetic resonance: board of trustees task force on standardized protocols. *J Cardiovasc Magn Reson.* 2008;10(1):35.
6. Thomson LEJ, Fieno DS, Abidov A, et al. Added value of rest to stress study for recognition of artifacts in perfusion cardiovascular magnetic resonance. *J Cardiovasc Magn Reson.* 2007;9(5):733–740.
7. Cerqueira MD, Weissman NJ, Dilsizian V, et al. Standardized myocardial segmentation and nomenclature for tomographic imaging of the heart: a statement for healthcare professionals from the Cardiac Imaging Committee of the Council on Clinical Cardiology of the American Heart Association. *Circulation.* 2002;105(4):539–542.
8. Heijenbrok-Kal MH, Fleischmann KE, Hunink MG. Stress echocardiography, stress single-photon-emission computed tomography and electron beam computed tomography for the assessment of coronary artery disease: a meta-analysis of diagnostic performance. *Am Heart J.* 2007;154(3):415–423.
9. Abdel-Aty H, Zagrosek A, Schulz-Menger J, et al. Delayed enhancement and T2-weighted cardiovascular magnetic resonance imaging differentiate acute from chronic myocardial infarction. *Circulation.* 2004;109(20):2411–2416.
10. Cury RC, Shash K, Nagurney JT, et al. Cardiac magnetic resonance with T2-weighted imaging improves detection of patients with acute coronary syndrome in the emergency department. *Circulation.* 2008;118(8):837–844.
11. Wu KC, Zerhouni EA, Judd RM, et al. Prognostic significance of microvascular obstruction by magnetic resonance imaging in patients with acute myocardial infarction. *Circulation.* 1998;97(8):765–772.
12. Nijveldt R, Hofman MB, Hirsch A, et al. Assessment of microvascular obstruction and prediction of short-term remodeling after acute myocardial infarction: cardiac MR imaging study. *Radiology.* 2009;250(2):363–370.
13. Assomull RG, Lyne JC, Keenan N, et al. The role of cardiovascular magnetic resonance in patients presenting with chest pain, raised troponin, and unobstructed coronary arteries. *Eur Heart J.* 2007;28(10):1242–1249.
14. Northrup BE, McCommis KS, Zhang H, et al. Resting myocardial perfusion quantification with CMR arterial spin labeling at 1.5 T and 3.0 T. *J Cardiovasc Magn Reson.* 2008;10(1):53.
15. Schwitter J, Wacker CM, van Rossum AC, et al. MR-IMPACT: comparison of perfusion-cardiac magnetic resonance with single-photon emission computed tomography for the detection of coronary artery disease in a multicentre, multivendor, randomized trial. *Eur Heart J.* 2008;29(4):480–489.

16. Ortiz-Perez JT, Rodríguez J, Meyers SN, Lee DC, Davidson C, Wu E. Correspondence between the 17-segment model and coronary arterial anatomy using contrast-enhanced cardiac magnetic resonance imaging. *J Am Coll Cardiol.* 2008;1(3):282–293.
17. Beek AM, Kuhl HP, Bondarenko O, et al. Delayed contrast-enhanced magnetic resonance imaging for the prediction of regional functional improvement after acute myocardial infarction. *J Am Coll Cardiol.* 2003;42(5):895–901.
18. Kim RJ, Wu E, Rafael A, et al. The use of contrast-enhanced magnetic resonance imaging to identify reversible myocardial dysfunction. *N Engl J Med.* 2000;343(20):1445–1453.
19. Plein S, Schwittringer J, Suerder D, Greenwood JP, Boesiger P, Kozerke S. k-Space and time sensitivity encoding-accelerated myocardial perfusion MR imaging at 3.0 T: comparison with 1.5 T. *Radiology.* 2008;249(2):493–500.
20. Pennell DJ, Sechtem UP, Higgins CB, et al. Clinical indications for cardiovascular magnetic resonance (CMR): Consensus Panel report. *Eur Heart J.* 2004;25(21):1940–1965.
21. Messroghli DR, Bainbridge GJ, Alfakih K, et al. Assessment of regional left ventricular function: accuracy and reproducibility of positioning standard short-axis sections in cardiac MR imaging. *Radiology.* 2005;235(1):229–236.
22. Lyne JC, Gatehouse PD, Assomull RG, et al. Direct comparison of myocardial perfusion cardiovascular magnetic resonance sequences with parallel acquisition. *J Magn Reson Imaging.* 2007;26(6):1444–1451.
23. Elkington AG, Gatehouse PD, Cannell TM, et al. Comparison of hybrid echo-planar imaging and FLASH myocardial perfusion cardiovascular MR imaging. *Radiology.* 2005;235(1):237–243.

Chapter 28

Basic Adult Congenital Heart Disease (ACHD)

Andrew M. Crean

Basic Protocol in ACHD

1. Anatomy module (Section 19.3.1)
2. LV function module (Section 19.4)
3. Axial stack of SSFP cines from the diaphragm to the top of the aortic arch (equivalent to RV function module (Section 19.4))
4. MR angiography module in coronal orientation (Section 19.10)
5. Phase velocity mapping – through the main pulmonary artery and aorta to measure Qp and Qs (Section 19.6)

Optional

6. Thin slice cine imaging in nonstandard planes to answer specific questions, e.g., LVOT/RVOT obstruction, or coarctation
7. Differential pulmonary flow, or peak velocity measurements across stenosis
8. Late-gadolinium enhancement module for ventricular scar or to rule out thrombus (in a Fontan circuit for example) (Section 19.9.1)
9. Coronary MR angiography, thin slice steady-state free precession (SSFP), and DIR imaging are equally valid approaches if anomalous coronary origins are suspected (Section 19.10)
10. In plane and/or through plane velocity encoded gradient echo sequence to demonstrate abnormal flow patterns and shunts

28.1 Introduction

Over the last 15 years cardiovascular magnetic resonance (CMR) has indisputably become the reference standard for the anatomical and functional assessment of the heart in adult congenital heart disease (ACHD). The number of children with congenital heart disease surviving to adulthood continues to increase, with many having had complex repairs in childhood. Many develop problems relating to their underlying diagnosis and some suffer late complications of remote surgery – “fixed but not cured.” The role of the CMR physician is to provide a complete description of the anatomical and physiological findings; an accurate assessment of ventricular size and function; an appraisal of the imaging appearances post surgery; and – by integrating all of the above – to make a valuable contribution to the management of these complex patients.

28.2 CMR Versus Other Imaging Modalities

Because it is noninvasive, does not expose patients to ionizing radiation, and provides reproducible images and measurements, CMR is an ideal test for the initial diagnosis and follow-up of congenital heart disease. Echocardiography is the first-line imaging test, but CMR is often the more definitive investigation to confirm the diagnosis and to assess serial change and indications for surgery. In patients with MR-incompatible devices, computed tomography (CT) is an increasingly used alternative investigation, but it lacks the capability of flow measurement or myocardial scar depiction.

Tips and Tricks

- All first-time examinations should be fully monitored by a CMR physician to allow for protocol modifications if unsuspected pathology is detected.
- Always do a magnetic resonance angiography (MRA) for a first-time examination (and follow with a venous phase acquisition to collect “free” additional data at a cost of just one extra breath-hold).
- Look for areas of dephasing on the cine images – these often indicate the presence of unsuspected shunts or areas of static or dynamic obstruction and require further focused imaging.
- Thinner slices resolve areas of confusion in many cases.
- Access to clinical notes or letters is essential if the correct study to answer the clinical question is to be performed.

28.3 Coarctation of the Aorta

This is one of the commonest forms of congenital aortic anomaly and amongst the most straightforward to image by CMR. The majority of patients seen will have had surgical repair in childhood and will be followed routinely for evidence of recoarctation. A much smaller proportion will present late, in adult life, with a suspicion of coarctation from chest x-ray appearances (Fig. 28.1) and/or clinical findings.

Key imaging features to assess are given in Table 28.1.

Recognition of coarctation is generally not difficult. Either MRA or sagittal oblique cine imaging (“candy cane view”; see Chap. 22) may be used to assess the thoracic aorta – and there are arguments for performing both on the first visit. The former has the advantage that a 3D volume render may later be performed and is particularly helpful in understanding and demonstrating the tortuosity of the coarct segment to physicians less accomplished at mentally integrating multiple thin slice data sets (Fig. 28.2a). Cine imaging, however, has the advantage of revealing flow disturbance secondary to focal stenoses (Fig. 28.2b).

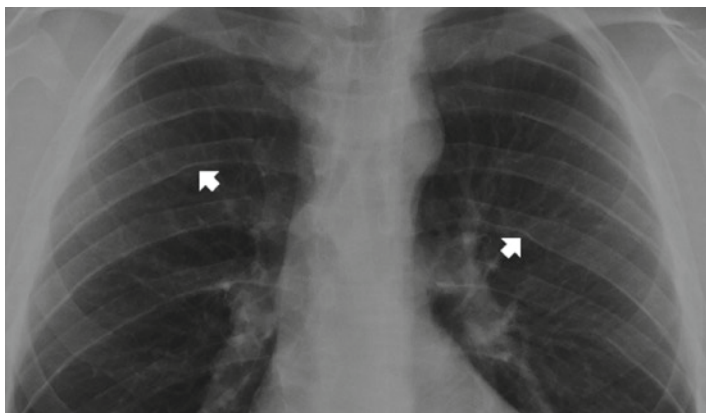


FIGURE 28.1. Appearance of rib-notching (*arrows*) on frontal chest x-ray.

TABLE 28.1. Possible CMR findings in coarctation of the aorta.

Repaired or unrepairs? (will probably not have had sternotomy - thoracotomy more usually)

Evidence of prior subclavian flap repair? (absent subclavian origin from arch)

Evidence of re-coarctation

Evidence of hypoplastic arch?

Evidence of collateral flow (large internal mammary or intercostal arteries)

Peak velocity across narrowing

Bicuspid aortic valve? Stenotic?

Evidence of aortopathy (associated with bicuspid valve)

Patch aneurysm? (if subclavian flap or Dacron patch repair)

Left ventricular hypertrophy if stenosis tight/long-standing or if associated aortic stenosis (measure LV mass)

Multiple levels of left heart or aortic obstruction (Shone complex)?

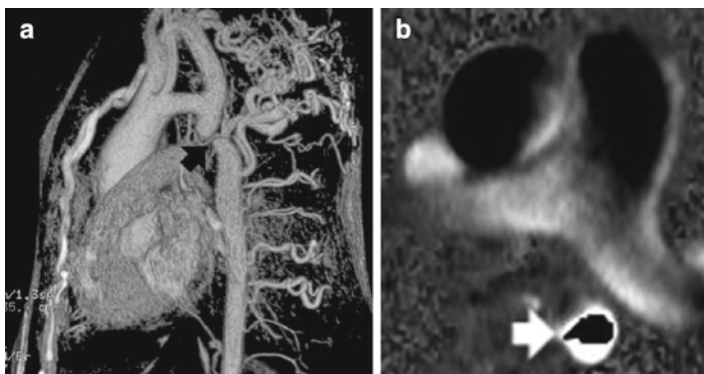


FIGURE 28.2. (a) Volume-rendered image of aorta shows coarct segment (black arrow) as well as provides an overview of the rest of the aorta with (in this case) multiple enlarged collaterals and a hypoplastic arch. (b) Phase velocity image at the level of the coarctation; the encoding velocity has been set lower than the actual velocity and aliasing has occurred.

It may sometimes be surprisingly difficult to establish whether the visualized stenosis is of functional significance or represents a “pseudocoarct.” A peak velocity on phase contrast imaging of >3 m/s (Fig. 28.2b), the presence of large collaterals (Fig. 28.2a), or elevated left ventricular (LV) mass all point to the former. Some patients with coarctation also have hypoplasia of the aortic arch. This is worth a comment particularly if a stent dilatation of the aorta is planned since relief of stenosis at the coarct site alone may not lead to significant reduction in LV pressure overload. Such cases are difficult to manage successfully and in extreme cases extra-anatomic bypass of the arch may be required (Fig. 28.3).

Common ancillary findings include bicuspid aortic valve and associated ascending aortopathy (see Chap. 22). In the context of a prior coarctation repair with either a flap of the subclavian artery or a Dacron patch, a focal weakness in the material used may give rise to focal aneurysmal dilatation years after surgery. Both true and false aneurysms may develop – distinction is rarely possible except at surgery.

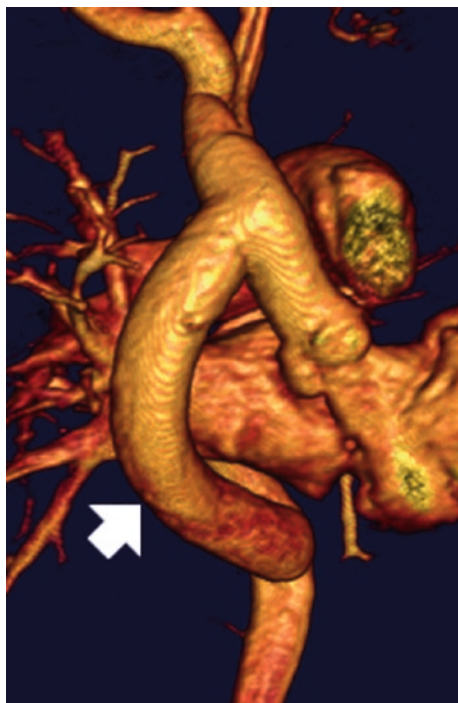


FIGURE 28.3. Volume-rendered image of the aorta post surgery for relief of arch obstruction. An extra-anatomic bypass has been performed with creation of a surgical conduit (arrow) between the ascending and descending portions of the thoracic aorta.

28.4 Tetralogy of Fallot

This is another common congenital condition – and one in which CMR surveillance has a major role to play. The cardinal tetrad of infundibular right ventricular (RV) stenosis, overriding aorta, ventricular septal defect (VSD), and RV hypertrophy (Fig. 28.4) is rarely seen since most patients will have been repaired in childhood. The occasional adult patient presents unrepaired and often cyanotic secondary to Eisenmenger complex. In most cases, however, the role of CMR is to demonstrate the almost invariable late consequences of surgery.

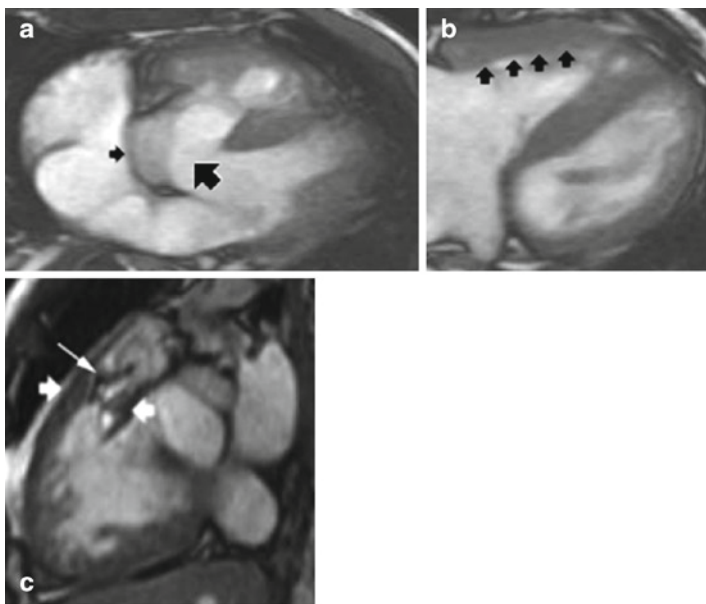


FIGURE 28.4. Features of unrepaired tetralogy. (a) Large nonrestrictive VSD (big arrow), overriding aorta (small arrow); (b) RV hypertrophy; (c) infundibular obstruction due to muscle bundles (thick arrows) – evidence of flow disturbance is seen as a linear black jet of spin dephasing (thin arrow).

In the past, relief of infundibular obstruction was performed by resection and patch enlargement of the right ventricular outflow tract (RVOT). In most cases a trans-annular style of repair meant that the pulmonary valve was either severely disrupted or completely excised. Unrecognized, in that era, were the late consequences of free pulmonary regurgitation (PR), which in most patients leads to progressive RV dilatation, impairment of function and secondary effort intolerance, or worse, life-threatening ventricular arrhythmia.

The principal role of CMR here is to monitor serial change in RV size and function. End diastolic volume should be indexed to body surface area for meaningful interpretation and a standardized method of contouring the endocardial surface

on cine images is required to avoid spurious changes in volume from being reported. It matters less whether measurements are made from an axial or short axis oblique cine stack as long as a consistent approach is taken for subsequent examinations. The goal of monitoring is to alert the ACHD physician to any genuine deterioration in RV size or function so that the optimal timing of pulmonary valve replacement can occur (Fig. 28.5).

Phase velocity mapping quantitates the PR fraction with precision (Fig. 28.5) but in reality adds little to echocardiographic assessment of the valve. MRA has a place at the initial examination since a significant minority of these patients will have unsuspected proximal pulmonary arterial (PA) stenoses (Fig. 28.6). Angiographic data facilitate interventional planning

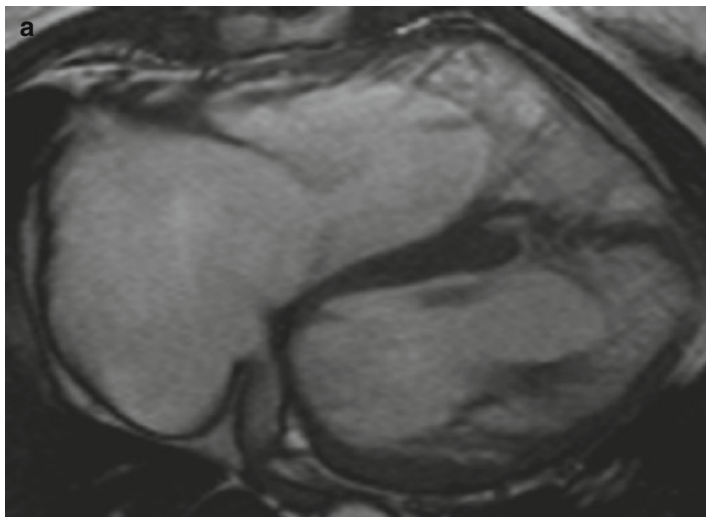


FIGURE 28.5. Late consequences of PR. (a) SSFP end diastolic frame showing a moderate-to-severe enlargement of the RV in a tetralogy patient with long-standing PR. (b) Flow curve generated from a phase velocity map acquired in the MPA. Forward systolic flow is normal (black arrow) but note significant reverse flow in diastole (grey arrow); regurgitant fraction is approximately 40% (i.e., essentially free incompetence).

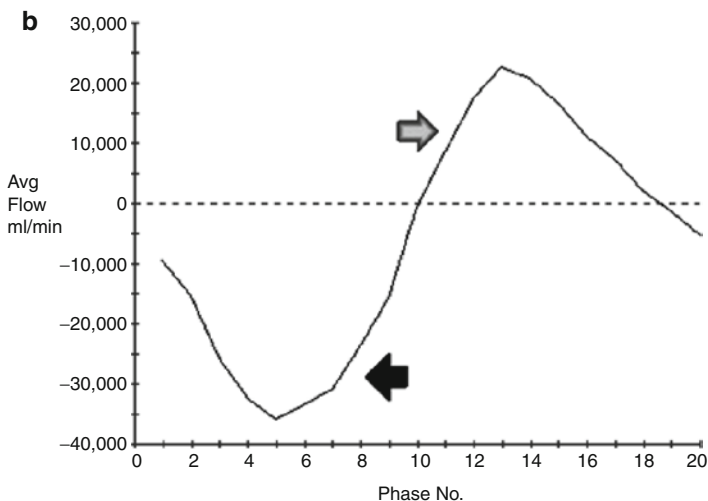


FIGURE 28.5. (continued)

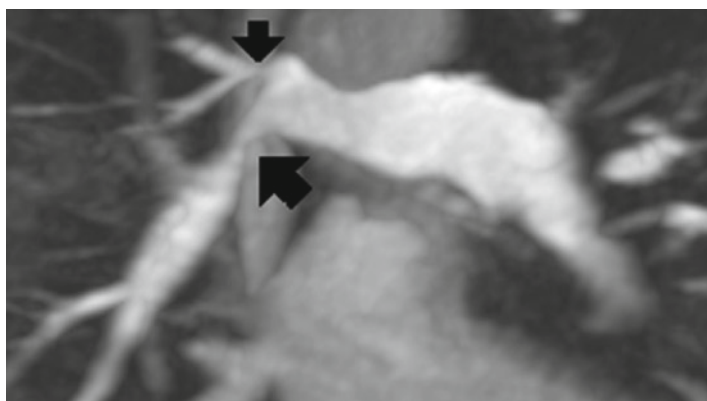


FIGURE 28.6. Maximum intensity projection image from a coronal MRA in a tetralogy patient. Several branch PA stenoses are apparent (arrows).

both here and also more proximally in the main pulmonary artery (MPA) when stent-mounted percutaneous pulmonary valve replacement is being contemplated.

28.5 Transposition of the Great Arteries

It is now rare to see unrepaired *d-TGA* (dextro-transposition of the great arteries) in an adult CMR practice. Repaired patients fall into two quite different groups: those having had surgery more than 15–20 years ago are likely to have had an *atrial switch* procedure – often known eponymously as a Mustard or a Senning procedure. In this operation patients are given a physiologically corrected circulation by means of an interatrial baffle which directs blue blood to the lungs and pink blood to the body. Unfortunately the procedure leaves the patient with the preexisting ventriculoarterial (VA) discordance such that the RV remains in place as the systemic ventricle facing systemic arterial pressure. Although the initial RV compensation is to hypertrophy in response to increased afterload, eventual symptomatic decline of RV function is the norm. In the context of discordant connections it is prudent to use terminology carefully so that the referring clinician understands what is being described. Terms such as “right” and “left” ventricle should be replaced with the more precise “subpulmonic (morphological left) ventricle” and “subaortic (morphological right) ventricle.”

Mustard/Senning patients are monitored by CMR not only for RV dysfunction and dilatation but also for late surgical complications such as baffle stenosis or leak. The former is readily detected by either MRA or thin slice cine imaging (Fig. 28.7). The latter is more challenging and requires careful planning of phase velocity maps parallel to the superior and inferior systemic venous baffles – even in expert hands leaks may go unrecognized and this is one of the few areas where invasive catheter angiography retains a degree of superiority.

More recently the technique of *arterial switch*, eponymously known as the Jatene operation, has been widely adopted. This involves restoration of VA concordance so that the patient is corrected both physiologically and anatomically. Potential complications include narrowing of the MPA as it straddles over the anterior aspect of the aorta (Fig. 28.8) as well as theoretical concerns about myocardial ischemia

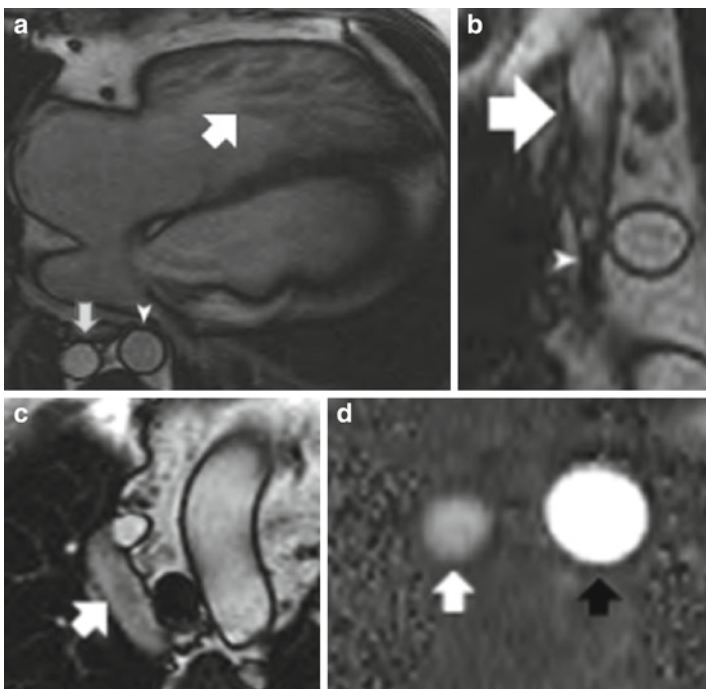


FIGURE 28.7. Baffle occlusion in a Mustard patient. (a) Axial SSFP diastolic frame showing an enlarged and hypertrophied systemic (*morphological right*) ventricle (*large white arrow*). Note the dilated azygous vein (*small white arrow*), which is almost as large as the aorta (*arrowhead*). (b) Sagittal cine image demonstrating the SVC (*arrow*), which becomes grossly narrowed distally as it forms the superior systemic venous baffle (*arrowhead*). (c) Extent of azygous engorgement is shown at level of azygous arch (*arrow*) close to its insertion into the SVC. Antegrade flow cannot occur through the stenosed baffle – confirmed by (d) phase velocity mapping of the azygous (*white arrow*) and descending aorta (*black arrow*) – normal cephalad azygous flow would be encoded black but here it is the same color as the descending aorta, indicating reverse flow.

resulting from stenosis formation at the coronary reimplantation sites. The true long-term complication rate of this operation remains to be established and the role of CMR is less well established than for atrial switch.

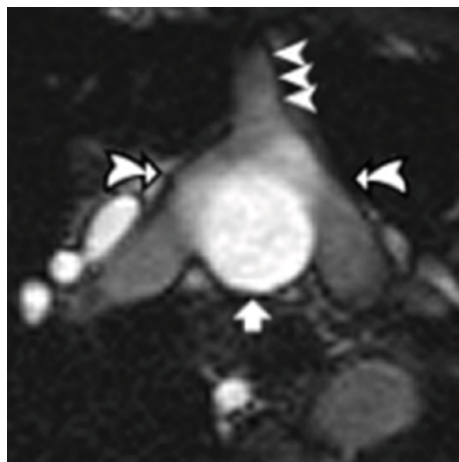


FIGURE 28.8. Axial SSFP image post Jatene operation (see text). The RPA and LPA (*curved arrows*) straddle the ascending aorta (*straight arrow*). This leads to some stretching and distortion of the MPA (*arrowheads*) which may cause a degree of RV outflow obstruction.

Less common but not rare in any large ACHD practice is the levo-transposition of the great arteries (*l-TGA*) or congenitally corrected transposition. The term is in truth a misnomer: in this situation both the atrioventricular (AV) and VA connections are discordant and thus – like the atrial switch population – they are physiologically but not anatomically corrected. A proportion of these patients will have come to medical attention late in the absence of any other associated defect. Their main problem is again progressive systemic RV decline. The double switch procedure restores anatomical continuity and, although performed in children, is seldom performed in adults. In the few reported cases the deconditioned subpulmonic (morphological left) ventricle is prepared to face systemic afterload during a

period of progressively tighter PA banding. CMR may be used to estimate serial change in a ventricular mass as a result of this “training” and hence guide timing of the operation. This approach remains controversial.

28.6 Coronary Anomalies

There are many described anomalies of coronary artery origin, course, or termination. Although CMR does not have the spatial resolution of conventional angiography, its 3D nature allows the course of the vessel to be more readily understood and the image quality is certainly sufficient for demonstration of coronary origin and proximal course. When a coronary arises from an aberrant location, it frequently has a slit-like origin as it passes within the wall of the aorta for a few millimetres, which may predispose to ischemia. Coronaries that pass between the aorta and RVOT are referred to as having a “malignant” course – the implication being that they may suffer dynamic compression between the two outflow tracts, again resulting in myocardial ischemia. Both mechanisms have been invoked to explain the increased risk of sudden death that such anomalies bestow.

The two key attributes of an ideal coronary imaging sequence are isotropic voxel sizes and a short acquisition window (to prevent motion-related blurring). There are dedicated sequences which come close to achieving this in a breath-hold (for a small targeted coronary volume) (Fig. 28.9a) or by using a navigated free-breathing sequence over 10–15 min (Fig. 28.9b). Although these sequences may require considerable experience, in reality adequate assessment of coronary origin and initial course can be made by black blood or cine imaging as long as the matrix is optimized and the *z*-axis resolution is improved by reducing slice thickness to 3–4 mm (Fig. 28.9c).

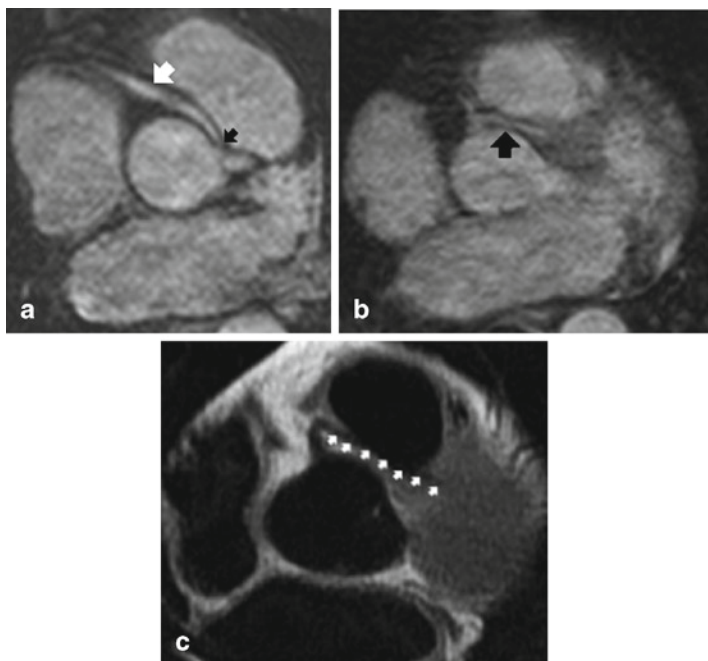


FIGURE 28.9. Coronary imaging. (a) Breath-held targeted coronary acquisition demonstrating an anomalous right coronary artery (RCA) (white arrow) arising from the left coronary sinus and taking a “malignant” course between the aortic root and RVOT. Note the narrow origin (black arrow), a common finding. (b) Free-breathing-navigated whole heart acquisition. Image quality is reduced compared to the targeted technique but a much larger volume of the heart can be covered. This patient has a malignant left main stem artery (arrow). (c) Standard double inversion recovery black blood 3 mm thick slice clearly shows the malignant left main coronary artery (arrows).

28.7 Partial Anomalous Pulmonary Venous Return (PAPVR)

Unexplained right heart dilatation in a young or middle-aged individual should prompt a search for left to right shunting. One of the most frequently missed causes is PAPVR (Fig. 28.10). Even when the diagnosis is made its frequent

concomitant – sinus venosus defect – is not always appreciated. The most frequent type of PAPVR involves drainage of the right upper and middle lobes to the superior vena cava (SVC). The second most common is the drainage of part or all of the left lung to the left innominate vein. Sinus venosus defect is related to the former and may either occur superiorly (more common) or inferiorly (rare). Diagnosis prior to the development of PA hypertension is essential if surgical intervention is to be successful.

The anomalous drainage is easily detectable with a coronal MRA (Fig. 28.10). Less straightforward is the sinus venosus defect, which is easy to miss unless specifically searched for. The author's practice is to use thin slice (5 mm) cine imaging in the axial plane through the region of the SVC/right upper

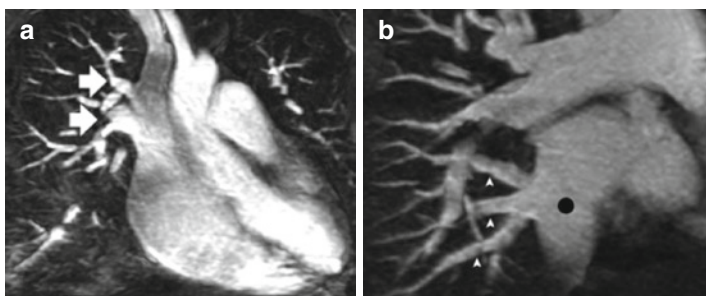


FIGURE 28.10. Partial anomalous pulmonary venous return. (a) Coronal maximum intensity projection (MIP), right upper and middle lobe veins drain to SVC (arrows); (b) coronal MIP, right lower lobe veins (arrowheads) drain to inferior vena cava (IVC) (black dot); (c) coronal MIP, single vessel (large arrow) draining entire right lung to IVC (small arrow); (d) axial SSFP image, superior sinus venosus defect (large arrow) between lower SVC (white dot) and upper left atrium (black dot) with anomalous upper lobe vein (small arrow) draining at site of defect; (e) coronal SSFP image, inferior sinus venosus defect (arrow) between left atrium (black dot) and IVC (white dot); (f) volume-rendered MRA, Scimitar syndrome with a single vein draining the right lung (large arrow) into the IVC (small arrow) and associated hypogenesis of the lung and systemic arterial supply (not shown). Note the presence of small bridging veins (arrowheads) between the scimitar vein and the left atrium.

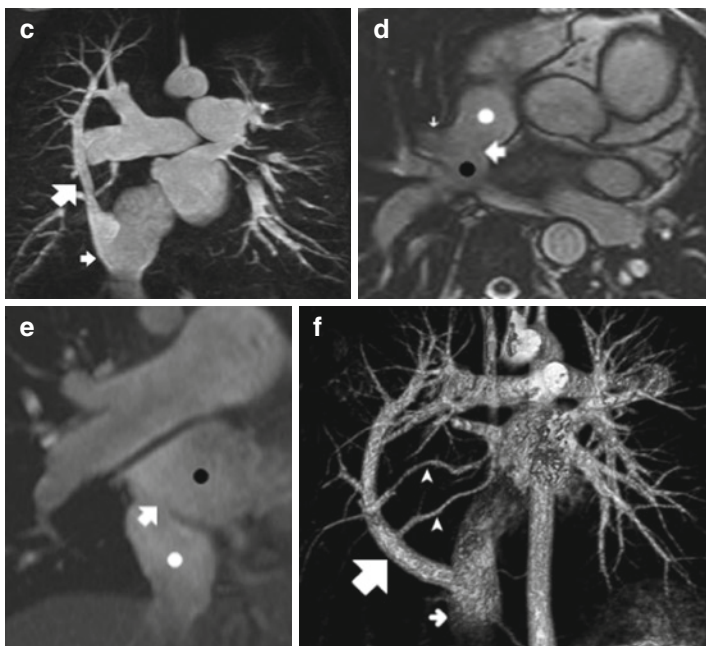


FIGURE 28.10. (continued).

pulmonary vein since this is where the defect is located (Fig. 28.10). Measurement of $Qp:Qs$ allows for noninvasive assessment of size of shunt. Indirect evidence of pulmonary hypertension should be sought (enlarged PAs with tortuous segmental branches). RV volume and function should be formally quantitated. Significant RV dilatation is never caused by right upper/middle PAPVR alone and almost invariably indicates the presence of a sinus venosus ASD.

28.8 Summary

CMR is invaluable in the assessment of ACHD patients, unique in its large field of view without ionizing radiation. With the three basic techniques of CMR – cine imaging, MRA, and phase velocity mapping – 99% of all necessary information can be elucidated for enhancing patient management.

CMR Report in ACHD

1. Morphology (descriptive)
 - a. Simple lesions
 - b. Complex lesions
 - i. Situs
 - ii. Ventriculoarterial relationship
 - iii. Artioventricular relationship
 - iv. Pulmonary venous connection
 - v. Systemic veins and connections
 - vi. Septal defects
 - vii. Valvular lesions (including atresia)
 - viii. PAs (and systemic to pulmonary artery collaterals where present)
 - ix. Aorta
 - x. Others
2. RV and LV volumes with and without indexing to body surface area
3. PA and aortic dimensions (diameters)
 - a. MPA
 - b. Left and right pulmonary arteries
 - c. Aortic measurements at selected levels (see Chapter 22)
 - d. Shunt or conduit (minimum and maximum)
4. Blood flow, velocity
 - a. Pulmonary/systemic flow ratio (Qp:Qs)
 - b. Valve (if regurgitant) (name of valve)
 - i. Forward flow
 - ii. Regurgitant flow
 - iii. Regurgitant fraction
 - c. Valve (if stenotic) (name of valve)
 - i. Peak velocity (gradient)
 - ii. Other (eg., cusp morphology, valve area)
 - d. Coarctation
 - i. Peak velocity (gradient)
 - ii. Collateral flow estimate
 - e. PA flow
 - i. MPA
 - ii. LPA
 - iii. RPA
 - iv. Shunt or conduit flow (name of shunt or conduit)
 - v. Peak velocity (conduit)

Key Points CMR in ACHD

1. Congenital heart patients require lifelong surveillance in most cases.
2. CMR is the method of choice for assessment of complex anatomy, ventricular function, surgical/interventional planning, and postoperative surveillance.
3. CMR for ACHD cannot be entirely driven by protocol and in many cases requires protocol modification “on the fly” for adequate assessment of pathology.
4. Terminology is all-important in ACHD reporting – care is required in the naming of ventricles and AV valves, especially where anatomy is complex or confusing.
5. The MR imager plays a key role in the ACHD team and should be available to present imaging data at regular multidisciplinary meetings to aid management planning.

Chapter 29

Pulmonary Vein Assessment

Sven Plein and John P. Greenwood

CMR Protocol for Pulmonary Vein Assessment

1. Anatomy module (Section 19.3.1)
 2. LV function module (Section 19.4)
 3. Breath-hold non-gated contrast-enhanced MRA performed in the coronal projection encompassing the pulmonary veins and left atrium (Section 19.7)
 4. Optional
 - a. In-plane cine imaging of each individual pulmonary vein
 - b. Through-plane phase contrast flow analysis planned separately through each pulmonary vein
- Optional: LGE module (after ablation) (Section 19.9.1)

29.1 Introduction

There are two common clinical scenarios that generate a CMR referral specifically for assessment of the pulmonary venous anatomy. These are: (1) suspicion of anomalous pulmonary venous drainage, usually in the setting of a dilated right heart. (2) Assessment of the left atrial and pulmonary venous anatomy prior to an electrophysiological procedure. The former of these is fully covered in Chap. 28. 7, (congenital heart disease),

so this chapter will just focus on pre- and post-assessment for radiofrequency ablation procedures.

Radiofrequency ablation (RFA) of the pulmonary veins (PVs) and the left atrium has become a widely used procedure for the treatment of many forms of cardiac arrhythmia, in particular atrial fibrillation (AF). The morphology of the left atrium and the pulmonary veins is highly variable, and in around 1/3 of cases an anomaly of the PV can be found, such as a common left or inferior truncus or an additional right middle cardiac vein. Pre-procedural imaging by computed tomography, echocardiography and CMR is therefore today performed as a matter of routine to plan the interventional procedure, shorten its duration, and minimize complications. The 3D imaging data generated by CMR or CT can be integrated in clinical electrophysiological mapping systems to provide cardiac electrical-anatomical maps during the ablation procedure. Increasingly, CMR is used to delineate ablation lesions to measure procedural success and to assess possible procedural complications such as pulmonary vein stenosis, which occurs in 1 or 2% of cases and can be easily detected by CMR. The rare, but severe complication of atrioesophageal fistula can also be delineated by CMR, although CT is often preferred.

29.2 CMR Versus Other Imaging Modalities

In many institutions, cardiac CT is the method of choice for pre-procedural assessment of the pulmonary veins because of its availability, fast data acquisition, and high spatial resolution. However, the commercially available electrophysiological mapping software systems only produce low-resolution 3D electro-anatomical maps and so CMR imaging is equally adequate, if available. Also, cardiac CT is associated with substantial radiation and iodinated contrast exposure. As the main function of the 3D electro-anatomical mapping systems is to reduce procedural time and hence radiation exposure, CMR is likely to become an increasingly attractive alternative to acquire the 3D atrial maps.

29.3 CMR Protocol and Findings

The mainstay of CMR pulmonary vein assessment is contrast-enhanced magnetic resonance angiography of the pulmonary veins. This is usually performed as a breath-hold, non-gated, or ECG-gated acquisition in the coronal projection. Careful planning is essential to ensure that all of the pulmonary veins and left atrium are fully included in the field of view.

The following pulse sequence parameters are recommended for PV MRA:

- a. Gadolinium (0.1–0.2 mmol/kg) injected at 2–3 mL/s
- b. Slice thickness 1–2 mm; acquired spatial resolution in-plane 1–1.5 mm. If possible aim for isotropic voxels.
- c. 60–80 slices.
- d. Parallel acquisition used as available
- e. Single phase acquisition – breath-hold (typically 15–18 s), start the acquisition just after contrast leaves the RV as it is the pulmonary veins and LA that need optimal opacification.

Many CMR centers also perform through plane phase contrast imaging through each pulmonary vein. SSFP cines in the axial and SAX orientation can complement the imaging protocol. Following RF ablation, LGE imaging can be used to identify ablation scars to comment on procedural success.

29.4 CMR Analysis

Using advanced post-processing software, 3D volume-rendered images can be created to show the detailed anatomical arrangement of the left atrium and the pulmonary venous connections (Fig. 29.1). In the CMR report it is recommended to comment on the following:

1. Number of pulmonary veins (accounting for common trunks and accessory veins)
2. Exact anatomical arrangement in relation to the atria and/or systemic venous drainage (i.e., recognition of accessory or anomalous pulmonary veins). See Fig. 29.2.

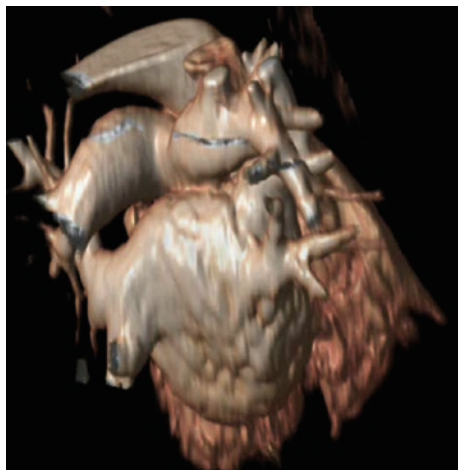


FIGURE 29.1. 3D volume-rendered image showing the posterior aspect of the left atrium and the pulmonary venous connections.



FIGURE 29.2. 3D reconstruction showing partial anomalous PV drainage (left upper pulmonary vein connected to the dilated innominate vein; SVC is also clearly dilated).

3. Maximum and minimal ostial diameter of each pulmonary vein (dependant on cardiac and respiratory phase)
4. Presence or absence of stenosis in each PV, especially in reporting post-ablation CMR exams (Fig. 29.3). Pre- and post-ablation images should be compared side by side.

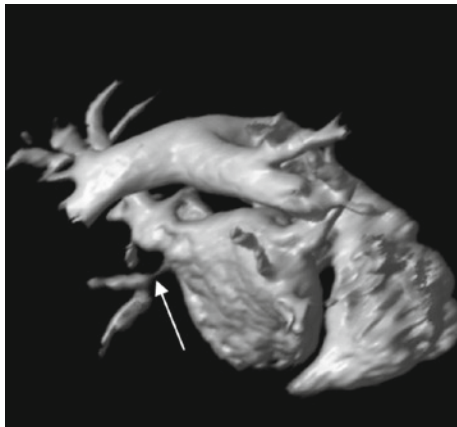


FIGURE 29.3. Post ablation MRA showing tight stenosis of the left lower pulmonary vein.

CMR Report for Pulmonary Vein Assessment

Morphology:

1. Number of pulmonary veins
2. Exact anatomical arrangement of pulmonary vein return including recognition of accessory or anomalous pulmonary veins
3. Presence or absence of stenosis in each PV, especially in reporting post-ablation CMR exams.

Quantitative elements:

1. Maximum ostial diameter of each pulmonary vein
2. Note the cardiac and respiratory phase during acquisition of images used for ostial measurements
3. Minimum ostial diameter of each stenotic pulmonary vein
4. Imaging technique used for measurements

Key Points CMR in Pulmonary Vein Assessment

1. Useful for planning ablation, during procedure, and for assessment of complications
2. Comparable measurements to CT

Chapter 30

Interventional Cardiovascular Magnetic Resonance Imaging

Tarique M. Hussain, Kawal Rhode, and Gerald F. Greil

30.1 Introduction

Rapid advances in the field of CMR have developed this modality to the extent that it can now be used to guide interventions. CMR provides exceptional 2D and 3D structural delineation for visualization and measurements. For these reasons, clinical programs using MRI guidance for cardiac catheterization have started and are showing promising results.¹

30.2 Interventional MRI Systems

Currently there are no dedicated safe MR-compatible catheters and devices for cardiovascular intervention commercially available. Therefore, it is still not possible to perform the complete procedure within the MR scanner. The immediate future of interventional MRI lies in exploiting multimodality imaging. A good example of this is the XMR system which combines X-ray and MRI by having both these modalities in the same room (Fig. 30.1).

30.2.1 *XMR Facility Design*

There are many design features that make this room different from standard MRI facilities. The XMR suite is designed so

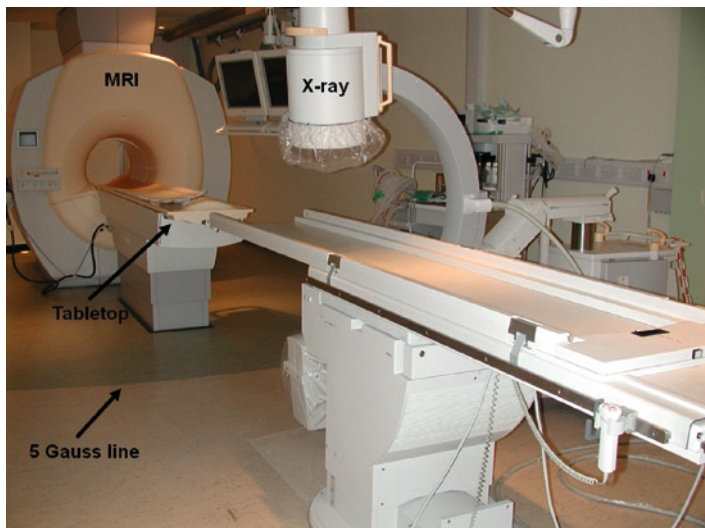


FIGURE 30.1. An XMR system combines X-ray and MRI by having both modalities in the same room with a tabletop design that allows patients to be moved from one modality to the other in a very short time. The table position is stored within the system, allowing image fusion between the MRI and X-ray system (XMRI) or even other imaging modalities (e.g., echocardiography). This system additionally allows the safe use of electronic devices, such as echocardiography machines and computer equipment, in the scanner room beyond the five-gauss line.

that half of the room is outside the five-gauss line of the magnet, permitting use of traditional instruments and devices in this area (including echocardiography and radiofrequency ablation equipment). A movable tabletop allows the patient to be moved between modalities easily. The paramount factor in the design, build, and operation of an XMR facility is safety and a comprehensive safety protocol needs to be drawn up to minimize possible hazards (Table 30.1).

TABLE 30.1. XMR facility – safety features.

-
1. Compulsory safety training of all MR interventional staff
 2. Specially designed clothes without pockets
 3. Safety entry restrictions during XMR intervention
 4. Clear demarcation of ferromagnetic safe areas within the room
 5. MR-compatible anesthetic and monitoring equipment
 6. Noise proof headphone systems for all staff within the room
 7. X-ray and RF shielded room
 8. Positive pressure air handling and filtration system
 9. Tethering of all ferromagnetic equipment to the wall/floor
 10. Safety checks whenever patient is transferred between X-ray and MRI to ensure that metallic instruments used for catheterization are not taken across to the MRI end of the room
 11. Written log of all safety infringements and regular review of safety procedures
-

30.3 MR Visualization Strategies

Crucial to the success of interventional MRI is real-time tracking and visualization of catheters, guide-wires and devices in the MR environment.

Several approaches have been proposed in terms of catheter tracking. They can be separated into *passive*, *active*, and *hybrid tracking* strategies.²

Passive techniques are comparable to X-ray fluoroscopy, whereby the device itself is imaged without the need of additional hardware. This method has been successfully employed to guide catheters in patients under MR.¹ The main challenge of all passive catheter tracking techniques is the concern regarding sufficient contrast between the instrument and its surrounding anatomy. Furthermore, real-time tracking limits the imaging to single-slice imaging with a limited field of view. *Active* tracking techniques employ small receiver coils,

incorporated in the catheter device for signal reception and/or transmission, which necessitates hardware modification. In addition, the main disadvantage is the concern regarding safety because these devices use intravascular coils as radio-frequency antennae and this makes the induction of an electric current and heating possible. The main advantage is that the tracking step can be performed independently to the imaging and so more detailed imaging (including 3D imaging) can be achieved.

Some approaches share both passive and active characteristics and are called *hybrid* techniques. Hybrid catheters can be tracked easily when compared to passive catheters and have a relatively better safety profile when compared to some of the active catheter designs.

30.3.1 Performing XMR Procedures

In general terms, there are two ways in which the XMR laboratory can be used.

30.3.1.1 X-ray Imaging as a Backup During MRI Cardiac Catheterization

The cardiac catheterization procedure is performed in the MR scanner after adequate arterial and/or central venous access has been obtained in the MR safe area (Fig. 30.1). The patient is then placed in the MR scanner after safety checks, including an operating theater-style check of all metallic objects used in the MR safe area. With real-time imaging, the end-hole or side-hole balloon angiographic catheter (4F–7F) is passively visualized with the balloon inflated with CO₂. It then can be tracked to the appropriate location for pressure measurement or deployment of a device. If catheter manipulation into a particular heart chamber or vessel using MR guidance alone is difficult, the patient is transferred back to the X-ray end of the room, where the catheterization can be continued under X-ray fluoroscopy (e.g., to use a guidewire

or a braided catheter). The patient can be transferred back to the MR scanner for further MR measurements once the catheter is satisfactorily positioned to continue the procedure.

30.3.1.2 Performing X-ray Fused MR-Guided Interventions

Interventional procedures and radiofrequency ablation of arrhythmias necessitate part of the procedure to be performed under X-ray fluoroscopy because the ablation catheters and delivery devices are not MR compatible. Therefore, MR imaging is performed at the beginning of the procedure for planning, during the procedure for guidance, and at the end of the procedure for evaluation.

Recently image fusion technology has been developed for image fusion between high-resolution MR imaging and electrophysiological models (Fig. 30.2). Several systems are on the market and are currently being evaluated for clinical utility.

Image fusion can be used for several different indications:

1. It can provide anatomical road-mapping by overlaying of 3D MR-derived anatomy onto live X-ray fluoroscopy
2. It can provide functional information overlay. Examples are motion from tagged MRI, or ablation lesion/ myocardial scar visualization from late enhancement MRI
3. It can provide 3D localization of devices within an MR image.
4. It can provide integration of data for biomechanical modeling.

Using these techniques, a number of clinical cardiac applications are listed (Table 30.2).

30.3.2 Physiological Information

Traditional cardiac catheterization involves invasive pressures and blood gas measurements to calculate systemic and pulmonary blood flow and resistance using the Fick principle. However,

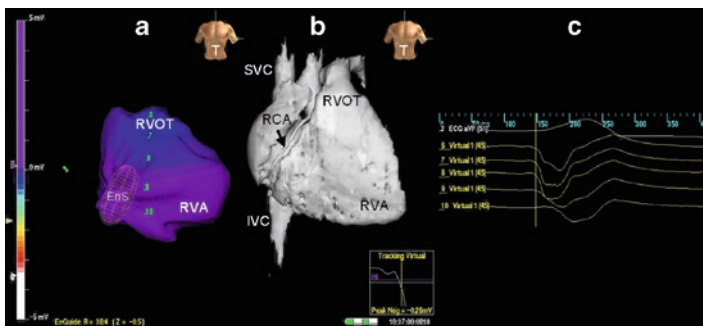


FIGURE 30.2. A 13-year-old patient was invasively treated for right ventricular outflow tract tachycardia. The geometric model, based on electrophysiology data (a) and the high resolution 3D magnetic resonance (MR) surface-rendered model (b), are presented side by side. Their spatial orientation within the thorax is shown by the thorax model (T). Their spatial coordinates are connected and movement of the electrophysiology model (a) results in the appropriate motion of the corresponding anatomic MR model (b). The 3D MR model (b) shows better anatomical details of the superior vena cava (SVC), inferior vena cava (IVC), right ventricular apex (RVA) and the right ventricular outflow tract (RVOT). The right coronary artery (RCA) can be seen in the 3D MR surface-rendered model (b), but not on the geometric model based on the electrophysiology data (a). The surface (2) and virtual (6–10) ECG signal generated from the Ensite Array® catheter (Ensite System St. Jude Medical) are displayed (c).

TABLE 30.2. Interventional XMR cardiovascular procedures.

Radiofrequency ablation for tachyarrhythmias and pacemaker implants

Interventional Procedures in Congenital Heart Disease

Guided cardiac biopsy

this is dependent on multiple measurements and this can be a considerable source of inaccuracy. In addition, in patients with large intracardiac shunts or high pulmonary blood flow, the accuracy is further reduced. However, velocity-encoded phase

contrast magnetic resonance (MR) enables noninvasive quantification of blood flow in major vessels. Cardiac output and the pulmonary-to-systemic flow ratio ($Q_p:Q_s$) measured using this technique have been shown to be more accurate. In addition, phase contrast MR has been validated in numerous phantom experiments. This allows for a more accurate method of quantification of pulmonary vascular resistance (PVR) in patients with pulmonary hypertension by using invasive pressure measurements and MR flow data.³

Assessment of global and regional ventricular function can also be carried out much more accurately with 2D cine SSFP or time resolved 3D SSFP cardiac MR than with X-ray angiography. This is particularly important when assessing right ventricular function, volume, and regional wall motion. Additional information can be obtained from myocardial tagging, delayed enhancement, or spectroscopy, and this can be combined with invasive pressure measurements or real-time volumes from conductance catheter measurements.

Finally, combining invasive pressure measurement with MR-derived blood flow and ventricular volumes also opens up interesting new ways of looking at pathophysiology. It allows the study of pulmonary vascular compliance, the derivation of ventricular pressure-volume loops, and the assessment of load-independent ventricular function.

30.3.3 Early Experiences

In our center, MR is used to assess PVR in patients as it offers a more accurate quantification of the PVR in humans and reduced exposure to ionizing radiation.³ XMR fusion technology is also being used to carry out interventional procedures in congenital heart disease such as stent implantation in patients with coarctation of the aorta (Fig. 30.3) as well as positioning of RF ablation devices within the heart (Fig. 30.4).

Another very promising area for clinical applications is the area of newly developed methods of scar imaging after electrophysiological ablation procedures. This allows assessment of the effectiveness of the ablation procedure. This can be

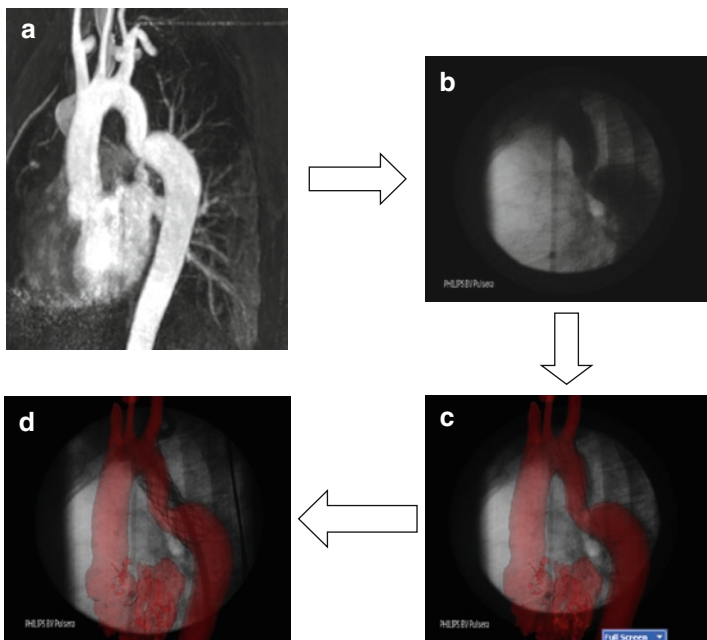


FIGURE 30.3. The three-dimensional (3D) contrast-enhanced magnetic resonance angiography (MRA) dataset of the aorta (**a**) is fused with the 2D angiography dataset (**b**) after injection of contrast agent (**c**). The high temporal resolution X-ray angiography 2D dataset (**b**) is used for implantation of a stent in the area of the coarctation. The 3D MRA/2D X-ray angiography fused dataset (**c**) is ideal for assessment of correct placement of the stent in the very complex 3D shape of the coarctation (**d**).

combined with the results of the electrophysiological mapping systems and 3D anatomic MRI imaging results. Using this unique XMR technology, we have carried out radiofrequency ablation in pulmonary veins, atria, and ventricles to successfully treat arrhythmias. This MR to X-ray registration method also allows us to relate the position of measured electrophysiology data to cardiac motion data from 3D MR images (Figs. 30.5 and 30.6).

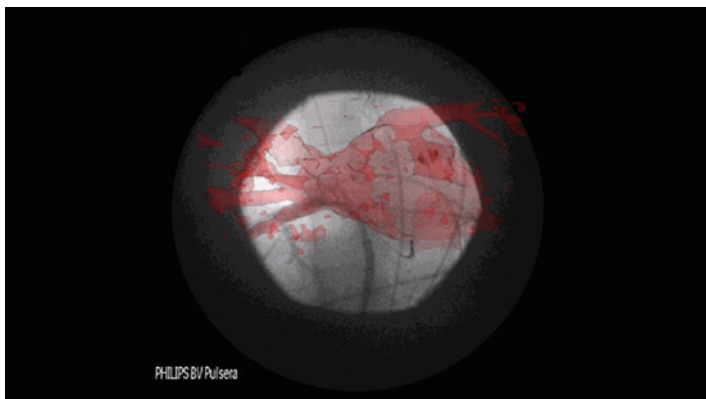


FIGURE 30.4. A 3D contrast-enhanced MRA dataset (*red*) of the left atrium is fused with 2D live X-ray fluoroscopy images (*greyscale*) during a radiofrequency ablation procedure to treat a patient with paroxysmal atrial fibrillation. Contrast injection into the lower branch of the right lower pulmonary vein shows good agreement with the MR overlay.

30.4 Future Perspectives

Several groups have demonstrated the immense potential of interventional CMR in animal models. The interventions have been shown to be feasible with passive and active catheter techniques that range from balloon angioplasty of arterial stenoses and stenting of vessels to atrial septal puncture and atrial septostomy. Device closure of atrial septal defects is another application that has been explored. MR-guided percutaneous pulmonary and aortic valve stent implantation has also been successfully carried out.

More complex interventions such as percutaneous coronary catheterization and intervention have also been demonstrated in healthy animals using MR. Balloon dilation of aortic coarctation in patients under MR guidance has also been performed. Recently, new MR-compatible guidewires and catheters have become available and interventions in

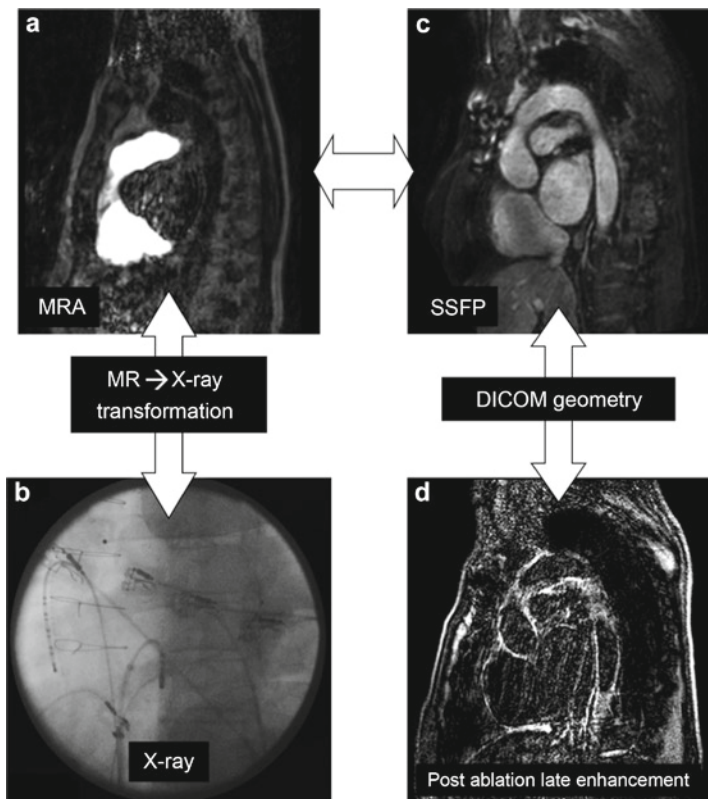


FIGURE 30.5. Using MRI for the measurement of ablation scar following a radiofrequency ablation for right atrial flutter. (a) A 3D MRA scan showing the right heart which is used to construct a 3D surface model of the right atrium; (b) an X-ray image showing the catheters present in the right heart; (c) a 3D SSFP whole heart post-contrast agent MR data set; and (d) a delayed enhancement image showing marked enhancement in the region of the right atrial floor. All the different types of image data were related by using image registration.

patients with congenital heart disease under MR guidance should be possible in the near future.

Further development of novel catheters and guidewires have been made possible by groups using targeted intramyocardial

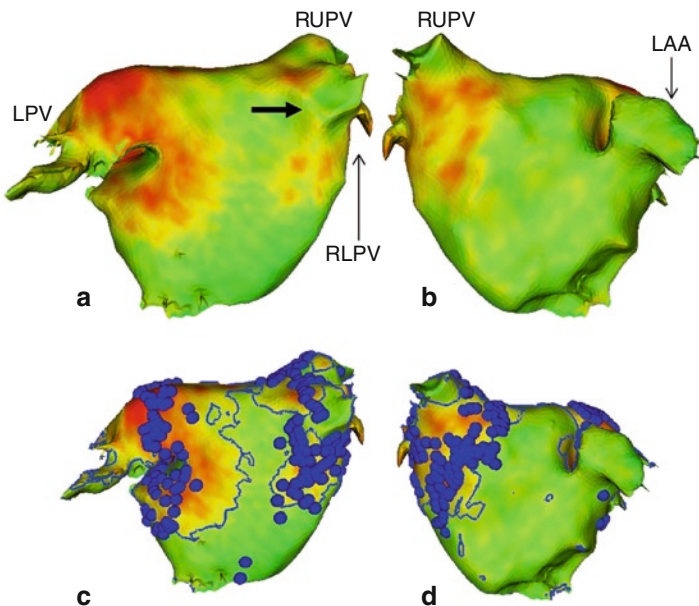


FIGURE 30.6. Mapping the late enhancement information from MRI to the 3D surface model for patient who underwent radiofrequency ablation for paroxysmal atrial fibrillation. **(a** posterior view & **b** anterior view) Enhancing regions are shown in red (most enhancing) and yellow (moderately enhancing) and non-enhancing regions are shown in green. The encirclement patterns around both left- and right-side veins are apparent. **(c** posterior view & **d** anterior view) The addition of the ablation points from NavX to show the good correlation between these points and the enhancing regions from the MRI data.

injection of progenitor stem cells in myocardial infarction in animal models.⁴ Also, using real-time MRI and direct apical access in porcine hearts, prosthetic aortic valves have been implanted in the beating heart. This breakthrough application may allow MR guidance of minimally invasive extra-anatomic bypass and beating-heart valve repair. MR guidance of intramyocardial gene therapy is another exciting field. Finally, three-dimensional electromechanical models of the heart have

also been created which allow simulation of cardiovascular pathologies in order to test therapeutic strategies and to plan interventions.

Acknowledgements We wish to thank in particular Reza Razavi and Carsten Shirra for their contribution to this work. Some of the work described in this chapter was performed at Guy's Hospital, London, UK, by a team of academic and clinical staff: Tobias Schaeffter, Sanjeet Hegde, Vivek Muthurangu, Marc Miquel, Redha Boubertakh, Andrew Taylor, Aaron Bell, Victoria Parish, Maxime Sermesant, Derek Hill, Stephen Keevil, David Hawkes, Jas Gill, Shakeel Qureshi, Eric Rosenthal, and Edward Baker in the Departments of Imaging Sciences, Pediatric and Adult Cardiology. We would also like to acknowledge the support of the anesthetic department as well as John Spence, Stephen Sinclair, Rebecca Lund, John Totman, and other staff from the Radiology Department who have provided considerable support.

References

1. Razavi R, Hill DL, Keevil SF, et al. Cardiac catheterisation guided by MRI in children and adults with congenital heart disease. *Lancet*. 2003;362:1877–1882.
2. Henk CB, Higgins CB, Saeed M. Endovascular interventional MRI. *Journal of Magnetic Resonance Imaging*. 2005;22:451–460.
3. Muthurangu V, Taylor A, Andriantsimavona R, et al. Novel method of quantifying pulmonary vascular resistance by use of simultaneous invasive pressure monitoring and phase-contrast magnetic resonance flow. *Circulation*. 2004;110:826–834.
4. Dick AJ, Guttmann MA, Raman VK, et al. Magnetic resonance fluoroscopy allows targeted delivery of mesenchymal stem cells to infarct borders in Swine. *Circulation*. 2003;108:2899–2904.

Index

A

- Acute intramural hematoma, 269–270
- Acute myocardial infarction
acute anterior MI, 428–431
acute inferior MI, 426–427
cine and LGE-CMR, 423
CMR role in, 426
complications, 425
vs. echocardiography, 422–423
edema imaging, risk assessment, 423
- microvascular obstruction, 424–425
- myocardial salvage, 424
- Adult congenital heart disease (ACHD)
aorta, coarctation
ancillary findings, 443
CMR findings, 442
extra-anatomic bypass, 443, 444
pseudocoart, 443
rib-notching appearance, 441, 442
volume-rendered image, 441, 443
- CMR
vs. computed tomography, 440
vs. echocardiography, 440
report, 455
- coronary anomalies, 451–452
- great arteries transposition

- axial SSFP image post Jatene operation, 448–450
- baffle occlusion, mustard/senning patients, 448, 449
- levo-transposition, 450–451
- partial anomalous pulmonary venous return (PAPVR), 452–454
- tetralogy of fallot
clinical features, 444–445
phase velocity mapping, 446, 447
- pulmonary arterial (PA) stenoses, 446, 447
- RV size and function, deterioration, 446
- Aliasing artifacts
frequency encoding direction, 168
- parallel imaging, 169–170
- phase encoding process, 167, 168
- short-axis image, heart, 167, 169
- Amyloidosis
aortic valve evaluation
LGE 4-chamber view, 321
- localizer and subsequent images, 319
- planimetry, 320
- systolic cine 4-chamber view, 320
- CMR, 318–319
findings on, 317–318
- protocol, 317

- report, 321
 - role, 317
 - differential diagnosis, 318
 - Anatomical and morphological imaging
 - T2^{*} relaxometry, 216–218
 - T1-weighted spin echo sequences, 212–214
 - T2-weighted spin echo sequences, 214–216
 - Aneurysm. *See* Aortic disease
 - Aortic disease, 276
 - aortic aneurysm
 - cardiac cycle, cine sequence, 274
 - focal enlargement, 272
 - MRA, 274
 - predisposing conditions for, 274–275
 - Valsalva measurement, 274
 - atherosclerosis, 269–273
 - candy cane view, aorta, 268
 - CMR protocol and report, 267, 277
 - CMR vs. CT, 268–270
 - Aortic dissection, 271–273
 - Arrhythmogenic right ventricular cardiomyopathy (ARVC)
 - CMR, 294
 - vs. CT, 292
 - findings on, 293
 - protocol, 290
 - report, 297
 - differential diagnosis, 293
 - palpitations, 294
 - axial cine images, 295–296
 - axial T1-weighted fast spin-echo images, 297
 - sagittal cine images, 296
 - standard long-axis cine image, 295
 - Task force criteria, 291–292, 297
 - Atherosclerosis
 - acute intramural hematoma, 269–270
 - aortic dissection, 271–273
 - penetrating atherosclerotic ulcer (PAU), 270–271
 - Atropine, 409–410
- B**
- Balanced steady state free precession (bSSFP), 118–121, 232
 - Benign cardiac tumors
 - fibromas, 366–367
 - hemangiomas, 368
 - lipoma, 364–366
 - myxomas, 364, 365
 - papillary fibroelastoma, 366
 - rhabdomyomas, 368
 - Binomial pulse. *See* Myocardial tagging
 - Black blood *vs.* bright blood imaging
 - double inversion preparation pulse
 - black blood preparation scheme, 105–107
 - blood pool signal suppression, 107, 108
 - gradient echo pulse sequence
 - bright blood imaging technique., 107
 - inflow enhancement, 108, 110
 - signal voids and vessel patency, 107
 - spin echo pulse sequence, 103–104
 - Boltzmann equation, 19
- C**
- Cardiac masses
 - benign (*see* Benign cardiac tumors)
 - CMR
 - vs. CT, 363–364
 - diagnosis, 373
 - protocol for, 361
 - report, 374
 - role, 361
 - tissue characteristics, 362
 - malignant (*see* Malignant cardiac tumors)

- primary, 363
- secondary, 363
- Cardiac motion
 - cardiac synchronization, 111, 112
 - cine gradient echo technique application, 121
 - cine imaging, 114–115
 - prospective *vs.* retrospective ECG gating, 117–118
- spoiled gradient echo *vs.* bSSFP
 - bSSFP sequence contrast behavior, 120–121
 - gradient echo pulse sequence, 118
 - spoiler gradient, 118, 119
- still imaging
 - application, 113
 - multiple slice acquisition, 114
 - triggering, 112, 113
- triggering *vs.* cine image gating
 - ECG gating, 116–117
 - ECG triggering, 115–116
- Cartesian data acquisition, 63–65
- Catheter tracking and visualization
 - active techniques, 465–466
 - hybrid techniques, 466
 - passive techniques, 465
 - X-ray imaging, 466–467
- Chemical shift artifact
 - gradient echo pulse sequences, 176–180
 - Larmor frequency, hydrogen nuclei, 175–177
 - spin echo-based pulse sequences, 176
- Churg–Strauss syndrome
 - CMR
 - findings, 314
 - protocol, 314
 - report, 318
 - role, 314
 - differential diagnosis, 315
 - pulmonary edema and pleural effusions, 315–316
- Cine imaging
 - cardiac phase, 114–115
 - cine gradient echo technique
 - application, 121
 - ECG triggering, 218–219
 - quantitation, 220–223
 - real-time, 219
 - triggering *vs.* cine image gating
 - ECG gating, 116–117
 - ECG triggering, 115–116
 - CMR report
 - adult congenital heart disease (ACHD), 455
 - amyloidosis, 321
 - aortic disease, 277
 - arrhythmogenic right ventricular cardiomyopathy, 297
 - cardiac masses, 374
 - Churg–Strauss syndrome, 316
 - congenital pericardial abnormalities, 360
 - constrictive pericarditis, 346
 - dobutamine stress CMR (DSCMR), 413
 - guidelines, 261
 - hypertrophic cardiomyopathy (HCM), 289
 - ischemic heart disease, viability assessment, 421
 - left ventricular non-compaction cardiomyopathy (LVNC), 302
 - myocardial perfusion CMR, 404
 - myocarditis, 308
 - pericardial effusion, 339
 - pericardial tumors, 354
 - pulmonary vein assessment, 462
 - sample report, 264
 - sarcoidosis, 313
 - siderotic cardiomyopathy, 326
 - structured approach
 - assessments, 262
 - clinical indications, 261–263
 - scan components, 262
 - Tako-Tsubo cardiomyopathy, 331
 - valvular heart disease, 385
 - CMR study
 - contraindications/safety
 - displacement, 194

- heating effects, 194, 195
 - internal devices, 194
 - missile effects, 193
 - MRI contrast agents, 195
 - nephrogenic systemic fibrosis (NSF), 195–196
 - scanner's magnetic field, 190–191
 - screening, 191–193
 - stress examinations, 197
 - ECG signals, 200–201
 - equipments, 198–200
 - indications, 189–190
 - patient preparation, 201–202
 - referral form, 187–189
 - safety issues, 197–198
 - scanner, 202
 - Coarctation, aorta**
 - ancillary findings, 443
 - CMR findings, 442
 - extra-anatomic bypass, 443, 444
 - pseudocoarct, 443
 - rib-notching appearance, 441, 442
 - volume-rendered image, 441, 443
 - Congenital pericardial abnormalities**
 - CMR**
 - vs. echocardiography, 356
 - protocol, 355
 - report, 360
 - role, 357
 - pericardial cyst, 355
 - CMR findings, 356
 - coronal HASTE image, 357
 - three-chamber cine image (SSFP), 359
 - TSE images, 358–359
 - pericardial defects
 - CMR findings, 356–357
 - partial defects, 355–356
 - Congenital valvular heart disease, 378–379**
 - Constrictive pericarditis**
 - CMR**
 - vs. CT, 341
 - vs. echocardiography, 341
 - indirect signs, 342
 - pericardial thickening, 341
 - protocol, 340
 - report, 346
 - role, 342
 - four-chamber cine image, 343
 - mitral in-flow, phase contrast flow mapping, 345
 - myocardial-tagged image, 344
 - T1-weighted TSE image, 344
 - MRI sequela, 341
 - physiological consequence, 340
 - Contrast-enhanced MR angiography, 228–231**
 - Coronary artery imaging**
 - module, 249
 - navigator-gated 3D fast/turbo gradient echo, 151–153
 - targeted technique, 244, 248–249
 - whole heart technique, 243
 - Cross-sectional anatomy**
 - axial black blood images, 252–256
 - coronal black blood images, 256–257
 - sagittal black blood images, 258
 - Customized views, 259**
- D**
- Dilated cardiomyopathy (DCM)**
 - CMR, 283, 284
 - findings on, 282
 - role, 281
 - vs. SPECT, 281
 - differential diagnosis, 282
 - family history, 280–281
 - heart failure, 283
 - Dipyridamole, 395**
 - Dobutamine stress CMR (DSCMR)**
 - diagnostic performance, 406
 - dobutamine
 - contraindications, 409
 - side effects, 409
 - vs. dobutamine stress
 - echocardiography (DSE), 405–406
 - end-systolic SA cine images, 412
 - image analysis, 410–411

procedure, 408
prognostic performance, 406–407
report, 413
role, 407
safety considerations, 408–409

E

Early and late gadolinium enhancement, 242–243
2D segmented inversion recovery gradient echo sequence, 240
EGE image, 241, 244
extracellular space, 240
intracellular space, myocardial necrosis, 240
Look locker sequence, 241, 245
module, 242
myocardial “nulling” changes, 240, 241
phase-sensitive IR-GRE (PSIR) sequence, 240
T1-weighted images, 240
Echocardiography *vs.* CMR
acute myocardial infarction, 422–423
adult congenital heart disease (ACHD), 440
congenital pericardial abnormalities, 356
constrictive pericarditis, 341
dobutamine stress CMR (DSCMR), 405–406
ischemic heart disease, 388
myocarditis, 303
pericardial effusion, 334
pericardial tumors, 347
valvular heart disease, 376
Echo planar imaging (EPI), 131–132, 232
Echo time (TE), 37–39, 87
Echo train length (ETL), 129

F

Faraday cage, 11
Fast imaging, image acquisition de-phasing, 134
EPI, 131–132

parallel imaging, 135–136
phase encoding steps, 133–134
turbo gradient echo
accelerated image acquisition, 130–131
real-time imaging, 131
segmented k-space, 129, 130
turbo spin echo
conventional spin echo pulse sequence, 127–128
echo train length, 129
Fibromas, 368–369
Flip angle, RF pulses
definition, 23
excitation pulse, 24–25
inversion pulse, 27–28
refocusing pulse, 27
saturation pulse, 25–26
Flow-related signal loss, 176
flow jets, 174–175
gradient echo-based pulse sequences, 174, 175
qualitative assessment, 174–175
velocity-related phase shift, 174
Fourier transform, 51–52
Free induction decay (FID), 29, 33–35
Frequency encoding gradient, 49

G

Gadolinium, 149
Ghosting artifacts
pulsatile blood flow motion
axial spoiled gradient echo image, 172–173
flow compensation, 174
phase difference, 172
respiratory motion, 171–172
Gradient echo *vs.* spin echo
difference, 101
field inhomogeneities, 97
low flip angle, 99
pulse sequence, 90–91
180° refocusing pulse, 99
RF pulse, 98, 100
transverse magnetization, 97–99
Gradient magnetic field, 3

H

- Hemangiomas, 361
 Hypertrophic cardiomyopathy (HCM)
 clinical signs, 285
 CMR
 findings on, 285–286
 protocol, 284
 report, 289
 role, 285
 differential diagnosis, 285
 LVOT obstruction
 cine 3 chamber view, 287
 cine images, 288
 LGE 2 chamber view, 288
 LGE 3 chamber view, 288
 LGE 4 chamber view, 289
 LGE short-axis view, 289
 microscopic and macroscopic studies, 284

I

- Image encoding and localization
 de-phasing gradient, 54–55
 frequency encoding
 arbitrary slice orientation, 51
 definition, 49
 Fourier transform, 49, 50
 image reconstruction, 55–56
 signal analysis, 51–53
 MR signal, 47
 phase encoding
 acquisition time, 59
 definition, 47–48
 2D Fourier transformation, 57–58
 image matrix, 57, 58
 image reconstruction, 55–56
 phase shift, 48–49
 proton magnetic moments, 56–57
 spatial resolution, 58–59
 pulse sequence, 54
 slice selection
 bandwidth, rf pulse, 47
 definition, 45

- Larmor frequency, 45
 rf excitation pulse, 45, 46
 Image localization and planning, CMR
 4-chamber cine, 208, 209
 HLA cine, 208
 image localizer, 206–207
 interactive, 211
 LVOT, 209, 210
 LV SA cine stack, 209, 210
 RVOT, 210, 211
 short axis (SA) cine, 208, 209
 trans-axial stack, 207
 VLA cine, 207, 208
 Imaging parameters and attributes
 2D and 3D imaging, 79–80
 3D imaging advantages, 80
 double in-plane spatial resolution, 75, 76
 factors affecting SNR, 77
 halve image acquisition time, 77, 78
 image matrix size, 69, 70
 image quality factors
 intrinsic signal amplitude, 71–72
 signal averaging, 72, 73
 SNR and receiver bandwidth, 73–74
 signal averaging nomenclature, 72
 signal-to-noise ratio, 70–71
 spatial resolution, image acquisition time, 69–70
 Infiltrative/storage diseases
 amyloidosis (*see Amyloidosis*)
 siderotic cardiomyopathy (*see Siderotic cardiomyopathy*)
 Inflammatory diseases
 myocarditis (*see Myocarditis*)
 sarcoidosis (*see Sarcoidosis*)
 vasculitis (*see Churg-Strauss syndrome*)
 Integral radiofrequency, 8–9
 Interventional MRI systems.
 See also MR visualization strategies

- catheter tracking
 active techniques, 465–466
 hybrid techniques, 466
 passive techniques, 465
- XMR facility design
 examination room, 463–465
 safety features, 464–466
- Ischemic heart disease
 acute myocardial infarction (*see*
 Acute myocardial infarction)
- CMR
 vs. computed tomography
 (CT), 388
 vs. echocardiography, 388
 hardware development, 434
 myocardial perfusion imaging
 without contrast, 435
 noninvasive arterial wall
 imaging, 435
 vs. nuclear scintigraphy, 389
 software development, 434
 targeted contrast agents, 435
- myocardial perfusion CMR (*see*
 Myocardial perfusion CMR)
- normal coronary arteries, positive
 markers
- secondary prevention therapy,
 433
- troponin-positive acute
 coronary syndrome, 433
- stress wall motion imaging (*see*
 Dobutamine stress CMR
 (DSCMR))
- viability assessment, LGE-CMR
 acute inferior ST-elevation MI,
 416–417
 anterior MI, 418–419
 fibrosis, 416
 functional improvement and
 complete recovery, 417
 vs. PET and SPECT, 414–415
 report, 425
 reversible ischemia and viable
 myocardium, 419–420
 role, 421
 transmural extent, 418, 421
- K
- K-space
 Cartesian data acquisition, 63–64
 centric/low-high k-space order,
 64, 65
 definition, 61–62
 2D Fourier transform, 65
 image space relation, 61
 linear phase encoding, 63–65
 MR signal echo, 65, 66
 MR signal relation, 67
 spatial frequency, 62–63
- L
- Larmor frequency, 8, 21
- Late gadolinium enhancement
 CMR (LGE-CMR). *See also*
 Early and late gadolinium
 enhancement
- viability assessment
 acute inferior ST-elevation MI,
 416–417
 anterior MI, 418–419
 fibrosis, 416–417
 functional improvement and
 complete recovery, 417
 vs. PET and SPECT, 414–415
 report, 421
 reversible ischemia and viable
 myocardium, 419–420
 role, 418
 transmural extent, 418, 421
- Left ventricular non-compaction
 cardiomyopathy (LVNC)
 CMR
 vs. cardiac CT, 298
 findings on, 299
 protocol, 298
 report, 304
 role, 300
 differential diagnosis, 299
 recurrent syncope
 cine images, 300–301
 LGE images, 301
- Left ventricular outflow tract
 (LVOT) obstruction

- cine 3 chamber view, 287
 cine images, 288
 LGE 2 chamber view, 288
 LGE 3 chamber view, 288
 LGE 4 chamber view, 289
 LGE short-axis view, 289
- Lipoma, 364–366
 Look locker sequence, 241, 245
 Lymphoma, 369–370
- M**
- Magnetic fields, 3
 Magnetic moment, 17
 Magnetic resonance (MR) echoes
 gradient echoes
 definition, 37
 echo time, 37–39
 spin echoes
 definition, 40–41
 magnetic field gradient, 41–42
- Magnetic resonance imaging (MRI)
- active and passive magnetic shielding, 14
 - decay, 33–34 (*see also* Free induction decay (FID))
 - examination room, 11
 - fringe field hazard
 - ASTM labelling system, 13
 - examination and controlled area, 11–12
 - gradient coil assembly, 6–8
 - hydrogen nuclei, 17
 - integral radiofrequency (RF)
 - body transmitter coil, 8–9
 - net magnetization, 17–19
 - proton spin, 17–18
 - receiver coil, 9
 - RF shielding, 11
 - superconducting magnet
 - cryostat, 4–5
 - shimming, 5–6
- Magnetic resonance visualization
- strategies
 - ablation scar measurement, 472
 - catheter tracking and visualization
 - active techniques, 465–466
- hybrid techniques, 466
 passive techniques, 465
- 3D contrast-enhanced MRA
- dataset and X-ray fluoroscopy fusion, 470, 471
 - future aspects, 471–474
 - late enhancement information mapping, 473
 - physiological information, 467–469
 - cardiac output, 469
 - global and regional ventricular function, 469
 - pulmonary blood flow, 468–470
 - pulmonary-to-systemic flow ratio, 469
 - stent implantation and coarctation, 469, 470
- XMR procedures
- cardiac catheterization, 466–467
 - image fusion, 467
- Magnetic susceptibility artifact
- de-phasing, 179
 - magnetic field, 178–179
 - signal loss, 179–180
- Malignant cardiac tumors
- lymphoma, 370
 - metastatic spread, 370
 - sarcoma, 368
- Metallic artifact, 180–181
- Multiple shot imaging, 129
- Myocardial infarction. *See* Acute myocardial infarction
- Myocardial perfusion CMR
- additional equipment, 398
 - angina
 - circumflex artery stenosis, 402
 - proximal LAD stenosis, 400–401
 - three-vessel coronary artery disease, 403
- balanced steady-state free precession (bSSFP), 232
- dark rim artifact, 235–236
- diagnostic performance, 391–392
- first-pass MR perfusion study, 232, 233

- first-pass perfusion CMR, 389
 hybrid echo planar imaging (EPI), 232
 image analysis, 399–400
 perfusion module, 235
vs. PET and SPECT
 contrast agents, 298
 data acquisition, 390
 diagnostic accuracy, 391
 ionizing radiation, 390–391
 spatial resolution, 390
 procedure, 396–397
 prognostic performance, 393
 protocol, 388
 pulse sequence
 data acquisition, 163
 single-shot gradient echo-based technique, 162–164
 quantitative assessment, 237–238
 report, 404
 role, 393
 safety considerations, 397
 semi-quantitative assessment, 238–239
 spoiled gradient echo, 232
 three short axis slices, 233–235
 vasodilator stress agents
 adenosine, 395
 contraindications, 397
 development, 395–396
 dipyridamole, 395
 side effects, 396
 visual assessment, 236–237
Myocardial tagging, 159–162, 223–225
Myocarditis
 acute chest pain
 cine 4-chamber view, 306
 LGE images, 307, 308
 STIR images, 306, 311
CMR, 307
vs. echocardiography, 303
 findings on, 304
 report, 308
 role, 302
 differential diagnosis, 304
Myxomas, 364
- N**
Nephrogenic systemic fibrosis (NSF), 195–196
Noninvasive arterial wall imaging, 435
Nuclear spin, 17
- P**
Papillary fibroelastoma, 366
Parallel imaging, 83, 135–136
Paravalvular abscess, 382–383
Partial anomalous pulmonary venous return (PAPVR), 452–454
Penetrating atherosclerotic ulcer (PAU), 270–271
Pericardial cysts, 372
Pericardial disease
congenital abnormalities (see Congenital pericardial abnormalities)
constrictive pericarditis (see Constrictive pericarditis)
pericardial effusion (see Pericardial effusion)
pericardial tumors (see Pericardial tumors)
Pericardial effusion
CMR
vs. echocardiography, 334
 findings on, 334–336
 protocol, 333
 report, 339
 role, 336
 etiology, 333
rheumatoid arthritis
 4-chamber cine image, 337–338
 real-time short axis cine image, 338
 T1 TSE image, 337
Pericardial tumors
CMR
 black blood images (TSE), 349
 CINE imaging (b-SSFP), 348–349
vs. coronary angiography, 348
vs. CT, 348

- delayed enhanced images, 349–350
vs. echocardiography, 347
first-pass perfusion imaging, 349
myocardial tagging, 349
post-contrast T1 TSE images, 349
protocol, 347
report, 354
role, 350
synovial sarcoma
angiogram, 353
cine SSFP 2-chamber and short axis views, 351
coronal cine image, 353
first-pass perfusion study, 352
TSE inversion recovery
delayed enhanced image, 352
- Phase contrast velocity encoding, 228
See velocity encoded cine gradient echo
- Phase encoding CMR
acquisition time, 59
definition, 47–48
2D Fourier transformation, 57–58
image matrix, 57, 58
image reconstruction, 55–56
phase shift, 48–49
proton magnetic moments, 56–57
spatial resolution, 58–59
- Phase encoding gradient, 47–48
- Phase-sensitive IR-GRE (PSIR)
sequence, 240
- Prosthetic valves, 382, 383
- Proton density, 91
- Pseudotumors, 37
- Pulmonary valve (PV) stenosis, 380–382
- Pulmonary vein assessment
clinical scenarios, 457
CMR
analysis, 459–461
vs. cardiac CT, 458
findings, 459
- protocol, 457, 459
report, 462
- Pulse sequence
black blood FSE/TSE
re-inverted myocardial tissue, 146–147
spin echo, 145–146
black blood turboSTIR, 147–148
cine gradient echo
real-time imaging, 155
retrospective gating, 153–154
- frequency selective fat suppression
- Larmor frequency, 141–143
pros and cons, 143
spoiler gradient, 142, 143
z-magnetization, 141
- image contrast and weighting, 90–91
- inversion recovery fast/turbo gradient echo
- late enhancement technique, 149–151
- TI-scout, 151
- viability imaging, 149, 151
- long TR and short TE, 92
- long TR and TE, 94
- myocardial perfusion
data acquisition, 163
single-shot gradient echo-based technique, 162–164
- myocardial tagging
grid tagging, 160–161, 163
modulating gradients, 159, 162
- navigator-gated 3D fast/turbo gradient echo, coronary arteries
- gradient echo pulse sequence, 151
- T2-preparation scheme, rf pulse, 152–153
- selective tissue saturation
application, 141
90° rf pulse, 140
- short TR and long TE, 95
- short TR and TE, 93
- STIR and turbo STIR

- inversion recovery, 143
 - pros and cons, 145
 - slice-selective 180° inversion pulse, 142–143
 - spin echo, 145
 - tissue saturation, 139–141
 - TR and TE
 - image acquisition parameters, 87
 - MR signal echo amplitude, 90
 - transverse magnetization, 87–89
 - velocity encoded cine gradient echo
 - bipolar gradient pulse pair, 155
 - de-phasing and re-phasing, 155–156
 - phase maps, 157
 - velocity encoding direction, 157–158
 - velocity map, 157–159
 - VENC, 159, 160
- R**
- Radiofrequency interference artifacts, 182–183
 - Radiofrequency (RF) magnetic field, 3
 - Referral form, CMR study, 187–189
 - Relaxation times
 - MRI signal decay, 33–34
 - spin-spin interaction, 34–35
 - T2* decay, 35–36
 - T1 time constant
 - saturation recovery, 31–32
 - significance, 33
 - Repetition time (TR), 87
 - Resonant frequency. *See* Larmor frequency
 - Respiratory motion
 - effects, 123
 - image degradation, 123
 - navigator echo, 125
 - pneumatic bellows device, 123, 124
 - respiratory gating
 - data acquisition, 123–124
 - gating threshold, 124–125
- patient respiratory cycle monitoring, 123, 124
 - RF coils, cardiovascular magnetic resonance, 85
 - RF pulses and echoes
 - flip angle
 - excitation pulse, 24–25
 - inversion pulse, 27–28
 - refocusing pulse, 27
 - saturation pulse, 25–26
 - gyromagnetic ratio, 21
 - magnetization
 - coherence and precession, 22–23
 - longitudinal and transverse components, 24
 - net magnetization, 22
 - MR-active nuclei, 22
 - MRI signal, 28–30
 - Rhabdomyomas, 368
- S**
- Sarcoidosis, 309
 - acute cardiac involvement, 310–311
 - apical short-axis STIR image, 312
 - follow-up study, 312
 - LGE images, 312, 313
 - long-axis cine images, 311
 - STIR images, 311
 - CMR
 - findings on, 309–310
 - protocol, 309
 - report, 313
 - role, 309
 - differential diagnosis, 310
 - Sarcoma, 368–369
 - Segmented k-space gradient echo imaging. *See* Multiple shot imaging
 - SENSE aliasing artifacts, 169–170
 - Siderotic cardiomyopathy
 - cardiac and liver iron overload
 - axial T2* map, liver, 326
 - coronal scout image, 324
 - mid-cavity short-axis T2* measurement, heart, 325

- systolic cine 4-chamber view, 325
- CMR, 322–324
findings on, 323
protocol, 322
report, 326
role, 323
differential diagnosis, 323
- Signal to noise ratio (SNR), 70–71
coil array, 83, 86
integral body coil, 83, 84
multielement coils, 83, 86
- Spin echo pulse sequence, 90
- Spin washout effect, 103, 105
- Synovial sarcoma
angiogram, 353
cine SSFP 2-chamber and short axis views, 351
coronal cine image, 353
first-pass perfusion study, 352
TSE inversion recovery delayed enhanced image, 352
- T**
- T1
relaxation, 31–33
weighting, 91, 93, 96, 146, 212, 213
- T2
relaxation, 33–35
weighting, 91, 94, 96, 97, 146, 214
- T2*, 216
relaxation, 35–36, 91, 94, 96, 97
weighting, 91, 94, 96, 97, 146, 214
- Tagging *See* Myocardial Tagging
- Tako-Tsubo cardiomyopathy
cine images, apical ballooning, 330
- CMR, 329
vs. echocardiogram, 327
findings on, 328
protocol, 327
report, 331
role, 328
differential diagnosis, 328
- LGE images, myocardial necrosis, 330
- STIR images, 330
- Tetralogy of fallot (TOF)
clinical features, 444–445
phase velocity mapping, 446
pulmonary arterial (PA) stenoses, 446, 447
RV size and function, deterioration, 445
- Thrombus masses, 370–371
- Time-of-flight magnetic resonance angiography (TOF MRA), 109
- Troponin-positive acute coronary syndrome, 433
- V**
- Valvular heart disease
CMR, 334
vs. echocardiography, 376
indications, 376, 377
protocol, 375
report, 385
role, 376
congenital, 378–379
paravalvular abscesses, 382–383
prosthetic valves, 382, 383
regurgitation, 379–380
stenosis, 380–382
vegetations, 382
- Vasculitis. *See* Churg-Strauss syndrome
- Vasodilator stress agents
adenosine, 395
contraindications, 396
development, 395–396
dipyridamole, 395
side effects, 396
- Velocity encoded cine gradient echo
advantage, 225
bipolar gradient pulse pair, 155
de-phasing and re-phasing, 155–156
magnitude and phase images, 226
module, 227
phase maps, 157

- post-processing software, 226–227
velocity encoding direction, 157–158
VENC, 159, 160
- Vertical field open MR systems, 5, 6
- Viability assessment. *See also* Late gadolinium enhancement
CMR (LGE-CMR)
cine imaging, 415
contractile reserve, 415
late gadolinium enhancement
acute inferior ST-elevation MI, 415–416
fibrosis, 416–417
- functional improvement and complete recovery, 417
transmural extent, 417, 418
- Voxel volume, 69, 70
- W**
- Whole heart technique, 243, 244
coronary artery rest periods, 247
3D coronary data set,
SoapBubble™ software, 247, 248
Lung–diaphragm interface, 245–246
pulmonary artery bifurcation, 245–246